U.PORTO
FEUP FACULDADE DE ENGENHARIA
UNIVERSIDADE DO PORTO

Torque Loss in Tapered Roller Bearings Lubricated with Axle Gear Oils

Nuno André Maia Rodrigues

Porto, October 2016

Faculdade Engenharia da Universidade do Porto
Departamento de Engenharia Mecânica

Torque Loss in Tapered Roller Bearings Lubricated with Axle Gear Oils

Nuno André Maia Rodrigues

Master's Degree Dissertation presented to Faculdade de Engenharia da Universidade do Porto

Dissertation supervised by:

Doctor Carlos M. C. G. Fernandes
Researcher of INEGI

Doctor Jorge H. O. Seabra
Full Professor of FEUP

Porto, October 2016

LaTeX
Torque Loss in Tapered Roller Bearings Lubricated with Axle Gear Oils
N. A. M. Rodrigues
2016
FEUP-U.PORTO

to my family

Acknowledgements

Long was the way to get here, and I want to express my acknowledgement to Faculdade de Engenharia da Universidade do Porto (FEUP), which provided all the resources to my Master's Degree in Mechanical Engineering graduation.

To INEGI/CETRIB (Instituto de Ciência e Inovação em Engenharia Mecânica e Engenharia Industrial/Unidade de Tribologia, Vibração e Manutenção industrial) for the opportunity, the conditions and resources to develop this project.

I am thankful to my both supervisors, Doctor Carlos Fernandes and to Professor Jorge Seabra for sharing their vast knowledge and expertise, from the first moment. Their patient, dedication, guidance and permanent support were essential throughout the semester, and without them this work would not be accomplished.

A special thanks to the outstanding CETRIB engineers Beatriz Graça, David Golçalves, José Brandão, Marroua Hammami, Pedro Marques and Ramiro Martins, for the numerous information exchanges that without doubt enriched this project. A word must be also addressed to my Master Degree colleagues for all the suggestions and advices.

To my parents, Manuel and Antónia, my brother, Diogo, and grandmother, Alice. All the comprehension, continuous encouragement and love that they always gave me, pushing me forward my whole life.

To my princesinha Joana, for all the unconditional love and unwavering support, believing in my abilities whatever the situation I was in, not only in this degree, but at life in general. I am eternally grateful to her.

To my grandfather Almiro da Cruz Maia.

Abstract

Fuel economy on vehicles is in the agenda of governments, manufacturers and consumers. Gearbox and differential are responsible for 13 % of the mechanical energy losses in a light duty vehicle. Tapered roller bearings, included in the final drive unit, are subjected to a wide range of load, temperature and rotational speed conditions, playing an active role on energy losses and heat generation. The lubricant sealed for life on a differential container, perform an important role in controlling energy losses and providing efficient and durable operation.

In this study, five multigrade oils (1 mineral and 4 synthetic) were analysed considering its rheological properties and chemical composition (additives). Tests with cylindrical roller thrust bearings were performed under boundary lubrication regime for 24h in order to understand the influence of additives on the friction behaviour and rolling bearing wear. Further analysis were performed on both rolling bearing surfaces and oil. Roughness measurements were performed on raceways. XPS analysis were performed on roller elements to investigate the tribofilm formation. Oil analysis including DR ferrography and analytical ferrography were performed to study the severity of the wear.

Friction torque measurements were performed on tapered roller bearings with the five oils, under two different axial loads, three different temperatures and a wide range of rotational speeds, allowing to compare the torque losses for each oil.

The results showed that both oil base, viscosity and additive package had a great influence tribofilm formation and friction behaviour of rolling bearings.

Resumo

A economia de combustível dos veículos está na agenda dos governos, fabricantes e consumidores. A caixa de velocidades e o diferencial são responsáveis por 13 % das perdas de energia mecânica num veiculo ligeiro. Os rolamentos de rolos cónicos, incluídos no diferencial do eixo tarseiro, estão sujeitos a uma grande gama de forças, temperaturas e velocidades de rotação, tendo um papel ativo nas perdas de energia e geração de calor. O lubrificante incluído e utilizado para toda a vida útil do diferencial, desempenha um papel importante no controlo das perdas de energia bem como promove um funcionamento eficiente e duradouro.

Neste estudo, cinco óleos multigraduados (1 mineral e 4 sintéticos) foram analisados tendo em consideração as suas propriedades reológicas e composição química (aditivos). Foram realizados testes com rolamentos axiais de rolos cilíndricos em regime limite de lubrificação durante 24h para se perceber a influência dos aditivos na perda de binário e no desgaste do rolamento. Medições de rugosidades foram realizadas nas pistas. Foram realizadas análises dos rolos por XPS para investigar a geração de tribofilme. Ferrografia de leitura direta e ferrografia analítica foram realizadas nos óleos para investigar a severidade do desgaste.

Foram realizadas para os cinco óleos medições de perda de binário nos rolamentos de rolos cónicos, para duas cargas axiais diferentes, três temperaturas diferentes e uma larga gama de velocidades de rotação, o que permitiu comparar as perdas para cada óleo.

Os resultados mostraram que tanto a base como a viscosidade e os aditivos do óleo tiveram uma grande influência na geração de tribofilme e no binário resistente dos rolamento.

Keywords

Drivetrain

Differential

Axle Gear Oil

Cylindrical Roller Thrust Bearing

Friction Torque

Coefficient of Friction

Film Thickness

Tapered Roller Bearing

Tribofilm

Palavras-Chave

Transmissão

Diferencial

Óleo para Engrenagem Hipóide

Rolamento Axial de Rolos Cilíndricos

Binário de Atrito

Coeficiente de Atrito

Espessura de Filme

Rolamento de Rolos Cónicos

Tribofilme

Contents

List of Figures

List of Tables

List of Symbols

a	contact semi-width	m
a_i	ASTM D341 constant	-
A_C	contact area	m^2
A_S	sampling area	μm^2
A_P	spectrum peak area	-
A_t	atomic concentration	%
b	face width	mm
C	basic dynamic load rating	kN
C_0	basic static load rating	kN
C_F	auxiliary pressure factor	$m^4.N^{-1}$
d	rolling bearing inner diameter	m
d'	pich diameter	mm
d_m	rolling bearing mean diameter	m
d_l	dilution factor	-
d_r	tapered roller mean diameter	m
d'_r	cylindrical roller mean diameter	m
D	rolling bearing outer diameter	mm
D_L	ferrometric index for the amount of large particles	-
D_S	ferrometric index for the amount of small particles	-
e	rolling bearing SKF calculation factor	-
$E_{1,2}$	Young modulus of elasticity for roller and race	Pa
E^*	equivalent Young modulus of elasticity	Pa
E_{be}	binding energy	eV
E_{ke}	ejected electron kinetic energy	eV
E_r	calculated error for optimized model	-
$fexp$	experimental factor	-
F_a	axial load applied on rolling bearing	N
F'_a	axial gear load	N
F_{am}	axial minimum load applied on rolling bearing	N
F_n	normal load applied at the contact	N
$F_{n_{max}}$	maximum normal load applied at the contact	N
F_r	radial load applied on rolling bearing	N
F'_r	radial gear load	N
F'_u	tangential gear load	N
G	non-dimensional material parameter	-
G_{rr}	rolling torque factor that depends on the bearing type, geometry and loads	-
G_{sl}	sliding torque factor that depends on the bearing type, geometry and loads	-
h_0	film thickness at the centre of the line contact	m

h_{0c}	corrected film thickness at the centre of the line contact	m
h_v	photon energy	eV
H_{VI}	kinematic viscosity at 40°C of an oil with VI=100	cSt
H_s	dimensionless Hersey number	-
i_{gb}	gearbox ratio	-
i_{diff}	differential ratio	-
I	intensity	CPS
J_r	line contact coefficient	-
$k_{1,2,3}$	°Engler to cSt conversion constants	-
K	thermal conductivity	W.m.$^{-1}$K^{-1}
K_a	external axial load	-
K_{rs}	replenishment/starvation constant	-
K_Z	bearing type related geometry constant	-
l	contact length	m
l'	rolling bearing relative positions	mm
l_S	sampling length	μm
L	non-dimensional lubricant thermal parameter	-
L_C	centre location of roughness measurements	mm
L_E	exterior location of roughness measurements	mm
$L(E_{be})$	linear background function	-
L_{VI}	kinematic viscosity at 40°C of an oil with VI=0	cSt
m	outside radial module	mm
m_i	ASTM D341 constant	-
M_{drag}	drag friction torque	N.mm
M_t	total friction torque	N.mm
M_{rr}	rolling friction torque	N.mm
M_{seal}	bearing seals friction torque	N.mm
M_{sl}	sliding friction torque	N.mm
M_{r1}	peak material ratio	%
M_{r2}	valley material ratio	%
n	rolling bearing superior/inner race rotational speed	rpm
n_i	ASTM D341 constant	-
n_r	number of ordinates	-
N_{eng}	engine rotational speed	rpm
N_{in}	input differential shaft rotational speed	rpm
N_{VI}	auxiliary variable to determine VI	-
p	pressure	Pa
p_{max}	maximum Hertzian pressure	Pa
P	equivalent dynamic bearing load	kN
P_0	equivalent static bearing load	kN
P_B	rolling bearing power losses	W
P_{eng}	engine power	W
rs	number of different rotational speeds	-
$R_{1,2,3}$	rolling torque constants dependent on rolling bearing type	-
R_a	arithmetical mean deviation roughness	μm
R_e	cone distance	mm
R_k	core roughness depth	μm
R_{ku}	kurtosis of roughness profile	-
R_{max}	maximum peak-to-valley height	μm
R_{pk}	reduced peak height	μm
R_q	root mean square deviation roughness	μm
R_{sk}	skewness of roughness profile	-
R_{vk}	reduced valley depth	μm
R_x	equivalent radius of contact in the x direction	m
R_{x1}	roller contact radius in x direction	m

R_{x2}	race contact radius in x direction	m
$R^{x,y,z}$	loads on rolling bearing position on x,y, z directions	N
R_z	mean peak-to-valley height	-
s_d	standard deviation	-
s_g	specific gravity	-
s_{Gold}	Gold's constant	-
S_m	peak spacing	mm
$S_{1,2}$	sliding friction constants dependent on rolling bearing type	-
S_a	arithmetical mean deviation height	μm
S_{pm}	modified Stribeck parameter	-
S_p	maximum peak height	μm
S_q	root mean square deviation height	μm
S_v	maximum valley depth	μm
S_{ku}	kurtosis of surface topography	-
S_{sk}	skewness of surface topography	-
S_z	maximum mean peak-to-valley height	μm
$S(E_{be})$	Shirley background function	-
T_{eng}	engine output torque	N.m
T_{in}	input torque on differential	N.m
t	oil flow time	s
t_{Gold}	Gold's constant	-
t_{ref}	water flow time	s
T	working temperature	K
T_{ref}	reference temperature	K
U	non-dimensional velocity parameter	-
U_1	contact roller velocity	$m.s^{-1}$
U_2	contact raceway velocity	$m.s^{-1}$
U_{2c}	contact raceway velocity at centre of the contact line	$m.s^{-1}$
U_R	rolling speed	$m.s^{-1}$
U_S	sliding speed	$m.s^{-1}$
U_{VI}	kinematic viscosity at 40°C of a selected oil	cSt
V_e	dimensionless slip rate parameter	-
Y_{VI}	kinematic viscosity at 100°C of a selected oil	cSt
Y	rolling bearing dynamic axial load factor	-
Y_0	static axial load factor for the bearing	-
W	non-dimensional load parameter	-
W_n	load per contact length unit	$N.m^{-1}$
z	number of rollers	-
$Z(x)$	profile height function	-
$Z(x,y)$	topography height function	-
$Z_{1,2}$	number of pinion or gear teeth	-
α	piezoviscosity coefficient	Pa^{-1}
α_n	normal pressure angle	rad
α_t	radial pressure angle	rad
α_{tec}	thermal expansion coefficient	$°C^{-1}$
β	thermoviscosity coefficient	K^{-1}
β_m	spiral angle	rad
γ	shaft angle	rad
$\delta_{1,2}$	pitch cone angle	rad
ϵ	load factor	-
η	dynamic viscosity	Pa.s
η_0	dynamic viscosity at the inlet contact temperature	Pa.s
η_{ref}	dynamic viscosity at p=0	Pa.s
θ	working temperature	°C
θ_{ref}	reference temperature	°C
κ	viscosity ratio	-
λ_c	cut-off length	mm
Λ	specific film thickness	-

μ_{bl}	coefficient of friction in boundary film conditions	-
μ_{EHL}	coefficient of friction in full film conditions	-
μ_{sl}	sliding friction coefficient	-
ν	kinematic viscosity	cSt
ν_1	rated kinematic viscosity	cSt
ρ	density	g.cm^{-3}
ρ_{ref}	reference density at 15 °C	g.cm^{-3}
σ	composite surface roughness	μm
τ	shear stress	Pa
$\upsilon_{1,2}$	Poisson's ratio for roller and race	-
ϕ_{bl}	weighting factor for the sliding friction coefficient	-
ϕ_{ish}	inlet shear heating reduction factor	-
ϕ_{rs}	kinematic replenishment/starvation reduction factor	-
ϕ_A	feeding conditions correction factor	-
ϕ_R	surfaces roughness correction factor	-
ϕ_T	heating correction factor	-
Φ_T	working function	-
ψ	contact angle	rad

List of Acronyms

ACBB	Angular Contact Ball Bearings
ACEA	Association des Constructeurs Européens d'Automobiles
AGMA	American Gear Manufacturers Association
API	American Petroleum Institute
ASTM	American Society for Testing and Materials
AWD	All Wheel Drive
BAC	Bearing Area Curve
COF	Coefficient of Friction
CPS	Count Per Second
CPUC	Wear Particle Concentration
DIN	Wear Particle Concentration
DIN	Deutsches Institut für Normung
DR	Direct Reading
EHD	Elastohydrodynamic
EHL	Elastohydrodynamic Lubrication
EPA	Environmental Protection Agency
ESCA	Electron Spectroscopy for Chemical Analysis
FWD	Front Wheel Drive
FWHM	Full Width at Half Maximum
ICP-AES	Inductively Couple Plasma - Atomic Emission Spectroscopy
ICP-OES	Inductively Couple Plasma - Optical Emission Spectroscopy
ISUC	Severity of Wear Particles
ISO	International Organization for Standardization
LW	Lower Part
PAO	poly-alpha-olefin oil nature
PLP	Percentage of Large Particle
RMS	Root Mean Square
ROI	Region of Interest

RSF	Relative Sensitivity Factor
RTB	Cylindrical Roller Thrust Bearing
RWD	Rear Wheel Drive
TWD	Two Wheel Drive
SAE	Society of Automotive Engineers
SUV's	Sports Utility Vehicles
TRB	Tapered Roller Bearing
UHV	Ultra High Vacuum
UP	Upper Part
VI	Viscosity Index
VSI	vertical scanning interferometry
XPS	X-ray Photoelectron Spectroscopy
4WD	Four Wheel Drive

Chapter 1

Introduction

The vehicles economical and environmental impact have been challenged the automotive industry to improve the efficiency on lubrication mechanisms, not only on increasing the vehicle fuel economy but also on extending the lifetime of the components.

87 % of the mechanical power loss are associated to frictional resistance where 13.2 % of this mechanical energy is lost on transmission and other parts of the driveline (see Figure 1.1), where are included the rolling bearings assembled on differential. The type of rolling bearing assembled and the differential operating conditions, such as temperature, loads and speeds, are parameters that determine the axle efficiency.

In the current work will be studied the performance of axle gear oils in terms of torque loss on tapered roller bearings used on a differential.

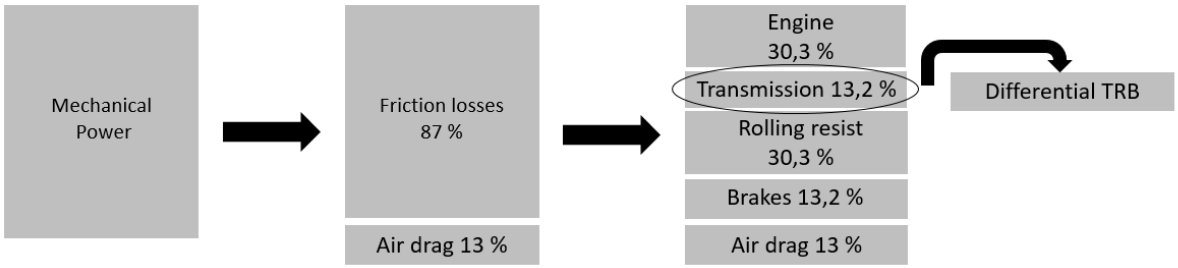

Figure 1.1: Sources of mechanical loss energy.

1.1 Objectives

The main objective of this work was to analyse the influence of different multigrade oil formulations, including three axle gear oils and two axle gear oil candidates (engine oils), on rolling bearing wear and friction torque losses.

The wear analysis was performed on cylindrical roller thrust bearings tested under extreme contact pressure and temperature conditions. The tribofilm formation was characterized.

Operating conditions of the tapered roller bearings used on a differential was studied and torque loss tests were performed under similar conditions.

The SKF torque loss model was calibrated using the experimental results. Reference values of boundary and full film coefficient of friction were obtained for each oil tested.

1.2 Document Structure

The present document has the following chapters:

Chapter 2 - Vehicle transmissions: A literature review was done, introducing different types of transmission configurations, types of differentials and its component parts, including gear types and rolling bearings. Also a brief introduction to differential lubricant requirements was made along with a physical and chemical characterization of five multigrade lubricants.

Chapter 3 - Rolling Bearings: Rolling bearing kinematics and roller-race contact pressure equations were described. A description of the available methods to predict the film thickness of the contact was done. SKF model was used as an engineering tool to quantify different torque loss sources on rolling bearings and also to calculate the coefficient of friction. The Hersey number and Stribeck curve concepts were introduced as a way to relate the coefficient of friction with the lubrication regime.

Chapter 4 - Tribofilms: A concise introduction of the surface protection layer tribofilm was done. Tests were performed to promote the tribofilm formation on cylindrical roller thrust bearing surfaces and evaluate the influence of lubricant formulation. Roughness measurements on rolling bearing races and XPS measurements on rollers were performed to check the lubricant effect on surface protection and tribofilm generation. Also direct reading and analytical ferrography analysis were executed on tested oils to evaluate and compare the amount of wear.

Chapter 5 - Torque Loss in Tapered Roller Bearings: A succinct description of the typical operating conditions on TRB presented in a light duty rear differential was done to define the laboratory operating conditions. Different tests on two different TRB were performed at different loads, temperatures and rotational speeds to evaluate the torque losses and coefficient of friction, for the five oils selected. It was also study the influence of the running-in period on the torque loss results. The reference values μ_{bl} and μ_{EHL} were determined for each lubricant and operating conditions to predict the TRB's total friction torque using the SKF model.

Chapter 6 - Conclusions and Future Work: The conclusions of the thesis were presented and possible future works were suggested.

Chapter 2

Lubricants for Vehicle Transmissions

The drivetrain is responsible to deliver the power produced by the engine to the driving wheels, under the form of rotation and torque. Several components are included in the automotive transmission system such as the clutch, gearbox, propeller shaft, differential and final drive shafts, as presented in Figure 2.1. The main objectives of transmission design are efficiency, higher torque capacity and reduced size [1] [2].

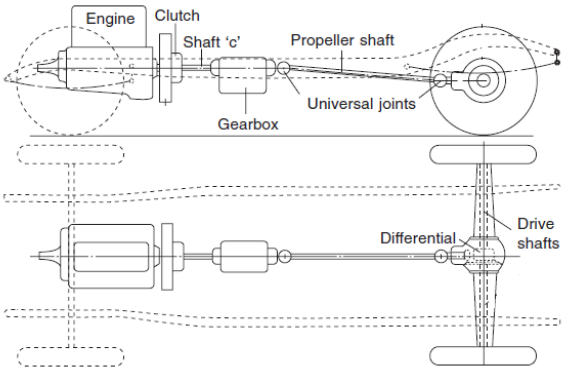

Figure 2.1: Components of transmission [1].

2.1 Transmissions Configurations

The location of the engine and the drive wheels depends on the type of the vehicle, so different configurations are possible. The engine could be located in the front, in the middle or in the rear, but currently it is found in the front for the most of the passenger vehicle, once brings an improve of weight distribution and this ensure better stability. On the other hand, the drivetrain configuration can be divided in two types: TWD (two-wheel drive) or AWD (all-wheel drive). The difference between these two types of arrangements is the number of sets of wheels that are responsible to transfer the engine power. On the TWD case, a single pair of wheels is responsible to transmit the power to the road, in the other hand on AWD case both pairs transfer the traction [3].

2.1.1 Two-Wheel Drive

The TWD configuration is the most common technology on passenger cars and is divided in two different layouts: FWD (front-wheel drive) and RWD (rear-wheel drive). As the name indicates, with FWD the power from the engine is delivered to the front wheels and with RWD the opposite occurs.

2.1.1.1 Front-Wheel Drive

This is the dominant type of drivetrain found in passenger vehicles with moderate engine power levels. Considering front engine location, the gearbox and differential are in a single unit. This disposition is often employed, because it is a compact arrangement, as presented in Figure 2.2(a), that frees up space inside the cabin [3].

The two biggest advantages of this layout are the good traction provided in slippery surfaces at low speed, because the weight of the engine and transmission components are located over the front wheels, and weight reduction, due to the absence of driveshaft, which offers better fuel economy and less carbon dioxide emissions. This arrangement have although some disadvantages related with weight transfer: under great linear accelerations or when the vehicle is climbing a slope the drive wheels could lose traction [4].

2.1.1.2 Rear-Wheel Drive

For this arrangement, in the majority of the cases, the engine, the clutch and the gearbox unit are in the front of the vehicle and separated from rear differential by the propeller shaft, as showed in Figure 2.2(b). This layout is generally used in sports car, since allows bigger engines in longitudinal disposition. However less cabin space is available due to the propeller shaft assembly along the vehicle and the rear differential. The main advantages reside in better handling obtained, due to the weight improvement distribution, and an increase of traction on drive wheels during a heavy linear acceleration. Thus this layout is less costly and it has easier maintenance since is mechanically simpler [4].

A major disadvantage lies on a less fuel efficiency vehicle, due to the weight increase associated to the propeller shaft and real differential power losses. Also, is more difficult to handling on low grip surfaces, such as wet road with ice or snow and gravel [4].

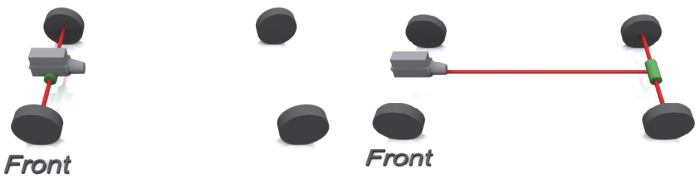

(a) FWD [4]. (b) RWD [4].

Figure 2.2: Two-Wheel Drive arrangements.

2.1.2 All-Wheel Drive

In AWD configuration, as the name indicates, all wheels are capable of deliver the engine power, once the two axles can be driven at the same time. It's usually seen on sport utility vehicles (SUVs) and trucks, although nowadays a few sedan, coupé and hatchback have this

drivetrain. There are two types of all-wheel drive configuration that limit how off road the vehicle are capable of, AWD or four-wheel drive (4WD) [4].

AWD arrangement could work permanently with two driving axles or only with one. When front and rear axles have open differentials, only a set of wheels has traction. Although, when the wheels begin to slip and spin, the other axle is activated and the car starts to function in AWD mode, through the use of a viscous coupling, as shown in Figure 2.3(a). When front, rear axles and viscous coupling are replaced by limited slip or TORSEN differentials, as shown in Figure 2.3(b), the engine torque is distributed permanently for both axles in 50%:50% or 33%:66% ratios. This technology has a huge growth in the last years, due to a more precise handling, similar self-steering properties under different weather conditions and an improved vehicle movement in slippery surfaces. However it has disadvantages associated to greater technical complexity, higher costly maintenance and increased weight related to two added differentials and consequently less fuel efficiency [3].

4WD layout typically has a transfer box between the gearbox and the rear axle, showed in Figure 2.3(c), and one open differential in each axle. Normally it works in TWD mode. The function of transfer box is to split the drive from the main gearbox to both front and rear axles. In the most of cases it has some sort of selectable internal differential or viscous coupling to allow front and rear drives turn at different speeds if needed. This layout is commonly use in trucks an off road vehicles [1].

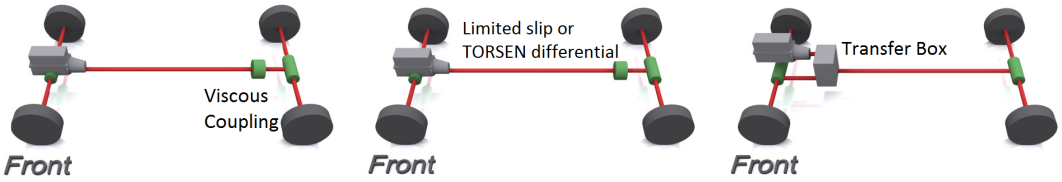

(a) Non-Permanent AWD [4]. (b) Permanent AWD [4]. (c) 4WD [4].

Figure 2.3: All-Wheel Drive arrangements.

2.2 The Differential

The differential is a mechanical device that allows two wheels on the same axle turn at different rates, divides the torque input between two driveshafts and also acts as the final gear reduction in the driveline [1].

As part of drivetrain, the differential is assembled on a live axle. If the vehicle has FWD or RWD layout only one differential is needed, however when has AWD or 4WD arrangement, it's necessary frequently three differentials, one between the gearbox output and the two live axles and one in each axle. This allow the entire front and rear axles to spin at different speeds to each other [3].

2.2.1 Differential Types

As mentioned in previous section different types of differentials are used. Due to the multiplicity of production designs, in the next section will be introduced four types of axle differentials: open, self-locking and locking differentials.

2.2.1.1 Open Differentials

Open differentials, shown in Figure 2.4, are the most common type and they supply the same torque at each shaft output. The input pinion gear 1 is the one that is driven from the drivetrain. The ring gear is driven by the pinion and its greater diameter is what gives that final gear reduction. Attached to the ring gear is the differential cage 2, that contained two captive bevel pinions 3 by the differential shaft 5, that it must rotate with the cage, but it's free to spin on is own axis. The torque applied through the pinion gear axle drive is transmitted through the differential cage and the differential shaft to the differential bevel pinions and from there to the axle bevel gears 4 which are torsionally locked to the axle shafts 6 [3].

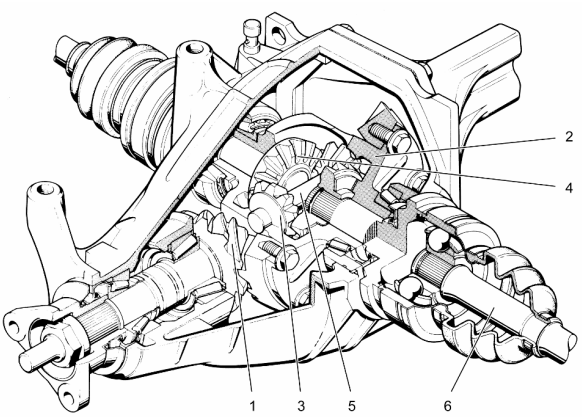

Figure 2.4: Open differential [3].

When the car moves in a straight line, the wheels rotate at the same speed as the differential cage and the differential pinions are stopped. On the other hand, when the vehicle is turning, the differential pinions rotates on is own axis and the differential cage rotates with different velocity than the bevel output gears.

This type of differential has one major drawback. When one wheel is in contact with a slippery surface, this differential will send the majority of the power to the slippery wheel and the vehicle won't be able to move [3].

2.2.1.2 Self-Locking Differentials

Also known as limited-slip differential, these are differentials with a compensating action that is deliberately restricted. These differentials are designed to overcome the scenario outlined in previous section and enables the torque transmission to one wheel even when the other wheel is spinning. However, when the both wheels of the axle need to rotate at different speeds due to a corner, the adaptation is slightly restricted [3].

- Multi-Plate Clutches

Typically the multi-plate clutches differential is the most used in passenger vehicle that use self-locking differentials. It has the same construction scheme of an open differential, but it has two additional components, spring pressure plates and clutch packs, as shown in Figure 2.5(a). The steel plates and the friction material are packed between the output bevel

gear and the differential cage and locked with the gear, known as clutch pack. The spring nestled in the cage, between the two output pinions, push the output bevel gears and pressure the steel plates to the wall of the differential case. Thus, the spring will always give a thrust force, so the clutch is always going to try to behave as if the car was moving in a straight line by attempting to make both output gears spin at the same speed as the ring gear and cage [3] [1].

- Worm Gears - TORSEN Diferentials

The internal components of a self-locking worm gears differential are different of a bevel gear differential. Instead bevel differential gear and bevel output gear it has worm wheels, worm gears and spur gears, as shown in Figure 2.5(b).

As in an open and self-locking differential, the driving ring gear 1 is attached to the differential cage 2 and the power is transferred to six worm wheels 3 that are contained in the differential cage by the differential shafts. Each end of the worm wheel 3 has a spur gear 4, that are engaged with the spur gear toothing of neighbouring worm gear. Considering half of the mechanism, the worm gear 5 is torsionally locked to the axle output shaft 6 and engaged with three worm wheel 3, that won't be able to spin the worm gear 5 [3].

When the vehicle moves straight ahead, the worm wheels that don't spin on is owned axes, will push and turn the worm gears and both output shafts will rotate at the same speed. When this happen the entire mechanism moves as a single unit [5].

When the vehicle is turning, the output shafts has different speeds and the worm gear, that rotates faster, will force the corresponding worm wheels spin on is own axes. On the other half of the mechanism, the worm wheels spin on the opposite direction and the spur gears will make sure that the two sided worm wheels will spin at same speed [3] [5].

When one wheel is in contact with a slippery surface the speed change is transferred to the corresponding worm wheels. Thus, the worm wheels form the one half of the mechanism deliver the speed difference to the others worm wheels, since they were connected through spur gears. As mentioned above, the worm wheels won't be able to turn the corresponding worm gear and the entire mechanism will turn as block [1] [3] [5]. Nowadays this differentials are rarely used.

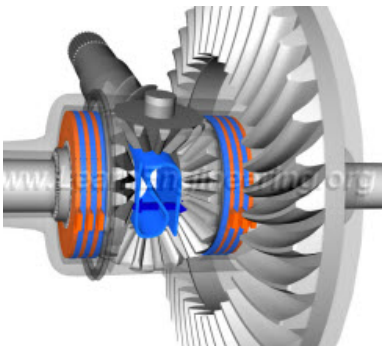

(a) Multi-plates clutches [6].

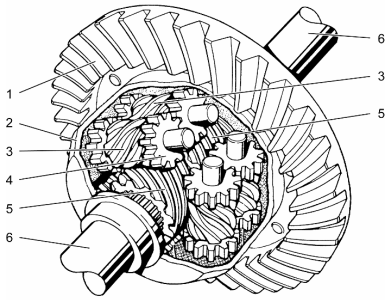

(b) Worm gears - TORSEN [3].

Figure 2.5: Self-locking differentials.

2.2.1.3 Locking Differentials

A locking differential has the same constructive base of an open differential. However, it has an actuation system, electronic, pneumatic or hydraulic, that locks the two output gear together as if they were a solid axle, as shown in Figure 2.6.

It was design to overcome the limitation of a standard open differential, because it transfer the torque transmission to one wheel, when the other loses grip or suspended. In this scenario a locking differential deliver 100 % of torque to wheel in contact with the surface, forcing both wheels rotate at same speed [5].

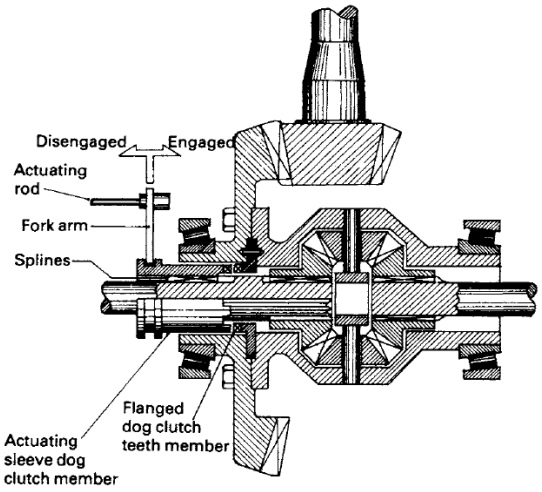

Figure 2.6: Lock differential [5].

2.2.2 Differential Parts

In the below section will be presented the main components of a differential, such as the different types of gears and the bearings typically used.

2.2.2.1 Gearing Mechanisms

As stated in previous section, spur gears, bevel gears and worm gears can be seen in a differential, depending on its disposition in powertrain and type.

In the most of the cases, spur gear are used in a front engine vehicle with a FWD layout [3].

Bevel gears and hypoid gears are apply in the majority of RWD and AWD vehicles, due to a longitudinal disposition of the engine. Commonly they are used in open, locking and self-locking differentials with multi-plate clutches. Hypoid gears are used on the input pinion and the ring gear, and bevel are used in gears inside differential cage between the differential pinions and the output gears [3].

Worm gears are employed in TORSEN differentials, between the gears inside the differential cage and the output worm gears [3].

In Figure 2.7 are disposed the types of gears presented in differentials.

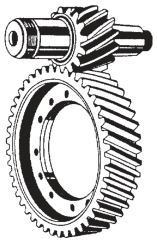

(a) Helical spur gears [7].

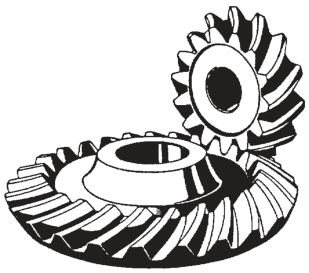

(b) Bevel gears [7].

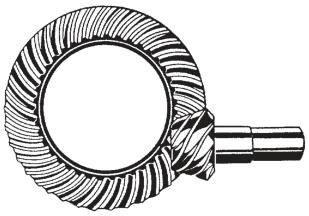

(c) Hypoid gears [7].

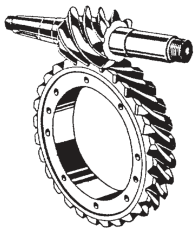

(d) Worm gears [7].

Figure 2.7: Types of gears assembled in differentials.

2.2.2.2 Rolling Bearings

Depending on the axle design, subjected loads, gear contact loads, vehicle weight and operating lifetime different bearings are available to implement. The assembly space onto the shaft can be a decisive factor for bearing selection. Considering the differential as a separated final drive unit, a set of four bearings are applied. Two bearings assembled on the pinion input shaft and the others on the output shafts to support the differential cage. Once thrust and radial loads are transmitted by the gear meshing to supports, tapered roller bearing (TRB) or double-row angular contact ball bearings (ACBB) are required, showed in Figure 2.8(a) and 2.8(b), respetively [8].

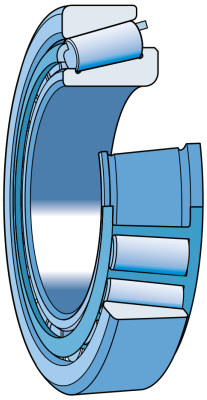

(a) Tapered roller bearing [9].

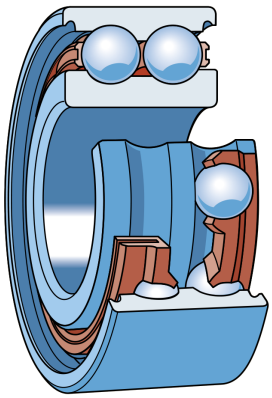

(b) Double row angular contact ball bearing [9].

Figure 2.8: Types of bearings assembled in differentials.

2.3 Differential Lubrication

The effort of automotive manufacturers to improve fuel efficiency in vehicles is inevitably dependent on gear axles performance which is one of the sources of power loss in driveline. Smaller gear axles with lower gear ratios has been constructed to acquire this goal, although this design modifications, associated to higher torque engines, lead to an increase of operating temperature. Operation parameters (load, speed and temperature), gear and bearing design (metallurgy and surface condition) and lubricant parameters (viscosity and composition) are the key variables that can be changed to improve axle gear efficiency [2] [10].

In lubrication perspective, it is possible reduce the energy axle losses and extend its operating lifetime by improving the lubricant formulation. Thus, a proper lubricant ensures a suitable lubrication regime, both in gears and bearings, which prevents high wear rates, while assures a convenient heat evacuation [8] [10]. Furthermore, the lubricant provides adequate protection against oxidation, rust, corrosion and foaming by protecting the mating surfaces [8]. The hypoid gears, are the most difficult lubricant applications. The high rate of sliding between the gear teeth tends to wipe lubricant films from the tooth surfaces. Thus, as the offset between the shaft centre lines is increased the amount of sliding in proportion to rolling increases, exacerbating the problem [11].

2.3.1 Lubricant Requirements

Depending on gear design and geometries, contacts, loads, speeds and kinematics different gear lubricants are required. To assure that a lubricant is capable of ensure a proper axle gear lubrication it must be subjected to different tests, settled for professional entities, according to the gear type mechanism. American Society for Testing Materials (ASTM) is one of this entities which define the tests on lubricants, as shown in Figure 2.9 [12].

Test	Description	Characteristics measured
ASTM L-33	Gear test using differential assembly	Resistance to corrosion in presence of moisture
ASTM D 6121	Gear test using complete axle assembly	Resistance to gear distress under low-speed, high-torque conditions
ASTM L-42	Gear test using complete axle assembly	Resistance to gear distress (scoring) under high-speed, shock-load conditions
ASTM L-60	Bench test using spur gears	Oxidative stability
ASTM D 5704	Bench test using spur gears	Thermal and oxidative stability and deposits
ASTM D 5662	Bench test	Seal compatibility
ASTM D 5579	Gear test	Transmission cyclic durability (waived for approved lubricants)
ASTM D 5182	Gear test	Spur gear wear
ASTM D 130	Bench test	Stability in the presence of copper and copper alloys
ASTM D 892	Bench test	Foaming tendencies

Figure 2.9: ASTM oil tests: Measured characteristics in different gears and assemblies [12].

According to the variables mentioned in the paragraph above, to facilitate a proper lubricant selection, two current oil lubricant specifications are followed by the automotive industry: viscosity and service [12] [13].

2.3.1.1 Viscosity Specifications

Gear oil viscosity is the most important parameter that controls the fluid film thickness. Viscosity is characterized by fluid resistance to shear deformation and are dependent on temperature, shear rate and pressure. The relationship between the oil temperature and viscosity is an important parameter and quite problematic for axle efficiency. When the operating temperature is high the viscosity is low and if it's below a limit, it will cause higher wear or even damages on surfaces contact. On the other hand higher viscosity lubricant can be used to provide the necessary protection, however it will promote higher power losses [8] [10]. To overcome this problem, multigrade gear oils has been progressively adopted, since they can maintain the film-forming characteristics for a greater range of temperatures, due to a higher Viscosity Index (VI) obtained by high VI synthetic base oils or with polymeric additives also known as VI improvers. This additives must be selected with caution, since under severe gear mechanical shearing, polymeric degradation may occurs causing viscosity drop, resulting in lower lubricant film thickness and eventually equipment failure [12].

Mineral base or fully synthetic base oil are currently used in differential. However, a fully synthetic oil have unique physical and chemical properties compared to mineral lubricant [8].

Multigrade automotive gear oils are composed also by pour point depressant (used in mineral oils) and performance packages, which are included antiwear and extreme pressure additives, oxidation, corrosion and foam inhibitors and friction modifiers. The use of additives and base oils that complement each other it is imperative to ensure a convenient lubrication [10] [12].

- Viscosity Classification

Depending on the professional entity, such as Society of Automotive Engineers (SAE) , International Standard Organization (ISO), American Gear Manufacturers Association (AGMA) and American Society for Testing and Materials (ASTM) several widely oil viscosities classifications are used [13]. The multigrade oil designation is given by SAE, which is the most commonly classification used in automotive industry for power transmissions SAE J306 and combustion engines SAE J300, shown in Figure 2.10 and Figure 2.11, respectively.

SAE viscosity grade	Max. temp. for viscosity of 150 000 cP [°C]	Kinematic viscosity [cS] at 100°C	
		min	max
70W	-55	4.1	-
75W	-40	4.1	-
80W	-26	7.0	-
85W	-12	11.0	-
90	-	13.5	< 24.0
140	-	24.0	< 41.0
250	-	41.0	-

Figure 2.10: SAE classification: SAE J306 power transmissions oils [14].

SAE viscosity grade	Viscosity [cP] at temp [°C] max		Kinematic viscosity [cS] at 100°C	
	Cranking	Pumping	min	max
0W	3 250 at -30	30 000 at -35	3.8	-
5W	3 500 at -25	30 000 at -30	3.8	-
10W	3 500 at -20	30 000 at -25	4.1	-
15W	3 500 at -15	30 000 at -20	5.6	-
20W	4 500 at -10	30 000 at -15	5.6	-
25W	6 000 at -5	30 000 at -10	9.3	-
20	-	-	5.6	< 9.3
30	-	-	9.3	< 12.5
40	-	-	12.5	< 16.3
50	-	-	16.3	< 21.9
60	-	-	21.9	< 26.1

Figure 2.11: SAE classification: SAE J300 engine oils [14].

Multigrade oils designation include a "W", meaning winter, in the middle of two numbers, representing a SAE grade. The number on the left is directly related with the lubricant properties in cold conditions. The right number is related with the kinematic viscosity properties at 100 °C [14].

Though this chapter is related with differential lubrication, for the purpose of this work, was introduced the SAE classification for engine oils and a summary description was made, since comparison tests were performed for both oil types.

As showed in Figures above, power transmission oils have higher classification numbers than engine oils. This difference was adopted to facilitate the oil recognition and has nothing to do with the oil viscosity, as shown in Figure 2.12.

2.3.1.2 Service Specifications

Along with the viscosity requirements, axle gear oils are also classified according to its properties specifications for a defined application. American Petroleum Institute (API) and Association des Constucteurs Européens d'Automobiles (ACEA) are the two most used lubricant service classifications. However, ACEA specifications are restricted to gasoline and diesel light duty engine oils, A and B class respectively, catalyst compatible engine oils, C class, and heavy duty diesel engine oils, E class, and does not include gear oils classifications [13] [15]
.

The API created service designations for gear oils based on specific applications which involves different gear designs, operating conditions and the chemical and physical characteristics of the lubricant. Each designation is associated to a gear lubricant required performance for a specific type of automotive service, and are presented in Table 2.1 [16].

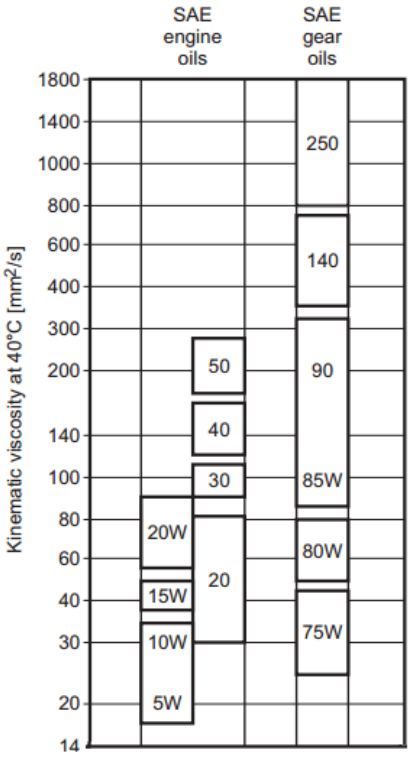

Figure 2.12: SAE classification: Viscosity comparison (adapted from [7]).

Table 2.1: API oil classification for power transmissions [16].

API service designation	Description	Status
GL-1	Lubricants for manual transmissions operating under such mild conditions that straight petroleum or refined petroleum oil may be used satisfactorily. Oxidation and rust inhibitors, defoamers, and pour depressants may be added to improve the characteristics of these lubricants. Friction modifiers and extreme pressure additives shall not be used.	Active
GL-2	Lubricants for automotive worm-gear axles operating under such conditions of load, temperature, and sliding velocities that lubricants satisfactory for API GL-1 service will not suffice.	Inactive
GL-3	Lubricants for manual transmissions operating under moderate to severe conditions and spiral-bevel axles operating under mild to moderate conditions of speed and load. These service conditions require a lubricant having load-carrying capacities exceeding those satisfying API GL-1 service but below the requirements of lubricants satisfying API GL-4 service.	Inactive
GL-4	Lubricants for axles with spiral bevel gears operating under moderate to severe conditions of speed and load or axles with hypoid gears operating under moderate speeds and loads. These oils may be used in selected manual transmission and transaxle applications where MT-1 lubricants are unsuitable.	Active
GL-5	Lubricants for gears, particularly hypoid gears, in axles operating under various combinations of high-speed/shock load and low-speed/high-torque conditions.	Active
GL-6	Lubricants for gears designed with a very high pinion offset. Such designs typically require protection from gear scoring in excess of that provided by API GL-5 gear oils.	Inactive
MT-1	Lubricants for non-synchronized manual transmissions used in buses and heavy-duty trucks. Lubricants meeting the requirements of API MT-1 service provide protection against the combination of thermal degradation, component wear, and oil-seal deterioration, which is not provided by lubricants in current use meeting only the requirements of API GL-1, 4, or 5.	Active

2.3.2 Lubricant Selection and Characterization

In this study five multigrade oils were used, all of them previously selected and characterized from a parallel work [17]. Three oils have applications in gearboxes and axles: TOTAL SYN FE 75W-90 (75W90), ELF SYN FE 75W-140 (75W140) and TOTAL RS FE 80W-90 (80W90); and the other two are suitable for both gasoline and diesel engines TOTAL QUARTZ INEO LONG LIFE 5W30 (5W30) and TOTAL QUARTZ RACING 10W50 (10W50). The first two gear oils and both engine oils have a synthetic base, and the 80W90 oil is mineral.

The gear oils 75W90 and 80W90 are classified according to API GL-4 and/or GL-5 and/or MT-1 standards and 75W-140 oil has de designation GL-5. Both 5W30 and 10W50 oils are not classified according to API power transmissions service specifications. The detailed information of lubricants provided by the manufacturers, can be found in the Appendix A, and the oil properties were compiled in the Table 2.2.

Table 2.2: Oil properties provided by the manufacturers.

Parameter	Unit	Standard	75W90 (PAO)	75W140 (PAO)	80W90 (MIN)	5W30 (PAO)	10W50 (PAO)
Density @ 15°C	[g/cm^3]	ASTM D4052	0.866	0.885	0.886	-	0.856
Viscosity @ 40°C	[cSt]	ASTM D445	101	183	115	67.5	115
Viscosity @ 100°C	[cSt]	ASTM D445	15	26.3	14.1	11.7	17.0
Viscosity Index	[-]	ASTM D2270	157	178	123	169	164
Pour Point	[°C]	ASTM D97	-51	-36	-33	-39	-45

To validate the manufacturers information, test analysis were made for each oil. To confirm the physical properties, viscosity measurements using a Engler's viscometer and density measurements using a densimeter were performed. Also a chemical characterization was made to measure the concentration of chemical elements on lubricant.

2.3.2.1 Engler Viscometry

Thermoviscosity characterizes the variation of the lubricants viscosity with temperature. For mineral and synthetic oils the viscosity decreases with temperature. An Engler's viscometer, presented in Figure 2.13, was used to measure the lubricant's viscosity. [13].

The Engler's viscometer consist in a cup with a small hole in the centre of the base which can be blocked by a wood stopper. The cup is surrounded by an oil bath fitted with a stirring device. The oil bath is heated by an electrical resistance and the temperature of the oil sample increase by heat transfer. Both oil sample and bath oil temperatures are controlled by two thermometers. A receiving goblet with 200 ml of capacity was centred below the container. When the desired temperature of the sample is achieved, the hole in the base of the cup is unblocked. The time taken to fill the 200 ml goblet was recorded according to IP 212/92 Standard [18].

The ratio between the time taken by the oil to fall through the hole (t) and the time taken by the water (t_{ref}) gives the degrees Engler, as shown in equation (2.1). The flow time of the water (t_{ref}), is 49.3 seconds at 20 °C.

$$^{\circ}Engler = \frac{t}{t_{ref}} \tag{2.1}$$

Figure 2.13: Engler's viscometer.

To convert Engler degrees to centiStokes (cSt) the equation (2.2) was used.

$$\nu = k_1 \cdot^{\circ} Engler + \frac{k_2}{^{\circ}Engler + k_3} \tag{2.2}$$

where k_1, k_2 and k_3 are parameters that depend on °Engler, and are defined in Table 2.3.

Table 2.3: Parameters (k_1, k_2 and k_3) value dependent on ° Engler.

	k_1	k_2	k_3
$^{\circ}Engler < 3$	14.867	75.568	-6.198
$^{\circ}Engler \geq 3$	7.624	-2.717	-1.522

In order to represent the variation of the viscosity with the temperature, it is necessary to apply a variation law to the experimental results. Vogel's law or ASTM standard can be used. In the case of this study the ASTM D341 [19] was used, but both laws have a similar behaviour and represent quite well the viscosity variation. Furthermore, in equation (2.3), ASTM law at 40, 70 and 100 °C is defined and for all oils $a_i = 0.7$ was assumed and it is possible to calculate the m_i and n_i constants.

$$\log\log(\nu + a_i) = n_i - m_i \cdot \log(T) \tag{2.3}$$

For all oils three measurements were taken, as showed in Table 2.4 and converted to cSt, Table 2.5. The ASTM D341 standard was used to calculate the oils constants (m_i and n_i). The viscosity variation with the temperature is presented in Figure 2.14.

The ASTM D341 constants (a_i, m_i and n_i) and the oil kinematic viscosity (ν), are useful to determine the thermoviscosity (β), given by the equation (2.4).

$$\beta = \frac{m_i \cdot (\nu + a_i)\ln(\nu + a_i)}{T \cdot \nu} \tag{2.4}$$

Table 2.4: Viscosity (ν) for the selected tested oils in °Engler.

	75W90 (PAO)	75W140 (PAO)	80W90 (MIN)	5W30 (PAO)	10W50 (PAO)
40 °C	15.27	27.25	16.76	9.00	15.25
70 °C	5.23	8.60	4.94	3.46	5.22
100 °C	2.63	3.73	2.33	2.04	2.64

Table 2.5: Viscosity (ν) for the five oils tested oils in cSt.

	75W90 (PAO)	75W140 (PAO)	80W90 (MIN)	5W30 (PAO)	10W50 (PAO)
40 °C	116.24	207.63	127.57	68.25	118.38
70 °C	39.17	65.15	36.87	24.91	39.10
100 °C	17.94	27.22	15.15	12.16	17.98

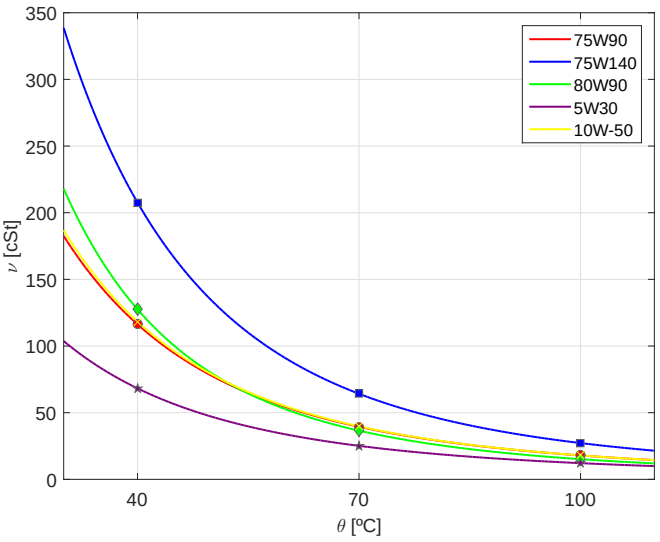

Figure 2.14: Viscosity (ν) variation with temperature (θ) for selected oils.

2.3.2.2 Viscosity Index

The VI, which a graphical representation is presented in Figure 2.15, is a dimensionless parameter to classify the change of viscosity between a temperature interval, 40 and 100 °C. *Dean and Davis* [20] proposed equation (2.5) to calculate the VI.

$$VI = 100 \cdot \left(\frac{L_{VI} - U_{VI}}{L_{VI} - H_{VI}} \right) \tag{2.5}$$

According to ASTM D2270 [18], for oils which the VI is higher than 100, the equation must be adapted as given by equations (2.6) and (2.7).

$$VI = \left(\frac{10^{N_{VI}} - 1}{0.00715} \right) + 100 \tag{2.6}$$

$$N_{VI} = \left(\frac{\log(H_{VI}) - \log U_{VI}}{\log(Y_{VI})} \right) \tag{2.7}$$

Where H_{VI} is the kinematic viscosity at 40 °C of an oil with a VI of 100, having the same kinematic viscosity at 100 °C as the oil whose viscosity index is to be calculated, L_{VI} is the kinematic viscosity at 40 °C of an oil of 0 VI having the same kinematic viscosity at 100 °C as the oil whose VI is to be calculated, U_{VI} is the kinematic viscosity at 40 °C of the oil whose viscosity index is to be calculated and Y_{VI} is the kinematic viscosity at 100 °C of the oil whose VI is to be calculated.

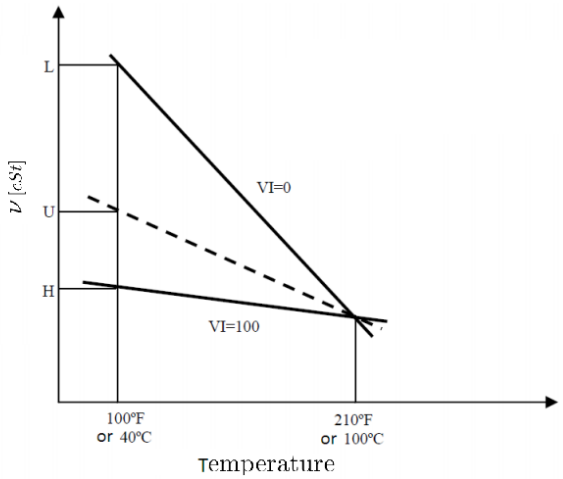

Figure 2.15: VI graphical representation. [13].

From all oils, the 75W140 has the highest viscosity at any temperature and also the highest VI. On the opposite, the 5W30 has the lowest viscosity values, but presents the second highest VI, as shown in Table 2.6, revealing a lower viscosity variation with temperature. At 40 °C and 100 °C 75W90 and 10W50 oils have similar viscosity and VI values. In comparison with 75W90 and 10W50 oils, 80W90 has higher viscosity value at 40 °C and lower at 100 °C, resulting in biggest viscosity variation due to the lowest VI, since is a mineral base oil.

Table 2.6: Kinematic viscosity (ν) at 40, 70 and 100 °C, ASTM constants (a_i, m_i and n_i), thermoviscosity (β) at 40, 70 and 100 °C, and Viscosity Index for selected oils.

Parameter	Unit	Standard	75W90 (PAO)	75W140 (PAO)	80W90 (MIN)	5W30 (PAO)	10W50 (PAO)
Viscosity @ 40°C	[cSt]	ASTM D341	116.2 (101)	207.6 (183)	127.6 (115)	68.3 (67.5)	118.4 (115,0)
Viscosity @ 70°C	[cSt]	ASTM D341	39.2	65.2	36.9	24.9	39.1
Viscosity @ 100°C	[cSt]	ASTM D341	17.9 (15)	27.2 (26.3)	15.1 (14.1)	12.2 (11.7)	18.0 (17,0)
a_i	[-]	ASTM D341			0.7		
m_i	[-]	ASTM D341	2.778	2.695	3.215	2.882	2.795
n_i	[-]	ASTM D341	7.249	7.093	8.348	7.457	7.293
Thermoviscosity @ 40°C ($\beta * 10^3$)	[K^{-1}]	ASTM D341	42.5	46.1	50.1	39.4	42.9
Thermoviscosity @ 70°C ($\beta * 10^3$)	[K^{-1}]	ASTM D341	30.4	33.2	34.6	28.0	30.5
Thermoviscosity @ 100°C ($\beta * 10^3$)	[K^{-1}]	ASTM D341	22.6	24.7	24.9	20.9	22.8
Viscosity Index	[-]	ASTM D2270	162 (157)	169 (178)	122 (123)	166 (169)	162 (164)

in Table 2.6, the manufacturer oil properties values are presented between brackets.

2.3.2.3 Piezoviscosity

The variation of the lubricant viscosity with pressure is characterized by its piezoviscosity. In elastohydrodynamic lubrication (EHL), where the lubricant pressure is between 0.5 and 4 GPa, the increase in viscosity is considerable and it is more important on naphthenic mineral oils than paraffin. For gears and rolling bearings, the piezoviscosity effect is important to characterize the lubricant film thickness [13].

The exponential relationship between pressure and viscosity is given by equation (2.8), proposed by *Barus* in 1983 [21].

$$\eta = \eta_{ref} \cdot \exp^{\alpha \cdot p} \tag{2.8}$$

where η is the dynamic viscosity at pressure p, η_{ref} is the dynamic viscosity at atmospheric pressure and α is the piezoviscosity coefficient dependent on temperature and pressure independent.

Knowing the temperature at the inlet of the contact and consequently the lubricant kinematic viscosity, it is possible to determine the piezoviscosity coefficient through *Gold's law*, equation (2.9), valid for a pressure of 0.2 GPa (common on inlet contact conditions).

$$\alpha = s_{Gold} \cdot \nu^{t_{Gold}} \cdot 10^{-9} \tag{2.9}$$

where s_{Gold} and t_{Gold} are *Gold's* constants, presented in Table 2.7 and dependent on the base oil of the lubricant (mineral, polialphaolefin, ester,...).

Table 2.7: Gold's (s_{Gold} and t_{Gold}) constants for selected oils at 0.2 GPa.

Parameter	75W90 (PAO)	75W140 (PAO)	80W90 (MIN)	5W30 (PAO)	10W50 (PAO)
s_{Gold}	7.382	7.382	9.904	7.382	7.382
t_{Gold}	0.1335	0.1335	0.139	0.1335	0.1335

In Table 2.8 is shown the piezoviscosity values at 40, 70 and 100 °C for the selected axle gear oils. The 80W90 oil presents the highest piezoviscosity values for all temperatures and the 5W30 oil presents the lowest values.

Table 2.8: Piezoviscosity (α) for selected oils.

Parameter	Unit	Standard	75W90 (PAO)	75W140 (PAO)	80W90 (MIN)	5W30 (PAO)	10W50 (PAO)
Piezoviscosity @ 40°C ($\alpha \times 10^{-8}$)	[Pa^{-1}]	/	1.3928	1.5050	1.9432	1.2973	1.3962
Piezoviscosity @ 70°C ($\alpha \times 10^{-8}$)	[Pa^{-1}]	/	1.2057	1.2867	1.6332	1.1353	1.2070
Piezoviscosity @ 100°C ($\alpha \times 10^{-8}$)	[Pa^{-1}]	/	1.0853	1.1474	1.4451	1.0304	1.0856

2.3.2.4 Density

The density is a fluid's property that varies its value with the temperature and pressure. When the pressure increases the fluid volume decreases and the density increases. When the temperature increases, in the case of the lubricants, the density decreases. The oils density tests were performed in order to understand their variation with temperature.

The reference density (ρ_{ref}) was considered at 15 °C, which is the reference temperature (T_{ref}) and the values are presented in Table 2.9.

Table 2.9: Density (ρ) at 15 °C and thermal expansion coefficient (α_{tec}) for selected oils.

Parameter	Unit	Standard	75W90 (PAO)	75W140 (PAO)	80W90 (MIN)	5W30 (PAO)	10W50 (PAO)
Density @ 15°C	[g/cm^3]	/	0.870 (0.866)	0.885 (0.885)	0.886 (0.886)	0.853 (-)	0.861 (0.856)
Thermal Expansion Coefficient $\times 10^4$	[-]	/	−7.2	−6.6	−7.6	−8.4	−7.6

The measurements were performed at three different temperatures with a densimeter,

Anton Paar presented in Figure 2.16. Due to a limitation of the equipment, it is only possible make reliable tests when the specimen temperature is below 40 °C [22].

Figure 2.16: Anton Paar densimeter.

The values measured are shown in Figure 2.17. These values were used to evaluate the thermal expansion coefficient (α_{tec}), according to equation 2.10.

$$\rho = \rho_{ref} \cdot (1 - \alpha_{tec} \cdot (T_{ref} - T)) \tag{2.10}$$

Where the ρ represents the density in at a temperature (T).

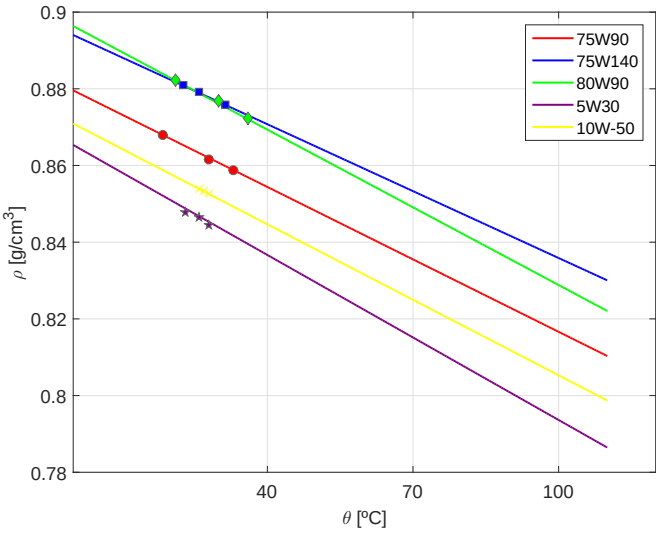

Figure 2.17: Density (ρ) variation with temperature (θ) for selected oils.

The 5W30 oil has the lower density to all range of temperatures. On the other hand, at 15 °C, 75W140 oil has lower density than the 80W90 oil, but the smallest density variation and the smallest volume variation with temperature, since the thermal expansion coefficient is smaller than all other oils, as presented in Table 2.9. Furthermore, at temperatures above 30 °C, 75W140 oil had the highest density.

2.3.2.5 Chemical Characterization - Inductively Coupled Plasma Atomic Emission Spectroscopy

Inductively coupled plasma atomic emission spectroscopy (ICP-AES), also known as inductively coupled plasma optical emission spectroscopy (ICP-OES) is a technique often used in oil chemical analysis. By ionization in an intense electromagnetic filed, it produces exited ions and atoms that emit detectable amounts of light at characteristic wavelengths, with intensities proportional to the concentration of the ion, and an atomic emission spectrometer (AES), measured and analysed the produced spectra [23].

ICP-AES is widely used method to measure the concentration or the presence of additive elements or the wear metals in the oil sample [24]. The technique was applied to all new selected oils, revealing the presence and the concentration of the chemical elements presented Table 2.10.

Table 2.10: Chemical composition for selected oils.

Chemical Composition	Units	75W90 (PAO)	75W140 (PAO)	80W90 (MIN)	5W30 (PAO)	10W50 (PAO)
Boron (B)	[ppm]	-	-	-	0	81
Barium (Ba)	[ppm]	<5	<5	<5	0	0
Calcium (Ca)	[ppm]	18	33	97	1795	2891
Magnesium (Mg)	[ppm]	1087	1093	936	6	17
Sodium (Na)	[ppm]	5	<5	<5	0	0
Phosphorus (P)	[ppm]	1622	1686	1436	783	958
Silicon (Si)	[ppm]	-	-	-	4	5
Tin (Sn)	[ppm]	8	8	7	0	0
Zinc (Zn)	[ppm]	7	12	23	899	1120

For the oils which have applications on gearboxes and axles (75W90, 75W140 and 80W90), it is seen higher concentrations of magnesium and phosphorus. Magnesium is used as a detergent additive which has the ability to suspend undesirable product from thermal and oxidative degradation. By its side phosphorus, presents a good performance as an oxidation inhibitor and as an anti-wear and extreme pressure additive. On the other hand, calcium, sodium and barium also used as detergent additives have residual concentration in these oils [25].

In 5W30 and 10W50 oils three elements are presented in higher concentrations: calcium, phosphorus and zinc. The calcium and phosphorus concentration is explained by the presence of detergents and EP/AW additives, respectively. Zinc is also used in oil as antiwear, extreme pressure and antioxidant agent. In 10W50 oil, a small concentration of boron is seen due to its friction modification property [25].

Chapter 3

Rolling Bearings

3.1 Lubrication in Rolling Bearings

Lubrication has the purpose to separate two nearby surfaces in relative motion with a film of intervening material. The lubrication mechanisms in conformal contacts, such as those encountered in hydrodynamic and hydrostatic bearings, are well described and defined and the reasons for their effectiveness are well understood. However, in highly loaded non-conformal contacts, such as those found in gears, cams and rolling bearings, the hydrodynamic lubrication mechanism isn't capable of give a suitable explanation. The wear rates of these components are very low and implies the existence of films thick enough to separate the contacting surfaces, that is inconsistent to the calculated values of hydrodynamic film thickness for such type of contacts [14, 26].

EHL is a form of hydrodynamic lubrication that considers the effect of elastic surfaces deformation and it is concerned with the fluid film formation and its thickness. The lubricant is entrained to the interior of the contact, where a layer is formed, due to the kinematics and geometry of bodies. High pressures are developed, since the surfaces are non-conformal and the contact areas are very small. In the case of rolling bearings these surfaces are the contact areas between the rolling elements and the raceways. As consequence, the lubricant is capable of significantly increase its viscosity and elastically deform those contacting surfaces [14].

In addition to film thickness and effective lubrication explanation, the understanding of EHL mechanism allows to interpret the complete spectrum of lubrication regimes, ranging from boundary to hydrodynamic [26, 27].

In the next sections bearings geometry and kinematics, contact pressure distribution, film thickness prediction, lubrication regimes, viscosity ratio and Stribeck diagram will be described.

3.1.1 Bearing Geometry and Kinematics

The relative motions of bearing components are crucial to evaluate their performance. Kinematic analysis determines the rolling and sliding contact speeds as well as spin angular velocity of raceways, required for lubricant film thickness calculation and subsequent bearing torque and temperature analysis [28].

For both cylindrical roller thrust bearing (RTB) and tapered roller bearings (TRB), the required geometrical dimensions for next calculations, which are unavailable in SKF catalogue, were established with resource of SKF CAD models and the SOLIDWORKS software.

3.1.1.1 Cylindrical Roller Thrust Bearings

A typical RTB is comprised of a pair of parallel thrust plates. A row of cylindrical rollers sits between the thrust plates and a cage retaining the rollers. Cylindrical roller thrust bearings experience a large amount of sliding as a result of the spin motion between the rollers and raceways. For this reason, cylindrical roller thrust bearings are limited to slow-speed applications.

Observing the Figure 3.1, the contact race velocity (U_{2c}) at the middle of the contact length $\left(\frac{l}{2}\right)$, is given by equation (3.1).

$$U_{2c} = \frac{d_m}{2} \cdot \frac{\pi \cdot n}{60} \tag{3.1}$$

Where d_m is the rolling bearing mean diameter and n the upper race rotation speed.

For rolling element, the contact speed along the entire contact line (U_1) is the same and equal to U_{2c}, equation (3.2).

$$U_1 = U_{2c} \tag{3.2}$$

On the other hand, the contact race velocity at the ends of contact line (U_{2c}) is also dependent on the roller length (l), given by equation (3.3).

$$U_2 = \left(\frac{d_m \pm l}{2}\right) \cdot \frac{\pi \cdot n}{60} \tag{3.3}$$

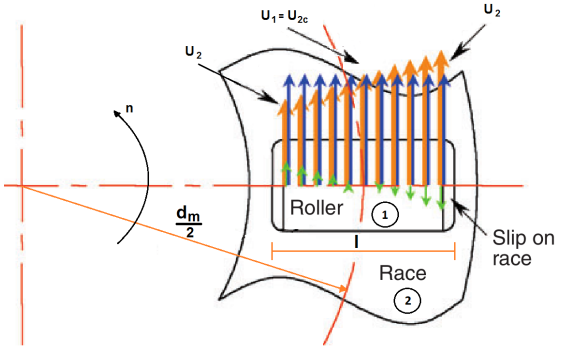

Figure 3.1: Cylindrical roller thrust bearing kinematics (adapted from [29]).

A detailed demonstration of the rolling bearing speed at desired points is done on the Appendix B.

3.1.1.2 Tapered Roller Bearings

TRB, as the name indicates, are composed by tapered rollers and tapered inner and outer races, which carries the load and also a cage, providing the rollers spacing out function around the races. The tapered rollers are guided between the races by a accurately positioned flange, the rib [5].

The inner and outer races have different contact angles, since its geometry is based on the cone principle. The extension lines of the working surfaces and tapered roller axis converge at a common apex point on the rotation bearing axis, showed in Figure 3.2.

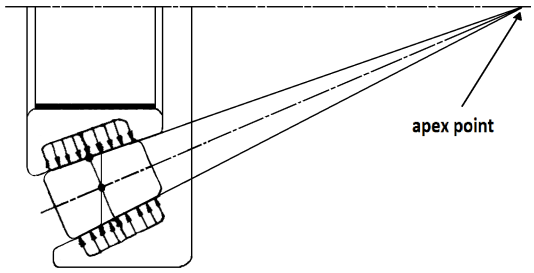

Figure 3.2: Tapered roller bearing principle (adapted from [5]).

Inner and outer race converging design make the track circumferences, at the large and small roller ends, greater and smaller, respectively. The different surface velocities are adjusted by track transition circumferences. As result, true rolling motion of the rollers on the raceways over the full length of the line contact is established [28].

With support of Figures 3.3(a) and 3.3(b) it is possible to determine the contact velocities in the middle of the contact line for both tapered roller (U_1) and inner/outer race (U_2), given by equation (3.4).

$$U_1 = U_2 = \left(\frac{d_m + d_r \cdot cos(\psi)}{2}\right) \cdot \frac{\pi \cdot n}{60} \tag{3.4}$$

Where d_r is the tapered roller mean diameter, n the inner race speed and ψ is the contact angle, given according to *Eschmann et al.* [30] by equation (3.5) where e is a calculation factor given by the manufacturer and dependent on TRB series.

$$\psi = \arctan \frac{e}{1.5} \tag{3.5}$$

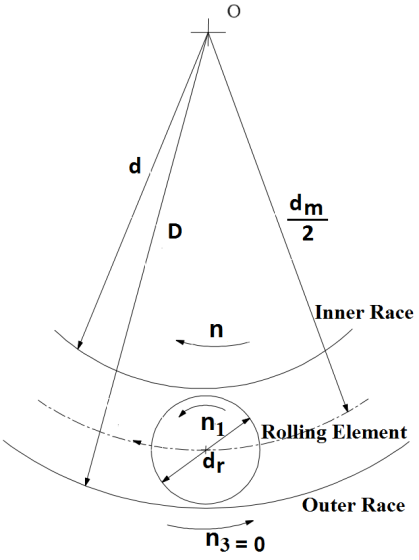

(a) Angular velocity.

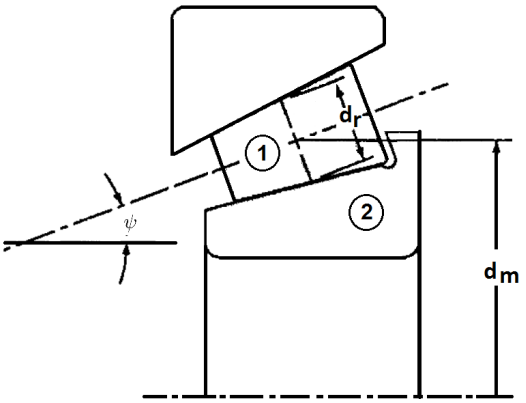

(b) Simplified internal geometry (adapted from [27]).

Figure 3.3: Tapered roller bearing schematic representations.

3.1.2 Contact Pressure Distribution

Theoretical contact pressure distribution can be determined from the analytical expressions based on the elasticity theory established by Hertz [14].

In RTB and TRB, there is a theoretical line contact between the rolling elements and the raceways, which is transformed in a narrow rectangular area, due to the elastic deformation. The dimensions of this area depends on the contact loads, bearing dimensions and material properties of the contacting bodies. In Figure 3.4 is presented the contact area for two parallel cylinders.

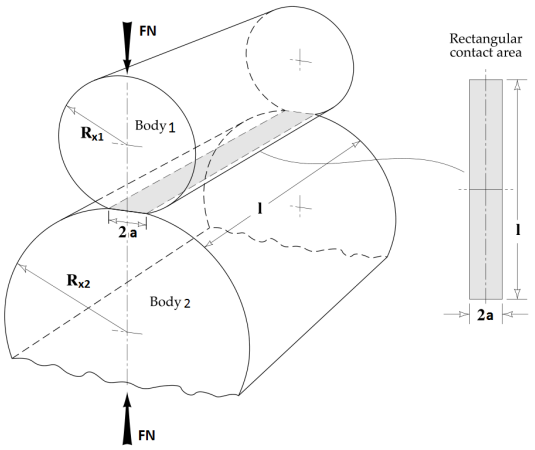

Figure 3.4: Parallel cylinders: contact geometry [14].

Knowing the curvature radius (R_{x1} and R_{x2}) and the material properties for both bodies, Poisson's ratio (υ_1 and υ_2) and Young's modulus (E_1 and E_2), it is possible to determine the equivalent radius (R_x) and the effective Young's modulus (E^*), given by the equations (3.6) and (3.7), respectively.

$$\frac{1}{R_x} = \frac{1}{2}\left(\frac{1}{R_{x1}} + \frac{1}{R_{x2}}\right) \tag{3.6}$$

$$\frac{1}{E^*} = \left(\frac{1-\upsilon_1^2}{E_1} + \frac{1-\upsilon_2^2}{E_2}\right) \tag{3.7}$$

In equations (3.8) and (3.9) are expressed the maximum Hertz pressure (p_{max}) and semi-width (a), respectively.

$$p_{max} = \sqrt{\frac{2 \cdot F_n \cdot E^*}{\pi \cdot l \cdot R_x}} \tag{3.8}$$

$$a = \sqrt{\frac{2 \cdot F_n \cdot R_x}{\pi \cdot l \cdot E^*}} \tag{3.9}$$

Where F_n is the normal load applied on the bodies and l the length of contact area.

Maximum Hertzian pressure in rolling bearings assume commonly values between 1 and 4 GPa [28]. In Figure 3.5 is presented the typical Hertzian pressure distribution in the contact area.

The pressure distribution on a Elastohydrodynamic (EHD) contact is very similar to Hertzian pressure. So, the profile of the lubricant film is very similar to the deformed surfaces

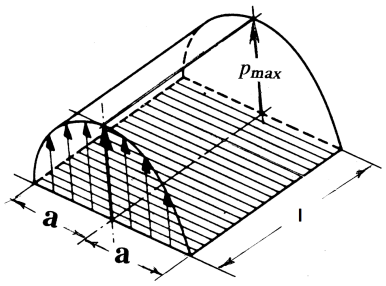

Figure 3.5: Parallel cylinders: contact pressure distribution [31].

geometry. Figure 3.6 shows a comparison between EHL pressure and the Hertzian pressure of a dry contact and also the film thickness distribution.

The fluid film pressure wave increases from the inlet and reaches a maximum equal to the maximum Hertz pressure at the centre of the contact area. After that, pressure decreases, but rises again with a sharp spike near the outlet side, which justify the lower thickness in the film in that region [31].

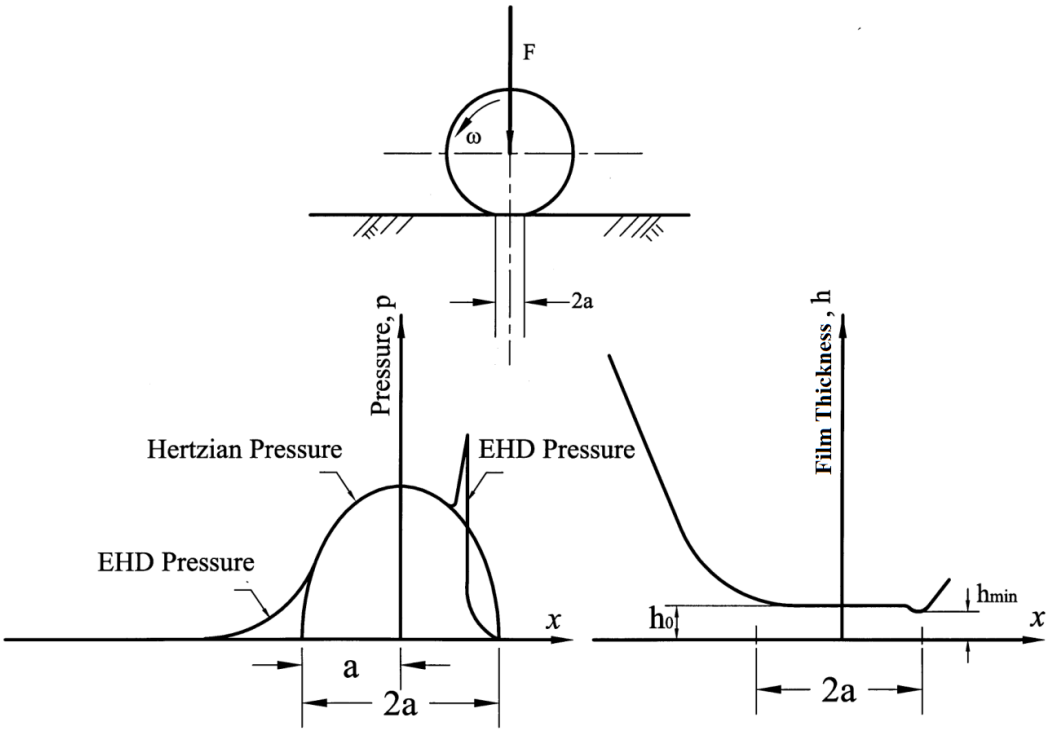

Figure 3.6: Pressure wave and film thickness distribution in elastohydrodynamic lubrication [31].

3.1.3 Film Thickness Prediction (Dowson and Higginson Model)

Dowson and Higginson [32], in 1959 described an iterative procedure for solving the complex elastohydrodynamic lubrication problem, that not only yielded a wide range of solutions during the next decade, but also enabled them to derive an empirical minimum film thickness

formula for line contacts. This prediction implicates an isothermal contact between smooth surfaces and fully flooded lubrication. In 1961 *Crook*, prove experimentally that rolling speed plays a crucial role and load has an insignificant importance in film thickness [27].

In operating rolling bearings, there are several simultaneous contacts between raceway and rolling elements. Furthermore, the same conditions are not ensured for all of the contacts, which make it complicate to assure that predicted film thickness is representative for all contacts of bearing.

The film thickness (h_0) in line contacts is given by equation (3.10).

$$h_0 = 0.975 \cdot R_x \cdot U^{0,727} \cdot G^{0,727} \cdot W^{-0,091} \tag{3.10}$$

U, G and W are non-dimensional numbers, representing the velocity, material and load parameters and are given by the equations (3.11), (3.12) and (3.13) respectively.

$$U = \frac{\eta \cdot U_R}{2 \cdot R_x \cdot E^*} \tag{3.11}$$

$$G = 2 \cdot \alpha \cdot E^* \tag{3.12}$$

$$W = \frac{F_n}{R_x \cdot E^* \cdot l} \tag{3.13}$$

Dynamic viscosity (η) and the piezoviscosity (α) values are given for the conditions at the inlet contact and the rolling speed (U_R) is given by equation (3.14).

$$U_R = U_1 + U_2 \tag{3.14}$$

As described above, the calculation of film thickness does not takes into account the heating of the lubricant in contact inlet (ϕ_T), the feeding conditions (ϕ_A) and the surfaces roughness (ϕ_R), which must be corrected through the expression defined in equation (3.15) [13].

$$h_{0c} = \phi_T \cdot \phi_A \cdot \phi_R \cdot h_0 \tag{3.15}$$

However, currently only the temperature parameter is taken into account to correct the film thickness (h_{0c}) (equation (3.16)), since surface roughness parameter are expressed on specific film thickness parameter.

$$h_{0c} = \phi_T \cdot h_0 \tag{3.16}$$

The heating effect in the inlet contact occurs as a result of high shear deformation in lubricant film, due to the pressure gradient and the rolling and sliding speeds. Thus, this shear deformation creates high energy dissipation, that leads to an increase of temperature and consequently a decrease of film thickness [13]. The thermal reduction factor is defined in equation (3.17).

$$\phi_T = \left[1 + 0.1(1 + 14.8 \cdot V_e^{0.83}) \cdot L^{0.64}\right]^{-1} \tag{3.17}$$

V_e and L are non-dimensional parameters, representing the slip rate and the lubricant thermal properties given by equations (3.18) and (3.19), respectively.

$$V_e = \frac{|U_1 - U_2|}{(U_1 + U_2)} \tag{3.18}$$

$$L = \frac{\beta \cdot \eta \cdot (U_1 + U_2)^2}{K} \tag{3.19}$$

Lubricant thermoviscosity (β) and thermal conductivity (K) values are given for the conditions at the inlet contact.

Thermal conductivity is given by equation (3.20).

$$K = \frac{0.12 \cdot \left(1 - \frac{0.005}{3} \cdot \theta\right)}{sg} \tag{3.20}$$

Where sg is the specific gravity of the oil.

Typical values for V_e lie in a range between 0.03 and 0.06. This values are proposed even when there is no sliding speed in the full length of contact line like occurs in TRB contacts. For RTB it was consider $V_e = 0.06$ according to equation (B.37) and for TRB $V_e = 0.05$ taking into account a previous study performed by *Fernandes* [21].

3.1.4 Lubrication Regime and Specific Film Thickness

In 1967 *Tallian*, [33] developed a concept that links the effect of surface roughness with lubricant film thickness, the specific film thickness (Λ), which can be calculated by equation (3.21).

$$\Lambda = \frac{h_{0c}}{\sigma} \tag{3.21}$$

Where σ is the composite roughness of contact surfaces depending on the surface roughness of the roller and the race that is defined by equation (3.22).

$$\sigma = \sqrt{R_{q1}^2 + R_{q2}^2} \tag{3.22}$$

R_{q1} and R_{q2} represent the root mean square (RMS) deviation of the roughness profiles for rolling element and raceway, respectively.

Typical values of R_q depending on the rolling bearing element are presented in Table 3.1.

Table 3.1: RMS roughness values for type of rolling bearing element [13].

Bearing rolling element	R_q $[\mu m]$
Precision balls	0.05
Balls	0.18
Cylindrical and spherical rollers	0.36
Tapered and needle rollers	0.23

Four different lubrication regimes are considered: hydrodynamic, full film, mixed film and boundary film, which the last three are included in EHL. The definition of lubrication regime is related with characteristic values of specific lubricant film thickness.

In Table 3.2 are defined EHL regimes observed in rolling bearings.

Table 3.2: Rolling bearing's EHL regimes [13].

$\Lambda = \frac{h_{0c}}{\sigma}$	Lubrication Regime
$\Lambda \geq 3.0$	Full film
$1.0 < \Lambda < 3.0$	Mixed film
$\Lambda \leq 1.0$	Boundary film

However, for other applications, where elastic deformation of the surfaces is negligible, the hydrodynamic regime is observed and is characterized for very thick film, with a specific film thickness superior in ten times the full film conditions value ($\Lambda > 10 \cdot \Lambda_{EHD}$) [13].

In full film regime, a minimum lubricant film thickness, which is superior to composite roughness, allows to completely separate the surfaces [13,26].

Mixed film occurs when the tallest asperities of contacting surfaces can occasional cross all the lubricant film and contact the other surface [13,26].

Boundary film develops when the lubricant film is very low. Considerable contact asperities occurs separated only for a few layers of molecules. Thus, the chemical properties of the lubricant are of crucial importance [13,26].

In Figure 3.7 are shown the EHL regimes described above.

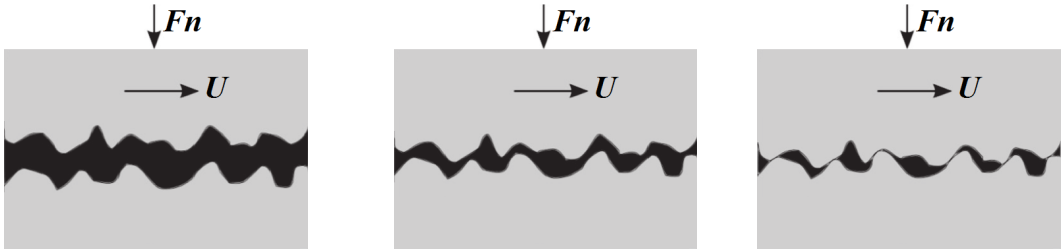

(a) Full film [26]. (b) Mixed film [26]. (c) Boundary film [26].

Figure 3.7: Elastohydrodynamic lubrication regimes.

3.1.5 Viscosity Ratio

Viscosity ratio (κ) is a dimensionless parameter that allows to evaluate a lubricant capability to properly separates the rolling contact surfaces. A minimum viscosity value is established to provide $\kappa = 1$, according to the bearing mean diameter and depending on lubricant viscosity. As proposed by SKF [9], this parameter should be calculated according to the abacus presented in Figure 3.8 for bearing operating conditions at service temperature and is defined by equation (3.23).

$$\kappa = \frac{\nu}{\nu_1} \tag{3.23}$$

For a operating viscosity (ν) lower than the rated viscosity (ν_1) to assure $\kappa = 1$, the lubricant isn't capable of separate the surfaces, and metal to metal contact may occur. Furthermore, when $\kappa < 0.4$, extreme pressure additives must be added to lubricant due to considerable

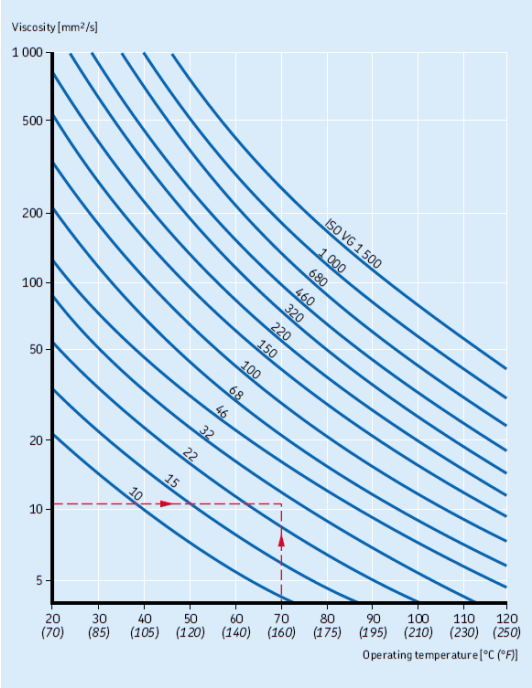

Figure 3.8: SKF abacus to determine the rated kinematic viscosity ([9]).

metal contact. For $\kappa \geq 1$ a minimum film is ensured and for $\kappa \geq 4$ full film conditions are reached [9].

Another method to calculate the parameter is defined by ISO 281 [34], which relates, for linear contacts, the κ with Λ according the equation (3.24).

$$\kappa = \Lambda^{1.296} \tag{3.24}$$

However, for TRB considerable differences can be observed on determination of viscosity ratio. In Figure 3.9 is presented a comparison between both methods to determine κ values.

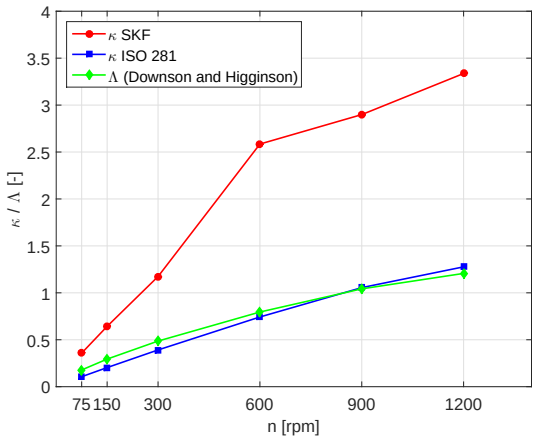

Figure 3.9: Comparison between determined viscosity ratio (κ) values obtained from SKF abacus and ISO 281 and specific film thickness (Λ).

3.1.6 Hersey number and Stribeck diagram

Stribeck's diagram is a common tribological tool to describe the frictional behaviour of a lubricated contact during the transition between different lubrication regimes. It shows the relationship between the dimensionless *Hersey* number and the coefficient of friction (COF), which depends on lubricant's dynamic viscosity (η), the sliding contact speed (U_S) and the load per length unit (W_n), and it's defined in equation (3.25) [27].

$$H_s = \frac{U_S \cdot \eta}{W_n} \tag{3.25}$$

Where the sliding speed is given by $U_S = U_2 - U_1$.

Observing Figure 3.10, it is possible to establish a relationship between the lubricant film thickness in the contact and the Hersey number, since generally small values are associated to negligible lubricant films and consequently higher coefficient of friction, about $\mu \approx 0,1$ or higher, which correspond to boundary film condition, represented in zone 1. With the increase of Hersey number, a thin film is generated and it is capable of separate the surfaces. The COF quickly decreases and reach a minimum value $\mu \leq 0.01$, represented in zone 2, corresponding to mixed film regime. For higher Hersey numbers, the film is thick enough to separate completely the contacting surfaces without any metal to metal interaction. The friction coefficient slightly increases, represented in zone 3, corresponding to full film EHD regime. Zone 4 includes zone 3, which correspond to hydrodynamic regime. However, for high Hersey values, the film thickness is 10 times thicker than in full EHD regime and the coefficient of friction continues to increase [27].

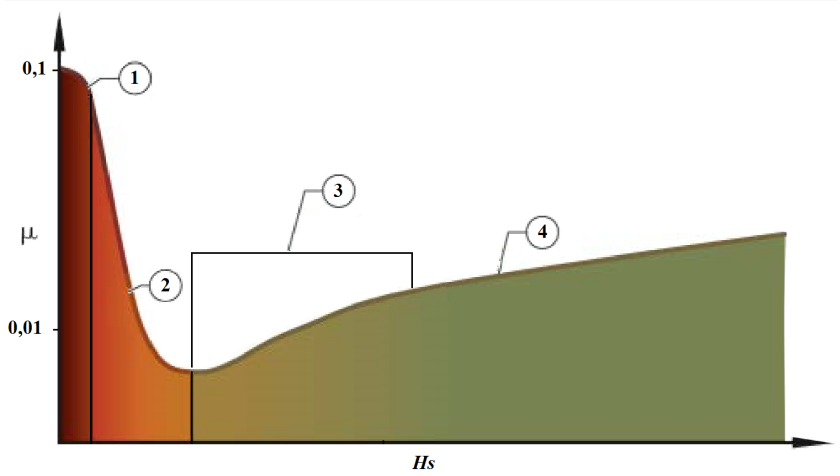

Figure 3.10: Stibeck diagram (adapted from [35]).

The effect of pressure rise in inlet contact results in higher lubricant viscosity expressed by the piezoviscosity parameter. However, Hersey number doesn't take this parameter into account. *Brandão* [36] suggested the modified Hersey number given by the equation (3.26).

$$S_{pm} = \frac{U_S \cdot \eta \cdot \alpha^{\frac{1}{2}}}{F_n^{\frac{1}{2}}} \tag{3.26}$$

For the purpose of the present study, the modified Hersey parameter (S_{pm}) was used instead of the Hersey number (H_s), where for ($S_{pm} < 10^{-9}$) the contact is under boundary

lubrication regime and for ($S_{pm} > 10^{-7}$) it is under full film lubrication regime.

3.2 Rolling Bearing Losses

The resistance developed on bearings movement, is responsible for mechanical power loss and heat generation. The friction depends on the bearing type, size and series, loads, operating speed, lubricant quantity and its properties and several other factors [9,37].

Bearings manufacturers such as SKF and FAG have been developing models based on experimental measurements that predict the torque loss in rolling bearings [21]. In this thesis, it was selected the SKF model for calculating the frictional moment, in order to analyse the obtained results.

Increasing bearing rotational speed or lubricant viscosity, friction torque has different behaviour, as shown in Figure 3.11. In zone 1, corresponding to the start up period, the friction torque decreases, as result of lubricant film formation, until reach a minimum value. As viscosity or rotational speed increases, the lubricant film thickness also increases and the bearing enters into the full EHL, corresponding to zone 2. In this zone the friction torque is continuously increasing. If these two parameters are continually increasing, friction torque reaches a plateau, corresponding to zone 3, caused by kinematic starvation and inlet shear heating effects [9].

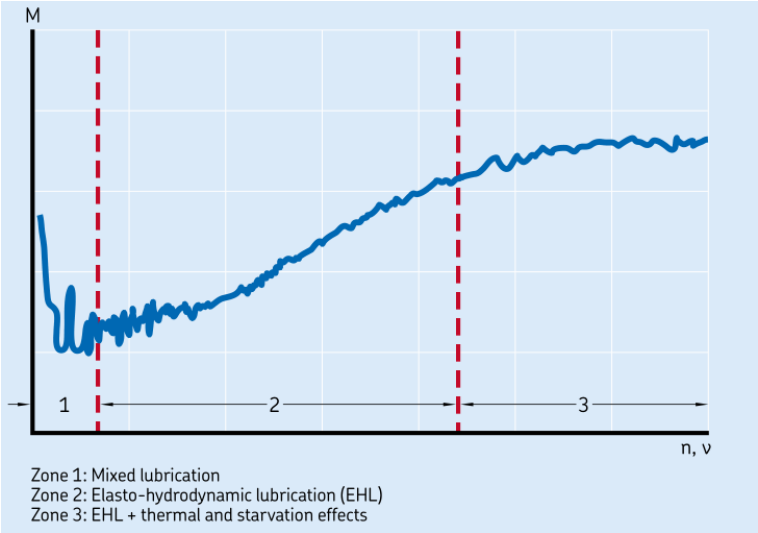

Figure 3.11: Bearing frictional torque as function of speed or viscosity [9].

3.2.1 SKF Friction Torque Model

There are different sources of friction present both in dry or lubricated contacts. The SKF friction model assume four different physical sources of friction torque in rolling bearings: rolling torque (M_{rr}), sliding torque (M_{sl}), drag losses (M_{drag}) and seal losses (M_{seal}), as given by equation (3.27) [9].

$$M_t = M_{rr} + M_{sl} + M_{drag} + M_{seal} \tag{3.27}$$

Knowing the total friction torque and the rotational speed, it is possible to calculate the power loss according to equation (3.28) [9].

$$P_B = M_t \cdot \frac{2 \cdot \pi \cdot n}{60} \tag{3.28}$$

In the present thesis, 3 sets of bearings were used:

- 81107 TN cylindrical roller thrust bearing;
- 30203 J2 tapered roller bearing;
- 320/28X/Q tapered roller bearing.

In the following sections will be explained in more detail, the four physical mechanisms of friction loss.

3.2.1.1 Rolling Friction Torque

Rolling friction mechanism is always present in rolling contacts. However, purely rolling contacts does not exist, it is a mathematical idealization to represent reality. Since elastic deformation occurs, the conditions to micro-sliding in surfaces are provided, which are considered in sliding friction torque [38].

Rolling friction losses are related with energy dissipation that occurs due to removal of the excess of lubricant from the contact, elastic hysteresis in steel deformation and the adhesion forces between surfaces, which might be measured according to equation (3.29) [38].

$$M_{rr} = \phi_{rs} \cdot \phi_{ish} \cdot G_{rr} \cdot (\nu \cdot n)^{0.6} \tag{3.29}$$

- **Load distribution in rolling contacts**

It depends on the external loads applied on the bearing and its geometry, which is included by the bearing type, mean diameter size and number and size of rolling elements. The influence of bearing load is represented by G_{rr} variable and geometry parameters are represented by R_1 and R_2. The equations to calculate load parameter and geometric variables dependent on bearing type and series are presented in Table 3.3 [38].

Table 3.3: Rolling bearing load rolling torque constant (G_{rr}) and geometric variables (R_1 and R_2) for different type of bearings [9].

Bearing	G_{rr}	R_1	R_2
RTB 81107	$G_{rr} = R_1 \cdot d_m^{2.38} \cdot F_a^{0.31}$	2.22×10^{-6}	-
TRB30203J2	$G_{rr} = R_1 \cdot d_m^{2.38} \cdot (F_r + R_2 \cdot Y \cdot F_a)^{0.31}$	1.76×10^{-6}	10.9
TRB 320/28X/Q	$G_{rr} = R_1 \cdot d_m^{2.38} \cdot (F_r + R_2 \cdot Y \cdot F_a)^{0.31}$	2.38×10^{-6}	10.9

- **Inlet shear heating**

The lubricant film formation depends on the conditions at the inlet contact area. Only a small portion of lubricant available is dragged into the high pressure zone. The lubricant that does not get into the contact creates a reverse flow between the ball and the raceway, as shown in Figure 3.12 [38].

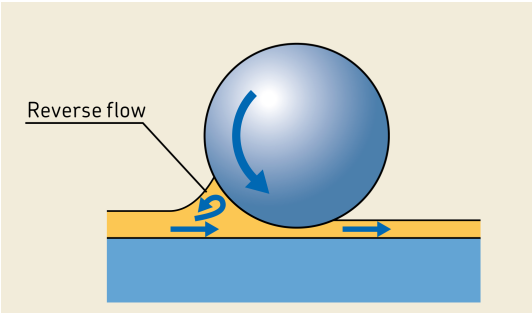

Figure 3.12: Reverse flow at the inlet of the contact [9].

The recirculation leads to energy dissipation through heat generation that increases the temperature, and consequently, decrease the lubricant viscosity. Lowering viscosity causes a film thickness decrease at the contact area that provides lower rolling friction. This factor is given by equation (3.30), that takes into account the rotational speed, the rolling bearing mean diameter and the lubricant viscosity. The ϕ_{ish} variation is shown in Figure 3.13 [38].

$$\phi_{ish} = \frac{1}{1 + 1.84 \times 10^{-9}(n \cdot d_m)^{1.28} \cdot \nu^{0.64}} \tag{3.30}$$

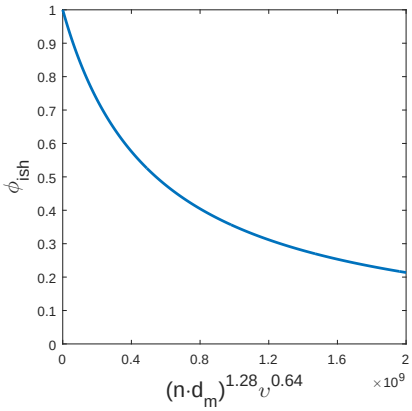

Figure 3.13: Inlet shear heating factor variation [9].

- **Kinematic replenishment/starvation**

When the rolling elements rotate at high speeds or the lubricant viscosity is high, the local lubricant replenishment may not be ensured and the adjacent rolling element suffer from kinematic starvation. The lubricant takes a amount of time to flow back from the sides to the centre of raceway. If the following rolling element passes before the replenishment needed

time, the amount of lubricant in the inlet of the contact is lower and consequently the film thickness will be reduced, decreasing the rolling friction. This effect is given by equation (3.31), dependent on rolling bearing type geometric constant K_Z, dimensions, oil lubricant's viscosity, speed rotation and lubrication method (oil bath, grease or oil jet) [38].

$$\phi_{rs} = \frac{1}{\exp\left[K_{rs} \cdot \nu \cdot n \cdot (d+D) \cdot \sqrt{\frac{K_Z}{2(D-d)}}\right]} \tag{3.31}$$

The geometric constant are represented in Table 3.4.

Table 3.4: Rolling bearing geometric constant K_Z [9].

Rolling bearing	K_Z
RTB 81107	4.4
TRB30203J2	6
TRB 320/28X/Q	6

The replenishment/starvation factor K_{rs} depends on the lubrication method. For low level oil bath and oil jet lubrication, takes the value 3×10^{-8} and 6×10^{-8} for oil-air and grease lubrication [9]. All the tests were performed at low level oil bath.

3.2.1.2 Sliding Friction Torque

Sliding friction is always present in rolling bearings, generating higher friction losses, mainly at low speeds. SKF splits in two, micro and macro sliding, the sources of sliding friction [38].

As refered in Section 3.2.1.1, microslip is present in rolling contacts, since the surfaces are subjected to heavy loads in small contact areas causing surface distortion due to elastic deformations.

Macroslip is caused by contact between two surfaces of bigger geometries. For instance, in roller/raceway contact on thrust bearings, only the mid point in all contact line has no slip.

According to the slip profile in the contact area and depending on the the film thickness/roughness ratio, there are two ways to produce sliding friction losses: lubricant shearing or/and asperity contact, and is given by the equation (3.32).

$$M_{sl} = G_{sl} \cdot \mu_{sl} \tag{3.32}$$

- **Lubricant shearing**

When the full film regime is reached, a thick lubricant film is present in the contact and shear stress across these film comes up, due to the slippage between the surfaces. The coefficient of friction, which depends on the normal load and shear stress (lubricant's rheology), a coefficient is present and can be calculated according to equation (3.33) [38].

$$\mu_{EHL} = \frac{1}{F_n} \int_{A_c} \tau dA_c \tag{3.33}$$

- **Asperity contacts**

Depending on the lubrication regime, some surface to surface interaction could exist in contacts. When the film thickness is not sufficient to completely separate the surfaces some asperity interaction occurs, resulting in an increase of sliding friction. As consequence, the coefficient of friction of the asperities (μ_{bl}) is larger than shearing the oil (μ_{EHL}).

The μ_{bl} is dependent on lubricant's additive packages and their capacity to generate a protective layer in the surface, that decreases the asperity resistance. On the other hand, the coefficient of friction depends on the bearing type and base oil.

The SKF model defines the sliding coefficient of friction in boundary layer as $\mu_{bl} = 0.15$. However, this value must be experimentally fitted according to lubricant additives since for boundary lubrication sliding coefficient of friction (μ_{sl}) usually ranges from 0.05 to 0.15 [26].

For sliding coefficient of friction in full-film conditions, the values proposed by SKF are dependent on the rolling bearing's geometry and the base oils [9]. In Table 3.5 are presented the reference values for sliding coefficient of friction for both boundary (μ_{bl}) and full film regime (μ_{EHL}) .

Table 3.5: Sliding coefficient of friction for boundary or full-film lubrication conditions [9].

Reference COF	Cylindrical roller thrust bearings	Tapered Roller Bearings
μ_{bl}	0.15	0.15
μ_{EHL}	0.02	0.002

The equation (3.34) gives the sliding coefficient of friction for a particular condition, taking into account the lubricant's performance under full and boundary lubrication regimes.

$$\mu_{sl} = \phi_{bl} \cdot \mu_{bl} + (1 - \phi_{bl}) \cdot \mu_{EHL} \tag{3.34}$$

The parameter ϕ_{bl} presented in equation (3.34), is a weighting influence factor for the asperity and lubricant shearing mechanisms. This factor is given by equation (3.35), and decreases with the increase of rotational speed and lubricant's viscosity, as shown in Figure 3.14. In other words, increasing the film thickness the coefficient of friction will be reduced due to lower influence of contact asperities. The ϕ_{bl} value will tends to 0 and the friction losses will be mainly dependent on lubricant shearing [9].

$$\phi_{bl} = \frac{1}{\exp^{[2.6\times10^{-8}\cdot(n\cdot\nu)^{1.4}\cdot d_m]}} \tag{3.35}$$

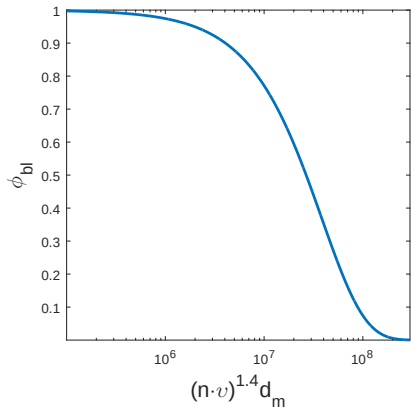

Figure 3.14: Weighting factor variation with rotating speed and viscosity [9].

The influence of the bearing's load in sliding friction is given by G_{sl} being its geometry and bearing series expressed by S_1 and S_2 parameters, presented in Table 3.6.

Table 3.6: Rolling bearing load sliding torque constant (G_{sl}) and geometric variables (S_1 and S_2) for different type of bearings [9].

Rolling bearing	G_{sl}	S_1	S_2
RTB 81107	$G_{sl} = S_1 \cdot d_m^{0.62} \cdot F_a$	0.154	-
TRB30203J2	$G_{sl} = S_1 \cdot d_m^{0.82} \cdot (F_r + S_2 \cdot Y \cdot F_a)$	0.017	2
TRB 320/28X/Q	$G_{sl} = S_1 \cdot d_m^{0.82} \cdot (F_r + S_2 \cdot Y \cdot F_a)$	0.014	2

3.2.1.3 Seal Friction Torque

When bearing rotating part is sliding against a seal, the resistance generated can not be disregarded. The losses induced by the contact with seals may exceed the other sources of friction loss and represent a large percentage of the total friction. [9].

3.2.1.4 Drag Friction Torque

For oil bath lubrication, bearings are partially or completely submerged. When bearings are rotating, the moving parts are in the presence of an additional friction source, induced by oil drag, which increase the total friction torque. According to SKF, drag losses are dependent on bearing rotational speed, oil level and viscosity, bearing dimensions, geometry and size of oil compartment and even the external oil agitation [9].

3.2.1.5 Effect of Centrifugal Forces and Spinning

When a bearing is rotating, centrifugal forces emerge in the contact, which will influence the lubrication. The effect is more relevant at high speeds. The sliding friction will reduce with the increase of speed until, at a certain speed, this tendency will be inverted and the sliding resistance increase again. This increasing is explained by the increase of centrifugal forces

from rolling elements in outer raceway contact. According to SKF, this effects are considered in friction model through G_{rr} and G_{sl} [38].

3.2.2 Experimental Sliding Coefficient of Friction Determination

All rolling bearings used in this work have small dimensions and were tested at low rotational speeds, so the drag losses are small when compared with rolling and sliding losses and weren't considered. Moreover both RTB and TRB don't have seals, so seal friction torque was also ignored.

As result, the total friction torque loss in tested rolling bearings is given by equation (3.36).

$$M_t = M_{rr} + M_{sl} \tag{3.36}$$

To calculate the experimental sliding coefficient of friction two considerations are assumed:

- The total friction torque (M_t) from SKF model is considered equal to the total friction torque measured (M_t^{exp}), leading to the equation (3.37):

$$M_t = M_t^{exp} = M_{rr} + M_{sl} \tag{3.37}$$

- The experimental rolling friction torque(M_{rr}^{exp}) is considered equal to the SKF rolling friction torque (M_{rr}), determined for the experimental operating temperature, rotational speed and load conditions, which leads to the equation (3.38):

$$M_{rr}^{exp} = M_{rr} \tag{3.38}$$

As consequence, the experimental sliding friction torque (M_{sl}^{exp}) is given by equation (3.39).

$$M_{sl}^{exp} = M_t^{exp} - M_{rr} \tag{3.39}$$

According to the equation (3.32), M_{sl} is dependent on two variables, G_{sl} and μ_{sl}. Therefore, knowing M_{sl}^{exp} it is possible to define the experimental sliding coefficient of friction (μ_{sl}^{exp}), equation (3.40).

$$\mu_{sl}^{exp} = \frac{M_{sl}^{exp}}{G_{sl}} \tag{3.40}$$

3.2.3 Coefficient of Friction Optimization

The SKF model described in Section 3.2.1 is an engineering tool that predict in certain cases the friction torque with accuracy. However, in most of the cases the experimental results indicate a great discrepancy with the prediction. One of the causes to the divergence is related with the additive package, which affect the rolling bearing COF. Furthermore, many variables are involved in the model prediction and need to be fitted to a particular case. Taking into account these, the SKF model was optimized based on the experimental results for constant

load and temperature and for different operating speeds, according to the procedure proposed by *Fernandes et al.* [39].

According to SKF friction torque model, the sliding coefficient of friction is predicted by equation (3.34) and it is dependent on three variables: weighting lubrication factor (ϕ_{bl}), sliding coefficient of friction under boundary-film regime (μ_{bl}) and sliding friction coefficient under full-film regime (μ_{EHL}). The ϕ_{bl} is known, since is dependent on viscosity, rotational speed and mean diameter. The μ_{bl} and μ_{EHL} values are defined by SKF and could be optimized.

Using the equation (3.34) and SKF values for μ_{bl} and μ_{EHL} (Table 3.5) it is determined a sliding coefficient of friction (μ_{sl}), different from the experimental sliding coefficient of friction (μ_{sl}^{exp}) obtained by equation (3.40).

The optimization process relies in minimization of the difference between the μ_{sl} and μ_{sl}^{exp}, by adjusting the μ_{bl} and the μ_{EHL} on equation (3.34). *Solver* function of *Excel* software was used to optimize the sliding coefficient of friction through a non-linear fitting method and three conditions were imposed:

- For each set of results at different rotational speeds: $\sum_{i=1}^{rs} \mu_{sl}^{exp} - \mu_{sl}^{SKF} = 0$, where rs is the number of different rotational speeds tested for each constant load and temperature conditions.
- $\mu_{EHL} > 0.001$
- $\mu_{bl} > \mu_{EHL}$

As a result of this process a optimized sliding coefficient of friction (μ_{sl}^{opt}) is obtained and the minimum difference value named error is determined.

Chapter 4

Tribofilms Characterization

Optimal friction efficiency in lubricated contacts is achieved with mixed film regime, which is characterized by interactions between the surfaces asperities.

Unlike the full film regime, where the rheological lubricant properties influence the friction losses, in mixed and boundary film regime the chemical composition of the lubricants has crucial influence in the contact behaviour [40]. During the asperities interactions, chemical reactions between lubricant anti-wear/extreme pressure additives and the surfaces occurs. A thin film, the tribofilm, is deposited on surface as shown in Figure 4.1 [26].

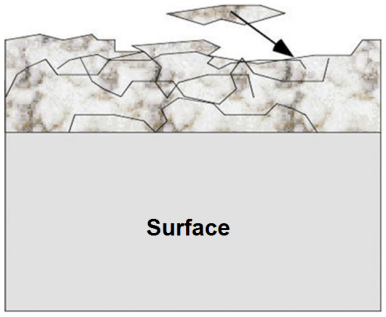

Figure 4.1: Surface modification in tribological contact: formation of tribofilm [41].

Depending on the additive package, tribofilm protect the surfaces from excessive wear, extending its lifetime and/or reduce the friction losses [42]. Under severe load conditions, anti-wear additives produce tribofilms that are difficult to shear off and protect a surface from eventual damage caused by the opposite surface asperities. Thus, it has lower friction modifying properties. On the opposite, friction modifiers additives deposit on the substrate several arrays of multimolecular layers. Due to the reduced adhesion between them, the outer layers can be easily sheared off, providing a low coefficient of friction [25].

4.0.1 Experimental Planing

In order to understand and compare the tribofilm phenomenon and its relationship with surface wear in the five oils, presented in Section 2.3.2, and also for a better comprehension of friction behaviour, a series of tests and analysis were performed with RTB 81107 TN. Friction torque measurements were been performed. After each test the used oil was collected and the rolling bearings were properly stored. Concluded all the friction torque measurements, different analysis were done to rolling bearings and to oil samples. Roughness measurements were performed on raceways, rollers were analysed in a X-ray photoelectron spectrometer and a direct reading and analytical ferrography analysis were performed to the oil samples.

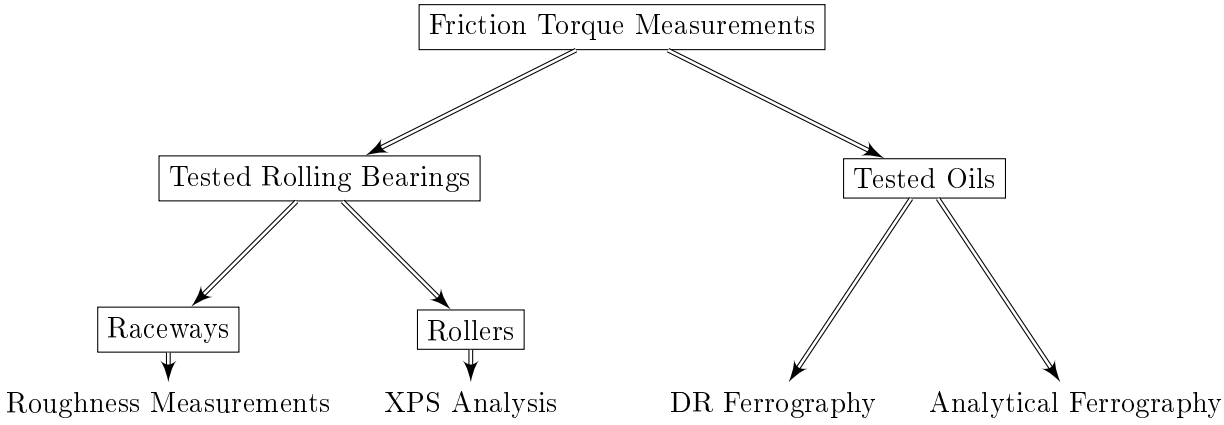

Figure 4.2: Experimental followed plan.

4.1 Experimental Friction Torque Measurements

In order to measure the total friction torque generated in a rolling bearing and compare its performance with the available lubricants for analysis, a series of tests were performed in a modified four-ball machine (Cameron-Plint TE 82/7752), shown in Figure 4.3(a). The four-ball arrangement was removed and the equipment was adapted to include a rolling bearing assembly, shown in Figure 4.3(b). The assembly developed by Cosseau *et al.* [43], shown in Figure 4.4, allows to measure the total friction torque and the operating temperature in multiple points of the arrangement.

The rolling bearing assembly is divided in two parts: the upper part (UP) which connect to the machine shaft and the lower part (LW), which transmit the torque to the torque cell (11) . The shaft adapter (6), connected to the machine shaft by a Morse cone, holds the bearing upper race (5). The bearing lower race (3) is mounted in the lower race support (2), which is fitted to bearing house (1). Also a seal (7) and a cover (8) are used in the superior part of the bearing house to prevent external contamination and oil leakage.

The LW is composed by the torque cell (11) and two plates (9 and 13), that protect the torque cell, support the whole upper assembly (9) and provides a support base (13) to the entire assembly. Each plate has three pins (10 and 12) to ensure a proper connection with the bearing house and the machine lower shaft.

Two electrical resistances and a set of five thermocouples (I-V) are included to heat, measure and control the temperature. Furthermore, chamber and room temperatures are

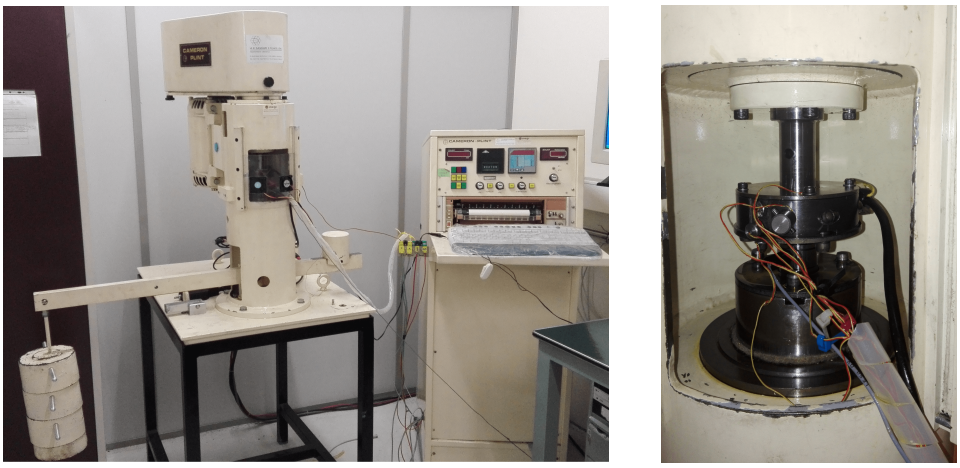

(a) Overview. (b) Bearing house assembly.

Figure 4.3: Cameron-Plint TE 82/7752 four-ball machine.

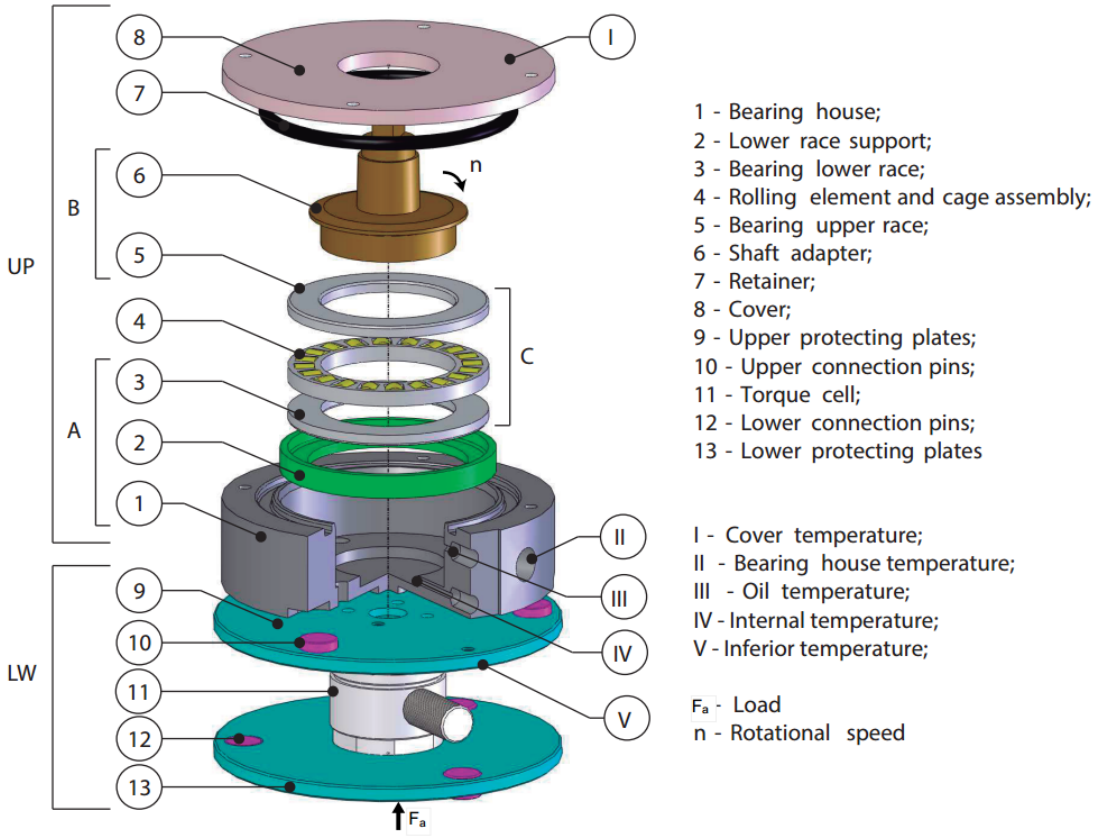

Figure 4.4: Schematic view of the rolling bearing assembly [21].

also measured by two thermocouples. Thermocouples (I, II and V) measure the external temperatures of the bearing house in order to evaluate the heat evacuation. Thermocouple (III) is placed near to the rolling bearing and gives feedback to a PID controller which control

the two electrical resistances, assuring a temperature variation always below than ±1 °C. Thermocouple (IV) gives the temperature inside bearing assembly. All the thermocouples are type K and have a measuring range between −40 °C and 200 °C, with sensibility of 41 μV°C $^{-1}$.

In operation, the UP is mounted over the LW. The axial load (F_a) is applied on the lower plate and the rotational speed (n) is applied to the shaft adapter. The upper race movement is transmitted to the rollers and cage assembly (4). The friction torque due to the movement is transmitted to the torque cell through the bearing house and measured with a piezoelectric torque cell (KISTLER 9339A), which ensures high-accuracy measurements (±1 Nmm). These measurements are given by the changing of electric current on the piezoelectric crystals, which must be amplified since the variation is very small. However, the accuracy of the torque cell measurements is dependent on the small temperature variations (±2 °C) and limited data acquisition time (less than 120 s). This restrictions are related to the piezoelectric sensors and must be respected to avoid the drift effect.

During the tests, two fans with 38 mm diameter running at 2000 rpm provide continuous forced air convection ensuring steady conditions inside the chamber.

With this equipment and replacing the components (2) and (6) it is possible test four different types of rolling bearings of different sizes, as shown in Table 4.1 . However, due to bearing house and four-ball machine, the geometrical rolling bearing dimensions are limited. The torque measurements were performed with a cylindrical roller thrust bearing (RTB 81107 TN).

Table 4.1: Main characteristics of rolling bearings which can be tested [9].

Designation	Principal Dimensions			Basic load ratings		Limiting Speed
	d	D	H/B/T	C	C_0	
	[mm]	[mm]	[mm]	[kN]	[kN]	[rpm]
Single direction trust ball bearings						
51103	17	30	9	11.14	21.2	12000
51107	35	52	12	19.90	51	7500
Cylindrical roller thrust bearings						
81102 TN	17	28	9	11.2	27	8500
81107 TN	35	52	12	29	93	5600
Single row angular contact ball bearings						
7203	17	40	12	11	5.85	22000
7204	20	47	14	13.3	8.15	18000
Single row tapered roller bearings						
30302 J2	15	42	14.25	22.4	20	18000
30203 J2	17	40	13.25	19	18.6	18000
320/28 X/Q	28	52	16	31.9	38	13000

4.1.1 Test Conditions

As mentioned in Chapter 4, the tribofilm generation occurs due to contact surface asperities, resulting from boundary film conditions. The tests performed were defined under the operating conditions presented in Table 4.2, to promote the tribofilm deposition. Temperature was defined at 110 °C, maximum four-ball machine load (7 kN) and minimum rotating speed (75 rpm) were applied. Furthermore, to increase the contact pressure in the rolling contact, 15 of 20 rollers were removed. Higher temperatures reduces the lubricant's viscosity and consequently the film thickness in the contact also decrease. Low rotating speed affects directly the rolling speed between the rollers and the races decreasing the lubricant capacity to generate a film thick enough to separate both surfaces. Although load has an effect less evident on the film thickness, higher load contact values promote severe conditions.

Table 4.2: Operating conditions of rolling bearing friction torque tests.

Temperature [°C]	Load [kN]	Rotational speed [rpm]	Running period [hours]
110	7	75	24

In Figure 4.5 is presented a RTB 81107 TN drawing with its geometrical dimensions and Table 4.3 presents contact and surface characteristics for a RTB 81107 TN. A comparison between the contact pressure under 7 kN load for both 5 and 20 rollers is done. The roughness measurements were taken from a previous study developed by *Fernandes* [21], where $R_{q1} = R_{q2} = 0.1$ μm.

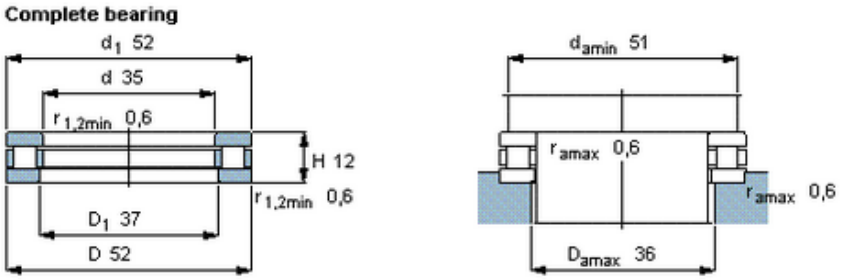

Figure 4.5: RTB 81107 TN representative scheme and geometrical dimensions (adapted from [9]).

Table 4.3: Rolling bearings contact parameters and surface characteristics.

No. Rollers [-]	R_x [m]	l [m]	a [μm]	p_{max} [MPa]	σ [μm]
5	5×10^{-3}	5×10^{-3}	87.9	2.03	0.14
20			43.9	1.01	

4.1.2 Test Procedure

As stated in Section 2.3.2, five oils were tested.

To perform the friction torque measurements, a test procedure was followed which were included the rolling bearing preparation, the bearing house assembly on four-ball machine and the measurement procedure:

1. External ventilation was turned on an hour before the first measurements, to ensure air renewal in the room;
2. A new rolling bearing was unpacked and 15 rollers were removed. The rolling cage with the remaining five rollers, upper and lower races were cleaned in a ultrasound bath of petroleum ether for 3 minutes to remove the original oil;
3. The four-ball machine, computer and torque cell were turned on, and the test parameters were input;
4. Rolling bearing races assembly (Figure 4.4):
   (a) Upper race (5) was mounted in the shaft adapter (6);
   (b) Lower race (3) was mounted in the lower race support (2) and both mounted in bearing house (1) sealed to prevent the oil leakage;
5. (A) and (B) sets from Figure 4.4, bearing cage (4) and housing cover (8) were cleaned in a ultrasound petroleum ether bath for 5 minutes, to remove contaminants;
6. Thermocouples (III and IV) were mounted in bearing house and rolling cage was also assembled;
7. 14 ml of oil was added, ensuring the fluid level to reach the centre of the roller element as advised by the rolling bearing manufacturer;
8. Bearing house assembly:
   (a) (B) set was inserted over the rolling cage;
   (b) Retainer (7) and cover (8) were assembled;
   (c) Thermocouples (I and II) were assembled;
   (d) Electrical resistances were assembled in bearing house (1);
   (e) Both LW and thermocouple (V) were inserted in the lower machine shaft. The UP was assembled in the superior shaft, shown in Figure 4.3(b);
9. Two fans were inserted in chamber entrance area and turned on;
10. The rolling bearing was run-in 5 minutes with a 1 kN of axial load, at rotational speed of 75 rpm and at temperature of 110 ^{o}C;
11. With the four-ball machine turned off, a load of 7 kN was applied. Then the machine was turned on and the load, speed and temperature conditions were kept along the 24h of test;
12. Torque measurement procedure:

(a) Torque data acquisition was turned on and 1000 acquisition points were recorded;

(b) The four-ball machine and the fans were turned off and the data acquisition continues up to 5000 points and them was turned off. The fans were turned off to keep the temperature steady while the motor was off;

(c) All temperatures and torque measurement were stored;

(d) The four-ball machine and the fans were turned on again;

13. Item 12 was repeated for the number of measurements desired, usually 4. The set of measurements were always performed in 10 minutes and the temperature variation between measurements was less than 1.5 °C;

14. In the end of each test, oil was collected and the rolling bearing was stored to further analysis.

It should be noted that two sets of measurements were performed. The first set of was performed 1 hour after the test start, and the second was implemented 23 hours latter of the first set of measurements. As described in Item 13, four measurements were performed by each set and selected the three closest friction torque values. Thus the average of these three values were considered as the result of each set of measurements.

4.1.3 Experimental Results

The RTB tests were performed according to the procedure described previously.

4.1.3.1 Operating Temperatures

In Figure 4.6, is shown the operating temperatures of each oil tested. The left bar correspond to the temperature value recorded after one hour and the right bar corresponds 24 hour of test.

It was observed very similar operating temperatures between the beginning (1h) and the end (24h) of each test. The variation found is within the accuracy range of the thermocouples.

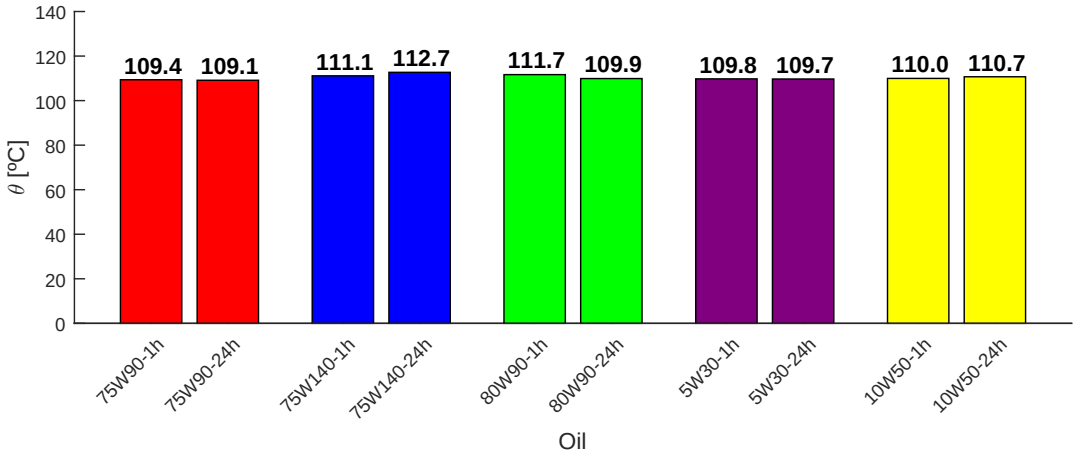

Figure 4.6: Operating temperatures (θ) after 1h and 24h of test for each oil.

In Table 4.4 is presented the viscosity (ν) and piezoviscosity (α) values calculated for both operating temperatures. The oil properties allow to understand the frictional behaviour of RTB 81107 TN.

Table 4.4: Kinematic viscosity (ν) and piezoviscosity (α) at 110 ^{o}C determined to 1h and 24h of test for each oil.

Parameter	Units	Measurement time	75W90	75W140	80W90	5W30	10W50
ν	[cSt]	1h	14.64	20.97	11.52	10.00	14.47
		24h	14.71	20.25	11.98	10.02	14.25
α	$[Pa^{-1}]$	1h	1.0563	1.1082	1.3910	1.0039	1.0546
$(\alpha \times 10^{-8})$		24h	1.0570	1.1030	1.3987	1.0041	1.0525

4.1.3.2 Specific Film Thickness

The test conditions were chosen in order to measure the friction torque on rolling bearings under boundary lubrication conditions. The specific film thickness in RTB was calculated according to the *Dowson and Higginson* equation (3.10) [32] in the centre of the roller-raceway linear contact. In Figure 4.7 it is shown that for all the oils tested the rolling bearings were run at the expected lubrication regime since $\Lambda << 1$.

Since all the conditions were kept along the test, the specific film thickness difference observed for each oil, occurs due to different operating temperatures (Figure 4.6) and different surface roughness (Table 4.8). At 24h, it was assumed raceway roughness (R_{q2}) as the mean value of the two measurements performed at exterior and centre of the race.

For all the oils a decrease of specific film thickness was found when comparing both 1h with 24h tests. The highest decreases were found in 5W30 and 10W50 oils and correspond to 41 % and 32 %, respectively.

Comparing the results, 5W30 oil presented the lowest specific film thickness, as expected, due to its lower viscosity and piezoviscosity. On opposite, 75W140 oil presented the highest Λ value, resulting from its highest viscosity when compared with the other oils. However, the piezoviscosity value is lower than the highest value presented for the 80W90 oil. Despite of 80W90 oil presented the highest piezoviscosity value, the viscosity is only higher than 5W30 oil. For this reason, it presented a similar Λ value to 10W50 and 75W90.

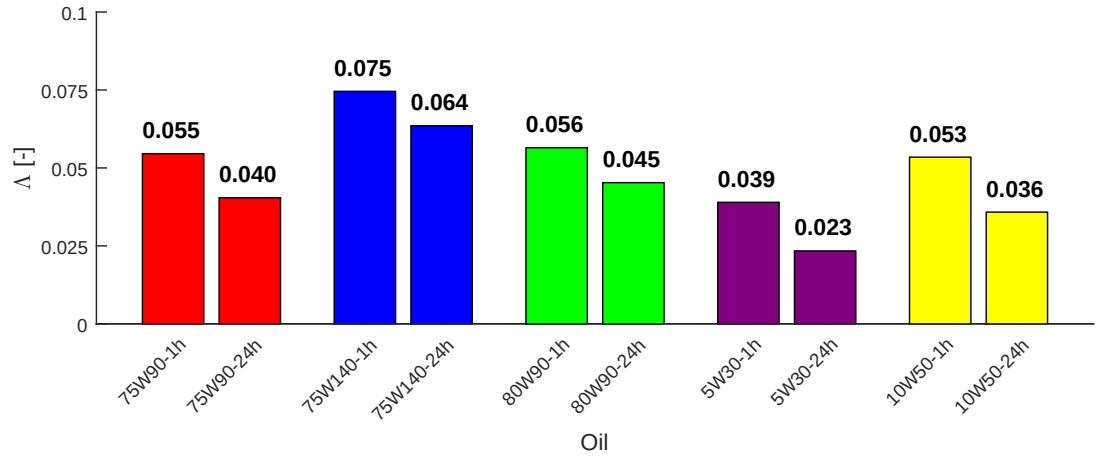

Figure 4.7: Calculated specific film thickness (Λ) at 110 °C after 1h and 24h of test for each oil.

4.1.3.3 Total Friction Torque

In Figure 4.8 is shown the total friction torque for each oil.

For 75W90, 75W140, 80W90 and 5W30 oils, a friction torque reduction was observed after 24h of operation. The results were expected, due to possibility of tribofilm generation. However, for 10W50 oil a small increase of friction torque occurs. The highest reduction 7.5 % was achieved for 75W90 oil and on the opposite, 10W50 oil increase the friction torque by 0.4 % (within torque cell accuracy). 80W90 and 75W140 oils presented similar results for both measurements, which results in identical friction torque reduction, 4.6 % and 5.8 %, respectively.

For both set of measurements, 5W30 oil presented the highest M_t value. This result was expected due to its lowest specific film thickness. On the other hand, the 75W140 oil presented the lowest M_t value after 24 hour.

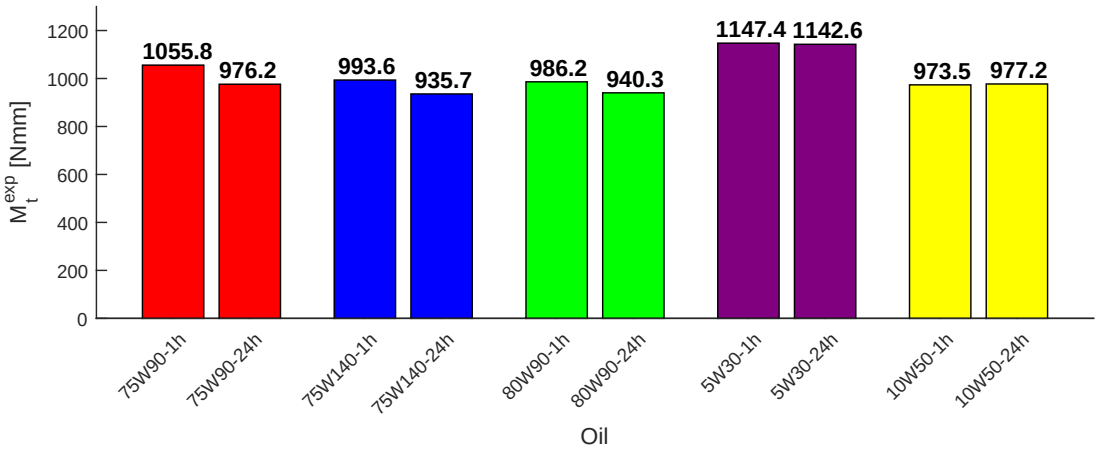

Figure 4.8: Experimental total friction torque (M_t^{exp}) after 1h and 24h of test for each oil.

4.1.3.4 Rolling and Sliding Friction Torque

The SKF friction torque model can be used to determine the rolling and sliding friction torque on a complete RTB (20 rollers). As mentioned in Section 4.1.1, these tests were performed with RTB with only five rollers. To overcome this restriction, experimental friction torque results with a complete RTB 81107 TN for the same oils, temperature, load and rotational speed, obtained by *Hammami* [17] were used.

According to equations (3.37), (3.38) and (3.39) established in Chapter 3.2.2 and knowing the total friction torque for 20 rollers ($M_t^{exp(20rollers)}$), it was possible to determine the rolling torque ($M_{rr}^{20rollers}$) and the experimental sliding torque ($M_{sl}^{exp(20rollers)}$).

In order to establish a relationship between both 20 and 5 rollers experimental total friction torque measurements, it was defined a experimental factor f^{exp}, given by equation (4.1).

$$f^{exp} = \frac{M_t^{exp(5rollers)}}{M_t^{exp(20rollers)}} \tag{4.1}$$

In Table 4.5 are presented the experimental factor for each measurement and oil.

Table 4.5: Experimental factor (f^{exp}) determined by set of performed measurements for each oil.

	Units	Measurement time	75W90	75W140	80W90	5W30	10W50
f^{exp}	[-]	1h	1.06	1.08	1.10	1.25	1.16
		24h	0.98	1.02	1.05	1.24	1.16

Knowing the experimental factor, it was possible to determine the experimental sliding friction torque, according to equation (4.2) and (4.3), assuming that rolling friction torque for five rollers is dependent on the rolling friction torque for twenty rollers and proportional to the experimental factor, given by equation (4.4).

$$M_{sl}^{exp(5rollers)} = f^{exp} \times (M_{rr}^{20rollers} + M_{sl}^{exp(20rollers)}) - M_{rr}^{5rollers} \tag{4.2}$$

$$M_{sl}^{exp(5rollers)} = f^{exp} \times M_{sl}^{exp(20rollers)} \tag{4.3}$$

$$M_{rr}^{5rollers} = f^{exp} \times M_{rr}^{20rollers} \tag{4.4}$$

It is important to note that f^{exp} is very close to one as presented in Table 4.5. On the other hand, it was known that the maximum contact pressure for a line contact is given by equation (4.5).

$$p_{max} = \sqrt{\frac{F_n}{C_F}} \tag{4.5}$$

Where C_F is a auxiliary pressure factor given by equation (4.6).

$$C_F = \frac{\pi \cdot l \cdot R_x}{2 \cdot E^*} \tag{4.6}$$

Since F_n is given by equation (4.7).

$$F_n = \frac{F_a}{z} \tag{4.7}$$

Where z is the number of rollers.

The contact pressure on both rolling bearings with 20 and 5 rollers is given by equations (4.8) and (4.9), respectively.

$$p_{20} = \sqrt{\frac{\frac{F_a}{20}}{C_F}} \tag{4.8}$$

$$p_5 = \sqrt{\frac{\frac{F_a}{5}}{C_F}} \tag{4.9}$$

The relation between the contact pressure with 20 and 5 rollers is expressed by equation (4.10).

$$\frac{p_{20}}{p_5} = \frac{\sqrt{\frac{\frac{F_a}{20}}{C_F}}}{\sqrt{\frac{\frac{F_a}{5}}{C_F}}} = \frac{1}{2} \tag{4.10}$$

Knowing that $M_{sl} = G_{sl} \cdot \mu_{sl}$, the relation between $G_{sl}^{20rollers}$ and $G_{sl}^{5rollers}$ is given by equations (4.11) and (4.12).

$$\frac{G_{sl}^{20}}{G_{sl}^{5}} = \frac{S_1 \cdot d_m^{0.62} \cdot F_a}{S_1 \cdot d_m^{0.62} \cdot F_a} \tag{4.11}$$

$$\frac{G_{sl}^{20}}{G_{sl}^{5}} = \frac{S_1 \cdot d_m^{0.62} \cdot 20 \cdot C_F \cdot p_{20}^2}{S_1 \cdot d_m^{0.62} \cdot 5 \cdot C_F \cdot p_5^2} = 4 \cdot \left(\frac{p_{20}}{p_5}\right)^2 = 4 \cdot \frac{1}{4} = 1 \simeq f^{exp} \tag{4.12}$$

Where F_a is given by equation (4.13).

$$F_a = z \cdot C_F \cdot p_{max}^2 \tag{4.13}$$

In Figure 4.9 are presented the calculated rolling friction torque for a RTB 81107 TN according to equation (4.4). It can be stated that rolling torque can be disregarded in comparison with sliding torque (about 2 % of total friction).

Despite the rolling bearings were running in boundary lubrication film for all the five tested oils and the lubricant viscosity be a property with secondary relevance in this regime, the minor rolling friction torque differences between the tested oils were dependent on this parameter. Also, since the running speed was low, the inlet shear heating (ϕ_{ish}) and the kinematic replenishment/starvation (ϕ_{rs}) factors, did not perform an important role in the rolling friction torque.

In Figure 4.10, it was observed that the experimental sliding friction torque is the major source of friction torque on the RTB. These results occurs, because rolling bearings were running in a boundary film regime ($\Lambda << 1$), revealing the contact interaction between the surface asperities.

75W140 oil presented the lowest sliding friction torque after 24h, and reduced its value in 5.4 % when compared with the 1h measurement. On the opposite, 5W30 oil presented

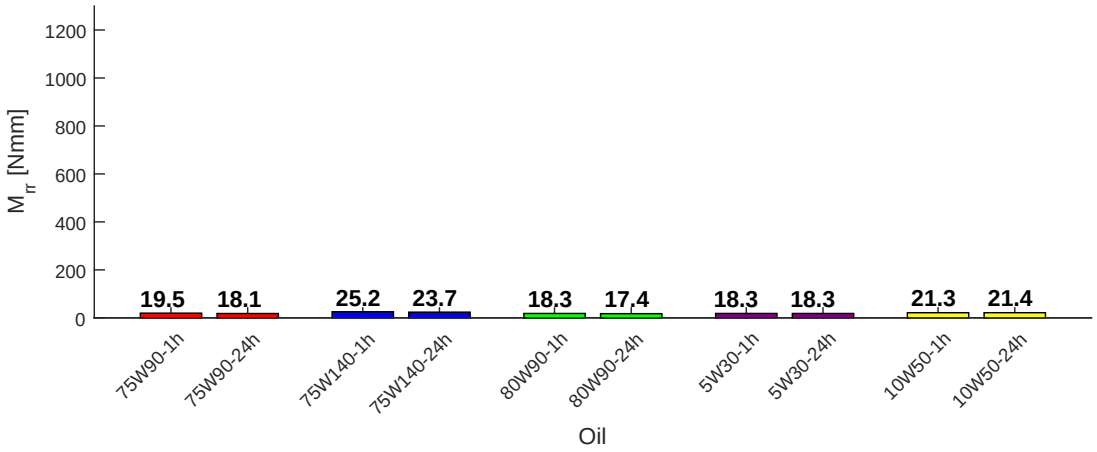

Figure 4.9: Rolling friction torque ($M_{rr}^{5rollers}$) after 1h and 24h of test for each oil.

the highest sliding torque values for both 1h and 24h measurements and the lowest reduction between measurements (0.4 %).

75W140 and 80W90 oils presented identical experimental sliding friction torque values for each set of measurements (1h and 24h). Moreover, the reduction observed on M_{sl}^{exp} for 80W90 oil was 4.6 %, which is lower than the M_{sl}^{exp} reduction obtained for 75W140 oil.

75W90 and 10W50 oils presented closely values for 24h measurements, although higher than 75W140 and 80W90. However, 75W90 oil presented the highest M_{sl}^{exp} reduction (7.5 %) when compared with the measurement at 1h. On the opposite, 10W50 oil presented an increase of sliding friction torque of 0.4 %.

As mentioned in total friction torque analysis, the major friction torque reduction between 1h and 24h tests occured in 75W90 oil, which could indicate a more effective tribofilm generation.

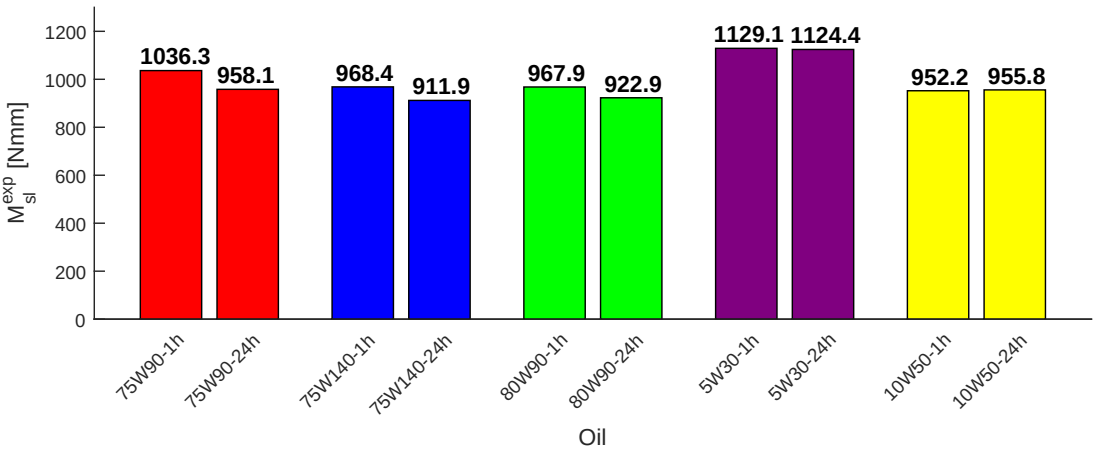

Figure 4.10: Experimental sliding friction torque ($M_{sl}^{exp(5rollers)}$) after 1h and 24h of test for each oil.

4.1.3.5 Sliding Coefficient of Friction

Experimental sliding coefficient of friction was determined according to equation (4.14).

$$\mu_{sl}^{exp} = \frac{M_{sl}^{exp}}{G_{sl}} \tag{4.14}$$

The analysis for sliding coefficient of friction is identical to sliding friction torque.

In Figure 4.11 is shown the change on sliding coefficient of friction from 0.0927 to 0.857 for 75W90 oil. It was the highest reduction observed for all the tested oils.

The sliding coefficient of friction values were found in the range 0.08-0.10, as expected for additised oils under boundary lubrication conditions [36, 39].

The contribution of the reference boundary coefficient of friction for the test was very high, since (ϕ_{bl}) was always close to 1 as shown in Table 4.6.

Table 4.6: Weighting factor (ϕ_{bl}) determined by set of performed measurement for each oil.

	Units	Measurement time	75W90	75W140	80W90	5W30	10W50
ϕ_{bl}	[-]	1h	0.980	0.967	0.986	0.988	0.980
		24h	0.980	0.968	0.985	0.988	0.981

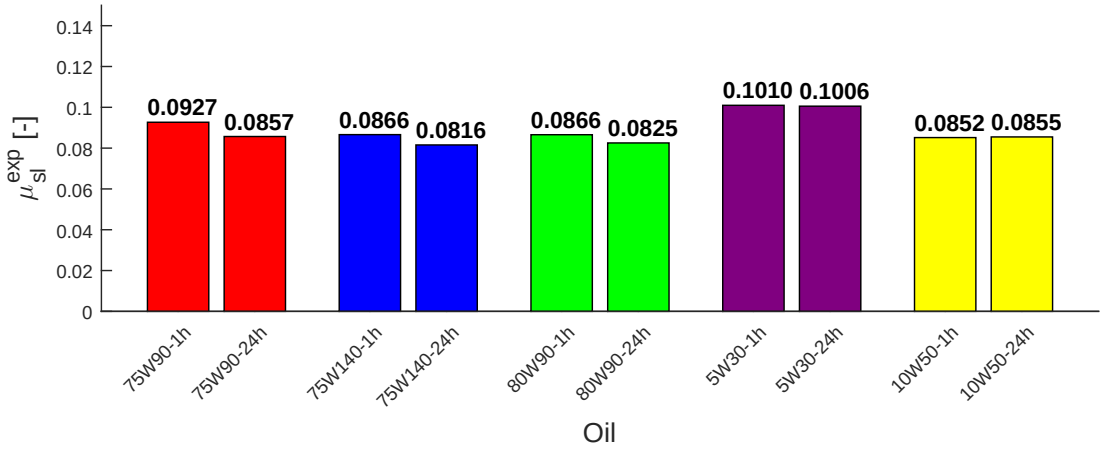

Figure 4.11: Experimental sliding coefficient of friction ($\mu_{sl}^{exp(5rollers)}$) after 1h and 24h of test for each oil.

Comparing 75W90 with 10W50 oils it was observed different coefficient of friction for 1h of test, revealing lower values to 10W50 oil, but similar results to 24h test despite the different additive packages.

For 80W90 oil, it was observed that despite 80W90 have a mineral base, presented lower coefficient of friction than 5W30.

Candidate axle gear oils (5W30 and 10W50) presented similar values for 1h and 24h measurements.

4.2 Roughness Measurements

According to *Mummery* [44], a surface is a boundary between a work-piece and its environment. Apart of its formation method, the surface topography contains irregularities or deviations from the projected nominal surface [45]. This occurs due to a variety of defects and distortions, ranging from bulk distortions to local microscopic irregularities, macro and micro-geometric deviations, having a strong influence on friction, wear and lubrication.

Surface texture includes lay, flaws, form errors, waviness and roughness as shown in Figure 4.12. Normally the principal direction of a surface pattern, lay, is given by the production method. The flaws are discrete interruptions on texture and they are unintentional, unexpected and unwanted. Form errors occurs when the surface presents gross deviations from the nominal shape for a very long wavelength. Considering a measuring length sample, waviness is an irregularity formed by fluctuations on surface with long wavelengths. It may result from machine or work-piece deflections, vibrations, heat treatment or warping strains. Roughness is the finer surface irregularity formed by fluctuations with short wavelength characterized by peaks (asperities) and valleys with different amplitudes and spacings [28].

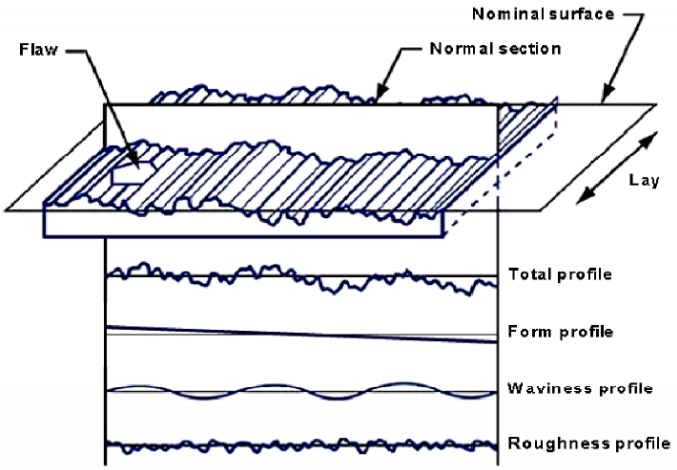

Figure 4.12: Representation of surface texture and profile subdivision [46].

Linear and areal methods are used to acquire the profile or the surface topography. As the name indicates, in linear roughness method, a single line on surface sample is measured, and in areal method a area of surface sample is measured. Data analysis and also both areal and linear parameters are described in Appendix C.

For the most engineering and manufacturing surfaces, two measurements techniques are used to acquire the data surface: contact or non-contact methods [28].

Several instruments are available to measure the surface topography. For this study, it was used 3D optical microscope (BRUKER^{TM}NpFlex), showed in Figure 4.13 which is an optical non-contact equipment.

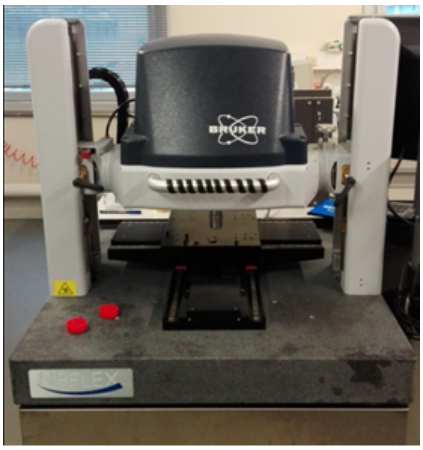

Figure 4.13: Bruker^{TM}NpFlex.

4.2.1 Measurement Procedure

As mentioned in Section 4.2 the measurements were performed with a non contact equipment, using an optical vertical scanning interferometry (VSI) technique.

For surface characterization it was measured only the lower raceway of the rolling bearings, since both raceways are subjected to the same kinematic conditions. For each raceway, one measurement was performed and 3D parameters were analysed, in similar location for all the samples, as shown in Figure 4.14. Then with the same sample area, 2D parameters were analysed in two different locations: one at the centre (L_C) and another at the outer side of the raceway (L_E), at 0.75 mm from the border. The purpose of this approach was to compare the surface condition on a location, where roller-raceway contact occur without slippage (centre location) and the outer side, where it was expected the maximum sliding speed between the roller-raceway contact.

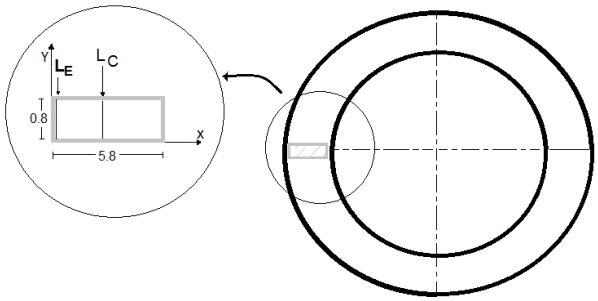

Figure 4.14: Scheme of measurement locations performed on each RTB 81107 TN inferior raceway.

4.2.2 Surface Roughness Results

As mentioned in Section 4.2.1, the surface area was measured, so areal parameters were used to characterize the surface. In this study, it was acquired data from a sample area with 5.8 mm of length (radial direction) and 0.8 mm of width, as shown in Figure 4.14. However, it was also possible for the same surface sample to analyse particular locations with roughness

parameters.

In order to provide a better comprehension of the results obtained for each raceway, the parameters were divided by category, surface and roughness, as presented in Table 4.7 and Table 4.8, respectively.

Comparing S_a and S_q parameters it was observed considerable differences between tested raceways and a new raceway. Except 5W30 raceway, it was verified a decrease of these two parameters for all the test. However, since these parameters represent the entire area, would be interesting to have some roughness information in two different locations: L_C and L_E. Furthermore, for all the raceways, the R_a and R_q values at L_E location were higher than the L_C, revealing the effect of the slippage on surface wear. Taking into account all the tested raceways, it was observed that 5W30 and 10W50 presented higher values in both measurement locations in comparison with the other raceways. These results could indicate a different additive behaviour of package on the surface's wear. On the other hand, 75W140 raceway presented in both locations, the lowest R_a and R_q values from all the lubricants.

S_{sk} parameters allow to differentiate surfaces with identical S_a and S_q as it was the case of 75W90 and 80W90 or 5W30 and 10W50. Taking into account the S_{sk} parameter, it was observed that all the raceways presented negative values, which denotes a higher concentration of material at the top of the surface. However, 75W90 raceway presented a higher value (-0.89) than 80W90 (-0.75), revealing a higher concentration of material on the top of the surface in 75W90 raceway. On 5W30 and 10W50 raceways it was observed, that 5W30 had a higher value of S_{sk} than 10W50 race.

Considering all the raceways, it was verified a decrease in R_{Sk} from L_C location to L_E location. This result was expected since at the L_E location a higher slippage is presented and more surface material was removed being in agreement with the R_z parameter that presented an increase of values for L_E location. The differences in R_z between L_C and L_E locations were more significant for 75W90, 75W140 and 80W90 raceways. The R_z values for both locations were higher for 5W30 and 10W50 races, revealing higher differences between the valleys and the peaks.

Comparing roughness parameters R_{pk} and R_{vk} at both locations, 5W30 and 10W50 raceways presented the highest values for both parameters, revealing the highest peaks and depths above or below the core roughness, which is consistent with R_z results, showing more wear on these surfaces in comparison with 75W90, 75W140 and 80W90. On the other hand, 75W140 raceway revealed the lowest values, no matter the measurement location.

Table 4.7: 3D surface parameters on raceway.

Sample	S_a [μm]	S_q [μm]	S_p [μm]	S_v [μm]	S_z [μm]	S_{sk} [-]	S_{ku} [-]
New	0.144	0.193	1.678	1.982	3.660	-0.62	5.15
75W90	0.120	0.166	1.619	2.050	3.669	-0.89	8.36
75W140	0.088	0.125	1.450	7.006	8.457	-0.89	14.51
80W90	0.122	0.167	2.572	1.932	4.504	-0.75	7.12
5W30	0.159	0.218	1.947	2.981	4.927	-0.92	6.23
10W50	0.139	0.190	2.739	2.210	4.949	-0.68	6.34

Table 4.8: 2D roughness parameters considering two different locations on raceway.

Sample	Position	R_a [μm]	R_q [μm]	R_{max} [μm]	R_z [μm]	R_{sk} [-]	R_{ku} [-]	R_k [μm]	R_{pk} [μm]	R_{vk} [μm]	M_{r1} %	M_{r2} %
New	Centre	0.1215	0.1630	1.4671	1.1651	−0.28	5.54	0.3512	0.2053	0.2381	9.63	86.91
	Exterior	0.1232	0.1680	1.4815	1.1793	−0.54	6.06	0.3452	0.1991	0.2709	9.76	86.37
75W90	Centre	0.0933	0.1325	1.3238	1.0346	−1.20	8.46	0.2419	0.1390	0.2575	9.32	84.59
	Exterior	0.1427	0.1945	1.7889	1.3838	−0.55	6.65	0.4068	0.2349	0.2993	9.69	86.84
75W140	Centre	0.0777	0.1132	1.2964	0.9955	−1.11	10.75	0.2033	0.1386	0.2161	9.41	85.44
	Exterior	0.1018	0.1396	1.3868	1.1194	−0.33	6.78	0.2884	0.1857	0.2130	9.67	86.49
80W90	Centre	0.0947	0.1292	1.1765	0.9087	−0.73	6.67	0.2665	0.1369	0.2246	9.13	86.25
	Exterior	0.1325	0.1761	1.4990	1.1992	−0.33	5.13	0.3875	0.2067	0.2522	9.61	87.03
5W30	Centre	0.1453	0.2032	1.8025	1.5095	−1.16	7.16	0.3897	0.1989	0.3792	8.49	85.17
	Exterior	0.1710	0.2242	1.7663	1.4885	−0.44	4.42	0.4982	0.2351	0.3286	8.72	86.13
10W50	Centre	0.1217	0.1652	1.5359	1.2310	−0.76	6.43	0.3461	0.1790	0.2736	8.48	86.07
	Exterior	0.1501	0.2002	1.6687	1.3980	−0.19	4.81	0.4344	0.2521	0.2764	10.19	86.99

In Figure 4.15, Figure 4.16, Figure 4.17, Figure 4.18, Figure 4.19 and Figure 4.20 are presented the topographies performed for each raceway.

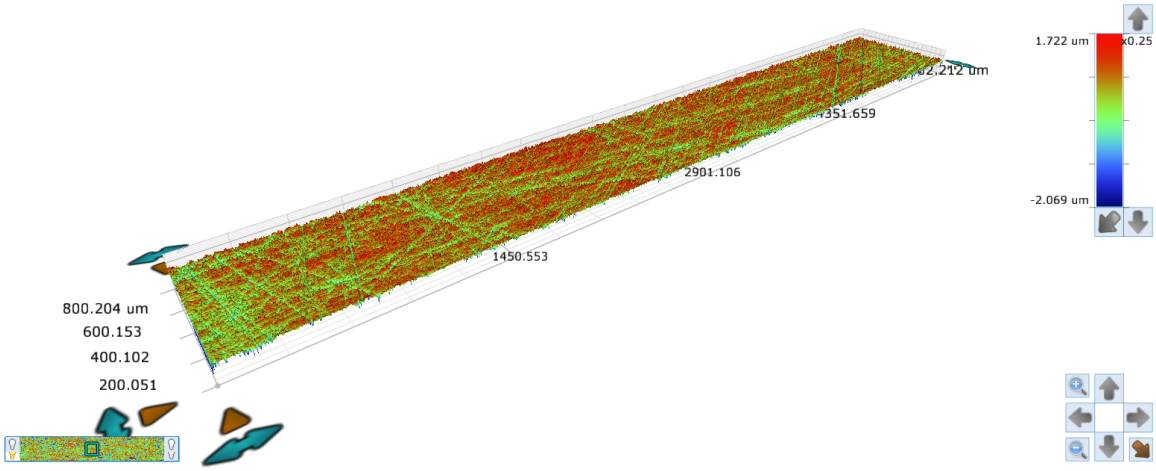

Figure 4.15: New RTB raceway surface.

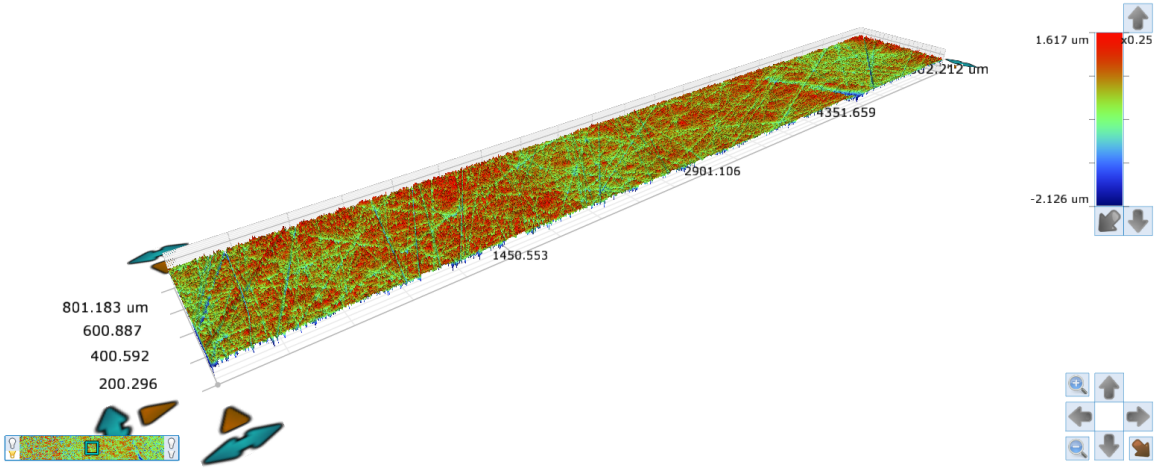

Figure 4.16: RTB raceway surface after 75W90 torque measurements test.

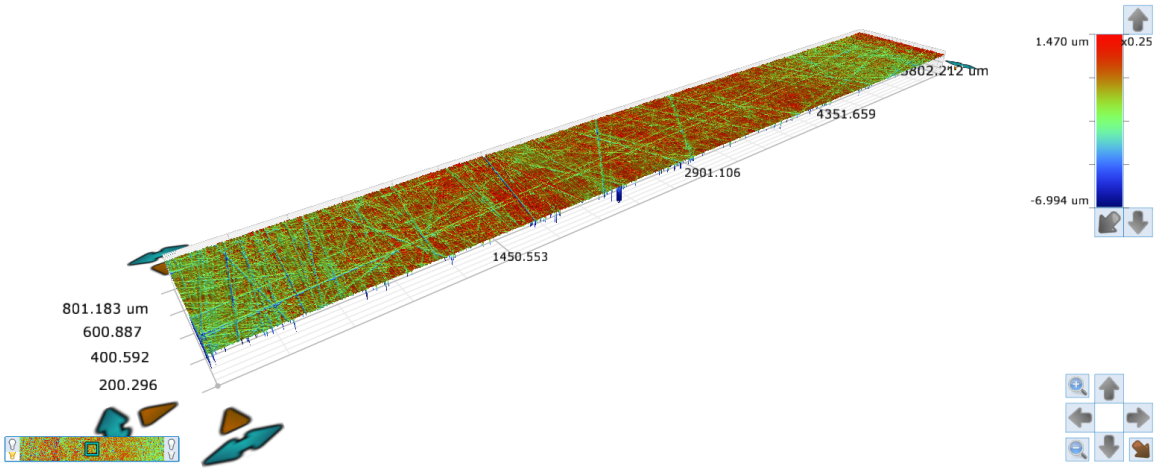

Figure 4.17: RTB raceway surface after 75W140 torque measurements test.

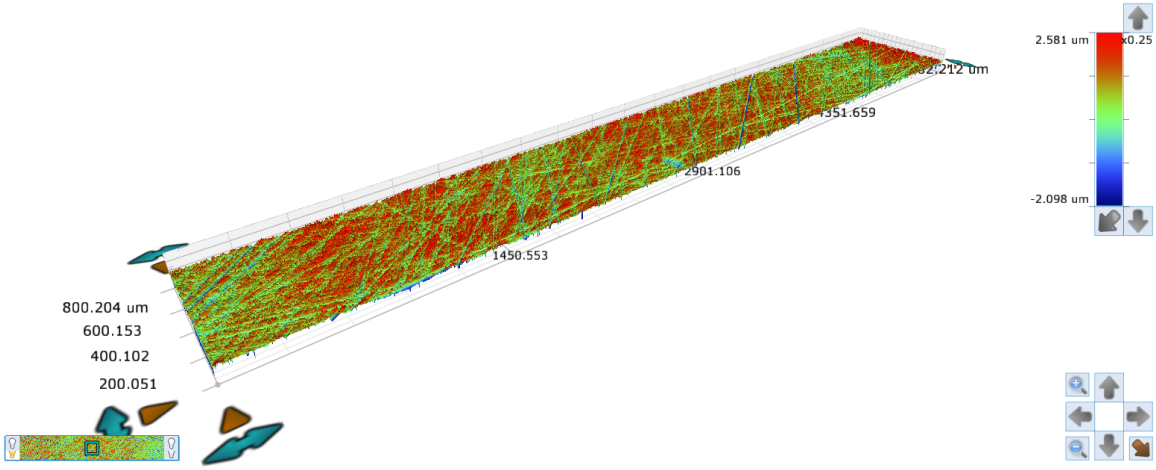

Figure 4.18: RTB raceway surface after 80W90 torque measurements test.

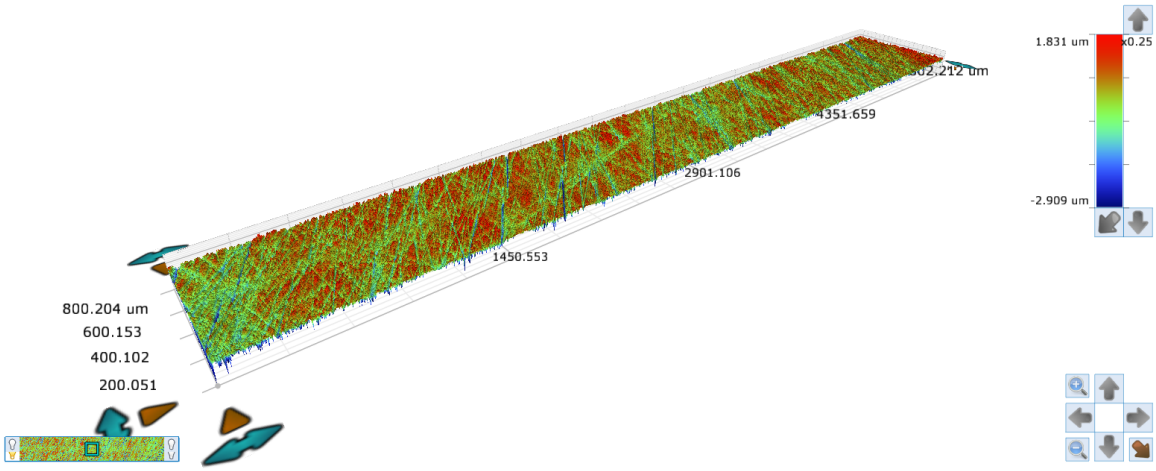

Figure 4.19: RTB raceway surface after 5W30 torque measurements test.

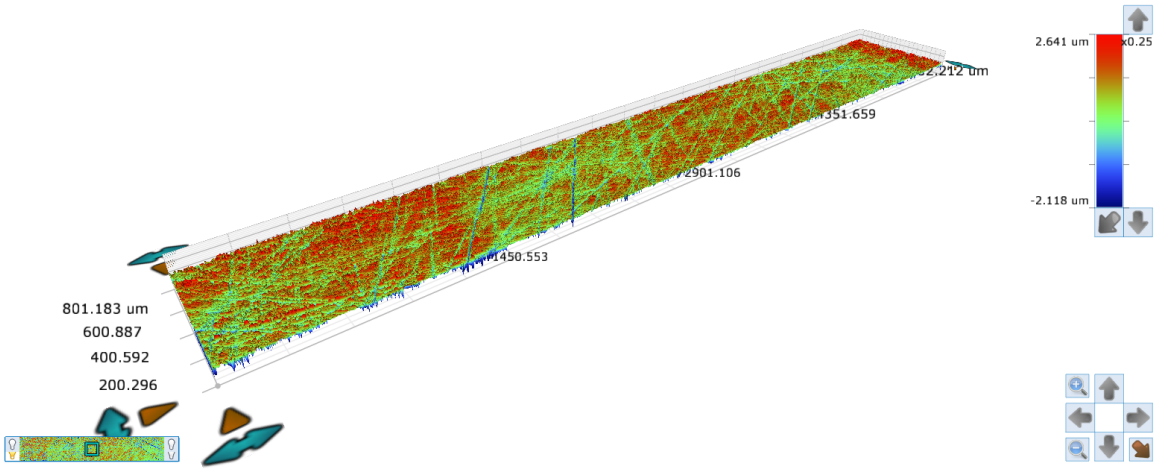

Figure 4.20: RTB raceway surface after 10W50 torque measurements test.

4.3 X-Ray Photoelectron Spectroscopy Measurements

X-Ray Photoelectron Spectroscopy (XPS) also known as Electron Spectroscopy for Chemical Analysis (ESCA), is a sophisticated analytical method to investigate the chemistry of a surface sample. It is a widely used surface analysis technique, due to its relative simplicity in use and data interpretation [47].

Based on photoelectric effect, the photoemission is used as an analytical tool, where the acquired data is represented by a XPS spectra. Figure 4.21 presents a surface sample which is irradiated by low-energy X-ray photons provided by the photon source.

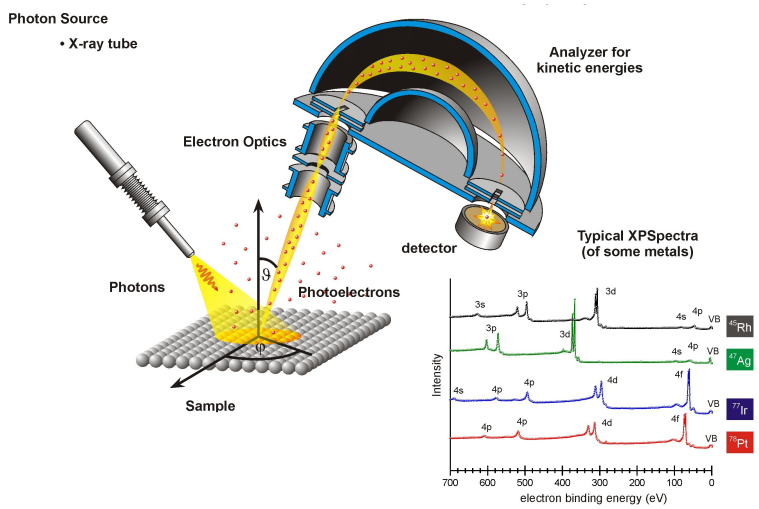

Figure 4.21: Scheme of basic components of XPS instrument [48].

The interaction between the X-ray photons of a specific energy and the sample causes electron

ejections from the chemical elements, located between 0 and 10 nm of depth. An electrostatic analyser detects the emitted electrons, according to their kinetic energy at the entrance of the detector, and by measuring their flux as a function of their kinetic energy, a spectra, representing the sample composition is obtained. In order to enable the emitted electrons to be analysed without interference from gas phase collisions, the entire process is performed under a ultra high vacuum (UHV) chamber ($< 10^{-7}$ Pa), which includes X-ray source, sample, electron analyser and detector equipments [47] [49].

Since XPS is a non-destructive technique, which allows evaluate the surface element composition, it is a excellent method to acquire information about the tribofilm presence at the rolling bearings surface contacts.

4.3.1 XPS Spectra Quantification

XPS is a quantitative technique that establishes a direct correspondence between the number of measured electrons, at a given transition energy, with the number of corresponding chemical elements presented in a surface sample. A XPS spectrum represents the number of electrons recorded at a sequence of energies and is given by intensity, counts per second (CPS), as a function of binding energy in eV. The binding energy is associated to the kinetic energy of a ejected electron, and is given by equation (4.15) [47].

$$E_{be} = h_v - E_{ke} - \Phi \tag{4.15}$$

Where E_{be} is the binding energy, h_v the photon energy, E_{ke}, the ejected electron kinetic energy and Φ the working function.

To evaluate all the interest chemical elements, the process is performed under continuum beam of photons with a known h_v energy, which depends on anode material. Knowing the kinetic energy of the measured emanated electrons, it is possible calculate the binding energy associated to each electron, which is the parameter that defines the atom and the atomic level [49].

To determine the atomic concentration (A_t) of the elements presented in the sample surface, it is necessary evaluate the XPS signal for each range of binding energy, correct the signal intensity dividing by a relative sensitivity factor (RSF), which is specific for each atom and atomic level, and normalized over all of the elements detected.

In XPS spectra are included the contribution from a background signal and also resonance peaks characteristic of the electrons in the surface atoms. However, the resonance peaks above the background are the significant features. Peaks characteristics, such as the intensity or the full width at half maximum (FWHM) are useful indicators. The peak intensity measure how much a material is at the surface and the broadening of the peak could indicates a change in the number of chemical bonds [47].

To make an accurate estimation of the number of the characteristic electrons, the background associated with each peak must be removed. There are several ways to remove the background, however in this section, will be only detailed the linear and the Shirley background.

- Linear background

The removal of a linear background, (Figure 4.22) is simple to implement, however is very sensitive to start and end position points. Its mathematical application is given by equation

(4.16) and is recommended for situations where a small background variation occurs.

$$L(E_{be}) = I_1 \frac{(E_{be2} - E_{be})}{(E_{be2} - E_{be1})} + I_2 \frac{(E_{be} - E_{be1})}{(E_{be2} - E_{be1})} \tag{4.16}$$

Where $L(E_{be})$ is the linear background function, E_{be1} and E_{be2} the energy binding at the start and end points and I_1 and I_2 the intensity at the start and end points.

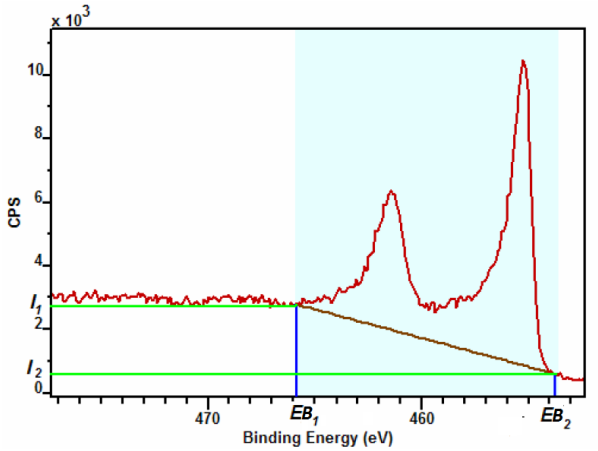

Figure 4.22: Applied linear background [47].

- Shirley background

The Shirley background presented in Figure 4.23 is represented by an S shape background and it involves a iterative determination process that tries to adopt the spectrum information using the areas A_{p1} and A_{p2} to obtain the background intensity $S(E_{be})$, which is proportional to the magnitude of the peak, at binding energy E_{be}:

$$S(E_{be}) = I_2 + (I_1 - I_2) \cdot \frac{(A_{p2}(E_{be}))}{(A_{p1}(E_{be}) + A_{p2}(E_{be}))} \tag{4.17}$$

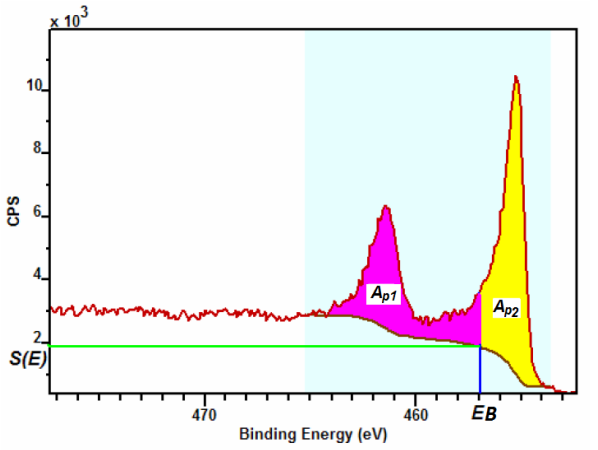

Figure 4.23: Applied linear background [47].

4.3.2 Experimental Procedure

In this study the surfaces were analysed with Kratos Axis Ultra HSA X-ray spectrometer presented in Figure 4.24, from the laboratory of "Unidade de Imagem, Microestrutura e Microanálise" (IMICROS) at "Centro de Materiais da Universidade do Porto" (CEMUP), with the settings presented in Table 4.9.

Figure 4.24: Kratos Axis Ultra HSA.

Table 4.9: Kratos Axis Ultra HSA settings.

X-ray source		Lens Mode	Iris aperture	Charge Neutraliser
Anode	Power			
Al (Monochomator) $h_v = 1486eV$	15 kV @ 150 W	Electrostatic	Slot	On

As stated in section 4.1.1, friction torque tests were performed under specific load, temperature and rotational speed, in order to promote a tribofilm deposition at the contact surfaces. In this study, the XPS measurements were performed on the RTB rollers. Since they are small bodies, it was possible to introduce several samples inside the Kratos Axis Ultra HSA chamber at the same time to perform the measurements. On the other hand, this task would be impossible with the rolling bearing raceways, and it would be necessary cut them, introducing contaminants or distortions to the samples.

To perform a correct tribofilm analysis, it was necessary to measure three different surfaces by XPS: a new clean roller removed from the RTB 81107TN, a tested roller from the friction torque tests and a new roller also removed from the RTB 81107TN, which was immersed in an oil bath at 110 °C for 24 hours (the same temperature and time conditions that the mechanically tested roller). All the rollers were cleaned at the same time, but in different cups, in a petroleum ether ultra sound bath for 10 minutes.

Depending on the roller condition, new, immersed in oil bath or tested, different roller locations were measured. After the friction torque tests, it was verified that for all the tested oils, all the rollers from RTB 81107TN presented a band mark in Z1 region as shown in Figure 4.25.

In order to figure out which differences on tribofilm layer deposition were present along the length of roller, three surface measurements were performed at Z1, Z2 and Z3 regions, as shown in Figure 4.25. Z1 region measurement was performed due to the mark presented in all the rollers. Z2 region, which is located at the opposite side of Z1, at the same distance from the right roller border, when compared with the distance between the Z1 region and the left border. Also a third region Z3 near to the roller border was measured. It was of the best interest that Z3 was precisely at the border, since the contact between the roller and the race didn't not occur. However, due to XPS measurement limitations it was impossible to analyse the border, so the region Z3 near to the border was selected.

On the other hand, for new and immersed rollers, only one measurement was performed at each surface, since both did not present any mark and similar layer was expected along their surface extension. Therefore, no particular region was specified for the rollers, however, this measurements were performed at the same location near the centre.

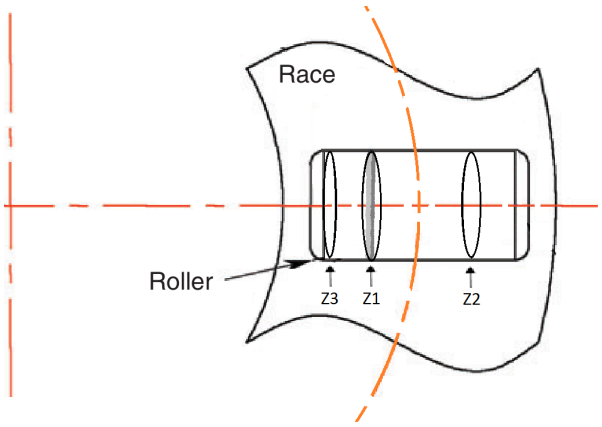

Figure 4.25: Scheme of performed XPS analysis on roller surface.

In all the measurements performed, the acquired data was restricted to a square sample area with 0.7 mm of side.

4.3.3 XPS Results

As mentioned in Section 4.3.2 three different sets of rollers were analysed by XPS at different surfaces regions. For all the analysis, the background presented on spectra were removed using both linear and Shirley background and according with each chemical element detailed spectra, it was applied the background that fitted better the spectra form. The measurement performed on new roller was intended to have the roller surface elements composition as it came from the manufacturer, since any contact occurs with the tested oils.

It was possible to observe in Table 4.10 that in the new roller's surface almost half of the atomic concentration correspond to the carbon, and also more than one third is associated to oxygen. Since the RTB came from the manufacturer previously lubricated, the carbon at these concentrations was related with the contact between the roller and the lubricant. Furthermore, XPS measurements collected information at depth up to 10 nm, so the surface oxidation layer had the major contribution to the spectrum. The hump presented in the spectrum of Figure 4.26 reveal that iron was at the deeper layers of the sample under a thin layer of lubricant's chemical elements.

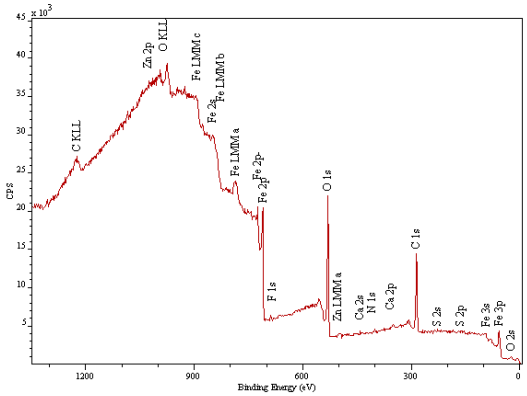

Figure 4.26: XPS spectra on a new RTB 81107 TN roller.

The region Z1 with a contact band, the Z2 at the same distance from left border than Z1 from the right and the Z3 region near the border were measured. Figure 4.27 presents the spectra of those three regions, for measurements performed with 75W90 oil.

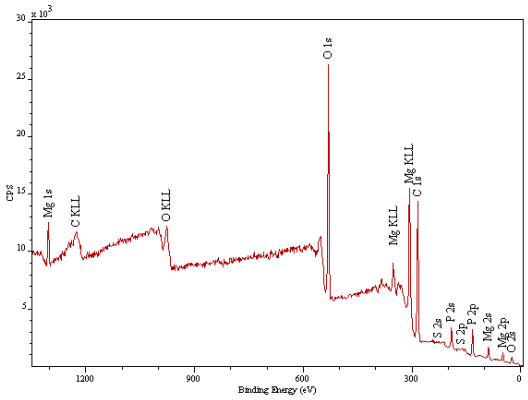

(a) ROI: Z1.

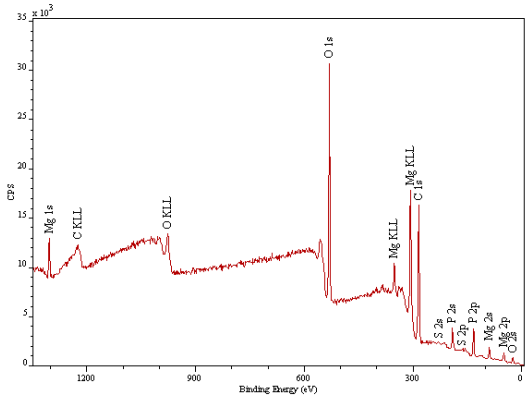

(b) ROI: Z2.

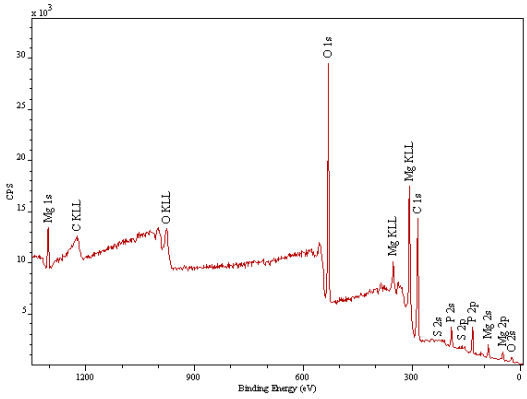

(c) ROI: Z3.

Figure 4.27: XPS spectra on RTB 81107 TN roller in three different locations for test performed with 75W90 oil.

It was observed that no substantial differences were registered, even when Z1 region was compared the with the other zones. For this reason, the tested rollers 75W140, 80W90, 5W30 and 10W50 were performed only in one chosen region, Z1. Moreover, all the detailed spectra of immersed and tested rollers samples are presented in Appendix D.

Taking into account the Table 4.10, higher carbon concentrations were found in all the rollers which were immersed at the oil bath in the oven, when compared with new roller, revealing that oil temperature affects the surface layer composition. The iron element concentration was lower for all the samples, revealing a thick hydrocarbon layer. On 75W90 and 80W90 rollers a small concentration of magnesium and phosphorus appeared, which is in agreement with the oils chemical composition. For 75W140 roller it was verified that magnesium was not shown up. On the other hand, for 5W30 and 10W50 rollers, besides appeared small calcium concentrations, no other elements were revealed.

It was observed in Figure 4.28(a), Figure 4.29(a), Figure 4.31(a) and Figure 4.32(a) that all the spectra presented the hump on the left zone, due to the iron presented on the surface under a layer of hydrocarbons. However for 80W90 roller this hump was less evident, which could be related with greatest oil adhesion to the surface due to the oil polarity.

Comparing the immersed and tested 75W90 rollers, it was possible to observe that the hump disappeared for spectrum of tested roller, which indicates the removal of the lubricant layer (Figure 4.28(b)). The carbon and oxygen concentration were similar to the new roller, as presented in Table 4.10 and the iron concentration decreased. However, higher concentrations in magnesium and phosphorus were registered, which is in agreement with the chemical composition of the oil, revealing the effect of mechanical work on the film deposition on surface.

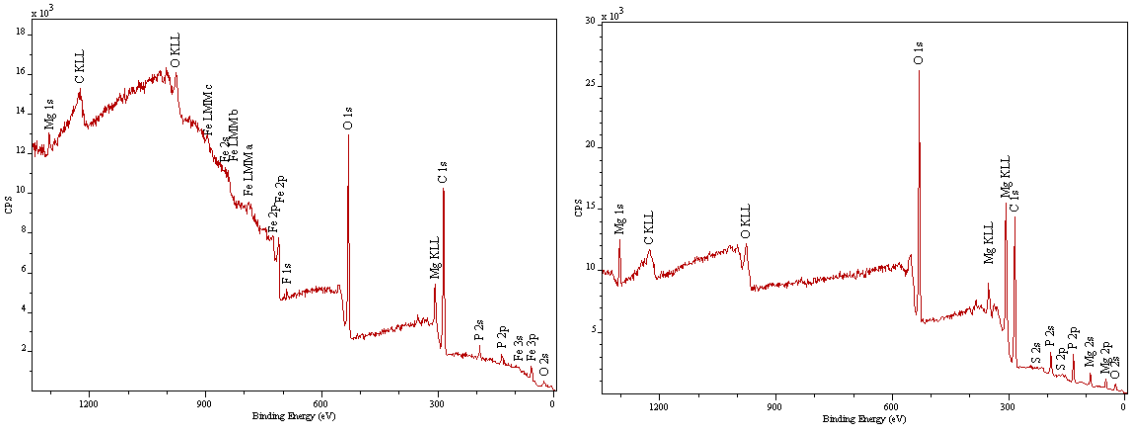

(a) Oven 24h roller.

(b) Tested 24h roller.

Figure 4.28: XPS spectra on RTB 81107 TN immersed and tested rollers, for tests performed with 75W90 oil.

For 75W140 rollers (Figure 4.29), the same conclusion was taken comparing both immersed and tested rollers. It was verified an increase of phosphorus concentration and the magnesium were also found (see Table 4.10). Furthermore, the tribofilm layer was more homogeneous and thicker than observed for in 75W90 case, since the iron element was no longer seen.

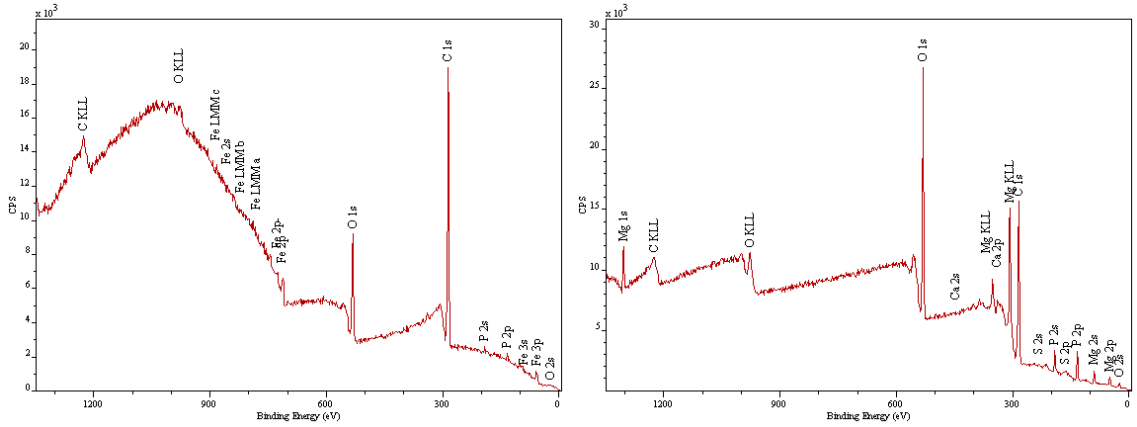

(a) Oven 24h roller. (b) Tested 24h roller.

Figure 4.29: XPS spectra on RTB 81107TN immersed and tested rollers, for tests performed with 75W140 oil.

80W90 surface measurements revealed for tested rollers a concentration increase of magnesium and phosphorus elements and the appear, in a slight concentration, of calcium and zinc (Table 4.10). This result is in agreement with the chemical composition of the oil. In Figure 4.30 are presented both immersed and tested rollers spectra.

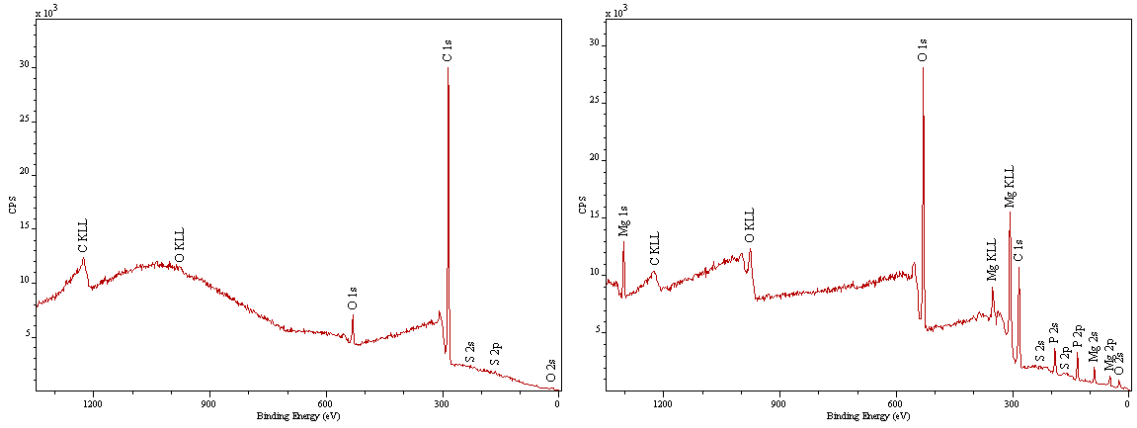

(a) Oven 24h roller. (b) Tested 24h roller.

Figure 4.30: XPS spectra on RTB 81107 TN immersed and tested rollers, for tests performed with 80W90 oil.

The 5W30 and 10W50 tested rollers presented phosphorus and zinc elements. Also, an increase of calcium was shown in both tested rollers in comparison with the immersed rollers. The appear of phosphorus and zinc and the increase of calcium on tested roller reveal the mechanical work effect on tribofilm generation.

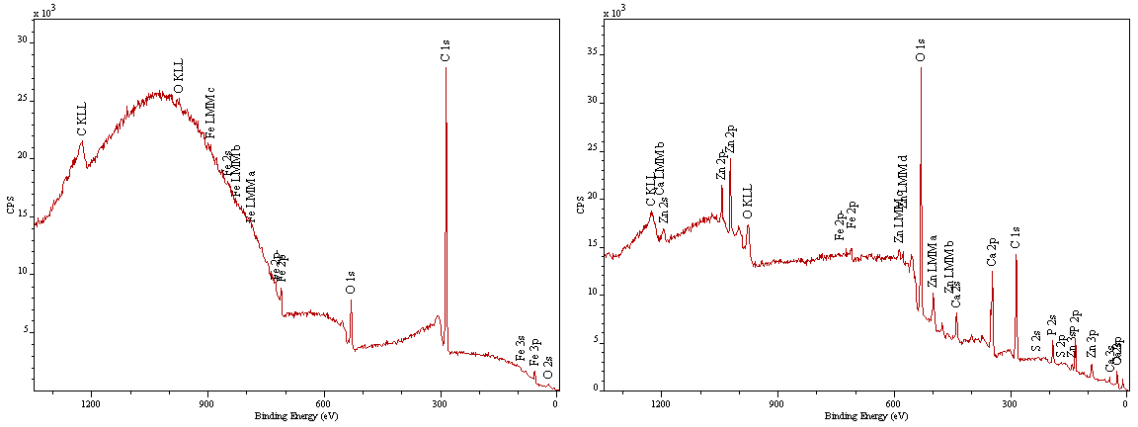

(a) Oven 24h roller. (b) Tested 24h roller.

Figure 4.31: XPS spectra on RTB 81107TN immersed and tested rollers, for tests performed with 5W30 oil.

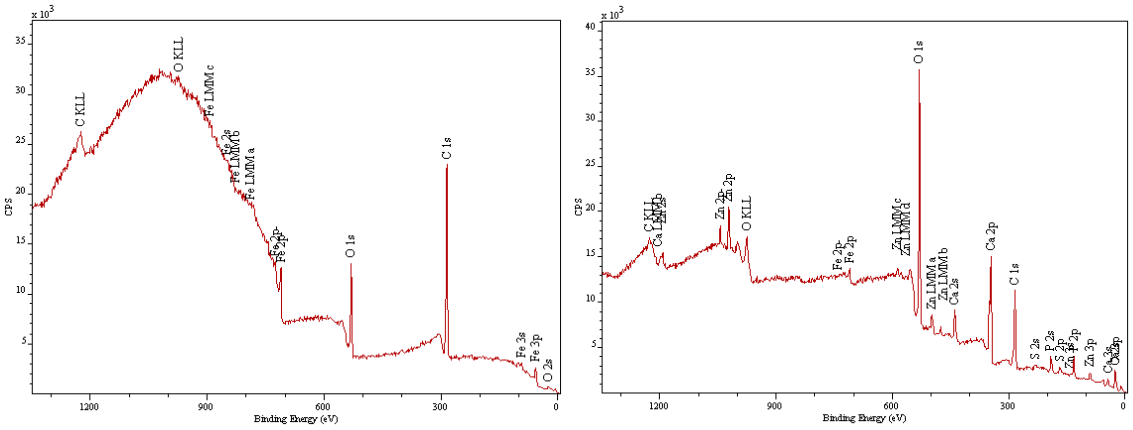

(a) Oven 24h roller. (b) Tested 24h roller.

Figure 4.32: XPS spectra on RTB 81107 TN immersed and tested rollers, for tests performed with 10W50 oil.

Comparing XPS results for 75W90 and 10W50, it was possible to observe that the replacement of magnesium on 75W90 for calcium on 10W50 as detergent additive and the inclusion of zinc as AW/EP additive on 10W50 oil, did not presented differences on sliding coefficient of friction at 24h of test ($\mu_{sl} = 0.086$) on both cases. However, as shown in friction torque results, for axle gear oil 75W90, the tribofilm generation reduced the coefficient of friction at 24h of test in comparison with the measurement performed at the beginning.

It was also observed for 5W30 and 80W90 oils, which present identical kinematic viscosity, that friction torque tests shown higher coefficient of friction for 5W30. The result could be explained by different additive package composition, giving the advantage for 80W90. This behaviour is even more interesting since 80W90 has a mineral base and 5W30 has a synthetic

base.

Despite all the tested surfaces presented tribofilm generation, 5W30 and 10W50 friction torque tests did not shown considerable changes in sliding COF (μ_{sl}) between measurements at 1h and 24h of test.

Table 4.10: Atomic concentration (A_t) and standard deviation (sd) (normalized at 100%) for RTB 81107 TN new, oven 24h (immersed) and tested 24h rollers performed with every oil.

Oil	Roller	Element/ Atomic level																	
		C 1s		O 1s		F 1s		Mg 1s		P 2p		S 2p		Ca 2p		Fe 2p		Zn 2p3	
		R.S.F. 0.278		0.78		2.62		0.486		0.668		1.83		2.96		3.73			
		A_t %	sd %	A_t %	sd %	A_t %	sd %	A_t %	sd %	A_t %	sd %	A_t %	sd %	A_t %	sd σ	A_t %	sd %	A_t %	sd %
-	New	45.13	0.62	34.15	0.48	0.58	0.14	-	-	-	-	1.17	0.68	0.82	0.19	18.14	0.34	-	-
75W90	Oven 24h	**59.69**	0.45	31.85	0.4	-	-	**0.77**	0.09	**2.24**	0.16	0.4	0.09	-	-	5.04	0.21	-	-
	Test 24h	48.83	0.39	**40.47**	0.35	-	-	**2.58**	0.06	**7.15**	0.11	0.45	0.08	-	-	0.52	0.16	-	-
75W140	Oven 24h	**78.26**	0.41	18.29	0.33	-	-	-	-	**1.33**	0.16	0.23	0.1	-	-	1.89	0.25	-	-
	Test 24h	53.79	0.36	**37.07**	0.33	-	-	**2.24**	0.05	**6.38**	0.1	0.5	0.08	-	-	-	-	-	-
80W90	Oven 24h	**93.65**	0.31	4.94	0.27	-	-	**0.15**	0.05	**0.48**	0.09	0.51	0.08	-	-	0.27	0.1	-	-
	Test 24h	39.11	0.43	**47.41**	0.38	-	-	**3.88**	0.06	**7.58**	0.11	0.6	0.08	**0.39**	0.04	0.39	0.04	**0.07**	0.04
5W30	Oven 24h	**87.97**	0.34	9.7	0.29	-	-	-	-	-	-	0.13	0.1	**0.44**	0.06	1.75	0.18	-	-
	Test 24h	38.87	0.46	**40.37**	0.39	-	-	-	-	**8.75**	0.13	1.21	0.1	**7.68**	0.08	0.83	0.24	**2.3**	0.09
10W50	Oven 24h	**72.65**	0.37	21.02	0.33	-	-	-	-	-	-	-	-	**0.49**	0.06	5.69	0.18	-	-
	Test 24h	35.01	0.42	**44.24**	0.35	-	-	-	-	**5.91**	0.12	2.01	0.09	**10.23**	0.09	1.29	0.18	**1.32**	0.18

4.4 Ferrography

Surface wear is always present in moving parts and regardless the wear mechanisms, different wear particles (debris) are generated. These particles, with distinct sizes, shapes, surface morphologies and colours, contain critical information on contact surfaces condition [50,51].

Ferrography is a sensitive and successful monitoring technique on the wear state of engineering systems. It is a method of particle separation based upon the interaction between an external magnetic field and the magnetic particles present in the lubricant [50].

Two ferrographic examination technique types may be performed depending on the study target. Determine the debris quantity and size are the first priority tests to recognize the severity of wear rate. Direct reading (DR) ferrography allows to evaluate quantitatively the concentration of ferrous particles in the lubricant. Analytical ferrography allows to determine the type and source of wear particles and also quantify its size [52].

In Figure 4.33 is shown the wear debris examination possibilities, and the relationship between the particles features and the wear characteristics.

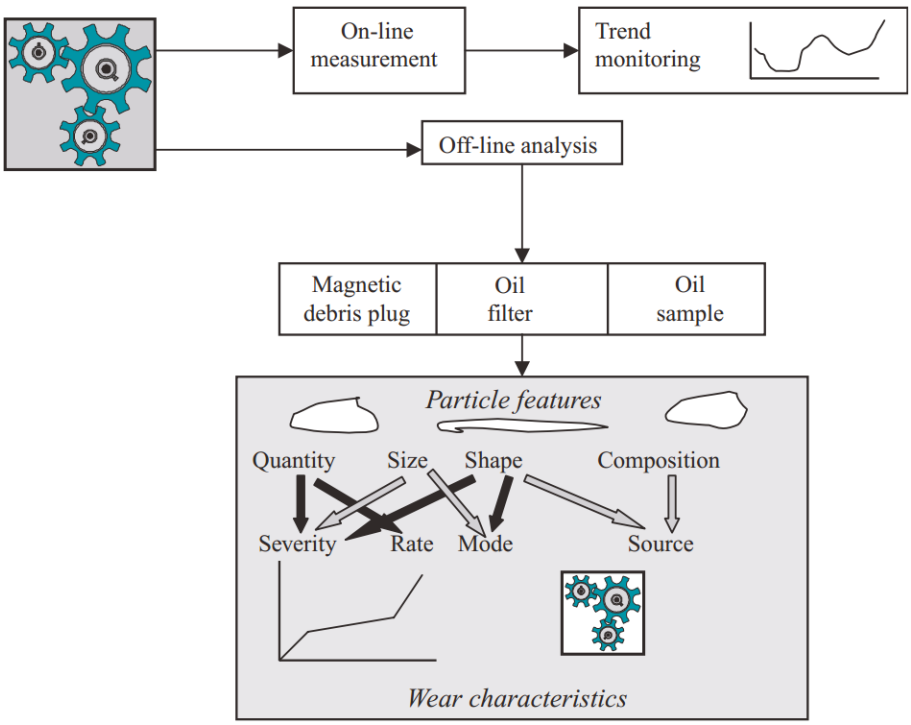

Figure 4.33: Basic components of wear debris analysis: characteristics and relationship to wear [52].

4.4.1 Direct Reading Ferrography

In order to measure the concentration of ferrous wear debris in used oil samples, and comparing the amount of particles among them, a Direct Reading Ferrograph (DR-III) was used, Figure 4.34.

An oil sample with 1 ml is flowed through a capillary tube, which is subjected to a powerful magnetic field. The particles are deposited along the tube by sedimentation or due

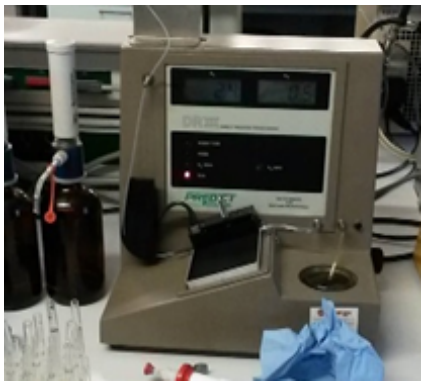

Figure 4.34: DR-III Direct reading ferrograph.

to the effect of the magnetic field, as shown in Figure 4.35 [53]. Larger particles, more than 5 μm, are the first to be deposited and are located in the beginning of the tube. Along the capillary length the particle size will reduce [54].

The optical system, composed by two light beams and optical detectors disposed in different locations, measure the light intensity across the capillary section and quantify the particle concentration, which is inversely proportional to the light intensity. Two values are measured D_L and D_S in DR-III. D_L index is related with the light/optical sensor assembled in the beginning of the tube and represent the concentration of bigger particles($> 5\mu m$). D_S, on the other hand, represents the concentration of smaller particles and is associated to light/optical sensor disposed at the end of the tube.

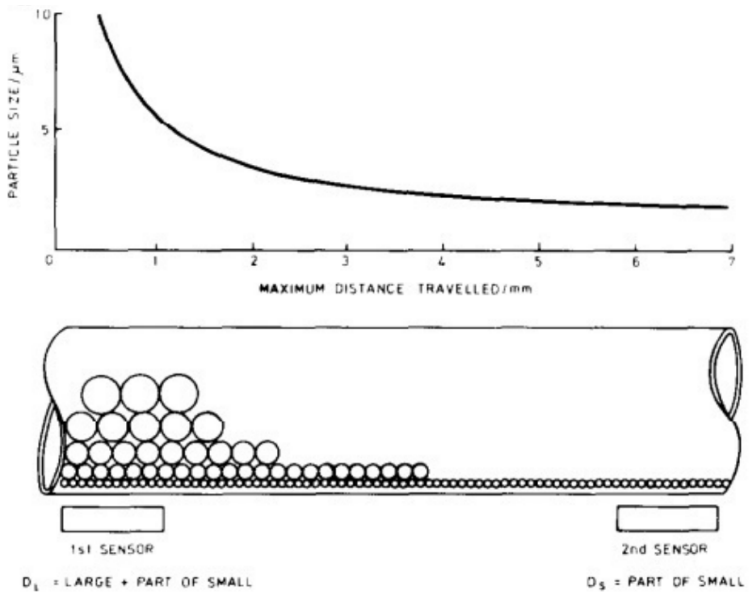

Figure 4.35: Deposit formation scheme [54].

Knowing the large D_L and small D_S particle indexes, it is possible to calculate three wear indexes: Wear Particle Concentration (CPUC), Severity of Wear Particles (ISUC) and

Percentage of Large Particles (PLP), given by equations (4.18), (4.19) and (4.20), respectively.

$$CPUC = \frac{D_L + D_S}{d_l} \tag{4.18}$$

$$ISUC = \frac{D_L^2 - D_S^2}{d_l^2} \tag{4.19}$$

$$PLP = \frac{100 \times (D_L - D_S)}{D_L + D_S} \tag{4.20}$$

To perform the DR ferrography analysis, both D_L and D_S indexes must be lower than 100. These values were guaranteed with a proper sample dilution. The parameter d_l represents the dilution factor and it was defined according to the oil particles contamination. If the sample had lower visible particles no dilution would be necessary. However, since the oil stored in the recipient shown deposited particles in the bottom, a dilution was done and the d_l was 0.1.

To perform the DR ferrography analysis, the oil samples were prepared and analysed according to the procedure described by *Graça et Seabra* [53].

4.4.1.1 Direct Reading Ferrography Results

The dilution factor, the results of D_L and D_S indexes and the calculated CPUC, ISUC and PLP indexes are presented in Table 4.11 .

Table 4.11: Direct reading ferrography results.

Factor/Parameter	Units	75W90	75W140	80W90	5W30	10W50
d_l	[-]	0.1	0.1	0.1	0.1	0.1
D_L	[-]	16.7	18.6	25.5	53.9	35
D_S	[-]	10.5	7.9	21.0	21.8	21.5
CPUC	[-]	272	265	465	757	565
ISUC	[-]	16864	28355	20925	242997	76275
PLP	[-]	22.8	40.4	9.7	42.4	23.9

It was observed that despite all the samples were diluted, high values of D_L and D_S were presented, which are associated to high wear rates. Axle gear oils 75W90 and 75W140 had the lowest wear particle concentration (CPUC). On the opposite, the oils 5W30 and 10W50 presented the highest CPUC, which is in agreement with the roughness results, that shown higher S_a and S_q values for 5W30 and 10W50 races. Thus, for 5W30 and 10W50 oils the wear severity (ISUC) was much higher than the other three oils. In particular, the 10W50 oil presented an ISUC four times higher than the 75W90 oil. It should be noted that, the main difference between the 10W50 and 75W90 oils is the additive package.

The 80W90 oil had the lowest PLP from all oils on the opposite to 5W30 oil. Furthermore, 5W30 oil presented a higher CPUC value than the 80W90 oil and a ISUC 11 times higher. This was a curious result, since 80W90 is a mineral base oil and 5W30 a synthetic base oil. Also, both oils had similar viscosity and the main difference is the additive package, which reveals in the 80W90 oil be much effective on surface protection.

It was clear that 75W140 had the highest surface protection effect from all the oils, since presented the lowest CPUC.

4.4.2 Analytical Ferrography

In analytical ferrography, a qualitative analysis describes the morphology characteristics of wear particles, relating them with its generation cause [55].

To perform this analysis, a ferrograph (FM-III) shown in Figure 4.36(a) was used to prepare the sample which was observed in a microscope. As in DR ferrography, it was applied a magnetic field to attract the wear particles. But in this case, the oil sample was pumped into a microscope slide, the ferrogram. The ferrogram was mounted above two permanent magnets, which attract the ferrous particles out of the oil flow, due to the the strong downward force, as shown in Figure 4.36(b). These particles are deposited in strings perpendicular to flow direction. After all the oil sample flows, in a 0.25 ml per minute rate, over the ferrogram, a solution of Tetrafluor Chloroethylene was pumped and flows over the ferrogram to fix the particles [51, 55]. The largest ferrous particles were deposited on the entry of the ferrogram where the oil first touches the glass slide. Along the ferrogram length, smaller ferrous particles can be found. Furthermore, non ferrous particles as copper and aluminium alloys or friction polymers were retained in the ferrogram, due to the acquired magnetism as a result of friction interaction with ferrous particles, or by gravity effect. On the opposite of ferrous particles, these were randomly deposited and did not acquire a specific orientation [56] .

To perform the ferrogram preparation, *Graça et Seabra* [56] procedure was followed.

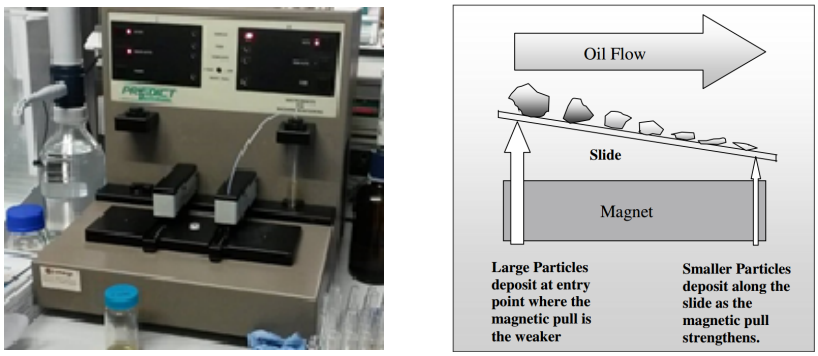

(a) Analytical FM-III ferrograph. (b) Ferrogram preparation [55].

Figure 4.36: Analytical ferrography: ferrogram preparation equipment.

An optical microscope with bichromatic lights (transmitted and reflected) (FERROSCOPE IV CH-2) was used to examine the ferrogram. Depending on the light scheme: filtered white, red or polarized reflected and filtered green or no light transmitted sources may be used to acquire the ferrogram particle information. The lighting scheme used was filtered white reflected and filtered green transmitted, and shows the metallic particles as shinning and non-metallic particles as green. Different magnification lenses, presented in Table 4.12, were available. The MA 10 lens was used to collect information from a great area and the the MA 50 lens was used to reveal particle details as size, shape and surface morphology. To acquire the photographic images a camera (OLYMPUS C-35DA-2) was mounted on the microscope, with a 2x magnification [51, 56].

4.4.2.1 Analytical Ferrography Results

The captured micro-photographies obtained in ferrogram analysis on the FERROSCOPE IV CH-2 were grouped in three figures giving an general overview of the results.

Table 4.12: Lenses available on FERROSCOPE IV CH-2.

Lens	Magnification	Total magnification
MA 10	10x	100x
MA 50	50x	500x
MA Plan 80	80x	800x

In Figure 4.37 it was observed that for oils 75W90, 75W140 and 80W90 were presented large particles at the core of the ferrogram, revealing a severe wear for the tested conditions. Furthermore, in both 5W30 and 10W50 analysis it was observed in Figures 4.37(d) and 4.37(e), respectively, a high concentration of medium size particles (> 5 μm), revealing an excessive wear. The concentration of particles verified was expected since DR ferrography analysis presented the highest values of CPUC, for 5W30 and 10W50.

For 75W140 oil samples it was observed dispersed medium and large particles, shown in Figure 4.37(b). This analysis confirms the results obtained for DR ferrography, which revealed low CPUC but high PLP. The same analysis could be done to 75W90 and 80W90 oils. In the 80W90 sample it was observed more small wear particles (Figure 4.37(c)) as expected due to the PLP result.

The sliding wear particle observed for 75W90 sample in Figure 4.38(a) was a consequence of high sliding speed in the roller-raceway contact.

The fatigue wear particles observed in 75W140 and 80W90 analysis, showed in Figure 4.38(b) and Figure 4.38(c) are a result of high cyclical stress in surfaces, due to the high pressure in rolling contacts.

For 75W90, 80W90 and 10W50 oil samples, corrosion wear particles were observed, as shown in Figure 4.39(a) and 4.39(b), 4.39(c), respectively.

In Appendix E is presented a full album of the micro-photographies obtained in ferrogram analysis grouped by oil.

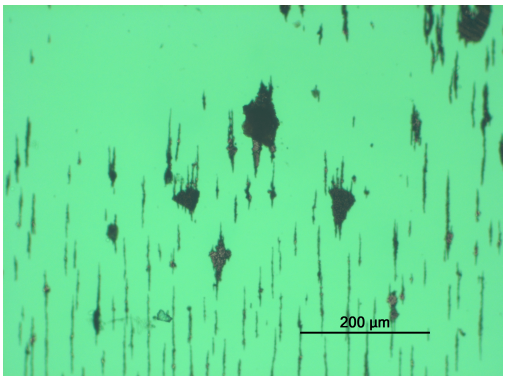

(a)

Oil: 75W90
Magnification: 200x Dilution: 0.01
Local: Core Light: White/Green
Description: Small and large ferrous particles.

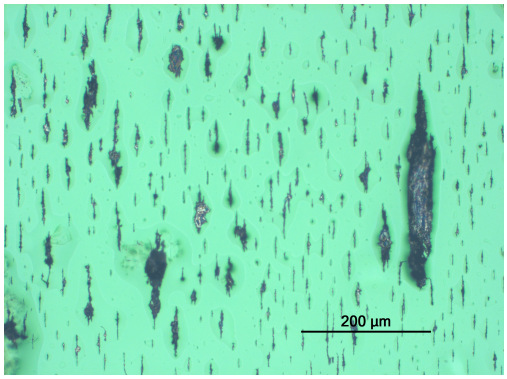

(b)

Oil: 75W140
Magnification: 200x Dilution: 0.01
Local: Core Light: White/Green
Description: Medium and large ferrous particles.

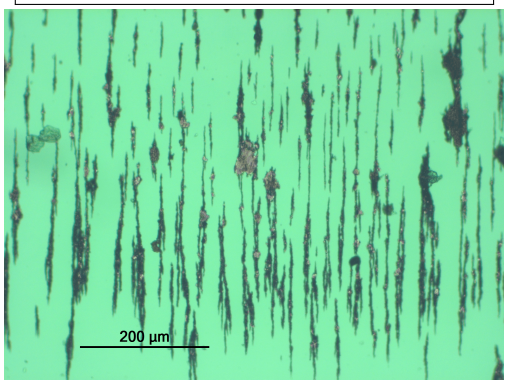

(c)

Oil: 80W90
Magnification: 200x Dilution: 0.01
Local: Core Light: White/Green
Description: Medium and large ferrous particles.

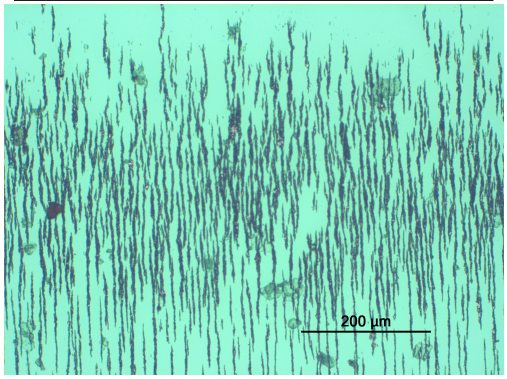

(d)

Oil: 5W30
Magnification: 200x Dilution: 0.01
Local: Core Light: White/Green
Description: Few large particles and medium ferrous particles.

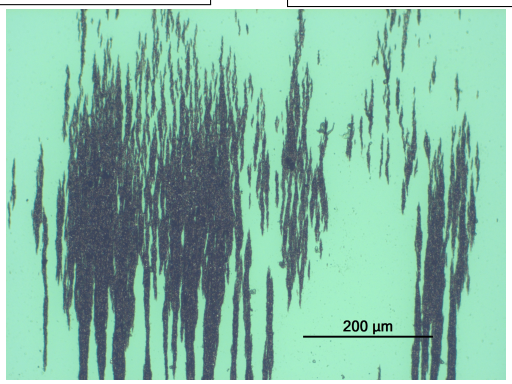

(e)

Oil: 10W50
Magnification: 200x Dilution: 0.01
Local: Midle Light: White/Green
Description: Medium wear particles agglomerated.

Figure 4.37: Analytical ferrography: overview pictures.

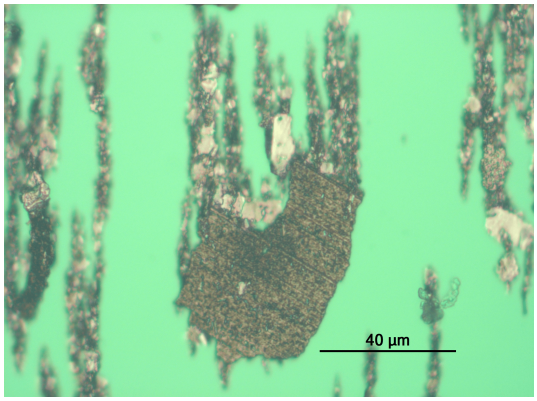

(a)

Oil: 75W90	
Magnification: 1000x	Dilution: 0.01
Local: Core	Light: White/Green
Description: Magnification of Figure 4.37(a). Large ferrous particle resulting of severe sliding wear.	

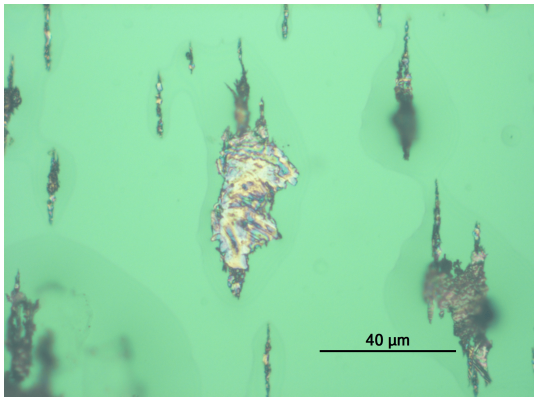

(b)

Oil: 75W140	
Magnification: 1000x	Dilution: 0.01
Local: Core	Light: White/Green
Description: Magnification of Figure 4.37(b). Large ferrous particle resulting from fatigue wear.	

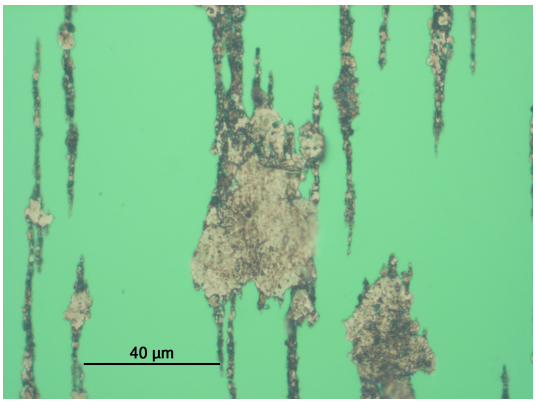

(c)

Oil: 80W90	
Magnification: 1000x	Dilution: 0.01
Local: Core	Light: White/Green
Description: Magnification of Figure 4.37(c). Large ferrous particle resulting of fatigue wear.	

Figure 4.38: Analytical ferrography: detail core pictures.

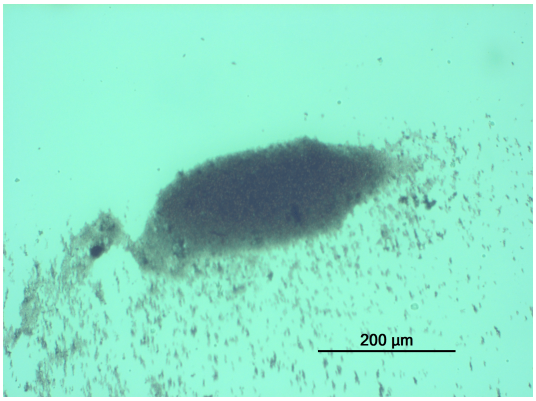

(a)

Oil: 75W90	
Magnification: 200x	Dilution: 0.01
Local: End	Light: White/Green
Description: Small wear particles cloud.	

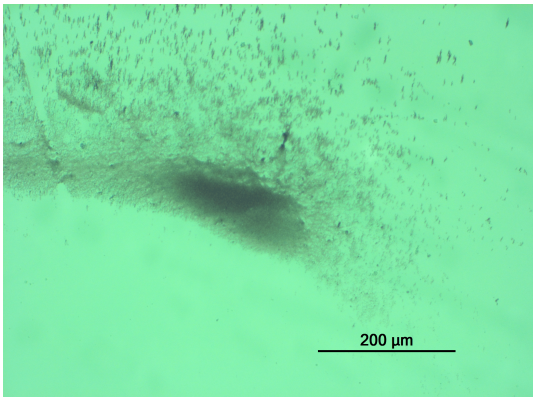

(b)

Oil: 80W90	
Magnification: 200x	Dilution: 0.01
Local: End	Light: White/Green
Description: Small wear particles cloud.	

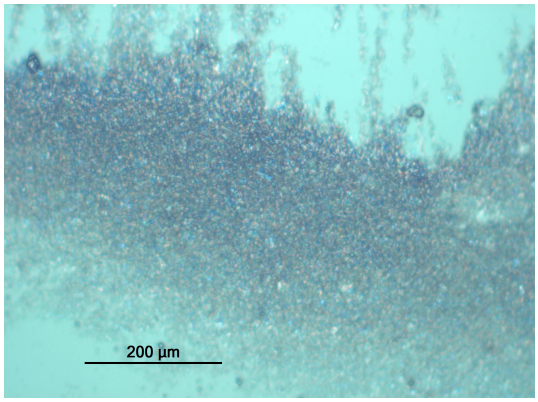

(c)

Oil: 10W50	
Magnification: 200x	Dilution: 0.01
Local: End	Light: White/Green
Description: Small wear particles indicating corrosive wear.	

Figure 4.39: Analytical ferrography: end of ferrogram.

Chapter 5

Torque Loss in Tapered Roller Bearings

The main purpose of this thesis is the evaluation of tapered roller bearings power loss, used in rear axle differentials. In order to understand the problem underlying variables and implement representative test rigs, it was made a preliminary analysis, to identify operating conditions of rear axle differentials.

5.1 A Light-Duty Differential

It was selected a BMW 7599469-02 differential, from a BMW F30 318d presented in Figure 5.1(a) and 5.1(b), with a transmission ratio of 1:3.231.

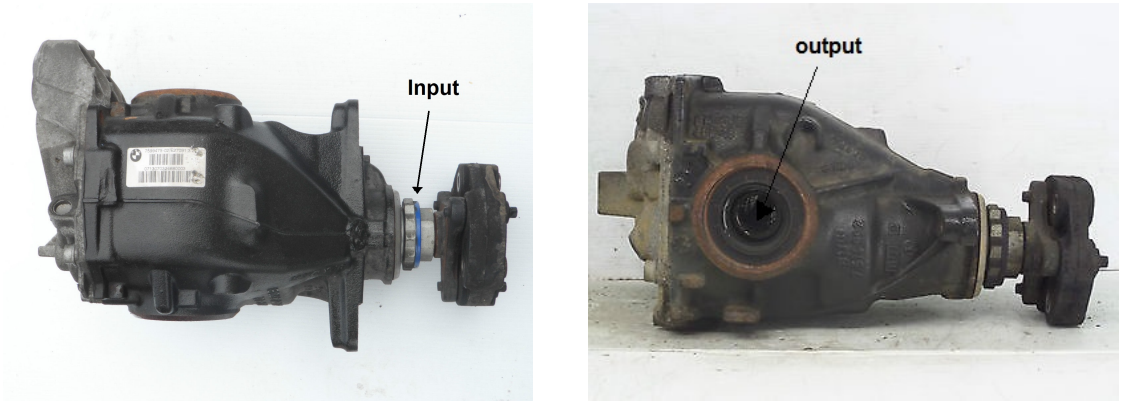

(a) Top view. (b) Front view.

Figure 5.1: BMW 7599469-02 differential.

5.1.1 Typical Operating Conditions

To obtain the meshing and rolling bearing loads, it was necessary to know the range of input torque and speed. In Appendix F, Figure F.1 shows the engine torque (T_{eng}) and the expected power (P_{eng}) diagram of a BMW 318d. The engine range of output torque is 225 up to 320 Nm, between 1000 and 4250 rpm. On the engine output is assembled a gearbox that

provides the speed and torque desired for the input differential shaft. The gearbox and final drive ratios are presented in Table 5.1.

Table 5.1: Gearbox and differential ratios [57].

	1	2	3	4	5	6	Reverse	Final Drive
Gear ratio	4.002	2.109	1.388	1	0.781	0.645	3.647	3.231
Overhall	12.93	6.81	4.48	3.231	2.52	2.08	11.78	-

Two different engine operating conditions were considered as shown in Table 5.2.

Table 5.2: Output engine conditions.

	Units	Engine condition 1	Engine condition 2
Torque T_{engine}	[Nm]	250	320
Speed N_{engine}	[rpm]	1500	3000

Since the gearbox ratio was known in advance and the output engine conditions were also specified, it was calculated the speed and torque conditions of the differential input shaft. The input torque and speed are shown in Table 5.3 and given by equation (5.1) and equation (5.2), respectively.

$$T_{in} = T_{eng} \cdot i_{gb} \tag{5.1}$$

$$N_{in} = \frac{N_{eng}}{i_{gb}} \tag{5.2}$$

Table 5.3: Input and output differential shafts torque and rotational speed.

Shifts	Engine condition 1 250Nm @ 1500rpm[1]				Engine condition 2 320Nm @ 3000rpm[2]			
	Input shaft		Output shaft		Input shaft		Output shaft	
	Torque [Nm]	Speed [rpm]	Torque [Nm]	Speed [rpm]	Torque [Nm]	Speed [rpm]	Torque [Nm]	Speed [rpm]
1	1000	374	3232	116	1280	749	4138	232
2	527	711	1703	220	674	1422	2180	440
3	347	1080	1121	334	444	2161	1435	669
4	250	1500	807	464	320	3000	1033	928
5	195	1920	630	594	249	3841	807	1188
6	161	2325	521	719	206	4651	666	1439
Reverse	-	-	-	-	1167	822	3770	254

[1] not full load
[2] full load

5.1.2 Rolling Bearings Operating Conditions

The real operating conditions of rolling bearings in a light-duty vehicle differential were collected to define the tests performed in laboratory.

5.1.2.1 Oil Operating Temperature

An Environmental Protection Agency (EPA) driving cycle test suggests that oil temperatures varies between 21 °C and 77 °C. Furthermore during a urban cycle the temperature rises from 21 °C to 50 °C, and in a highway cycle from 50 °C to 77 °C. However, in certain real life conditions, at fully rated axle capacity the temperatures can be far higher (more than 100 °C) [58].

5.1.2.2 Rolling Bearing Load

The loads or the pressure in the line contact between the raceway and the roller is a key parameter to design the experimental procedure. All the calculations made to obtain the contact pressure at the tapered roller bearing contact are presented in the Appendix F, and the light duty differential TRB's are presented in Table 5.4.

Table 5.4: Rolling bearings of light duty differential: main characteristics [9].

Bearing	Designation	Principal Dimensions			Basic load ratings		Dimensions		Calculation factors			No. Rollers
		d	D	T	C	C_0	d_1	C	e	Y	Y_0	z
		[mm]	[mm]	[mm]	[kN]	[kN]	[mm]	[mm]	–	–	–	–
A	32310 J2/Q	45	110	42.25	172	212	77.8	33	0.35	1.7	0.9	16
B	32308 J2/Q	40	90	35.25	117	140	62.9	27	0.35	1.7	0.9	16
C/D	32309 J2/Q	45	100	38.25	140	170	71.1	30	0.35	1.7	0.9	16

Figure 5.2 presents the location of TRB on the differential and on the free body diagram presented in Figure 5.3 are given the loads applied on rolling bearings (A, B, C and D) and the meshing point (M).

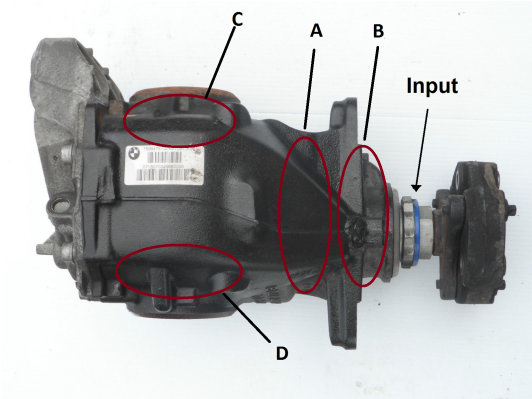

Figure 5.2: Vehicle moving forward.

In Figure 5.4 is presented the maximum pressure results by gearbox shift and condition for each rolling bearing.

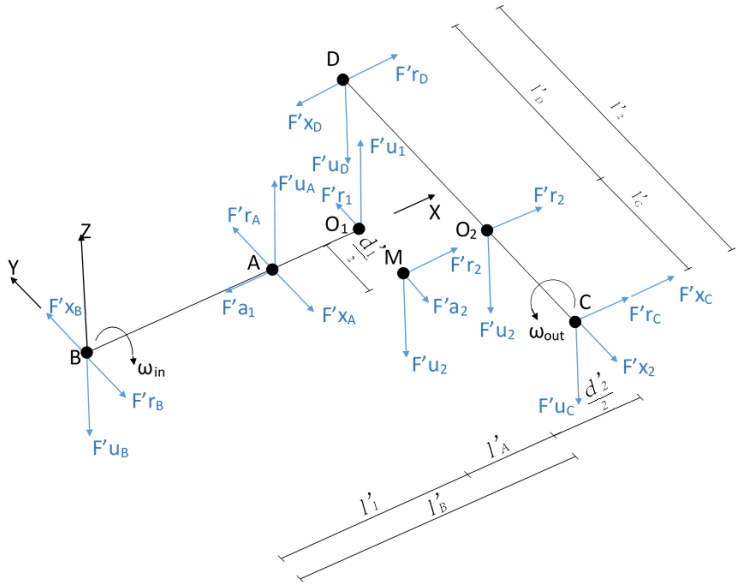

Figure 5.3: Vehicle moving forward load diagram.

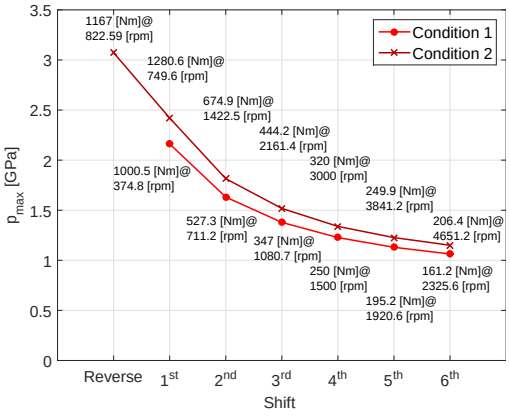

(a) Rolling bearing A.

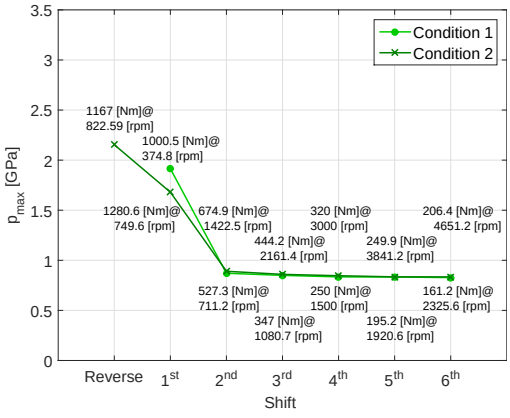

(b) Rolling bearing B.

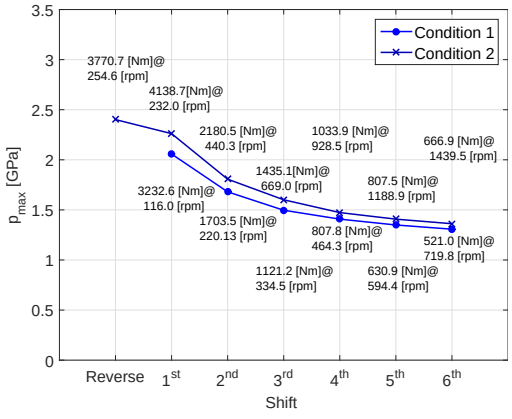

(c) Rolling bearing C.

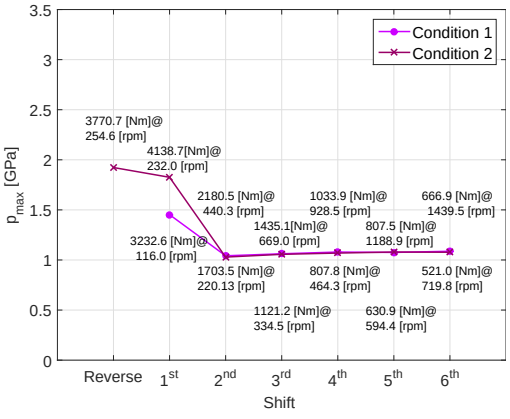

(d) Rolling bearing D.

Figure 5.4: Contact pressure (p_{max}) for both engine conditions for all selected rolling bearings.

For all rolling bearings, the pressure contact value decreases with lower gearbox transmission ratio. The rolling bearing A has higher contact pressure at higher gearbox ratios, and rolling bearing C has higher pressure for "4th", "5th" and "6th" gearbox shifts. The rolling bearings B and D have lower contact pressures for higher gearbox ratios comparing with the rolling bearings A and C.

Despite "reverse" shift has lower overall gearbox ratio than the "1st" gearbox shift, the contact pressure in all rolling bearings are higher. This occurs since the loads on the meshing point M are different due to rotation direction on the pinion shaft and the ring gear.

5.1.2.3 Rolling Speed

Rolling speed is also a key parameter to properly define the operating conditions. In Figure 5.5, the rolling speed variation with gearbox shift is presented, for each rolling bearing and for each condition.

The rolling speed range calculated was (1.2-14.9 m/s) for rolling bearing B, which is the one with lowest geometric dimensions. According to viscosity ratio (κ), above 2.5 m/s with a 40 cSt oil (75W90) the rolling bearing B, operate close to full film conditions (κ>2).

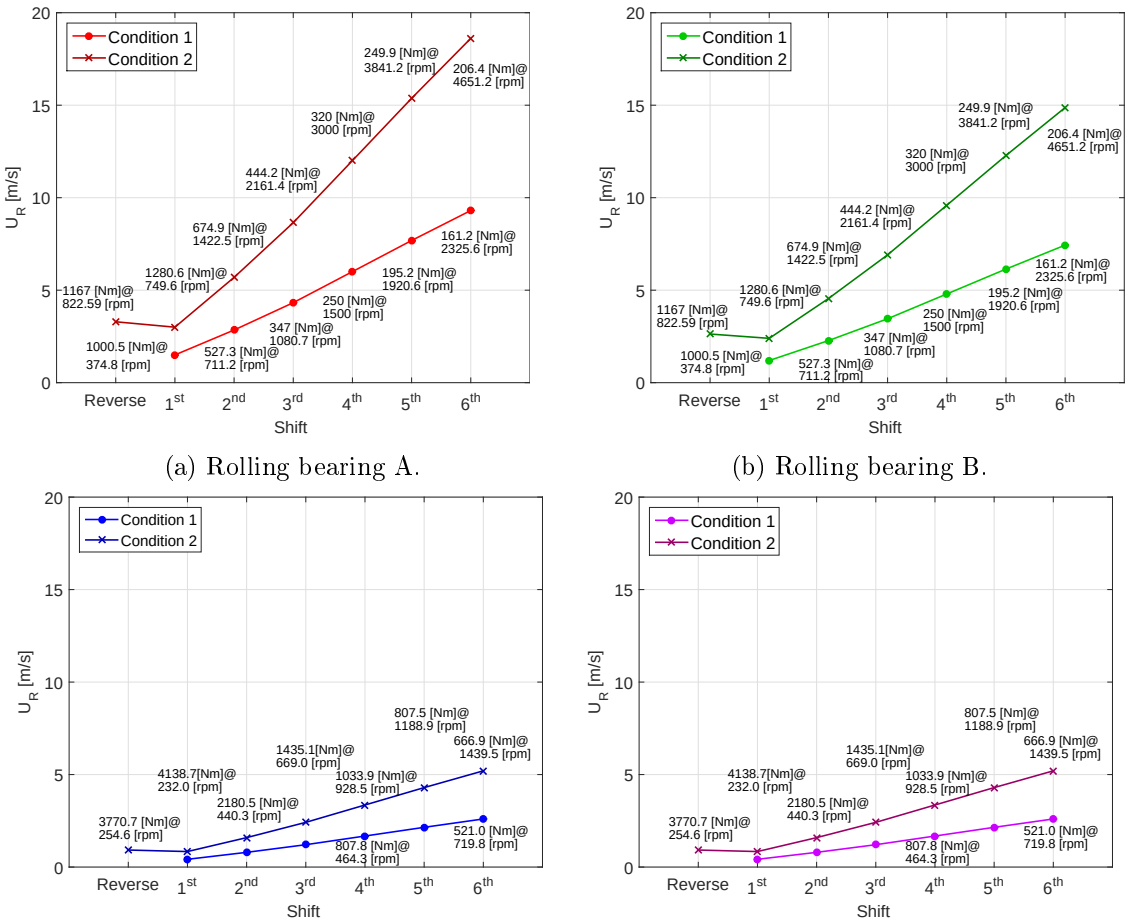

(a) Rolling bearing A.

(b) Rolling bearing B.

(c) Rolling bearing C.

(d) Rolling bearing D.

Figure 5.5: Rolling speed (U_R) for engine both conditions for all selected rolling bearings.

5.2 Friction Torque Measurments in TRB

To evaluate the total friction torque of tapered roller bearings for all the lubricating oils, it was performed a series of tests, using the same equipment described in Section 4.1. The rolling bearing assembly used a different shaft adapter (see Figure 5.6), developed to avoid misalignment of TRB, and a lower race support. Instead of a cone Morse connection, the superior part of the shaft adapter is a hollow shaft design to assemble on the machine input shaft. Furthermore, both pieces have a hole across their sections and perpendicular to their rotational axles with a screw applied to prevent the sliding effect among the two parts. The used TRBs also have different inner race diameters, as presented in Table 5.5 so different shaft adapters were used as well.

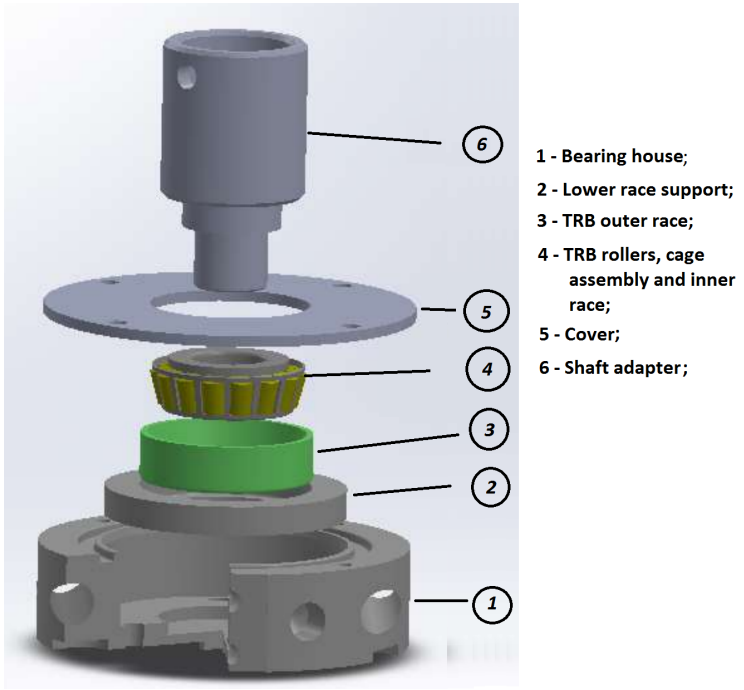

Figure 5.6: TRB assembly scheme.

5.2.1 Test Conditions

The tests performed were defined to simulate the same conditions presented on a typical TRB mounted in a rear differential. As seen in Section 5.1.2, these conditions are dependent on severeal factors including the bearing position on differential. Furthermore, taking into account only one rolling bearing from the assembly, operating conditions could vary in a wide range of temperatures, loads and rotational speeds. Temperature is a variable which can be easily adjusted to a desired value. Three temperatures were settled for the tests, 70 ^{o}C, 90 ^{o}C and 110 ^{o}C. However, define a range of contact pressures and rolling speeds on tested rolling bearing contacts, similar to the achieved in typical TRB mounted in a rear differential, was a hard task.

In the four-ball machine assembly it is impossible to test rolling bearings with the geometrical dimensions identical to the selected TRB, due to a bearing house size limitation,

leading to three TRB possibilities to perform the tests, according to Table 5.5. In Figure 5.7 a schematic drawing of a TRB is shown.

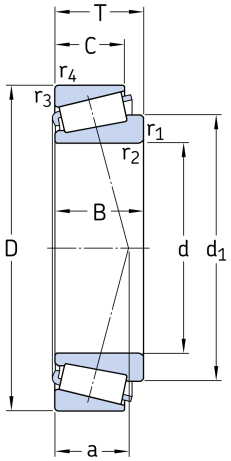

Figure 5.7: TRB draw.

Table 5.5: Main characteristics of TRB possibilities for test [9].

Rolling	Principal Dimensions			Basic load ratings		Dimensions		Calculation factors			No. Rollers
bearing	d	D	T	C	C_0	d_1	C	e	Y	Y_0	z
designation	[mm]	[mm]	[mm]	[kN]	[kN]	[mm]	[mm]	–	–	–	–
30302 J2	15	42	14.25	22.4	20	27.3	11	0.28	2.1	1.1	12
30203 J2	17	40	13.25	19	18.6	29	11	0.35	1.7	0.9	15
320/28X/Q	28	52	16	31.9	38	41.3	12	0.43	1.4	0.8	19

On the other hand, only axial loads can be applied in four-ball machine and limited to 7 kN, which is completely different from the loads presented in any rolling bearing mounted in a differential (see Table F.9). According to *Eschmann et al.* [30] for TRB subjected only to axial load, the normal load contact between roller and race is given by equation (5.3).

$$F_n = \frac{F_a \cdot \sin\psi}{z} \tag{5.3}$$

To perform the tests, two axial loads were settled, 4 and 7 kN, to ensure different contact pressures. Knowing the main geometric contact characteristics of the available rolling bearings, presented in Table 5.6, it was possible to calculate the pressure at the centre of the contact for each one, according to equation(5.4).

$$p_{max} = \sqrt{\frac{2 \cdot F_n \cdot E^*}{\pi \cdot l \cdot R_x}} \tag{5.4}$$

The maximum contact pressure in the centre of the rolling contact for both 4 and 7 kN axial load is also presented in Table 5.6. The TRB SKF 30203 J2 presents the maximum p_{max} and the TRB SKF 320/28X/Q presented the minimum value of p_{max} for both conditions. Also as shown in Figure 5.4 and Table 5.6, p_{max} on the rolling contacts for the available TRB for tests, was in the range of maximum pressure for typical rolling bearing's differential.

Table 5.6: TRB available for tests: contact roller raceways characteristics.

Designation	No. Rollers	R_{x1}	R_{x2}	l	σ	p_{max} @ $F_a = 4$ kN	p_{max} @ $F_a = 7$ kN
[-]	[-]	[m]	[m]	[m]	[μm]	[GPa]	[GPa]
30302 J2	12	3.91×10^{-3}	12.52×10^{-3}	10.76×10^{-3}	0.25	1.41	1.86
30203 J2	15	2.80×10^{-3}	11.72×10^{-3}	8.74×10^{-3}		1.44	1.91
320/28X/Q	19	2.95×10^{-3}	17.26×10^{-3}	12.16×10^{-3}		0.93	1.23

The operating rotational speeds range of four-ball machine equipment was from 75 up to 1200 rpm. 6 rotational speeds, 75, 150, 300, 600, 900 and 1200 rpm, were defined to perform the laboratory tests. According to equation (5.5) it is possible to determine the rolling contact speeds, presented in Table 5.7.

$$U_1 = U_2 = \left(\frac{d_m + d_r \cdot cos(\psi)}{2} \right) \cdot \frac{\pi \cdot n}{60} \tag{5.5}$$

Table 5.7: Contact rolling speed (U_R) in tested bearings.

Rotational Speed	Parameter	Unit	Test conditions 4KN / 7KN		
[rpm]			30302 J2	30203 J2	320/28X/Q
75	U_R	[m/s]	0.120	0.108	0.153
150			0.240	0.217	0.306
300			0.481	0.433	0.613
600			0.962	0.867	1.225
900			1.443	1.300	1.838
1200			1.924	1.734	2.451

On the other hand, on typical differential TRB's a great range of speeds are covered, and it was possible to observe that its rolling speed is much higher than the values available for the tests, Figure 5.5 and Table 5.7, respectively.

However, the main goal of the tests is to understand the behaviour of friction torque from boundary lubrication regime until being achieved the EHD lubrication regime. As presented in Section 5.1.2.3, differential's TRB achieve full film for 2.5 m/s, so, it was considered unnecessary to test all the differential speed range.

Since both TRB 30302 J2 and 30203 J2 have similar rolling bearing speeds and maximum contact pressure, only 30203 J2 was tested. Also TRB 320/28X/Q was selected due to its highest average rolling speed in comparison with 30302 J2 or 30203 J2, so it achieves easily full film conditions.

As stated in Section 2.3.2 five multigrade oils were tested. In Table 5.8 are presented the test conditions. For each oil, each TRB was tested at two loads 4 and 7 kN. For each load, three temperatures were applied (70, 90 and 110 °C) for six operating speeds (75 to 1200 rpm). The friction torque measurements were performed for each operating speed, according to the load and temperature defined. As in RTB measurements of Section 4.1.1, four measurements

were recorded, then the three closest values were selected and the average of these three values was considered as the result of each test condition.

Table 5.8: Operating conditions of TRB friction torque tests.

Parameter	Unit	75W90	75W140	80W90	5W30	10W50
Load	[kN]	4 and 7				
Temperature	[°C]	70, 90 and 110				
Operating speeds	[rpm]	75, 150, 300, 600, 900 and 1200				

In Table 5.9 are presented for five tested oils the viscosity (ν) and the piezoviscosity (α) at three temperatures conditions.

Table 5.9: Kinematic viscosity (ν) and piezoviscosity (α) at 70, 90 and 110 °C.

Parameter	Unit	75W90	75W140	80W90	5W30	10W50
Viscosity @ 70°C	[cSt]	39.2	65.2	36.9	24.9	39.1
Viscosity @ 90°C	[cSt]	22.8	35.5	19.8	15.1	22.8
Viscosity @ 110°C	[cSt]	14.5	21.7	12.0	10.0	14.4
Piezoviscosity @ 70°C	[Pa^{-1}]	1.2057	1.2867	1.6332	1.1353	1.2070
Piezoviscosity @ 90°C	[Pa^{-1}]	1.1206	1.1890	1.5001	1.0611	1.1207
Piezoviscosity @ 110°C ($\alpha_{Gold} \times 10^{-8}$)	[Pa^{-1}]	1.0547	1.1129	1.3993	1.0034	1.0544

5.2.2 Test Procedure

Before define the test procedure it was necessary taking into account that tapered roller bearings should have a running-in period. The running-in period is characterized for a significant amount of friction between the rolling elements and the raceways, and it can be identified by a temperature spike as presented in Figure 5.8. After reach the maximum operating temperature, a gradual decreasing in the temperature is observed until a stabilized value is achieved. It was observed in the tests performed that the time necessary to reach the stabilization temperature varies with the lubricant. So it was not defined a running-in time. Instead, it was defined that running-in period is complete when the temperature variation was less than one Celsius degree in a one running hour.

Taking into account the running-in, two different tests were defined. One where the measurements were recorded without being respected the running-in period, and other after the running-in procedure. The test without running-in was only performed for one oil, 10W50, and for a TRB type 30203 J2 with the main objective of compare the results in each scenario.

On the other hand, tests considering all the oils were performed after running-in period for TRB 320/28X/Q with the goal of understand the influence of lubricant formulation on friction torque loss.

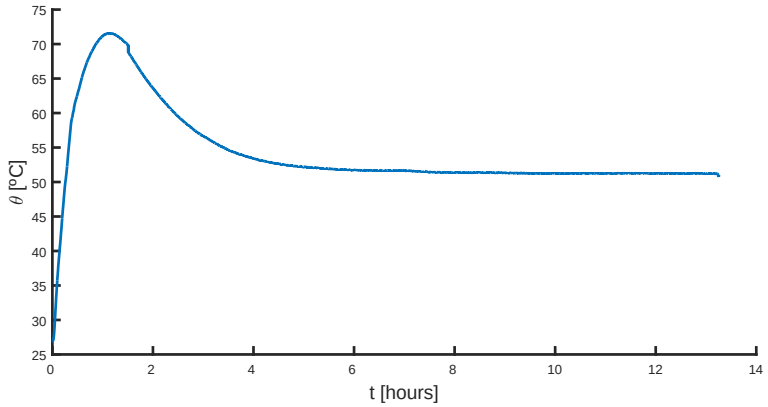

Figure 5.8: Temperature variation (θ) of tapered roller bearings during the running-in period (t).

The experimental procedure defined is similar to the Section 4.1.2 and only the differences will be described as follows:

1. New rolling bearing was unpacked and cleaned in a ultrasound bath of petroleum ether for 3 minutes to remove the original oil film;
2. Rolling bearing assembly (Figure 5.6):
   (a) Inner race (4), which includes also the tapered rollers and rolling cage was mounted in the shaft adapter (6);
   (b) Outer race (3) was mounted in the race support (2) and both mounted in bearing house (1) over a seal to prevent the oil leakage;
3. Depending on TRB 30203 J2 or 320/28X/Q, 4 ml or 8 ml of oil was added, respectively;
4. Initiation procedure:
   (a) Without considering running-in:
      i. A 5 minutes period with 1 kN of axial load were implemented, the rotational speed and the temperature were defined in 75 rpm and 70 °C, respectively;
      ii. With the four-ball machine turned off the load was applied, 4 kN.
      iii. The equipment was turned on and speed and temperature conditions were defined (the speed was defined in 75 rpm and temperature in 70 °C) during a 30 minutes period;
   (b) Considering running-in:
      i. A 5 minutes period with 1 kN of axial load were implemented, the rotational speed was defined in 600 rpm. Temperature were not defined (during this period TRB was running at free temperature);
      ii. With the four-ball machine turned off the load was applied, 7 kN.
      iii. The equipment was turned on at the same speed and temperature conditions during the desired period;

5. Measurement:

   (a) Torque data acquisition is turned on and recorded 1000 points;

   (b) Four-ball machine and fans were turned off and the data acquisition continues to record up to 5000 points and them turned off. The fans are turned off to keep the temperature steady;

   (c) All temperatures and torque measurement were saved;

   (d) Four-ball machine and fans are turned on;

6. Item 5 was repeated for the number of the measurements desired, usually 4. The set of measurements were always performed in 10 minutes and the temperature variation between measurements was less than 1.5 ^{o}C;

   - The following measurements:

7. Depending on the stage of the test, speed, temperature and load; speed and temperature or speed could vary:

   (a) Speed is increased to the subsequent;

      i. On a defined load and temperature, the speed is increased from 75 up to 1200 rpm (item 5 and item 6 are applied repeatedly for each operating speed);

   (b) Temperature is increased to subsequent;

      i. After recorded the 1200 rpm measurement, the rotational speed is reduced for 75 rpm and the temperature is increased from 70 up to 110 ^{o}C (item 7(a)i is applied for each temperature condition);

   (c) Load is increased to the subsequent;

      i. After recorded the 1200 rpm measurement at 110 ^{o}C, the rotational speed and temperature are reduced for 75 rpm and 70 ^{o}C, respectively and the item 7(a)i and item 7(b)i are applied for 7kN load condition;

   When any item, 7a, 7b or 7c, occurs a stabilization period of 30 minutes is followed.

8. Finished all the measurements and reached the end of item 7c, the worked oil was removed and the bearing was stored.

5.2.3 Influence of Running-in on Friction Torque

A TRB 30203 J2 was tested both with or without running-in procedure lubricated with 10W50 oil. The temperature was kept constant (when possible) and set at 70, 90 and 110 ^{o}C. Two axial loads were considered, 4 and 7 kN. The rotational speed was set for 6 different conditions (75, 150, 300, 600, 900, 1200) rpm.

On the test performed without running-in, the friction torque measurements started after 30 minutes of operation. However, on the test performed with the running-in, the torque losses were measured only after the maximum temperature peak was achieved and the temperature stabilized on a value considerably lower than the maximum peak.

For each trial, all the tests were performed with the same TRB 30203 J2.

5.2.4 Oil Operating Temperature

As mentioned in Section 5.2.2, the temperature is an important parameter to understand if a TRB completed the running-in period. In Figure 5.9 is showed the average of experimental temperature recorded for each friction torque measurement.

The tests where running-in period was not respected, the temperature inside the rolling bearing rise in almost all the load and temperature conditions. For the tests performed at 70 ^{o}C under both load conditions shown in Figure 5.9(a) and Figure 5.9(b), from 600 rpm in 4 kN condition and 300 rpm for 7 kN condition, the temperature increase significantly, an this increase is more pronounced in the 7 kN condition, due to the highest pressure values. In fact, for all the tests performed at 7 kN and 1200 rpm the temperature increase so significantly, higher than 130 ^{o}C, that there was not interest in record friction torque measurements.

On the other hand, tests where the running-in period occur, the temperature for both load conditions were maintained stable around the temperature defined.

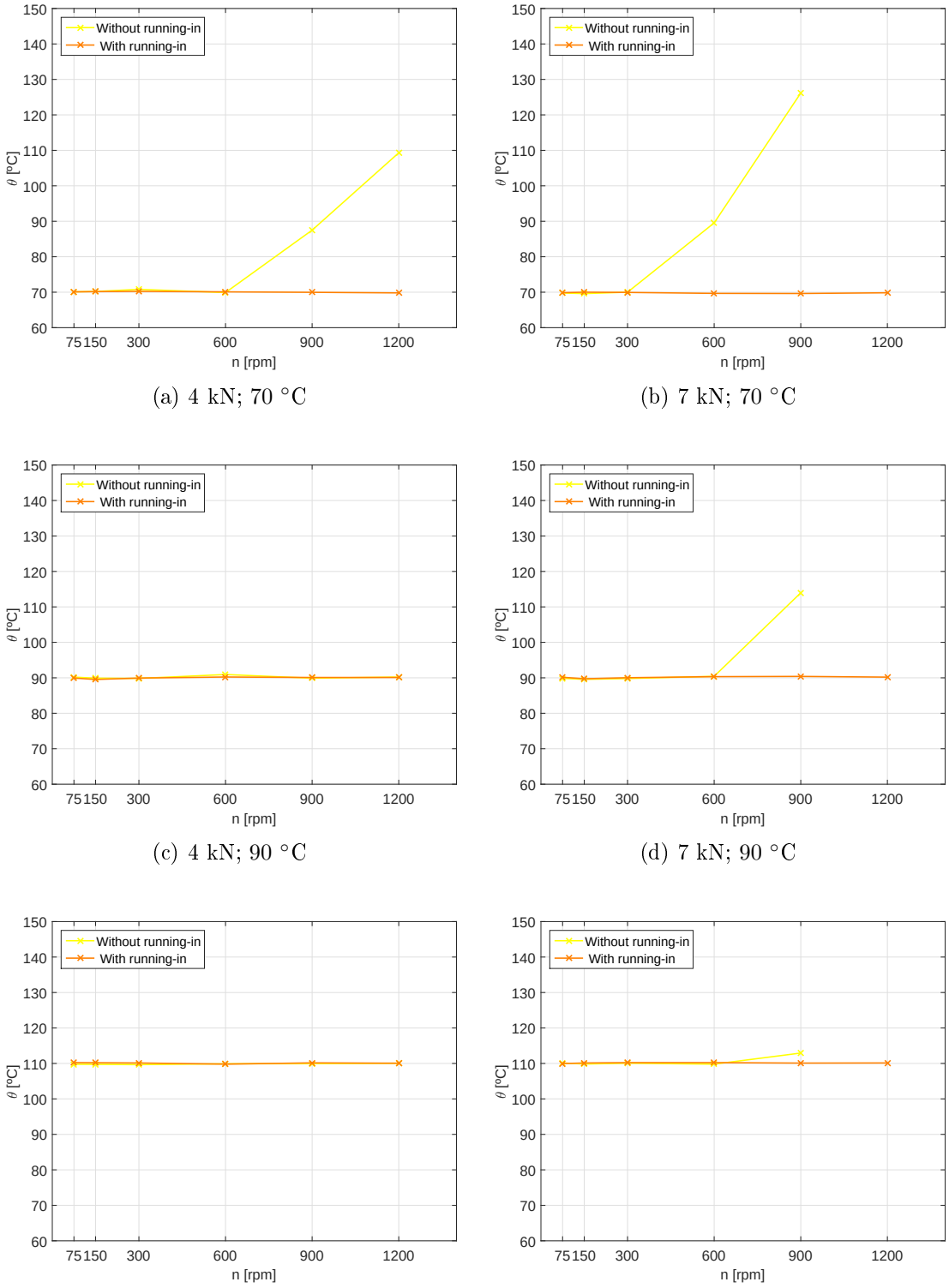

(a) 4 kN; 70 °C

(b) 7 kN; 70 °C

(c) 4 kN; 90 °C

(d) 7 kN; 90 °C

(e) 4 kN; 110 °C

(f) 7 kN; 110 °C

Figure 5.9: Effect of running-in on temperature (θ) behaviour, for pre-defined temperature values, with the increasing of rotational speed (n) and two load conditions for TRB 30203 J2 and oil 10W50.

5.2.4.1 Total, Rolling and Sliding Friction Torque

To be aware of the differences between the tests where the running-in period occur and the tests where it was not occur, Figure 5.10 presents the total experimental friction torque measurements, for all range of operating speeds, for each temperature and axial load. It was possible to observe that for all test conditions, without running-in period, the total experimental friction torque (M_t^{exp}) was always higher.

The major difference in M_t^{exp} occurs at 70 °C and 4 kN conditions as shown in Figure 5.10(a). With higher load and temperature the difference decreased, see Figure 5.10(f). This phenomenon was a result of the running-in process.

The M_t^{exp} measurements observed in Figure 5.10(b) from 300 up to 1200 rpm and Figure 5.10(d) from 600 up to 1200 rpm, shown very high differences between both test procedures. The M_t^{exp} increase observed, was associated to temperature increase, which resulted in lower dynamic viscosity (η), lower film thickness between the contact surfaces and higher coefficient of friction.

The SKF model was applied to the experimental results as suggested in Section 3.2. Rolling friction torque (M_{rr}), displayed in Figure 5.11, presented an opposite behaviour from total friction torque. Since the M_{rr} is mainly dependent on speed and viscosity, the test without running-in presented lower rolling torque due to higher operating temperature. However, the influence of M_{rr} in total friction torque is small, in comparison with M_{sl}^{exp}, as shown in Figure 5.12.

Comparing Figure 5.12(b) with Figure 5.12(d), above 600 rpm the M_{sl}^{exp} for test at 70 °C and 7 kN increased, however test at 90 °C and 7 kN had the opposite behaviour. On the other hand, for tests where the TRB running-in was applied, it was not verified this incident.

Moreover, apart the test at 70°C and 7kN for the TRB without the running in period, the M_{sl}^{exp} has a decreasing tendency for all the rotational speed range, which are related with the growth of specific film thickness along the increase of rotational speed.

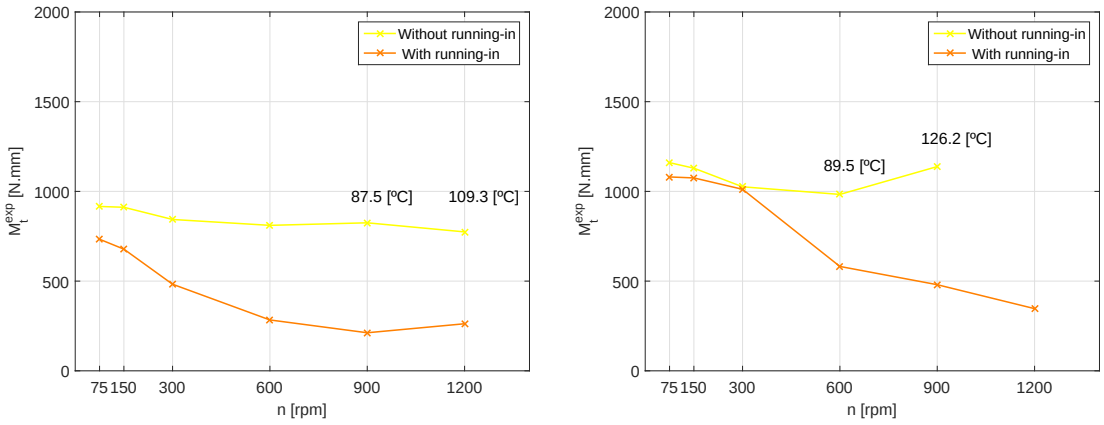

(a) 4 kN; 70 °C

(b) 7 kN; 70 °C

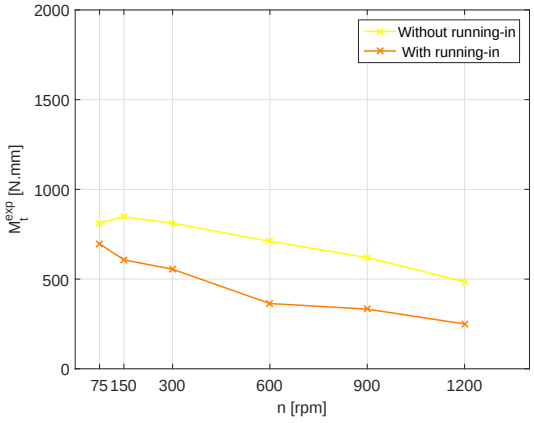

(c) 4 kN; 90 °C

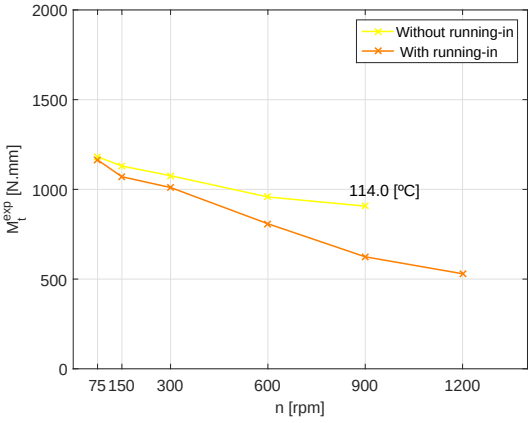

(d) 7 kN; 90 °C

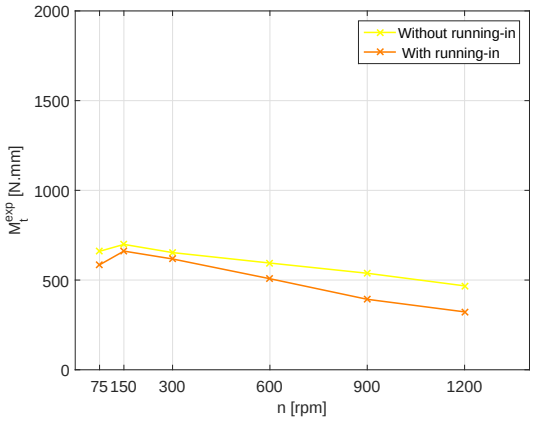

(e) 4 kN; 110 °C

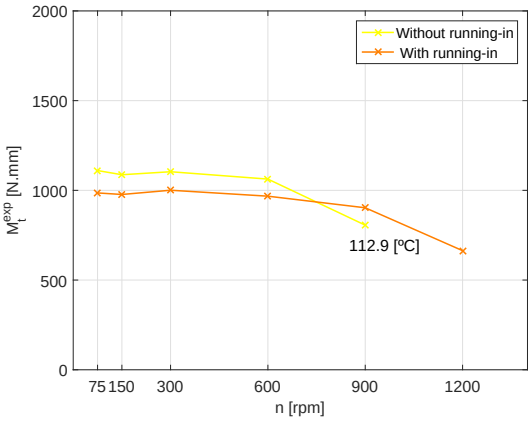

(f) 7 kN; 110 °C

Figure 5.10: Effect of running-in on experimental total friction torque measurements (M_t^{exp}) against rotational speed (n) for each temperature and load conditions for TRB 30203 J2 and oil 10W50.

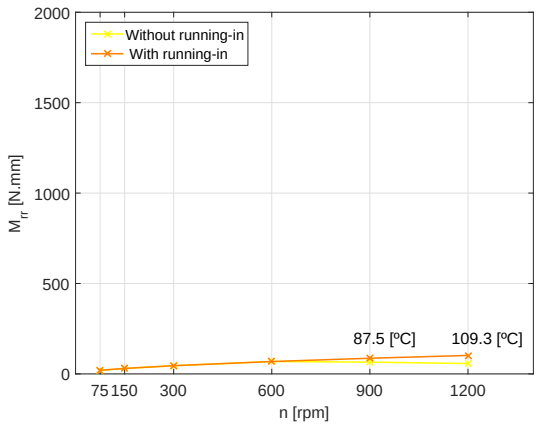

(a) 4 kN; 70 °C

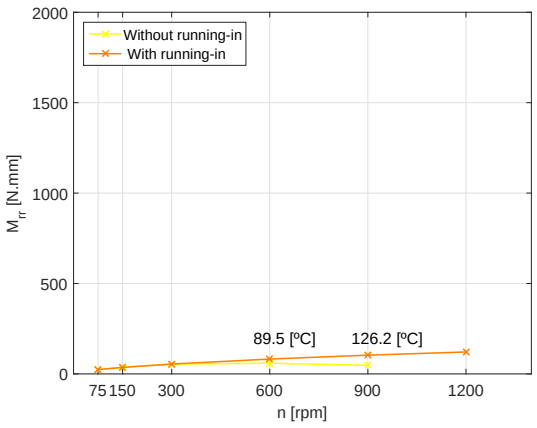

(b) 7 kN; 70 °C

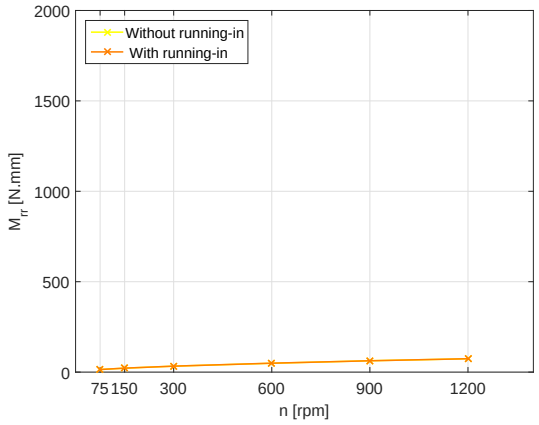

(c) 4 kN; 90 °C

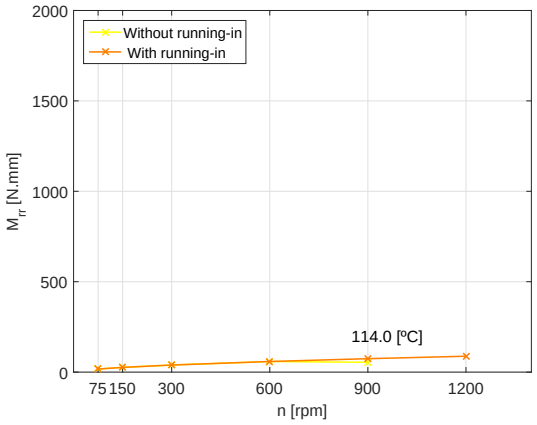

(d) 7 kN; 90 °C

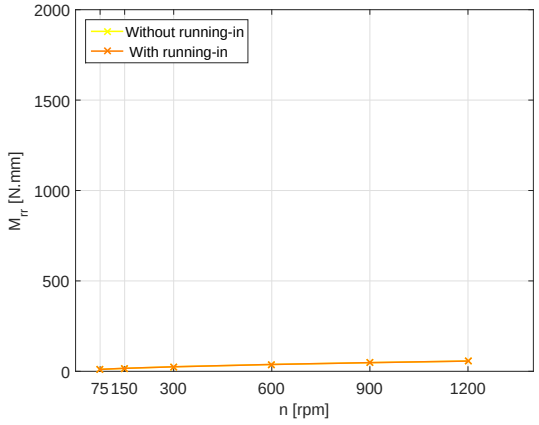

(e) 4 kN; 110 °C

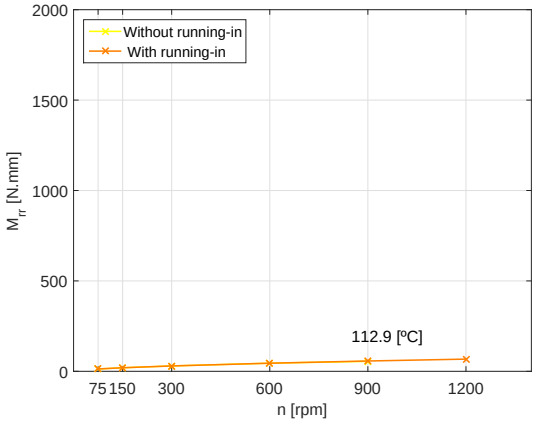

(f) 7 kN; 110 °C

Figure 5.11: Effect of running-in on rolling friction torque measurements (M_{rr}) against rotational speed (n) for each temperature and load conditions for TRB 30203 J2 and oil 10W50.

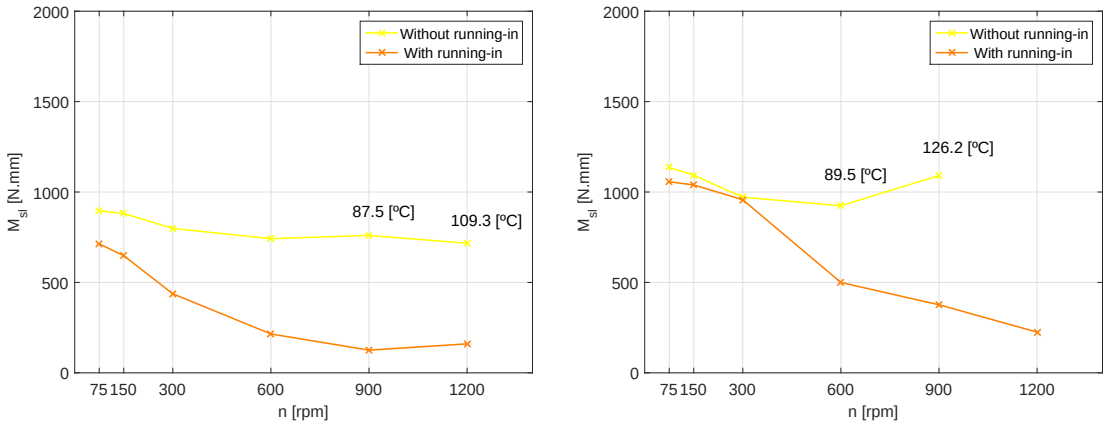

(a) 4 kN; 70 °C

(b) 7 kN; 70 °C

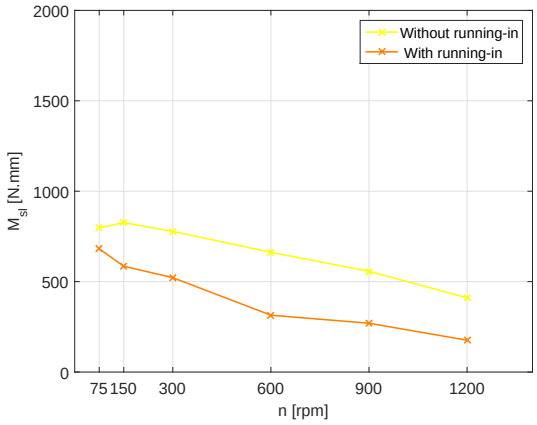

(c) 4 kN; 90 °C

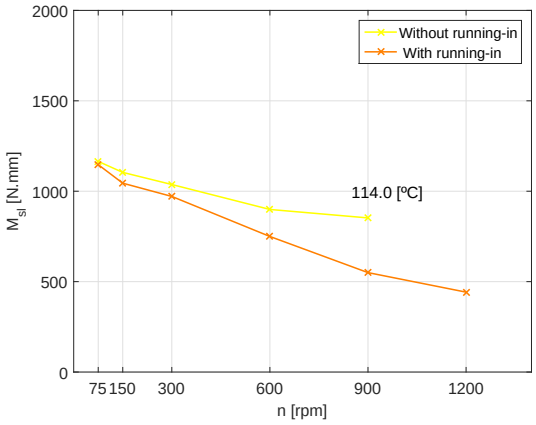

(d) 7 kN; 90 °C

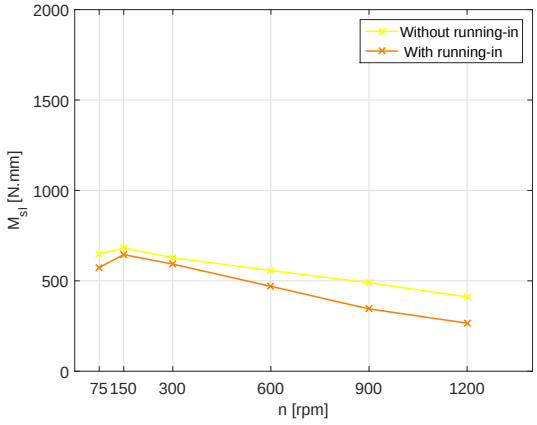

(e) 4 kN; 110 °C

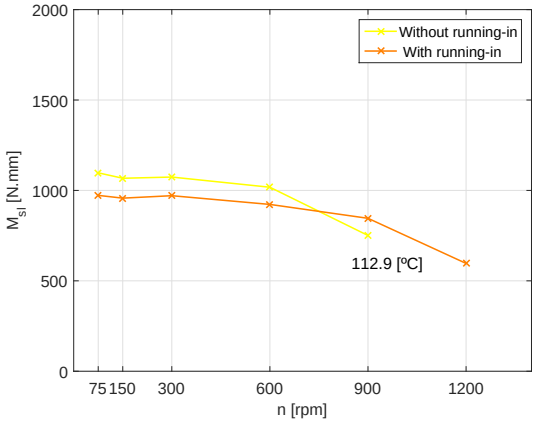

(f) 7 kN; 110 °C

Figure 5.12: Effect of running-in on experimental sliding friction torque measurements (M_{sl}^{exp}) against rotational speed (n) for each temperature and load conditions for TRB 30203 J2 and oil 10W50.

5.2.4.2 Sliding, Boundary and Full-Film Coefficient of Friction

In Section 3.2.2 it was mentioned the procedure to determine the experimental sliding coefficient of friction (μ_{sl}^{exp}) on rolling bearings, using the SKF model, which is given by equation (5.6).

$$\mu_{sl}^{exp} = \frac{M_{sl}^{exp}}{G_{sl}} \tag{5.6}$$

The results of μ_{sl}^{exp} were displayed in Figure 5.13. A decrease of μ_{sl}^{exp} with the increase of rotational speed was observed. The only exception is the test performed at 70 °C and 7 kN presented in Figure 5.13(b) for a test without running-in procedure.

For all the tests, the μ_{sl}^{exp} was always higher for the TRB where the running-in was not performed.

According to *Fernandes et al.* [39], it was possible to determine the boundary and full-film coefficient of friction, (μ_{bl} and μ_{EHL}) respectively, as described in Section 3.2.3.

In Table 5.10 are presented μ_{bl} and μ_{EHL} for all the test conditions. As expected despite the test at 7 kN at 110 °C, μ_{bl} and μ_{EHL} were always superior for the TRB without running-in. An exception was observed for μ_{EHL} of the tests performed at 7 kN and 110 °C. This happened because ϕ_{bl} varied from 0.987 to 0.528 and full film conditions are too far, having a lower effect on μ_{EHL} presented on equation (5.7), when the optimization process is done.

$$\mu_{sl} = \phi_{bl} \cdot \mu_{bl} + (1 - \phi_{bl}) \cdot \mu_{EHL} \tag{5.7}$$

To achieve a good model optimization ϕ_{bl} should vary from $\phi_{bl} = 0$ up to $\phi_{bl} = 1$ (see Table G.1 and Table G.2).

For both tests it was observed that μ_{bl} decrease with the rise of temperature and load, no matter if TRB was running-in or not.

Table 5.10: Boundary (μ_{bl}) and full-film (μ_{EHL}) friction coefficients determined for the six different (4 and 7 kN load and 70, 90 and 110 °C temperature) conditions, for the oil 10W50.

Test	Procedure	10W50	
		μ_{bl} [-]	μ_{EHL} [-]
70 °C @ 4 kN	Without running-in	0.252	0.179
	Running-in	0.207	0.001
90 °C @ 4 kN	Without running-in	0.239	0.084
	Running-in	0.172	0.001
110 °C @ 4 kN	Without running-in	0.188	0.033
	Running-in	0.166	0.001
70 °C @ 7 kN	Without running-in	0.188	0.080
	Running-in	0.186	0.024
90 °C @ 7 kN	Without running-in	0.182	0.072
	Running-in	0.181	0.010
110 °C @ 7 kN	Without running-in	0.176	0.001
	Running-in	0.155	0.068

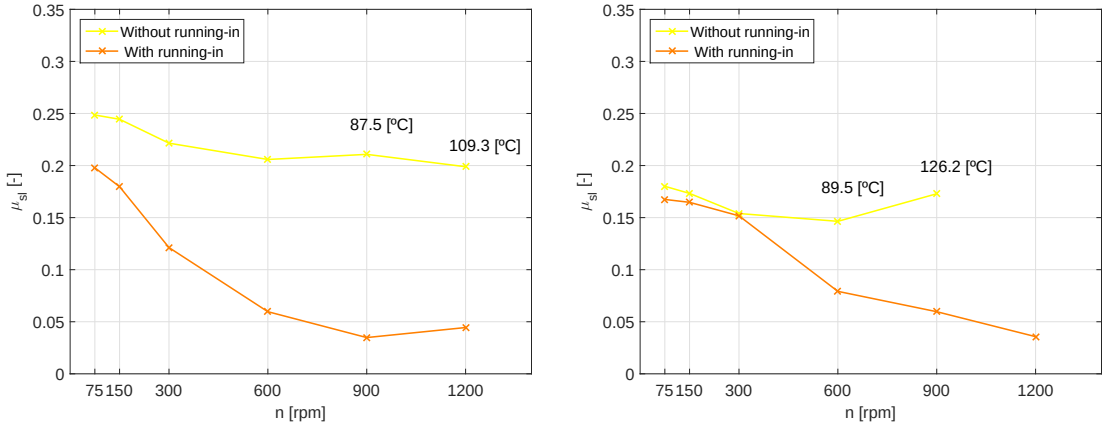

(a) 4 kN;70 °C

(b) 7 kN; 70 °C

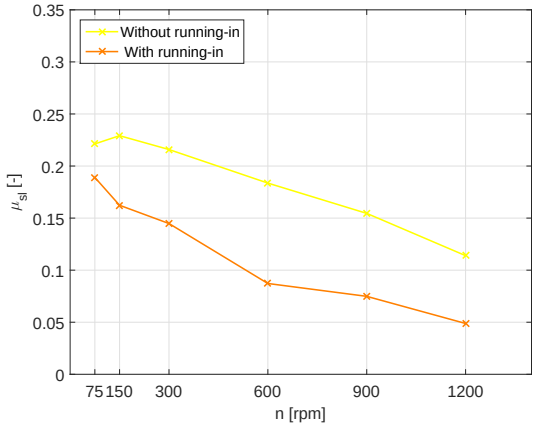

(c) 4 kN; 90 °C

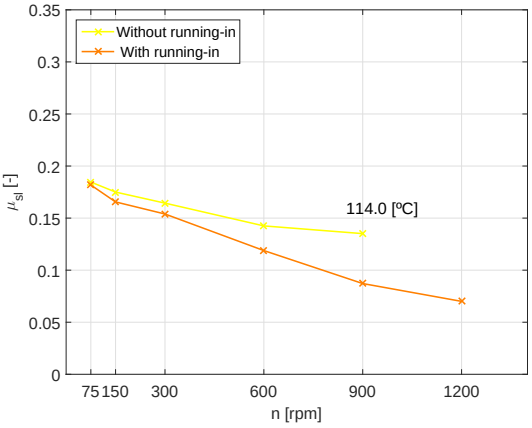

(d) 7 kN; 90 °C

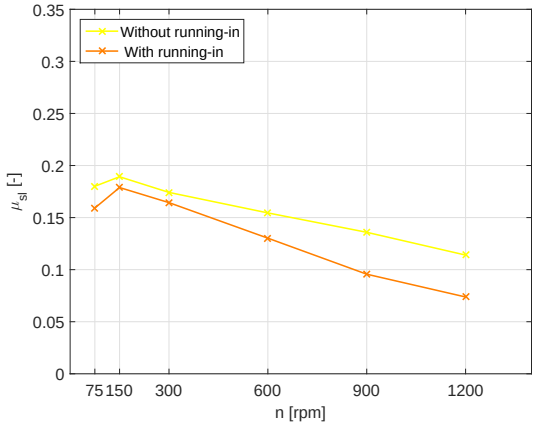

(e) 4 kN; 110 °C

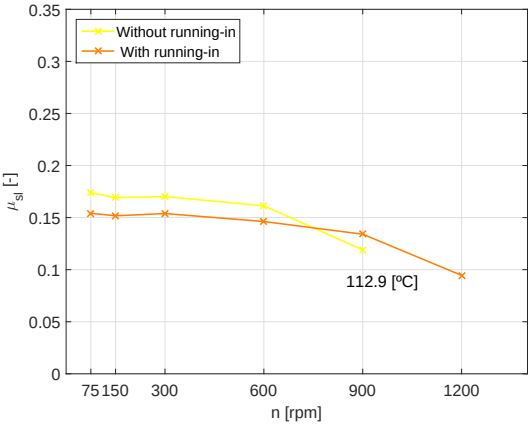

(f) 7 kN; 110 °C

Figure 5.13: Effect of running-in on experimental sliding coefficient of friction (μ_{sl}^{exp}) against rotational speed (n) for each temperature and load conditions for TRB 30203 J2 and oil 10W50.

5.2.5 Influence of Oil Formulation

In this section are presented the tests performed with TRB 320/28X/Q for the five oils, characterized in Section 2.3.2. The tests were performed for both loads (4 and 7 kN), including three temperatures (70, 90 and 110 °C) and six operating speeds (75, 150, 300, 600, 900 and 1200 rpm). Also, all the TRB tests were performed after the running-in period as mentioned in Section 5.2.2.

5.2.5.1 Specific Film Thickness and Viscosity Ratio Results

To evaluate the lubrication regime for the tests performed, specific film thickness and viscosity ratio were determined. Specific film thickness (Λ) was calculated at the centre of the contact line according to *Dowson and Higginson* equation, and κ was determined according to SKF.

The rated viscosity values for the TRB used in the tests were presented in Table 5.11.

Table 5.11: Rated viscosity (ν_1) determined for RTB 320/28X/Q for every rotational speeds (n).

Parameter		Unit						
Rotation Speed	n	[rpm]	75	150	300	600	900	1200
Rated viscosity	ν_1	[cSt]	180	100	55	25	22	18

The results obtained for both parameters for each oil at each tested condition for 4 kN are shown in Figure 5.14. Also in Appendix G is presented both parameters for 7 kN at all temperatures.

It was observed considerable differences between the calculated specific film thickness and the viscosity ratio as refered in Section 3.1.5. However under constant operating temperature, both Λ and κ increase with the increase of speed. Taking into account the κ values, it was also observed that all oils are running between boundary and mixed film regime, since $\kappa < 4$, even for 75W140 oil at 70 °C and 4 kN of axial load.

For a given load, when the temperature condition changed from 70 °C up to 110 °C, Λ and κ decreased their values for all rotational speeds tested, (compare Figure 5.14(a) with Figure 5.14(e) or Figure G.1(b) with Figure G.1(f) for instance).

The 75W140 oil presented the highest κ for all tested conditions. On the opposite, 5W30 oil presents always the lowest and κ values. In fact 75W140 oil presented for all tested conditions the highest viscosity values and the second highest operating piezoviscosity value, which are related with higher film thickness. On the other hand, 5W30 oil had the lowest viscosity and piezoviscosity values promoting the lowest Λ.

As expected, 75W90 and 10W50 oils presented similar Λ, since both have identical viscosity and piezoviscosity values for each temperature. 80W90 oil presented lower viscosity values than 75W90 and 10W50 but, had the highest piezoviscosity, promoting higher Λ values when compared with the refereed oils.

It was also observed, for a given load condition, that the difference between the highest and lowest Λ values decreased with the increasing temperature. This happened because the oil's viscosity is closer at 100 °C then at 70 °C.

For both load conditions, no major differences were found on Λ values when compared the same temperature and n conditions, since film thickness is not highly dependent on load.

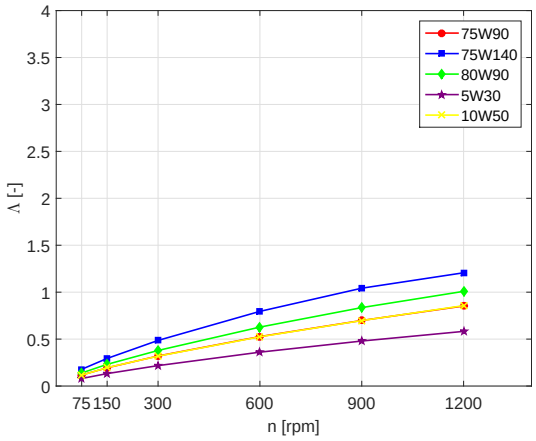

(a) 4 kN; 70 °C

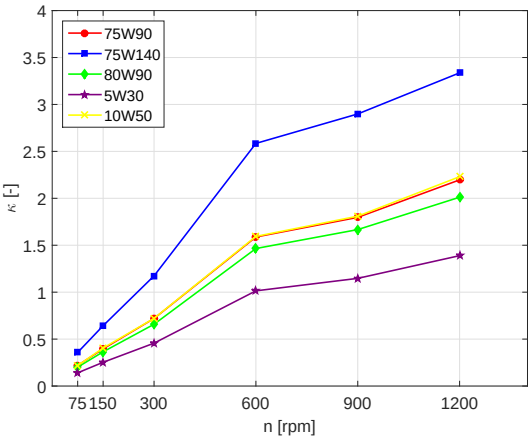

(b) 4 kN; 70 °C

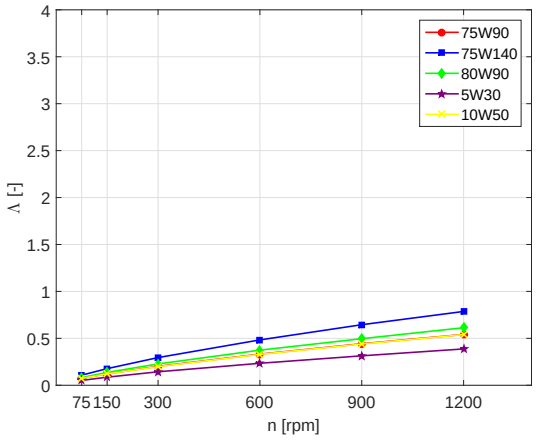

(c) 4 kN; 90 °C

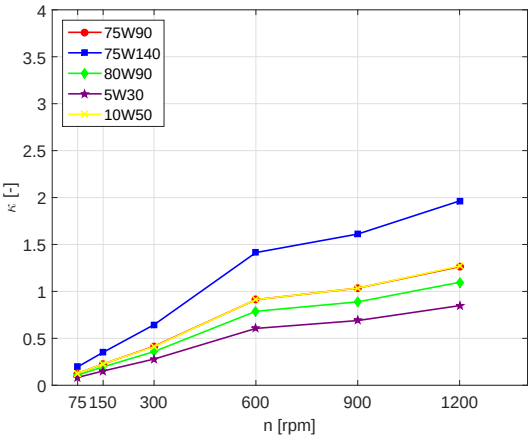

(d) 4 kN; 90 °C

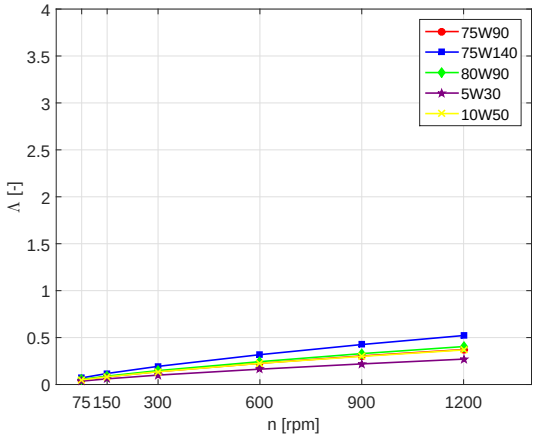

(e) 4 kN; 110 °C

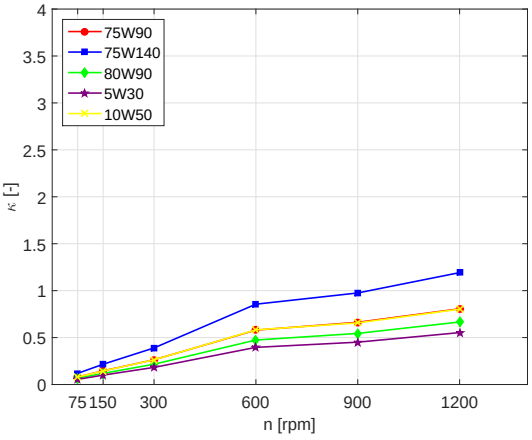

(f) 4 kN; 110 °C

Figure 5.14: TRB 320/28X/Q calculated specific film thickness (Λ) and viscosity ratio (κ) for all tested oils at 4 kN

5.2.5.2 Total Friction Torque Results

M_t^{exp} is the result of the measurements carried out on the four-ball machine, which are presented in Figure 5.15.

In general, it was observed that M_t^{exp} decreases with the increase of the rotational speed (n). The highest M_t^{exp} values at lower rotational speed (n) were related with the lower film thickness promoting metal-to-metal contact. Also, the lower M_t^{exp} for the highest rotational speed was expected since TRB evolved from boundary (75 rpm) to mixed lubrication regime (1200 rpm) for all the lubricants.

It was observed for friction torque measurements performed at a given load that, increasing the operating temperature, the total friction torque (M_t^{exp}) increased. It was expected, mainly for lower rotational speeds (75 up to 300 rpm), because higher temperature promote lower film thickness. Compare Figure 5.15(a), 5.15(c) and 5.15(e) or Figure 5.15(b), 5.15(d) and 5.15(f).

Increasing the rolling bearing's load, total friction torque (M_t^{exp}) increased for lower rotational speeds where boundary lubrication was present (75-300 rpm).

75W140 presented the lowest M_t^{exp} below 600 rpm, no matter the load and temperature. Above 600 rpm the total friction torque was higher for 75W140 because of its highest viscosity. The lowest results at lower rotational speeds (n) were in agreement with the results obtained for RTB tests. Also, closer to full film conditions (1200 rpm), higher viscosity presented higher friction. In Figure 5.15(a) it is shown a particular case where 75W140 oil presented the lowest M_t^{exp} for 75 up to 300 rpm and the highest values for 1200 rpm. The opposite behaviour was observed for 5W30 oil, which presented the second highest M_t^{exp} value for 75 rpm and the lowest for 1200 rpm.

10W50 and 75W90 oils present similar operating kinematic viscosity, piezoviscosity and the same base oil (PAO). Under these conditions it was expected to found similar friction torque behaviour, but 75W90 outperformed 10W50. However, the lubricants have quite different additive package which can explain the different friction behaviour observed, mainly under boundary lubrication conditions (75 up to 300 rpm) where the influence of additives is very important.

5.2.5.3 Rolling Friction Torque Results

As described in Section 3.2.1, the SKF model has the advantage to represent separately the different sources of friction torque. Rolling friction torque was calculated according to equation (5.8).

$$M_{rr} = \phi_{rs} \cdot \phi_{ish} \cdot G_{rr} \cdot (\nu \cdot n)^{0,6} \tag{5.8}$$

In Figure 5.16 was observed for all conditions the same increasing tendency of M_{rr} with the increase of n. However, for a given load at higher temperatures (90 and 100 °C) a lower increase and lower M_{rr} variation was observed, due to the lower oil's viscosity.

75W140 oil had the highest value of M_{rr} for all rotational speed range, and 5W30 had the lowest one, since presented the highest and lowest viscosity, respectively. As consequence with the increase of n, M_{rr} has a greater growth for 75W140 oil when compared with 5W30 oil. Furthermore, at a given load, the M_{rr} differences between both oils were lower for highest temperatures due to the the closer oil's viscosity at 110 °C than 70 °C.

75W90 and 10W50 oils presented identical M_{rr}, due to similar viscosity and piezoviscosity values. 80W90 oil presented lower M_{rr} than 75W90 and 10W50 since its oil viscosity is

lower than the other two.

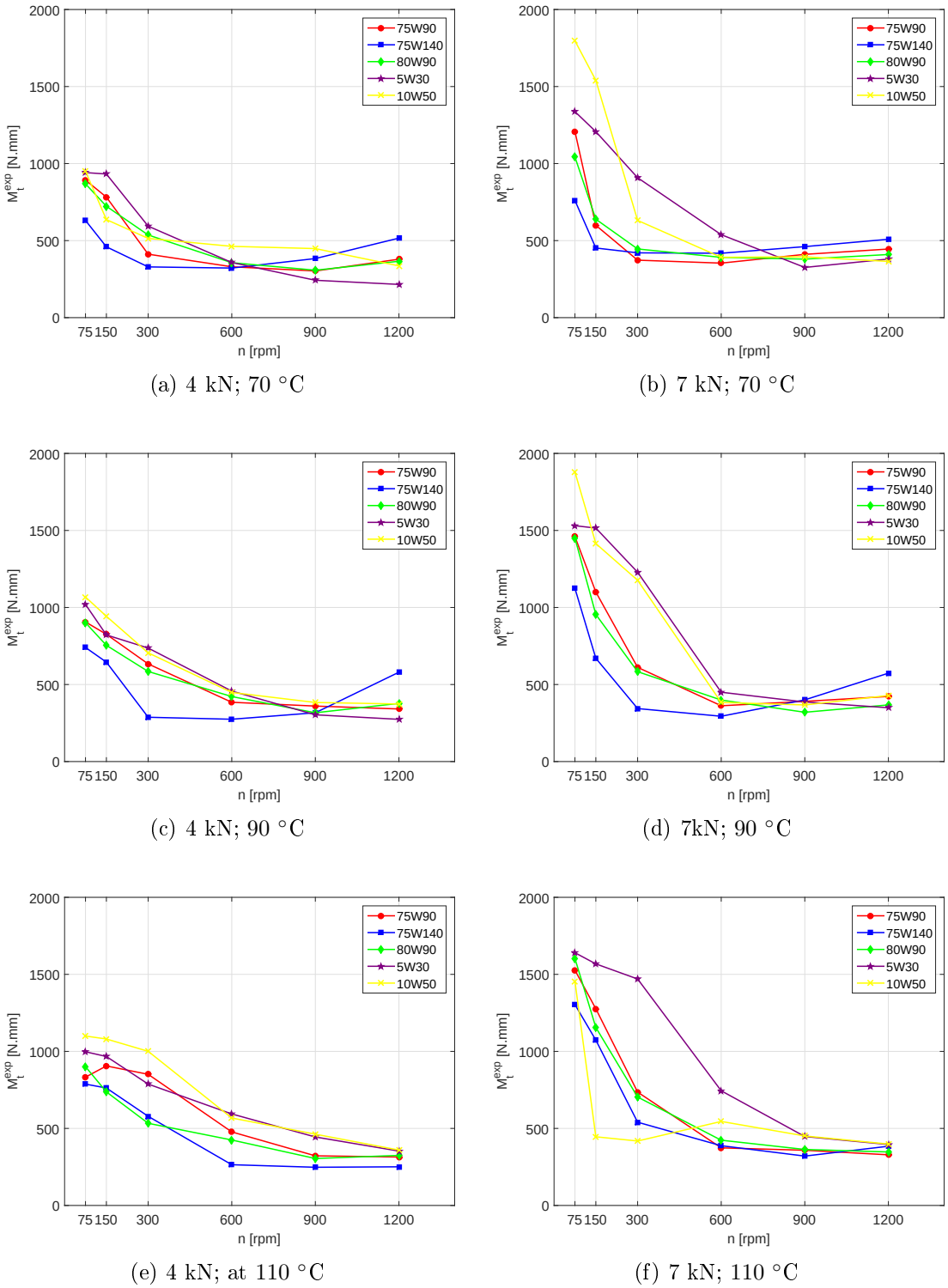

(a) 4 kN; 70 °C

(b) 7 kN; 70 °C

(c) 4 kN; 90 °C

(d) 7kN; 90 °C

(e) 4 kN; at 110 °C

(f) 7 kN; 110 °C

Figure 5.15: TRB 320/28X/Q experimental total friction torque measurements (M_t^{exp}) results against rotational speed (n) for all tested oils at each temperature and load conditions.

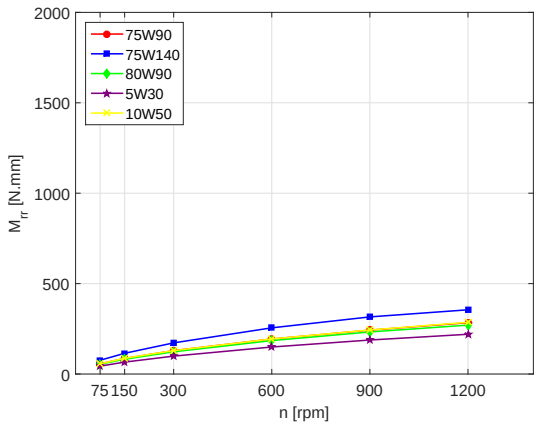

(a) 4 kN; 70 °C

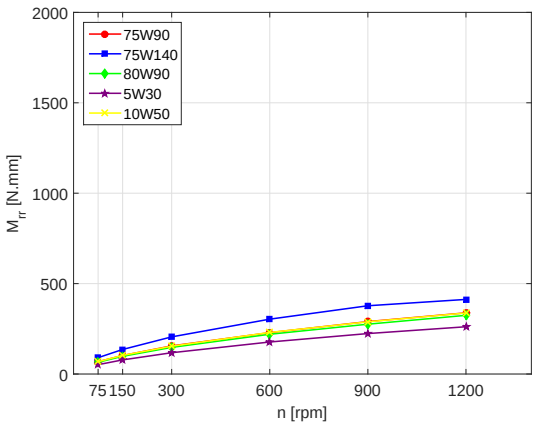

(b) 7 kN; 70 °C

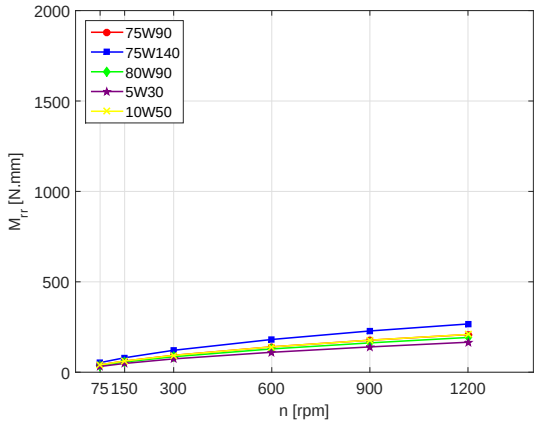

(c) 4 kN; 90 °C

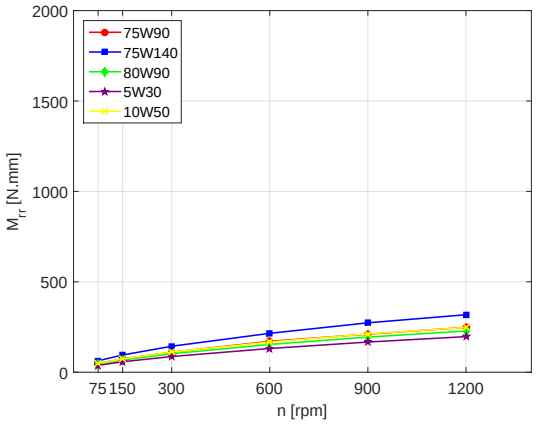

(d) 7 kN; 90 °C

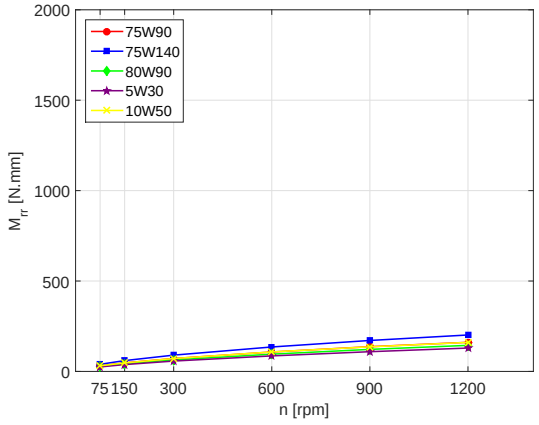

(e) 4 kN; 110 °C

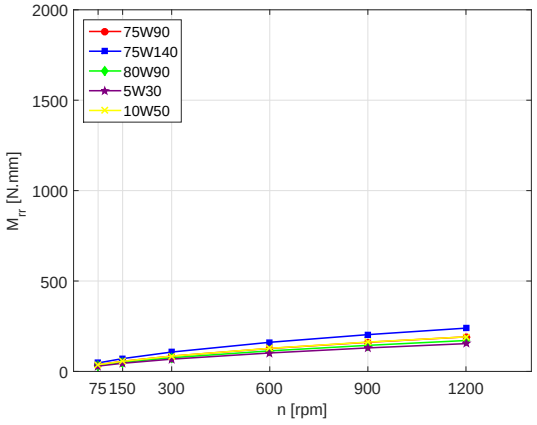

(f) 7 kN; 110 °C

Figure 5.16: TRB 320/28X/Q total friction torque (M_{rr}) results against rotational speed (n) for all tested oils at each temperature and load conditions.

5.2.5.4 Sliding Friction Torque Results

M_{sl}^{exp} values were calculated according to SKF friction torque model and the equation (5.9).

$$M_{sl}^{exp} = M_t^{exp} - M_{rr} \tag{5.9}$$

Increasing rotational speed (n), the trend of M_{sl}^{exp} is similar to that found for M_t^{exp}. Since the rolling torque increased with rotational speed (see Figure 5.16), the sliding friction torque decreased even faster than M_t^{exp} with speed. The M_{sl}^{exp} is dependent on the rolling bearing geometry and oil's COF. Evolving from boundary (75 rpm) to mixed or full film (1200 rpm) is expected to promote a reduction of COF and consequently of M_{sl}^{exp}, as shown in Figure 5.17.

Considering boundary lubrication operating conditions (75-150 rpm), 5W30 and 10W50 presented the highest sliding friction torque. On the other hand, 75W140 oil, which presented higher film thickness, for the same rotational speed (75-150 rpm) presented the lowest sliding friction torque (see Figure 5.17(a)).

When the speed increased, the oils presented similar sliding friction torque at 900 rpm. Above that, 75W140, which had the highest viscosity presented the highest sliding friction torque at 70 and 90 °C. Considering the viscosity ratio (κ) of 75W140 for 1200 rpm, the oil performed close to full film lubrication ($\kappa \simeq 3.5$), which promotes additional losses due to hydrodynamic effects. However, at 110 °C and 1200 rpm no matter the load it presented lower M_{sl}^{exp} values than other lubricants, since it performed under mixed lubrication regime due to the decrease of oil's viscosity.

Comparing 75W90 and 80W90 oils (similar viscosity specifications), presented similar sliding friction torque in spite of being completely different oil formulations, since, 75W90 is a PAO base oil and 80W90 is a mineral.

Despite similar Λ values for all tested conditions between 75W90 and 10W50 oils, 10W50 presented higher M_{sl}^{exp} values than 75W90. This result can be explained due to the different additive package.

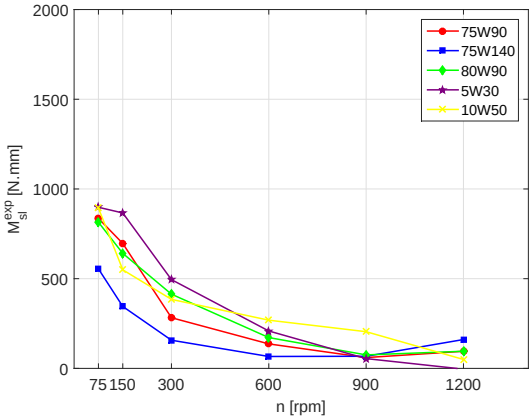

(a) 4 kN; 70 °C

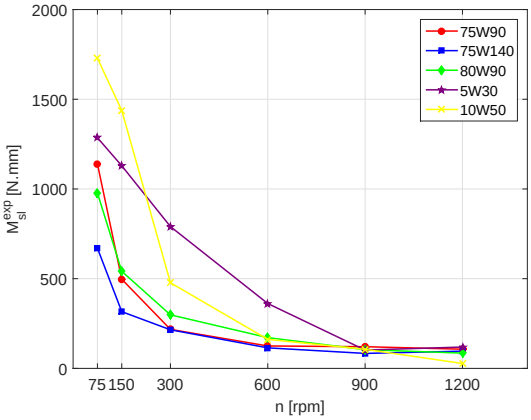

(b) 7 kN; 70 °C

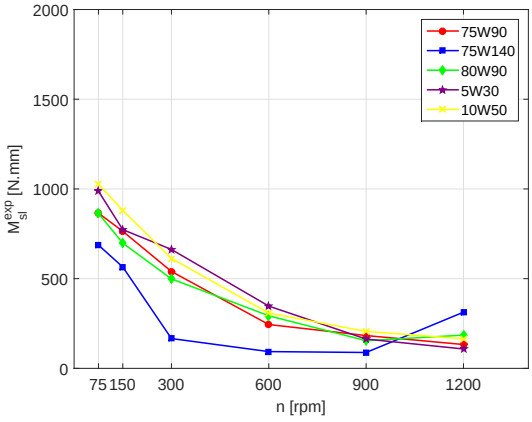

(c) 4 kN; 90 °C

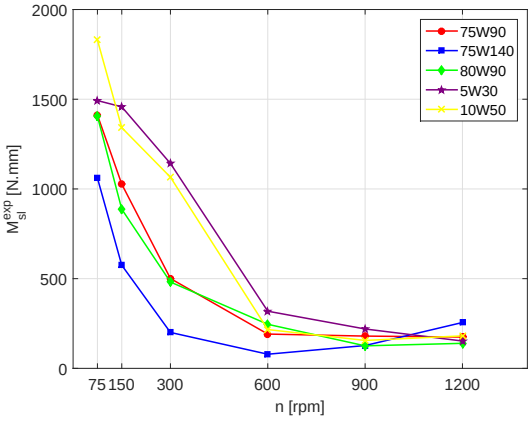

(d) 7 kN; 90 °C

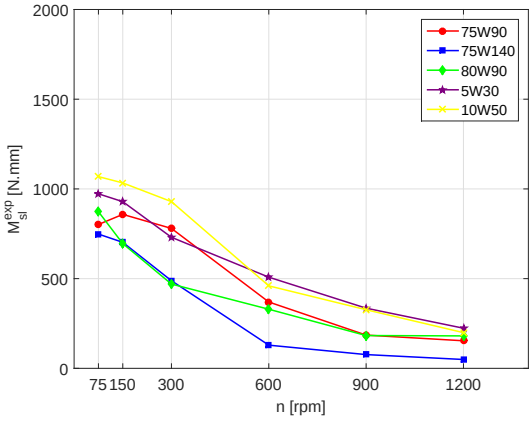

(e) 4 kN; 110 °C

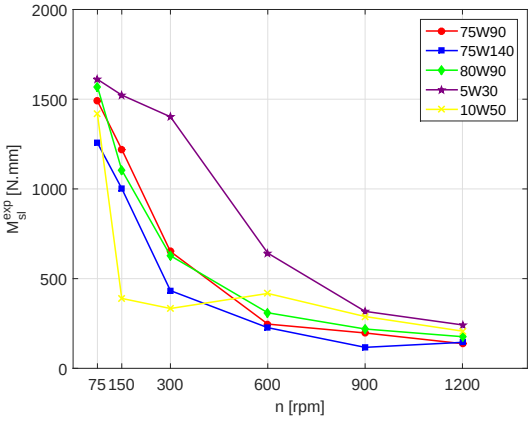

(f) 7 kN; 110 °C

Figure 5.17: TRB 320/28X/Q experimental sliding friction torque (M_{sl}^{exp}) results against rotational speed (n) for all tested oils at each temperature and load conditions.

5.2.5.5 Sliding Coefficient of Friction Results

The μ_{sl}^{exp} is determined according to equation (5.10) as stated in Section 3.2.2. It is dependent on the G_{sl} parameter and presented an identical behaviour to M_{sl}^{exp}, see Figure 5.18.

$$\mu_{sl}^{exp} = \frac{M_{sl}^{exp}}{G_{sl}} \tag{5.10}$$

In Figure 5.19 μ_{sl}^{exp} is plotted against S_{pm} parameter in order to identify the lubrication regime. Moreover it useful to compare μ_{sl}^{exp} for different oil formulations. For the majority of the tests, with the increase of the rotational speed and keeping the temperature and load constant, it was clear that lubrication regime evolves from boundary film to mixed film lubrication.

Furthermore, for 1200 rpm, 75W140 oil results at 70 and 90 ^{o}C and no matter the load as presented in Figure 5.19(a) and 5.19(c) or 5.19(b) or 5.19(d), respectively, shown that full film regime may exist. This result is in compliance with the analysis done in Section 5.2.5.1.

In Figure 5.18 is shown, as expected, that μ_{sl}^{exp} decrease with increasing rotational speed, according with the evolution of the lubrication regime. Also, for the same operating temperature but different load conditions it was observed that μ_{sl}^{exp} presented similar values for both 4 kN than 7 kN.

When operating temperature was increased, sliding COF slightly increased for the same rotational speed due to increment of conditions severity.

75W140 oil presented the lowest μ_{sl}^{exp} mainly at low rotational speeds due to its highest film thickness. Observing Figure 5.19, for lower rotational speeds (<900 rpm), no matter the applied load, 75W140 was more under a well defined mixed lubrication regime, while the other oils were in transition from boundary to mixed lubrication.

In Figure 5.18(a) and Figure 5.19(a) was shown a $\mu_{sl}^{exp} < 0$ for 5W30 oil at 1200 rpm. Since the sliding coefficient of friction is always superior to 0, it is impossible a TRB present such value. However, the result was a consequence of friction torque measurement uncertainties plus the SKF model limitations that could exist for the quantification of rolling torque (M_{rr}).

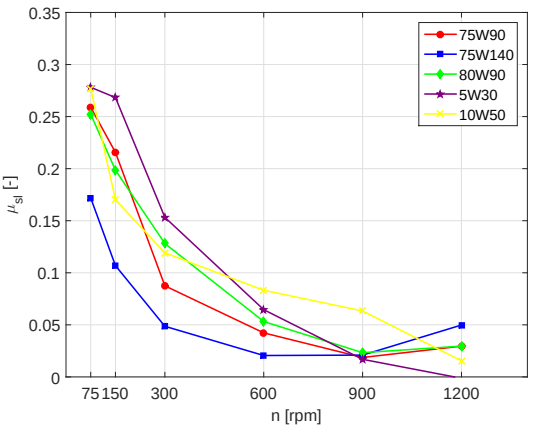

(a) 4 kN; 70 °C

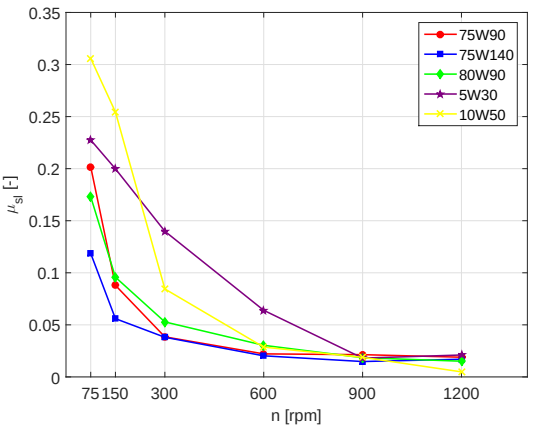

(b) 7 kN; 70 °C

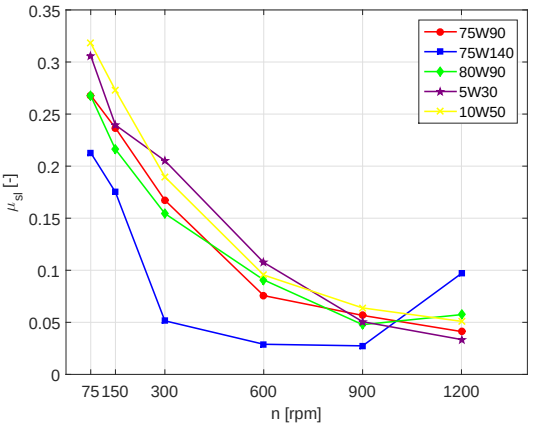

(c) 4 kN; 90 °C

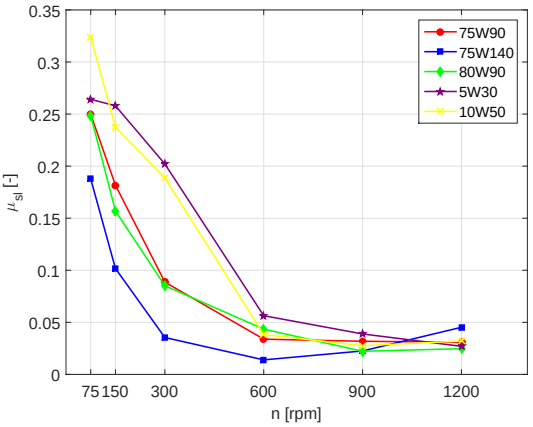

(d) 7 kN; 90 °C

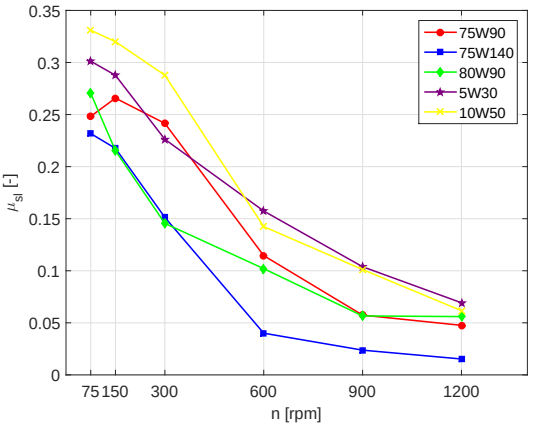

(e) 4 kN; 110 °C

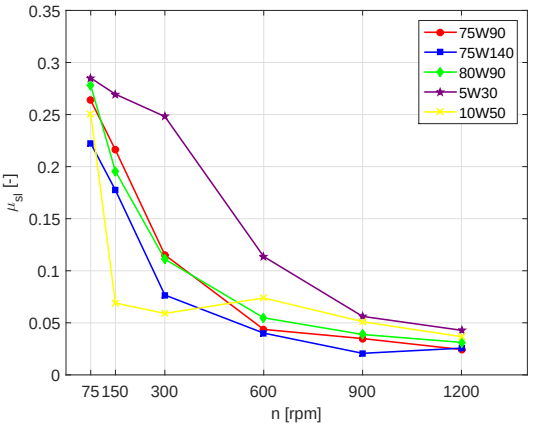

(f) 7 kN; 110 °C

Figure 5.18: TRB 320/28X/Q experimental sliding coefficient of friction (μ_{sl}^{exp}) results against rotational speed (n) for all tested oils at each temperature and load conditions.

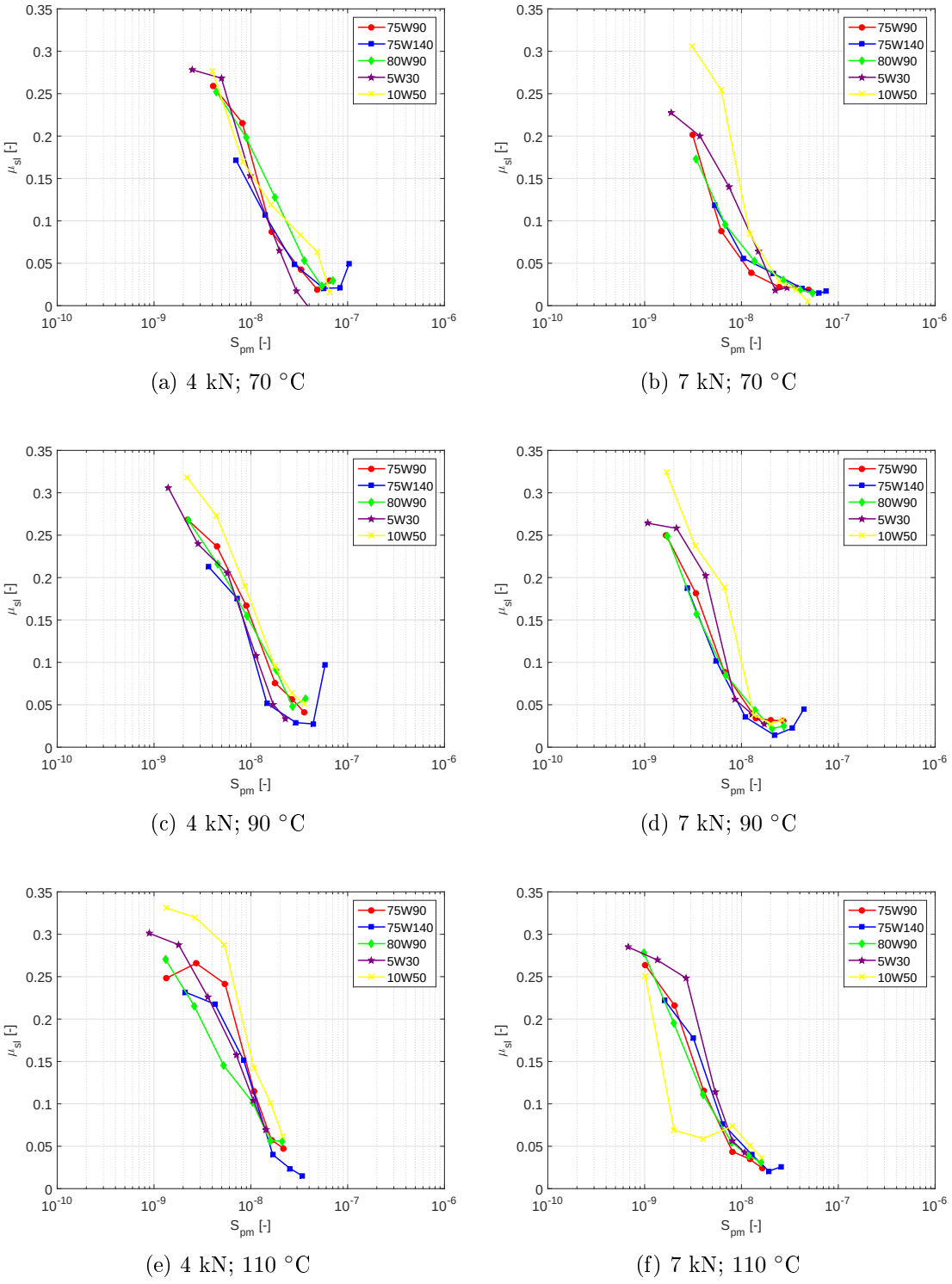

(a) 4 kN; 70 °C

(b) 7 kN; 70 °C

(c) 4 kN; 90 °C

(d) 7 kN; 90 °C

(e) 4 kN; 110 °C

(f) 7 kN; 110 °C

Figure 5.19: TRB 320/28X/Q experimental sliding friction coefficient (μ_{sl}^{exp}) results against modified Hersey parameter (S_{pm}) for all tested oils at each temperature and load conditions.

5.2.5.6 Reference Values for Boundary and Full Film Coefficient of Friction

As discussed in Section 3.2.3, it is possible to minimize the difference between the sliding coefficient of friction predicted by SKF (μ_{sl}^{SKF}) and the experimental values (μ_{sl}^{exp}), adjusting the μ_{bl} and μ_{EHL} through a non-linear fitting method. These values were obtained for each oil, load and temperature condition as presented in Table 5.12. The values were calculated for tests performed after the running-in procedure.

Table 5.12: Boundary (μ_{bl}) and full-film (μ_{EHL}) coefficient of friction determined for all tested oils.

Test	75W90		75W140		80W90		5W30		10W50	
	μ_{bl} [-]	μ_{EHL} [-]	μ_{bl} [-]	μ_{EHL} [-]	μ_{bl} [-]	μ_{EHL} [-]	μ_{bl} [-]	μ_{EHL} [-]	μ_{bl} [-]	μ_{EHL} [-]
70 °C @ 4 kN	**0.263**	0.001	**0.149**	0.020	**0.237**	0.001	**0.290**	0.001	**0.201**	0.036
90 °C @ 4 kN	0.259	0.001	0.207	0.002	0.226	0.001	0.236	0.001	0.299	0.001
110 °C @ 4 kN	0.253	0.001	0.189	0.001	0.156	0.043	0.244	0.001	0.327	0.001
70 °C @ 7 kN	0.105	0.010	0.080	0.015	0.114	0.006	0.222	0.001	0.311	0.001
90 °C @ 7 kN	0.199	0.001	0.119	0.010	0.104	0.001	0.231	0.001	0.260	0.001
110 °C @ 7 kN	0.131	0.001	0.117	0.001	0.123	0.001	0.268	0.001	0.071	0.037

Figure 5.20 presents the friction torque model optimized (M_t^{opt}) (lines) and the experimental values (M_t^{exp}) (markers) obtained for all the oils at every tested condition.

It was observed that calibrated model was not sufficient accurate to predict the experimental values for higher temperatures. However, despite the lack of accuracy at higher temperatures, at 70 °C the calibrated model fited properly, as shown is Figure 5.20(a). Furthermore, taking into account Table 5.12 it was observed that μ_{bl} at 70 °C and 4 kN is dependent on the oil's additive package 75W90/10W50.

In order to understand the lack of accuracy on the optimized model, the mean of the relative error ($\bar{E}_r$) between the μ_{sl}^{exp} and μ_{sl}^{opt}, given by equation (5.11) was calculated and presented in Table 5.13.

$$\bar{E}_r = \frac{\sum E_r}{rs} = \frac{\sum_{i=1}^{rs} \frac{\mu_{sl}^{exp} - \mu_{sl}^{SKF}}{\mu_{sl}^{exp}}}{rs} \tag{5.11}$$

With $rs = 6$.

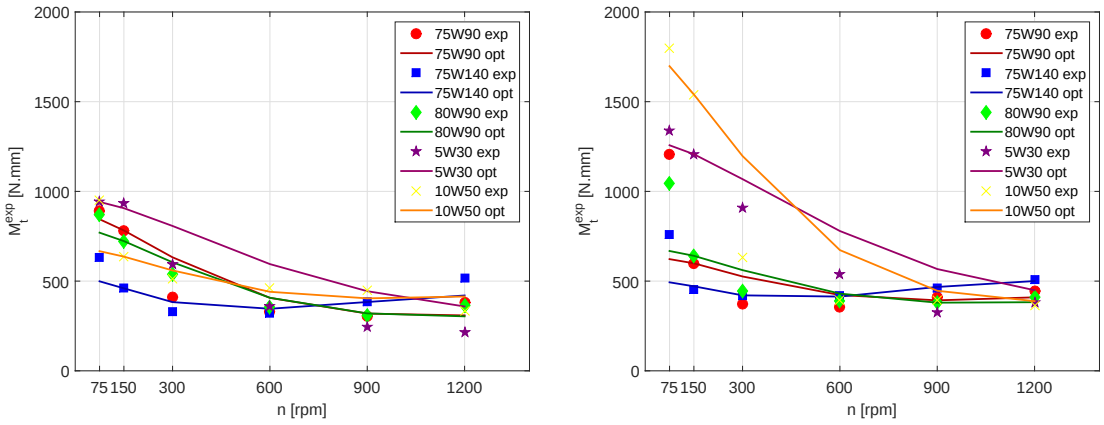

(a) 4 kN; 70 °C (b) 7 kN; 70 °C

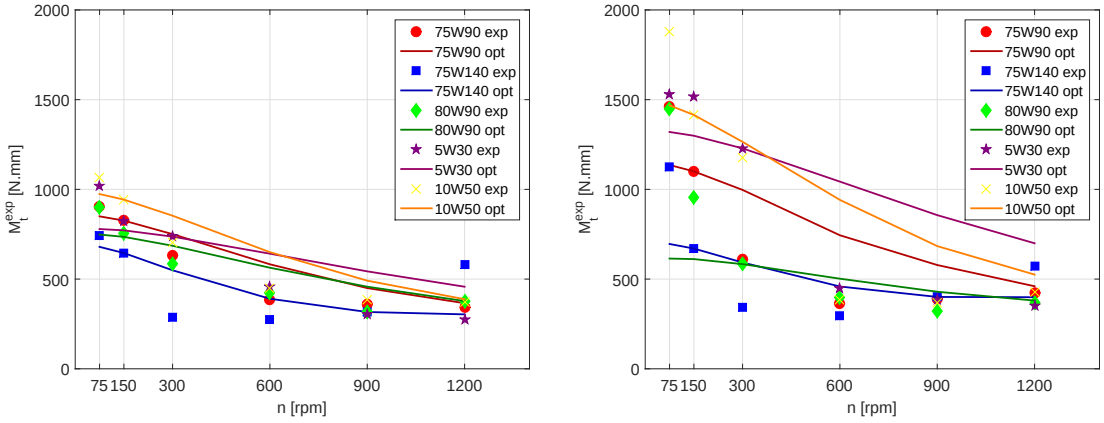

(c) 4 kN; 90 °C (d) 7 kN; 90 °C

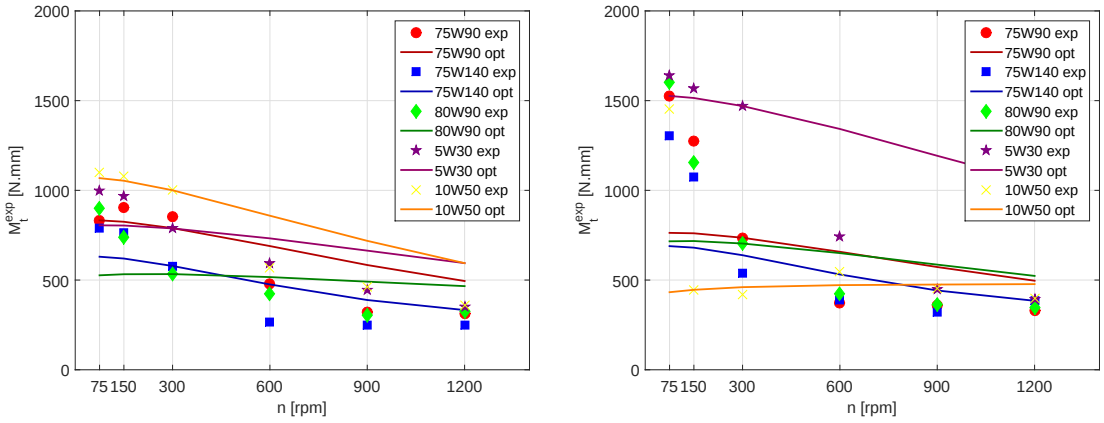

(e) 4 kN; 110 °C (f) 7 kN; 110 °C

Figure 5.20: TRB 320/28X/Q experimental total friction torque (M_t^{exp}) results and optimized total friction torque (M_t^{opt}) against rotational speed (n) for all tested oils at each temperature and load conditions.

Table 5.13: Mean error ($\bar{E}_r$) calculated for the optimized SKF model for each tested condition.

Load	Temperature	$\bar{E}_r$				
[kN]	[°C]	75W90	75W140	80W90	5W30	10W50
4	70	**0.401**	**0.257**	**0.233**	1.057	**0.384**
	90	0.294	0.631	0.301	0.667	0.266
	110	**0.555**	**0.924**	**0.467**	0.397	**0.442**
7	70	**0.375**	**0.110**	**0.220**	0.646	0.720
	90	0.710	0.736	0.394	1.099	0.909
	110	**0.732**	**0.463**	**0.618**	1.012	0.248

It was observed, that $\bar{E}_r$ increase with increase of temperature, for most of performed tests. A explanation to this fact is related with the covered rage of ϕ_{bl} on friction torque measurements, since to performed the optimization method it is necessary determine the μ_{sl} according to equation (5.12), which is dependent on this factor.

$$\mu_{sl} = \phi_{bl} \cdot \mu_{bl} + (1 - \phi_{bl}) \cdot \mu_{EHL} \tag{5.12}$$

To obtain a reliable optimized coefficient of friction (μ_{sl}^{opt}), it would be necessary to perform in each set of tests torque measurements where the extreme values of ϕ_{bl} were achieved, since ϕ_{bl} are correlated with lubrication regime, and for $\phi_{bl} = 1$ the rolling bearing is running under boundary film and for $\phi_{bl} = 0$ is running under full film regime.

So, higher ($\bar{E}_r$) values on the optimization process can be explained with Figure 5.21. For 5W30 oil, no matter the tested temperature for $n = 75$ rpm, $\phi_{bl} \simeq 1$. However, for $n = 1200$ rpm, ϕ_{bl} never reached 0, even for the lowest temperature where $\phi_{bl} = 0.146$, which corresponds to mixed lubricated condition. On the other hand, for 75W140 oil, at 70 °C and 4 kN it was observed for 75 rpm $\phi_{bl} = 0.861$ and for $n = 1200$ rpm, $\phi_{bl} = 0.001$, achieving the full film lubrication regime and consequently lower $\bar{E}_r$ (0.257).

As observed, with the increasing of temperature (from 70 to 110 °C), ϕ_{bl} increase its values for all rotational speeds, due to the decreasing oil's viscosity, revealing at the same time higher $\bar{E}_r$ (Table 5.13).

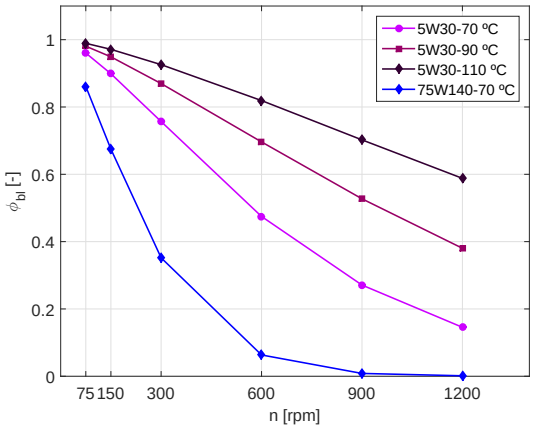

Figure 5.21: Weighting factor for 5W30 oil at 7kN and three temperatures and for 75W140 at 4 kN at 70 °C.

Chapter 6

Conclusions and Future Work

6.1 Tribofilm Formation and friction Torque on RTB 81107 TN

- Based on calculated Λ, all the test were performed under boundary lubrication regime;
- 5W30 oil presented the lowest specific film thickness and 75W140 the highest, due to the lowest and highest oil's viscosity at 110 ^{o}C, respectively;
- All the oils presented lower Λ after 24h, due to the increase in surface roughness (R_q) and the highest variation was observed for 5W30 and 10W50.

Taking into account the torque measurements performed after 1h and 24h of test:

- A decrease in total friction torque between measurements (1h and 24h) were observed for 75W90, 75W140, 80W90 and 5W30. 5W30 presented a slightly reduction (0.4 %). Also it was observed an increase for 10W50 oil. These results could be explained due to;
  - Tribofilm generation on contact surfaces;
- The highest decrease in total friction torque was observed for 75W90 oil (7.5 %), however 75W140 presented the lowest value after 24h between all the lubricants;
- 75W90 and 10W50 oils, with same viscosity, presented identical total torque losses after 24h even having different additive package;
- 80W90 is a mineral base oil but presented better torque loss results than other lubricants with the same viscosity (except 75W140) after 24h.

Taking into account the roughness measurements on raceways performed before and after 24h:

- For axle gear oils (75W90, 80W90 and 75W140) S_a and S_q parameters presented lower values than the candidate axle gear oils (5W30 and 10W50), revealing higher surface protection;
- For all the raceways much higher values of R_a and R_q were found on raceway border than on centre, due to the higher slippage between rollers and raceway;

- 5W30 and 10W50 raceways presented for both measurement locations the highest R_{pk} and R_{vk} parameters, which means that surfaces presented highest peaks and depths, revealing a higher wear in comparison with axle gear oils (75W90, 75W140 and 80W90).

Comparing the XPS analysis performed on a new sample, one immersed on oil bath at 110 ^{o}C and one tested roller, the following conclusions can be drawn:

- The rollers submerged in oil without mechanical work presented a thicker hydrocarbon layer than new rollers. However, no tribofilm formation was observed;
- 80W90 spectra of non mechanically worked roller presented a different shape due to a greatest oil adhesion to surface (lower atomic concentration of Fe);
- After mechanical work, the rollers spectra presented the chemical elements of the oil: presence of magnesium and phosphorus at higher concentrations on axle gear oils and presence of phosphorus, calcium and zinc on candidate axle gear oils;
- It can be concluded that all the lubricants promote the generation of a surface tribofilm. However, 5W30 and 10W50 oils did not presented a remarkable difference of COF between both friction torque measurments;
- Axle gear oils presented lower CPUC and ISUC in comparison with candidate axle gear oils;
- 75W140 oil had the lowest CPUC;
- Despite similar torque loss performance at 24h of test and tribofilm generation on roller surface, 10W50 presented higher CPUC than 75W90;
- Mineral base oil 80W90 presented lower CPUC and ISUC than 5W30 and 10W50 (PAO), revealing the effect of additive package on surface protection;
- 75W90, 75W140 and 80W90 oils, presented lower debris concentration on ferrogram, in agreement with surface roughness measurements and DR ferrography analysis.

6.1.1 TRB Friction Torque Losses

- Higher total friction torque values were observed for all tests without running-in;
- Increasing rotational speed for any given load and temperature, the total friction torque loss decreased;
- In general, 75W140 oil presented for all loads and temperatures and $n < 600$ the lowest values of total friction torque. On the opposite 5W30 oil presented the highest values.
- 75W140 oil presented always the highest specific film thickness for all tested conditions;
- According to the modified Stribeck parameter proposed by *Brandão*, the tests performed on TRBs were running under boundary and mixed lubrication regime, although for 75W140 oil the lubrication regime evolved for full film regime under certain conditions;
- The calculation of reference coefficient of friction (μ_{bl} and μ_{EHL}) values of SKF torque loss model, according to the method proposed by *Fernandes et al* presented better accuracy for lower temperature, since for higher temperatures the range of ϕ_{bl} values achieved is very short.

6.2 Future Work

There are several aspects that need to be further investigated:

- Study the reason of the band mark in cylindrical roller, tacking into account the rolling bearing kinematics: the effect of positive sliding on raceway and negative sliding on roller; in order to evaluate the wear, since no differences on rollers tribofilm was found in XPS results.
- Repeat all the TRB's tests with a running-in procedure with a well defined period time, to confirm the accuracy of the torque measurements;
- Perform tests not only with an axial load but also with a radial load, because it is the common in real practice;
- Perform tests on angular contact ball bearings (ACBB) with the same oil formulations in order to understand the torque loss differences between both rolling bearings, because ACBB can substitute TRB in some situations.

References

[1] T. Garrett, K. Newton, and W. Steeds, *The Motor Vehicle*. Butterworth-Heinemann, 2001.

[2] C. Wincierz, H. Klaus, and M. Muller, "Formulation of multigrade gear oils for high efficiency and low operating temperature," *SAE - Society of Automotive Engineers*, pp. 205–216, 2002.

[3] H. Naunheimer, B. Bertsche, J. Ryborz, and W. Novak, *Automotive Transmissions*. Springer, 2011.

[4] C. Longhurst, "Car bibles." `http://www.carbibles.com`. 2016-03-01.

[5] H. Heisler, *Advanced Vehicle Technology*. Butterworth-Heinemann, 2002.

[6] "Learn engineering - working of a limited slip differential." `http://www.learnengineering.org/2014/05/limited-slip-differential.html`. 2016-03-09.

[7] T. Mang and W. Dresel, eds., *Lubricants and Lubrication*. Wiley and Sons, 2007.

[8] A. S. KOLEKAR, *Lubrication and efficiency of rear wheel drive axles in road vehicle*. PhD thesis, Imperial College London, 2013.

[9] SKF, *SKF General Catalogue*, 2003.

[10] V. Bala, A. J. Rollin, and G. Brandt, "Rheological properties afecting the ffuel ecconomy of multigrade automotive gear lubricants," *SAE -Society of Automotive Engineers International Journal*, pp. 301–308, 2000.

[11] D. M. Pirro and A. A. Wessol, *Lubrication Fundamentals*. Marcel Dekker, 2001.

[12] G. E. Totten, *Handbook of Lubrication and Tribology*, vol. Volume I - Application and Maintenance. CRC Press, 2006.

[13] J. Seabra, A. Campos, and A. Sottomayor, *Lubrificação Elastohidrodinâmica*. FEUP, 2002.

[14] G. W. Stachoviak and A. W. Batchelor, *Engineering Tribology*. Butterworth-Heinemann, 2001.

[15] ACEA, "Acea european oil sequences," tech. rep., ACEA - European Automobile Manufacturers Association, 2012.

[16] API, "Lubricant service designations for automotive manual transmissions manual transaxles, and axles," tech. rep., API - American Petroleum Institute, 2013.

[17] M. Hammami, *Seminar: Efficiency and Wear in Automotive Gear Transmissions*, 2016.

[18] ASTM International, West Conshohocken, PA, *ASTM Standard D2270: Standard Practice for Calculating Viscosity Index from Kinematic Viscosity at 40 and* $100°C$, 1993.

[19] *ASTM D341-09: Standard Practice for Viscosity-Temperature Charts for Liquid Petroleum Products*, 2009.

[20] E. W. Dean and G. H. B. Davis, "Viscosity variation of oils and temperature," *Chemical and Metallurgical Engineering*, vol. 36, pp. 618–619, 1929.

[21] C. M. G. Fernandes, *Power Loss in Rolling Bearings and Gears Lubricated with Wind Turbine Gear Oils.* PhD thesis, Faculdade de Engenharia da Universidade do Porto, 2015.

[22] J. Seabra and J. Castro, eds., *Medição da Viscosidade e da Densidade de um Óleo Lubrificante a Várias Temperaturas*, 2010.

[23] G. E. Totten, ed., *Fuels and Lubricants Handbook: Thechnology, Properties, Performance and Testing.* ASTM Intenational, 2003.

[24] B. S. Fox, "Elemental analysis of lubricating grease by inductively couple plasma atomic emission spectroscopy (icp-aes)," *Journal of ASTM*, vol. 2, no. 8, 2005.

[25] L. R. Rudnick, ed., *Lubricant Additives Chemistry and Applications.* CRC Press, 2009.

[26] R. W. Bruce, *Handbook of Lubrication and Tribology*, vol. II - Theory and Design. CRC Press, 2006.

[27] B. J. Hamrock, S. R. Schmid, and B. O. Jacobson, *Fundamentals of Fluid Film Lubrication.* CRC Press, 2004.

[28] B. Bhushan, ed., *Modern Tribology Handbook*, vol. II - Materials Coating and Industrial Aplications. CRC Press, 2001.

[29] H. Fujiwara and K. Tamada, "Study of long-life thrust needle roller bearings used in low viscosity lubrication conditions," *NTN*, no. 73, pp. 40–47, 2005.

[30] P. Eschmann, L. Hasbargen, and K. Weigand, *Ball and Roller Baearings - Theory, Design and Application.* John Wiley and Sons, 1985.

[31] A. Harnoy, *Bearing Design in Machinery: Engineering Tribology and Lubrication.* CRC Press, 2002.

[32] D. Dowson and G. R. Higginson, *Elastohydrodynamic Lubrication.* Pergamon Press Ltd., 1966.

[33] T. E. Tallian, "On competing failure modes in rolling contact," *ASLE Transactions*, vol. 10 (4), pp. 418–439, 1967.

[34] ISO-281, "Rolling bearings - dynamic load ratings and rating life," standard, ISO - International Organization for Standardization, 2007.

[35] Schaeffler Technologies AG, *Lubrication of Rolling Bearings*, 2013.

[36] J. A. Brandão, M. Meheux, F. Ville, J. Seabra, and M. J. Castro, "Traction curves and rheological parameters of fully formulated gear oils," *Proceedings of the Institution of Mechanical Engineers, Part J: Journal of Engineering Tribology*, vol. 225, pp. 577–593, 2011.

[37] P. P. Amaro, "Friction torque in thrust ball and roller bearings lubricated with "wind turbine gear oils" at constant temperature," Master's thesis, FEUP - Faculdade de Engenharia da Universidade do Porto, 2012.

[38] G. Morales-Espejel, "Using a friction model as an engineering tool," *Evolution SKF*, pp. 27–30, 2006.

[39] C. Fernandes, P. Marques, R. Martins, and J. Seabra, "Gearbox power loss. part i: Losses in rolling bearings," *Tribology International*, vol. 88, pp. 298–308, 2014.

[40] A. Morina and A. Neville, "Understanding the composition and low friction tribofilm formation/removal in boundary lubrication," *Tribology International*, no. 40, pp. 1696–1704, 2007.

[41] S. Jacobson and S. Hogmark, "Surface modifications in tribological contacts," *Wear*, vol. 266, no. 3–4, pp. 370 – 378, 2009.

[42] A. Morina and A. Neville, "Tribofilms: aspects of formation, stability and removal," *JOURNAL OF PHYSICS D: APPLIED PHYSICS*, no. 40, pp. 5476–5486, 2007.

[43] T. Cousseau, B. Graça, A. Campos, and J. Seabra, "Experimental measuring procedure for the friction torque in rolling bearings," *Lubrication Science*, vol. 22, pp. 133–147, 2010.

[44] L. Mummery, *Surface Texture Analysis The Handbook*. Hommelwerke, 1992.

[45] T. R. Thomas, ed., *Rough Surfaces*. Longman Group Limited, 1982.

[46] New York: American Society of Mechanical Engineers, *ASME B46.1-1995 Surface Texture (Surface Roughness Waviness and Lay): An American National Standard*, 1996.

[47] N. Fairley, *CasaXPS Manual - 2.3.15- Spectroscopy*. Casa XPS, 2013.

[48] K. Jacobs, "Ultra high vacuum lab."`http://jacobs.physik.uni-saarland.de/english/instrumentation/uhvl.htm` 2016-08-17.

[49] J. M. Walls and R. Smith, eds., *Surface Science Techniques*. Pergamon Press Ltd., 1994.

[50] A. S. H. Makhlouf and M. Aliofkhazraei, eds., *Handbook of Materials Failure Analysis with Case Studies from the Chemicals, Concrete, and Power Industries*. Butterworth-Heinemann, 2016.

[51] O. Levi and N. Eliaz, "Failure analysis and condition monitoring of an open-loop oil system using ferrography," *Tribol Lett*, no. 36, pp. 17–29, 2009.

[52] B. J. Roylance, "Ferrography—then and now," *Tribology International*, no. 38, pp. 857–862, 2005.

[53] B. Graça and J. Seabra, *Trabalhos Práticos de Lubrificação: TPL4 - Análise de um Óleo por Ferrografia de Leitura Directa*, 3 ed., 2005.

[54] G. Poccock and S. J. Courtney, "Some quantitative aspects of ferrography," *Wear*, vol. 67, pp. 287–301, 1980.

[55] N. Govindarajan and R. Gnanamoorthy, "Ferrography - a procedure for measuring wear rate," *Indian Journal of Engineering and Materials Science*, vol. 15, pp. 377–381, 2008.

[56] B. Graça and J. Seabra, *Trabalhos Práticos de Lubrificação: TPL5 - Análise de um Óleo Lubrificante por Ferrografia Analítica*, 3 ed., 2005.

[57] P. Zal, "Automobile catalog." `http://www.automobile-catalog.com`. 2016-04-12.

[58] H. Xu, A. Singh, and D. Maddock, "Thermal mapping of an automotive rear drive axle," *SAE - Society of Automotive Engineers*, vol. 4, pp. 888–900, 2011.

[59] International Organization for Standardization, *ISO 4288: Geometric product specification (GPS). Surface texture. Profile method: Rules and procedures for the assessment of surface texture.*, 1996.

[60] F. Blateyron, *Good practices for the use of areal filters*, 2014.

[61] S. M. O. Tavares, *Analysis of surface roughness and models of mechanical contacts*, 2005.

[62] X. Jiang, H. Abdul-Rahman, and P. J. Scott, "Multi-scale freeform surface texture filtering using a mesh relaxation scheme," *Measurement Science and Technology*, vol. 24, no. 11, 2013.

[63] zygo, *Surface Texture Parameters*, 2013.

[64] "Olympus." `http:///www.olympus-ims.com/knowledge/metrology/roughness`. 2016-07-12.

[65] R. Leach, ed., *Characterisation of Areal Surface Texture*. Springer, 2013.

[66] SDP/SI -Stock Drive Products/Sterling Instrument, *Handbook of METRIC Drive Components D805*, 2010.

[67] G. Henriot, *Engrenages - Conception - Fabrication - Mise en oeuvre*. Dunod, 2013.

[68] D. Spindler and G. Von Petery, "Angular contact ball bearings for a rear axle differential," tech. rep., SAE- Society of Automotive Engineers - Warrendale (PA US), 2003. SAE Technical paper series.

[69] R. S. Hosokawa, R. Oliveira, D. M. Franco, and A. A. Vendrasco, "Doube row angular contact ball bearing for axle drives," *SAE- Society of Automotive Engineers - Technical Paper*, 2009.

[70] NSK, "Techical report," tech. rep., NSK Motion Conrol, 1991.

Appendix

Appendix A

Data Sheet Oils

TRANSMISSION SYN FE 75W-90

SYNTHETIC OIL FOR GEARS

USES

- Very high performance synthetic oil developed to meet the T.D.L. concept (**T**otal **D**rive **L**ine) for synchronised or non-synchronised manual gearboxes, axles and reduction gears.
- Recommended when filters are added to the lubrication system.
- Recommended for manual gearboxes and axles requiring API GL-4 or API GL-5 or API MT-1 level.

PROPERTIES

- Very high viscosity index.
- Increased Extreme-Pressure and antiwear properties for an optimized lubrication of hypoïd or non-hypoïd axles.
- Excellent antifoam, anticorrosion, antirust properties.
- Excellent thermal stability.
- Very low loss in viscosity through shear.
- Driving comfort.
- Excellent stability in service.
- Compatible with most types of synchronisers for an optimized lubrication of manual gearboxes.
- Very extended drain interval.
- Easy gear changes at low and high temperatures.
- Fuel saving.

CHARACTERISTICS

TRANSMISSION SYN FE	Unit	Grade SAE **75W-90**
Volumetric mass at 15°C	kg/m^3	866
Viscosity at - 40°C	mPa.s	66 000
Viscosity at 40°C	mm²/s	101
Viscosity at 100°C	mm²/s	15
Viscosity index	-	157
Flash point Cleveland	°C	190

The typical characteristics mentionned represent mean values.

SPECIFICATIONS

API MT-1
API GL-4
API GL-5
MACK GO-J
MACK GO-J
MAN 3343 type S (ex MAN 3343 type SL)
SAE J 2360
Meets the requirements for all RENAULT TRUCKS axles (very extended drain interval)
SCANIA STO 1:0
ZF TE-ML 02B, 05B, 07A, 12B, 16F, 17B, 19C

TOTAL LUBRIFIANTS
16, rue de la République
92800 PUTEAUX

TRANSMISSION SYN FE 75W-90
NOVEMBER 2006
N° MPR 11/06

TRANSELF SYNTHESE FE 75W-140

Fully synthetic lubricant for heavily loaded gearboxes and axles.

UTILISATIONS

Mechanical gearboxes and axles in trucks and light trucks

- For lubricating mechanical gearboxes and differentials in the most heavily loaded conditions.
- Particularly recommended when looking for greater ease of gear-shifting in cold weather as well as satisfactory gearbox operation when hot.

PERFORMANCES

API GL-5

- Meets the requirements of the highest extreme-pressure levels of the international API specification.

SCANIA, RENAULT

- Meets the requirements of the following manufacturers:
  - SCANIA : STO 1.0 (gearboxes, high mileage)
  - RENAULT : approval on OT1 Axle (Trafic 1st generation): n° 7711229320

CUSTOMERS BENEFIT

Super multigrade

Extended drain interval

Fuel saving

- Extreme-pressure and anti-wear properties enabling gearboxes or axles to function under the most severe conditions.
- High resistance to degradation, ensuring stable performance after prolonged use at high temperature.
- Outstanding anti-rust and anticorrosion properties even in the presence of water.
- Very high viscosity index and low pour point ensuring perfect lubrication at all temperatures.
- Good shear stability.
- Inert to seals even at high temperatures..
- Very high anti-foaming power thus guaranteeing a resistant lubricating film even at high speeds.
- Very good filterability allowing the lubrication of devices (gearboxes or axles) fitted with oil filters.

CHARACTERISTICS

CHARACTERISTICS	Unités	Grade 75W-140
Density at 15 °C	---	0.885
Kinematic viscosity at 40°C	mm^2/s	183
Kinematic viscosity at 100 °C	mm^2/s	26.3
Viscosity index	---	178
Pour point	°C	-36

The characteristics shown are mean values

TOTAL LUBRIFIANTS
16, rue de la République
92800 PUTEAUX

TRANSMISSION RS FE 80W-90

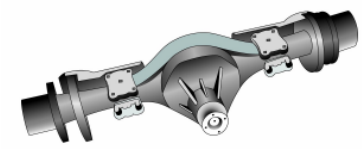

SEMI-SYNTHETIC OIL FOR GEARBOXES AND AXLES

APPLICATIONS

- Semi-synthetic oil with a high viscosity index for the lubrication of gears under severe conditions of use.
- Designed to meet the challenge of the T.D.L. (Total Drive Line) concept: high performance lubrication of hypoid axles as well as synchronized gearboxes, to simplify maintenance without any compromise on components durability.
- Is recommended for use on manual gearboxes, rear axles, or any gear assembly requiring API GL-4, API GL-5, API MT-1 or SAE J2360 levels of performance
- Allows extended service intervals up to 160 000 km on ZF axles and gearboxes (without Intarder), and more generally on all commercial vehicles hypoid axles.
- Suitable for use on Scania gearboxes

PROPERTIES

- Very good low temperature fluidity due to a high viscosity index, generating benefits during cold starts and limiting drag losses and fuel consumption.
- Very high extreme-pressure performance for optimal protection of gears and bearings against scoring and scuffing.
- Excellent antiwear, anticorrosion and antirust properties for the durability of components including gearbox synchronizers.
- Semi synthetic formulation, very resistant to oxidation and allowing extended drain intervals (up to 160 000 kms) compared to standard mineral.

CHARACTERISTICS

TRANSMISSION RS FE	Units	Grade SAE **80W-90**
Volumetric mass at 15°C	kg/m^3	886
Viscosity at 40°C	mm²/s	115
Viscosity at 100°C	mm²/s	14,1
Viscosity Index	-	123
Pour point	°C	- 33

The typical characteristics mentioned represent mean values.

SPECIFICATIONS

MAN 3343 type M (ex MAN 3343 type ML)
ZF TE-ML 02B, 05A, 07A, 12E, 16B, 17B,19B, 21A

Meets the performance requirements of the following international specifications :
API GL-4
API GL-5
API MT-1
MIL-PRF-2105E / SAE J2360

TOTAL LUBRIFIANTS
16, rue de la République
92800 PUTEAUX

QUARTZ INEO LONG LIFE 5W30

The new generation of Low SAPS engine oil specially formulated to meet the technical requirements of Volkswagen group vehicles. Its very high-tech performance optimises the way in which anti-pollution systems - such as Particulate Filters - operate.

APPLICATIONS

- QUARTZ INEO LONG LIFE 5W30 is suitable for all Gasoline and Diesel engines, including the most recent, which comply with Euro V polluting emissions reduction norms in particular.
- It optimises anti-pollution systems, Particulate Filters (PF) in particular.
- It provides engines with excellent protection against wear, ensures they stay ultra clean and allows for longer intervals between oil changes.
- It performs even in the most demanding driving conditions (city, major roads, motorways). It is suited to every kind of driving style, especially sporty, high-speed and all-season driving.

PERFORMANCE

International Standards — **ACEA** C3

OEMs approvals* — **VOLKSWAGEN** VW 504.00/507.00
BMW LL-04 – and Backward compatibility with BMW LL-01 (in Europe only)
MERCEDES-BENZ MB-Approval 229.51 – and Backward compatibility with MB-229.31
PORSCHE C30

CUSTOMER BENEFITS

Increased life of particulate filters	• Ensure the Particulate Filter lifetime, preventing it from getting clogged up prematurely (its metallic component content is lower than that of an oil made using conventional technology).
Respect for the environment	• Environmentally friendly, ensures that the engine's anti-pollution systems perform optimally.
Engine protection and cleanliness	• Provides the engine with excellent protection and ensures that it remains clean
Longer intervals between oil changes	• Exceeds standards in ensuring engine sustainability and satisfies the most demanding manufacturer service plans by allowing for extra-long oil change intervals, thanks to excellent resistance levels against oxidation.

SPECIFICATIONS

TOTAL QUARTZ INEO LONG LIFE	Method	Units	**5W-30 grade**
Kinematic viscosity at 40°C	ASTM D445	mm2/s	67,5
Kinematic viscosity at 100°C	ASTM 445	mm2/s	11,7
Viscosity index	ASTM D2270	-	169
Pour point	ASTM D97	°C	-39
OC Flash Point	ASTM D92	°C	240
TBN	ASTM D2896	mgKOH/g	6.2

The values given in this specifications table are typical values for information purposes only
**refer to the car handbook.*
For cars manufactured after 2007

TOTAL LUBRICANTS
562, avenue du Parc de l'île
92029 Nanterre Cedex
FRANCE

QUARTZ RACING 10W-50

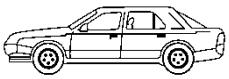

Synthetic multigrade oil for Gasoline and Diesel engines

USES

- **TOTAL QUARTZ RACING** has been developed to cover the most stringent requirements of both gasoline and diesel engines used in sport and intensive conditions
- **TOTAL QUARTZ RACING** is particularly suited to turbo-charged and multi-valved engines.
- **TOTAL QUARTZ RACING** can be used in the most difficult operating conditions (motorways, dense city traffic...), whatever the season.

PERFORMANCES

Specifications	ACEA 2008	A3/B4
	API	SN/ CF

CUSTOMER BENEFITS

- **TOTAL QUARTZ RACING**, thanks to its synthetic formulation, has an exceptional viscosity index and maintains the most resistant oil film even at high temperatures.
- **TOTAL QUARTZ RACING** provides an exceptional anti-wear protection of the engines, especially in the severest conditions of use.
- **TOTAL QUARTZ RACING** protects mechanical parts by ensuring an optimal lubrication as of the time of starting and fully preserves the engine power, thus contributing to its youth and strength.
- **TOTAL QUARTZ RACING** keeps the engine's most sensitive parts clean thanks to its advanced detergent and dispersive additivation.

CHARACTERISTICS

QUARTZ RACING	Units	SAE Grade **10W-50**
Volumetric mass at 15°C	kg/m^3	856
Viscosity at 40°C	mm²/s	115
Viscosity at 100°C	mm²/s	17,0
Viscosity index	-	164
Flash point Cleveland	°C	240
Pour point	°C	-45

The typical characteristics mentioned represent mean values.

Appendix B

Kinematic of Rolling Bearing

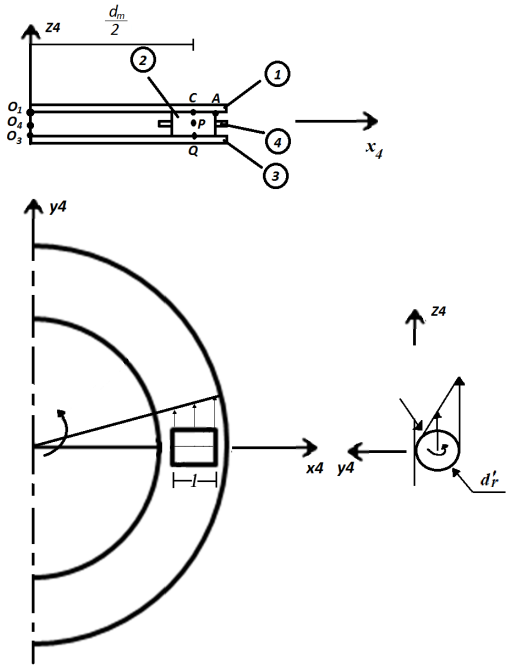

Figure B.1: RTB kinematic scheme.

$$\vec{\omega}_{10}\Big]_{S4} = \begin{Bmatrix} 0 \\ 0 \\ \omega_{10} \end{Bmatrix} \tag{B.1}$$

$$\vec{\omega}_{20}\Big]_{S4} = \begin{Bmatrix} \omega_{20x} \\ 0 \\ \omega_{20z} \end{Bmatrix} \tag{B.2}$$

$$\vec{\omega}_{30}\Big]_{S4} = \begin{Bmatrix} 0 \\ 0 \\ 0 \end{Bmatrix} \tag{B.3}$$

$$\vec{v}_{C_{10}}\Big]_{S4} = \vec{v}_{O_{10}} + \vec{\omega}_{10} \times \overrightarrow{OC} \tag{B.4}$$

$$\vec{v}_{C_{10}}\Big]_{S4} = \begin{Bmatrix} 0 \\ 0 \\ 0 \end{Bmatrix} + \begin{Bmatrix} 0 \\ 0 \\ \omega_{10} \end{Bmatrix} \times \begin{Bmatrix} \frac{d_m}{2} \\ 0 \\ 0 \end{Bmatrix} = \begin{Bmatrix} 0 \\ \frac{1}{2} \cdot d_m \cdot \omega_{10} \\ 0 \end{Bmatrix} \tag{B.5}$$

$$\vec{v}_{C_{20}}\Big]_{S4} = \vec{v}_{Q_{20}} + \vec{\omega}_{20} \times \overrightarrow{QC} \tag{B.6}$$

$$\vec{v}_{Q_{30}}\Big]_{S4} = \vec{v}_{Q_{20}}\Big]_{S4} = \vec{0} \tag{B.7}$$

$$\vec{v}_{C_{20}}\Big]_{S4} = \begin{Bmatrix} 0 \\ 0 \\ 0 \end{Bmatrix} + \begin{Bmatrix} \omega_{20x} \\ 0 \\ \omega_{20z} \end{Bmatrix} \times \begin{Bmatrix} 0 \\ 0 \\ d'_r \end{Bmatrix} = \begin{Bmatrix} 0 \\ -d'_r \cdot \omega_{20x} \\ 0 \end{Bmatrix} \tag{B.8}$$

$$\vec{v}_{C_{20}}\Big]_{S4} = \vec{v}_{C_{10}}\Big]_{S4} \Rightarrow \omega_{20x} = -\frac{d_m}{2 \cdot d} \cdot \omega_{10} \tag{B.9}$$

$$\vec{v}_{P_{20}}\Big]_{S4} = \vec{v}_{Q_{20}} + \vec{\omega}_{20} \times \overrightarrow{QP} \tag{B.10}$$

$$\vec{v}_{P_{20}}\Big]_{S4} = \begin{Bmatrix} 0 \\ 0 \\ 0 \end{Bmatrix} + \begin{Bmatrix} \omega_{20x} \\ 0 \\ \omega_{20z} \end{Bmatrix} \times \begin{Bmatrix} 0 \\ 0 \\ \frac{d'_r}{2} \end{Bmatrix} = \begin{Bmatrix} 0 \\ -\frac{d'_r}{2} \cdot \omega_{20x} \\ 0 \end{Bmatrix} = \begin{Bmatrix} 0 \\ \frac{d_m}{4} \cdot \omega_{10} \\ 0 \end{Bmatrix} \tag{B.11}$$

$$\vec{v}_{P_{20}}\Big]_{S4} = \vec{v}_{P_{40}}\Big]_{S4} = \vec{v}_{O_{3_{10}}} + \vec{\omega}_{40} + \overrightarrow{O_3P} \tag{B.12}$$

$$\vec{v}\,_{P_{20}}\Big]_{S4} = \begin{Bmatrix} 0 \\ 0 \\ 0 \end{Bmatrix} + \begin{Bmatrix} 0 \\ 0 \\ \omega_{40} \end{Bmatrix} \times \begin{Bmatrix} \frac{d_m}{2} \\ 0 \\ 0 \end{Bmatrix} = \begin{Bmatrix} 0 \\ \frac{d_m}{2} \cdot \omega_{40} \\ 0 \end{Bmatrix} \tag{B.13}$$

$$\vec{v}_{P_{20}}\Big]_{S4} = \vec{v}_{P_{40}}\Big]_{S4} \Rightarrow \omega_{40} = -\frac{1}{2} \cdot \omega_{10} \tag{B.14}$$

$$\vec{v}_{C_{14}}\Big]_{S4} = \vec{v}_{C_{10}} - \vec{v}_{C_{40}} = \vec{v}_{C_{10}} - \vec{v}_{P_{40}} \tag{B.15}$$

$$\vec{v}_{C_{40}}\Big]_{S4} = \vec{v}_{P_{40}} + \vec{\omega}_{40} \times \overrightarrow{PC} \tag{B.16}$$

$$\vec{v}_{C_{40}}\Big]_{S4} = \begin{Bmatrix} 0 \\ \frac{d_m}{2} \cdot \omega_{40} \\ 0 \end{Bmatrix} + \begin{Bmatrix} 0 \\ 0 \\ \omega_{40} \end{Bmatrix} \times \begin{Bmatrix} 0 \\ 0 \\ \frac{d'_r}{2} \end{Bmatrix} = \vec{v}_{P_{40}} \tag{B.17}$$

$$\vec{v}\,_{C_{14}}\Big]_{S4} = \begin{Bmatrix} 0 \\ \frac{d_m}{2} \cdot \omega_{10} \\ 0 \end{Bmatrix} - \begin{Bmatrix} 0 \\ \frac{d_m}{4} \cdot \omega_{10} \\ 0 \end{Bmatrix} = \begin{Bmatrix} 0 \\ \frac{d_m}{4} \cdot \omega_{10} \\ 0 \end{Bmatrix} \tag{B.18}$$

$$\vec{v}_{C_{24}}\Big]_{S4} = \vec{v}_{C_{20}} - \vec{v}_{C_{40}} = \vec{v}_{C_{10}} - \vec{v}_{C_{40}} \tag{B.19}$$

$$\vec{v}_{C_{24}}\Big]_{S4} = \begin{Bmatrix} 0 \\ \frac{d_m}{2} \cdot \omega_{10} \\ 0 \end{Bmatrix} - \begin{Bmatrix} 0 \\ \frac{d_m}{4} \cdot \omega_{10} \\ 0 \end{Bmatrix} = \begin{Bmatrix} 0 \\ \frac{d_m}{4} \cdot \omega_{10} \\ 0 \end{Bmatrix} \tag{B.20}$$

$$\vec{v}_{C_{14}}\Big]_{S4} = \vec{v}_{C_{24}}\Big]_{S4} \tag{B.21}$$

$$\vec{v}_{P_{20}}\Big]_{S4} = \vec{v}_{O_{4_{20}}} + \vec{\omega}_{20} \times \overrightarrow{O_4P} \tag{B.22}$$

$$\vec{v}_{P_{20}}\Big]_{S4} = \begin{Bmatrix} 0 \\ 0 \\ 0 \end{Bmatrix} + \begin{Bmatrix} \omega_{20x} \\ 0 \\ \omega_{20z} \end{Bmatrix} \times \begin{Bmatrix} \frac{d_m}{2} \\ 0 \\ 0 \end{Bmatrix} = \begin{Bmatrix} 0 \\ \frac{d_m}{2} \cdot \omega_{20z} \\ 0 \end{Bmatrix} = \begin{Bmatrix} 0 \\ \frac{d_m}{4} \cdot \omega_{10} \\ 0 \end{Bmatrix} \tag{B.23}$$

$$\omega_{20z} = \frac{\omega_{10}}{2} \tag{B.24}$$

$$\vec{v}_{A_{14}}\Big]_{S4} = \vec{v}_{O_{1_{14}}} + \vec{\omega}_{14} \times \overrightarrow{O_1A} \tag{B.25}$$

$$\vec{\omega}_{14}\Big]_{S4} = \vec{\omega}_{10} - \vec{\omega}_{40} \tag{B.26}$$

$$\vec{\omega}_{14}\Big]_{S4} = \begin{Bmatrix} 0 \\ 0 \\ \omega_{10} \end{Bmatrix} - \begin{Bmatrix} 0 \\ 0 \\ \frac{1}{2} \cdot \omega_{10} \end{Bmatrix} = \begin{Bmatrix} 0 \\ 0 \\ \frac{1}{2} \cdot \omega_{10} \end{Bmatrix} \tag{B.27}$$

$$\vec{v}_{A_{14}}\Big]_{S4} = \begin{Bmatrix} 0 \\ 0 \\ 0 \end{Bmatrix} + \begin{Bmatrix} 0 \\ 0 \\ \frac{\omega_{10}}{2} \end{Bmatrix} \times \begin{Bmatrix} \frac{d_m}{2} + \frac{l}{2} \\ 0 \\ 0 \end{Bmatrix} = \begin{Bmatrix} 0 \\ \frac{d_m + l}{2} \cdot \frac{\omega_{10}}{2} \\ 0 \end{Bmatrix} = \begin{Bmatrix} 0 \\ \frac{d_m + l}{4} \cdot \omega_{10} \\ 0 \end{Bmatrix} \tag{B.28}$$

$$\vec{v}_{A_{24}}\Big]_{S4} = \vec{v}_{P_{24}} + \vec{\omega}_{24} \times \overrightarrow{PA} \tag{B.29}$$

$$\vec{\omega}_{24}\Big]_{S4} = \vec{\omega}_{20} - \vec{\omega}_{40} \tag{B.30}$$

$$\vec{\omega}_{24}\Big]_{S4} = \begin{Bmatrix} \omega_{20x} \\ 0 \\ \omega_{20z} \end{Bmatrix} - \begin{Bmatrix} 0 \\ 0 \\ \omega_{40} \end{Bmatrix} = \begin{Bmatrix} \frac{d_m}{2 \cdot d'_r} \cdot \omega_{10} \\ 0 \\ \frac{\omega_{10}}{2} \end{Bmatrix} - \begin{Bmatrix} 0 \\ 0 \\ \frac{\omega_{10}}{2} \end{Bmatrix} = \begin{Bmatrix} \frac{d_m}{2 \cdot d'_r} \cdot \omega_{10} \\ 0 \\ 0 \end{Bmatrix} \tag{B.31}$$

$$\vec{v}_{A_{24}}\Big]_{S4} = \begin{Bmatrix} 0 \\ 0 \\ 0 \end{Bmatrix} + \begin{Bmatrix} \frac{d_m}{2 \cdot d'_r} \cdot \omega_{10} \\ 0 \\ 0 \end{Bmatrix} \times \begin{Bmatrix} \frac{l}{2} \\ 0 \\ \frac{d'_r}{2} \end{Bmatrix} = \begin{Bmatrix} 0 \\ \frac{d_m}{2 \cdot d'_r} \cdot \omega_{10} \cdot \frac{d'_r}{2} \\ 0 \end{Bmatrix} = \begin{Bmatrix} 0 \\ \frac{d_m}{4} \cdot \omega_{10} \\ 0 \end{Bmatrix} \tag{B.32}$$

$$\vec{U}_{S}\Big]_{S4} = \vec{v}_{A_{14}} - \vec{v}_{A_{24}} \tag{B.33}$$

$$\vec{U}_{S}\Big]_{S4} = \begin{Bmatrix} 0 \\ \frac{d_m + l}{4} \cdot \omega_{10} \\ 0 \end{Bmatrix} - \begin{Bmatrix} 0 \\ \frac{d_m}{4} \cdot \omega_{10} \\ 0 \end{Bmatrix} = \begin{Bmatrix} 0 \\ \frac{l}{4} \cdot \omega_{10} \\ 0 \end{Bmatrix} \tag{B.34}$$

$$\vec{U}_{S}\Big]_{S4} = \vec{v}_{A_{14}} + \vec{v}_{A_{24}} \tag{B.35}$$

$$\vec{U}_{S}\Big]_{S4} = \begin{Bmatrix} 0 \\ \frac{d_m + l}{4} \cdot \omega_{10} \\ 0 \end{Bmatrix} + \begin{Bmatrix} 0 \\ \frac{d_m}{4} \cdot \omega_{10} \\ 0 \end{Bmatrix} = \begin{Bmatrix} 0 \\ (\frac{d_m}{2} + \frac{l}{4}) \cdot \omega_{10} \\ 0 \end{Bmatrix} \tag{B.36}$$

$$V_e = \frac{||\vec{U_S}||}{||\vec{U_R}||} = \frac{\frac{l}{4} \cdot \omega_{10}}{(\frac{d_m}{2} + \frac{l}{4}) \cdot \omega_{10}} = \frac{l}{2 \cdot d_m + l} \tag{B.37}$$

Appendix C

Roughness Parameters

C.1 Roughness Filtering

On a profile, the measured roughness is a function of the bandwidth of the measurement, which means that is not an intrinsic property [28]. Thus, to measure roughness on a surface it is necessary differentiate it from waviness to a specific application. The procedure that allows to distinguish both is called filtering, and it involves identify the irregularities to be measured and isolating them (roughness) from the remainder (form and waviness) with a filter [45]. What defines the transition between roughness and waviness is the cut-off length. A small cut-off value, more than isolate the waviness could hide roughness information, while a large cut-off value would include the waviness in roughness measurement [44]. A correct cut-off length should be selected and according to *Mummery* [44] it might have about 2.5 times the peak-to-peak spacing of the profile roughness. In Table C.1 is presented the cut-off length information according to ISO 4288. For rolling bearings the value is defined in 250 μm.

Table C.1: Selection of cut-off filter (λ_c): ISO 4288 [59].

Cut-off λ_c [mm]	Peak spacing (periodic profiles) S_m [mm]	Measured roughness (non-periodic profiles) R_z [μm]	R_a [μm]
0.08	>0.013 - 0.04	>0.025 - 0.1	>0.006 - 0.02
0.25	>0.04 - 0.13	>0.1 - 0.5	>0.02 - 0.1
0.8	>0.13 - 0.4	>0.5 - 10	>0.1 - 2
2.5	>0.4 - 1.3	>10 - 50	>2 - 10
8	>1.3 - 4	>50 - 200	>10 - 80

Despite the main reason to use a filter is separate roughness from waviness and form, the filtration process is required for other purposes, for instance to correct the stylus effect on raw data, to clean up data measured with an optical probe or to compare data acquire with different instruments methods [60].

Analog and digital filters are available. Nowadays, digital filters are more used since they are simpler than analog, and it is possible to apply different cut-off lengths for the same profile measured. From the all filters available, Gaussian filter, which is a digital phase correct filter, is a standardised and a good general-purpose filter (ISO 11562) to determine the mean line profile. It is the filter used on the roughness analysis performed in this work [61].

In Figure C.1 is showed the process to perform a full analysis of surface. It can be divided in four parts: surface sampling and representation, decomposition and filtration, texture representation and mapping and characterization and parametrization [62].

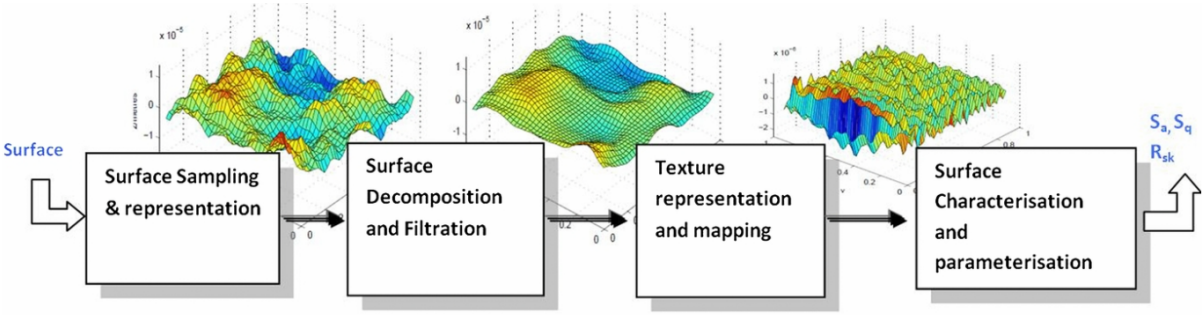

Figure C.1: Steps required to perform a full roughness analysis [62].

C.1.1 Profile and Areal Parameters

Depending on the method (linear or areal) to acquire surface information different parameters are used. In this section will be presented the parameters applied in profile and surface topography.

C.1.1.1 2D Parameters

The following parameters describes the profile amplitude and the material distribution.

- Arithmetical mean deviation of the roughness profile (R_a)

Used to monitor gradual changes on surface finish on a production process, due to the wear of the cutting tool. Expresses the arithmetical mean of the absolute profile values ($Z(x)$) in a sampling length (l_S), given by equation (C.1) and shown in Figure C.2 [44, 63].

$$R_a = \frac{1}{l_S} \cdot \int_0^{l_S} \mid Z(x) \mid dx \tag{C.1}$$

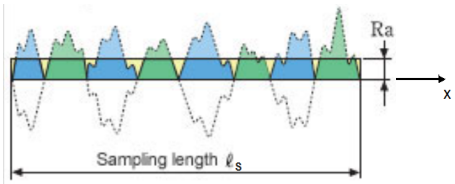

Figure C.2: Amplitude parameter: R_a [64].

- Root mean square deviation of the assessed profile (R_q)

The parameter R_q is more sensitive to peaks and valleys than R_a. It represents the average of the measured height taken within the evaluation length and measured from the mean linear profile, and it is given by equation (C.2) [44, 63]. In Figure C.3 is shown the R_q parameter.

$$R_q = \sqrt{\frac{1}{l_S} \cdot \int_0^{l_S} \mid Z(x)^2 \mid dx} \tag{C.2}$$

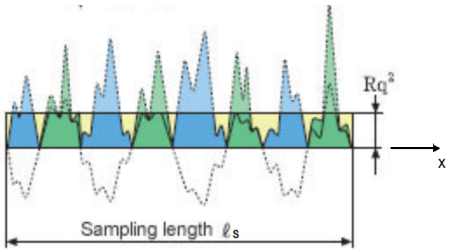

Figure C.3: Amplitude parameter: R_q [64].

- Maximum peak-to-valley height (R_{max})

As the name indicates, this parameter measures the greatest peak-to-valley distance (z_{pv}) in a defined sample length [44].

- Mean peak-to-valley height ($R_{z(DIN)}$)

For determination of $R_{z(DIN)}$, the sampling length is divided in five equal segments with the same length of λ_c, as shown in Figure C.4, and it is calculated the maximum peak to valley height (z_{pvi}) for each segment. The $R_{z(DIN)}$ is the average of the five (z_{pvi}), given by the equation (C.3), and it is more sensitive than R_a, since are examined profile heights and not averages [44].

$$R_{z(DIN)} = \frac{1}{5} \cdot \sum_{i=1}^{5} z_{pvi} \tag{C.3}$$

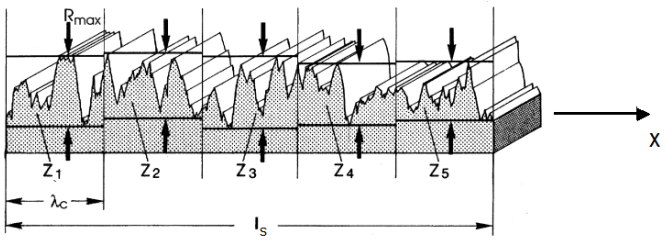

Figure C.4: Amplitude parameter: $R_{z(DIN)}$ and R_{max} [44].

- Skewness of the roughness profile (R_{sk})

R_{sk} is a statistical parameter (equation (C.4)) which indicates the profile symmetry about a mean line. Negative values expresses a concentration of material near the top of the surface, while positive skew is a result of a profile with low material concentration between peaks (see Figure C.5) [44,63].

$$R_{sk} = \frac{1}{n_r \cdot R_q^3} \cdot \sum_{i=1}^{n_r} y_i^3 \tag{C.4}$$

Where y_i is the ordinate height and n_r is the number of ordinates.

- Kurtosis of the roughness profile (R_{ku})

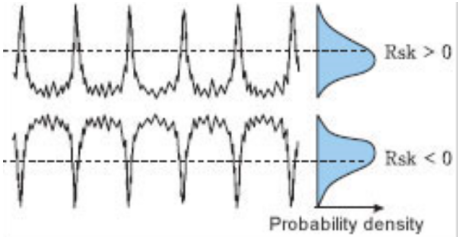

Figure C.5: Amplitude parameter: R_{sk} [64].

Kurtosis is a statistical parameter given by equation (C.5) which measure the randomness of heights and sharpness of a surface in a defined sampling length. For a sharp amplitude distribution ($R_{ku} > 3$), surface morphology presents large peaks and valleys. For a flat amplitude distribution ($R_{ku} < 3$), the surface profile presents many small, rounded peaks and valleys (see Figure C.6) [44,63].

$$R_{ku} = \frac{1}{n_r \cdot R_q^4} \cdot \sum_{i=1}^{n_r} y_i^4 \tag{C.5}$$

Where y_i is the ordinate height and n_r is the number of ordinates.

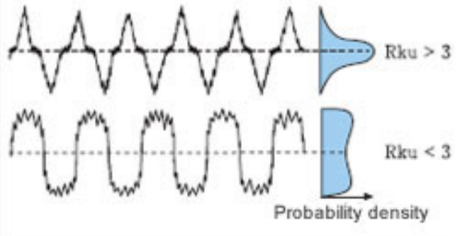

Figure C.6: Amplitude parameter: R_{ku} [64].

The parameters described bellow are related with the lubrication performance, and evaluate the plateau structure of the surface.

- Abbot-Firestone Curve

The *Abbot-Firestone* curve or also named bearing are curve (BAC) or material ratio curve, is a cumulative curve which represents the height distribution. BAC is counted from the highest point on the surface (where the curve equals 0 %) to its lowest point (where the curve reaches 100 %) and is created by drawing lines parallel to the datum and measuring the fraction of the line which lies within the profile [65]. In right side of Figure C.7 is represented the BAC curve.

The R_k family of parameters are calculated according BAC based on the ISO 13565-2:1996 standard, which is divided in three parts, that describes the core (R_k), the peaks (R_{pk}) and the valleys (R_{vk}), shown in Figure C.7.

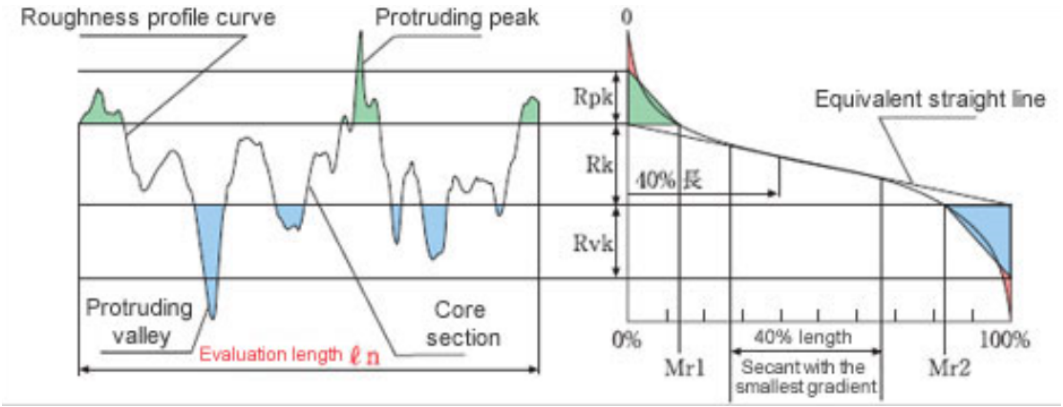

Figure C.7: Roughness profile and Abbot-Firestone Curve [64].

- Core roughness depth (R_k)

R_k is a measure of the core roughness of the surface with the predominant peaks and valleys removed. It is the long term running surface which will influence the performance and the life of the bearing surface.

- Reduced peak height (R_{pk})

Normally it is the top portion of the surface that will be worn away in the run-in period. This parameter is a measure of the peak height above the core roughness and represents the height of a triangle having a base equal to M_{r1}. Bigest R_{pk} implies a surface composed of high peaks providing small initial contact area and thus high areas of contact stress [44, 63].

- Reduced valley depth (R_{vk})

It is the lowest part of the surface that retains lubricant. This parameter is a measure of the valley depth below the core roughness and represents the height of a triangle having a base equal to M_{r2}. It is related to lubricant retention and debris entrapment [44, 63].

- Peak material ratio (M_{r1})

The material ratio at which R_{pk} and R_k meet. It represents the upper limit of the core roughness profile and the percentage of the surface that may be removed during running-in [44, 63].

- Valley material ratio (M_{r2})

The material ratio at which R_{vk} and R_k meet. It represents the lower limit of the core roughness profile [44, 63].

C.1.1.2 3D Parameters

The following parameters describes the topography amplitude.

- Arithmetical mean deviation height (S_a)

S_a is a 3D parameter expanded from 2D parameter R_a, and it is also used to monitor gradual changes on surface finish on a production process. Expresses the arithmetical mean of absolute height values ($Z(x,y)$) in a sampling area (A_S) and it is given by equation (C.6) and shown in Figure C.8 [64].

$$S_a = \frac{1}{A_S} \cdot \int_{A_S} \int \mid Z(x,y) \mid dxdy \tag{C.6}$$

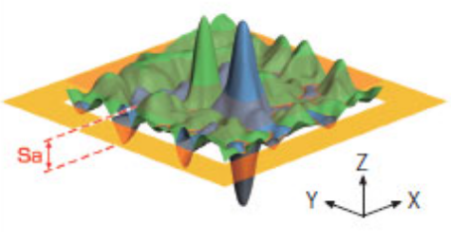

Figure C.8: Amplitude parameter: S_a [64].

- Root mean square deviation height (S_q)

The parameter S_q is more sensitive to peaks and valleys than S_a. It represents the average squared value of the measured height taken within the evaluation area and measured from the mean surface, and it is given by equation (C.7) [64]. In Figure C.9 is shown the S_q parameter.

$$S_q = \sqrt{\frac{1}{A} \cdot \int_A \int Z(x,y)^2 dxdy} \tag{C.7}$$

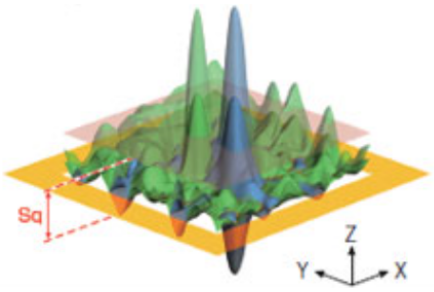

Figure C.9: Amplitude parameter: S_q [64].

- Maximum peak height (S_p)

This parameter, presented in Figure C.10, indicates the maximum value peak height (z_p) on the surface in the measured area, given by equation (C.8).

$$S_p = max(Z(x, y)) \tag{C.8}$$

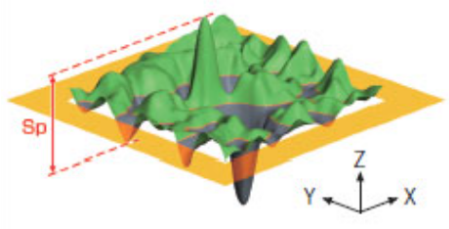

Figure C.10: Amplitude parameter: S_p [64].

- Maximum valley depth (S_v)

This parameter, (Figure C.11), indicates the maximum valley depth (z_v) on the surface in the measured area, given by equation (C.9).

$$S_v = min(Z(x, y)) \tag{C.9}$$

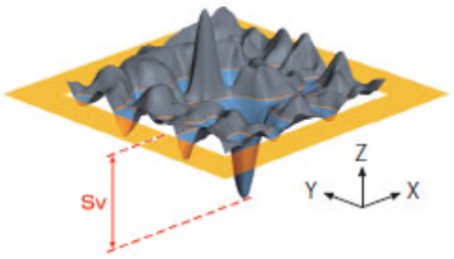

Figure C.11: Amplitude parameter: S_v [64].

- Maximum mean peak-to-valley height (S_z)

S_z expresses the sum of the maximum value of peak height (S_p) and the maximum value of valley depth (S_v) on the surface within the measured area (see Figure C.12). It is defined according two standards ISO and DIN. However, in this study only ISO standard will be discussed. The $S_{z(ISO)}$ is given by equation (C.10) [44].

$$S_{z(ISO)} = S_p + S_v \tag{C.10}$$

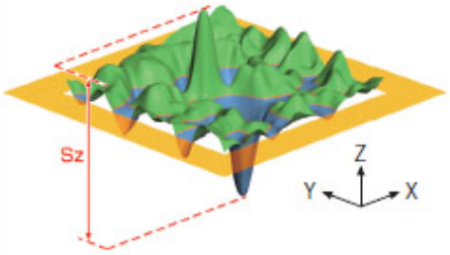

Figure C.12: Amplitude parameter: S_z [64].

- Skewness of the surface topography (S_{sk})

S_{sk} is a statistical parameter which indicates the profile symmetry about a mean surface. However, with this parameter it is not possible identify if the profile is equally distributed above or below the mean surface plane. Negative values expresses a concentration of material near the top of the surface, while positive skew is a result of a profile with low material concentration between peaks [44]. For surfaces having the same S_a the use of this parameter allows to differentiate them. In equation (C.11) is the presented the skewness parameter.

$$S_{sk} = \frac{1}{S_q^3}\left(\frac{1}{A_S}\int_{A_S}\int Z(x,y)^3 dxdy\right) \tag{C.11}$$

- Kurtosis of the surface topography (S_{ku})

Kurtosis (S_{ku}) is a statistical parameter and measure the randomness of heights and sharpness of a surface in a defined sampling area. This parameter can detect whether the profile spikes are equally distributed and measure the spikiness of the area. For a sharp amplitude distribution ($S_{ku} > 3$), surface morphology presents large peaks and valleys. For a flat amplitude distribution ($S_{ku} < 3$), the surface profile presents many small, rounded peaks and valleys, being a useful parameter in predicting component performance with respect to wear and lubrication retention. However it cannot stablish the difference between a hill and a valley [44,63]. In equation (C.12) is presented the skewness parameter.

$$S_{ku} = \frac{1}{S_q^4}\left(\frac{1}{A_S}\int_{A_S}\int Z(x,y)^4 dxdy\right) \tag{C.12}$$

Appendix D

XPS Detailed Spectra

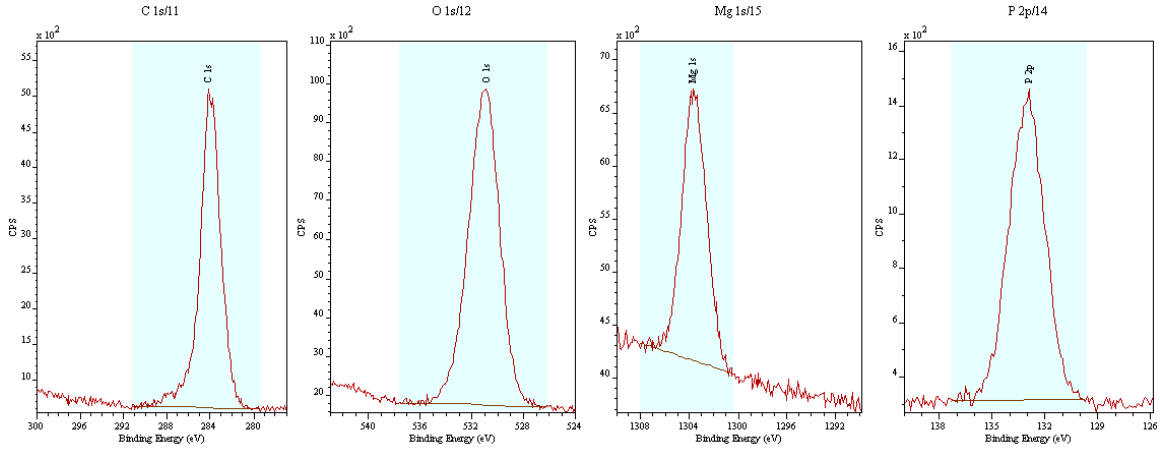

(a) Worked roller.

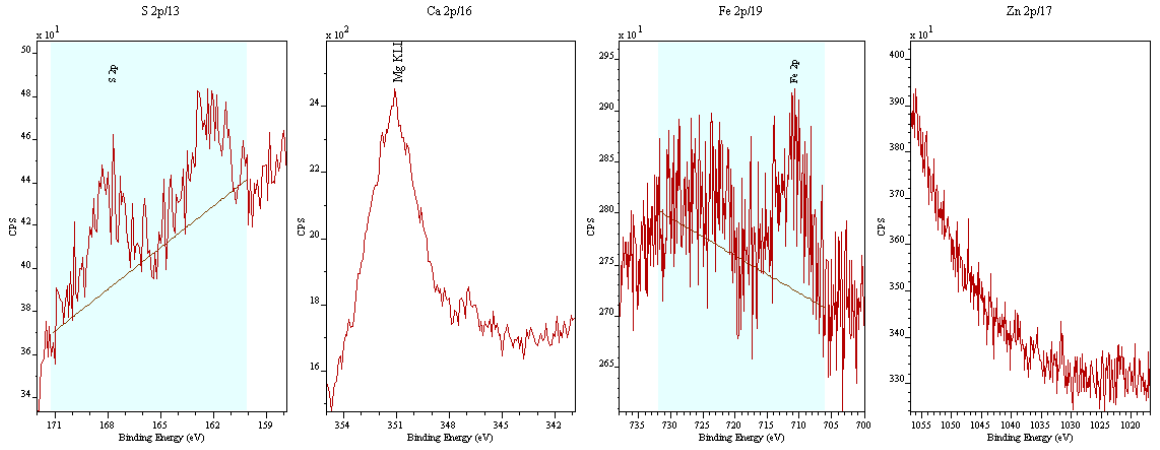

(b) Non-worked roller.

Figure D.1: XPS detail spectra on RTB 81107 TN tested 24h roller on Z1 region for tests performed with 75W90 oil.

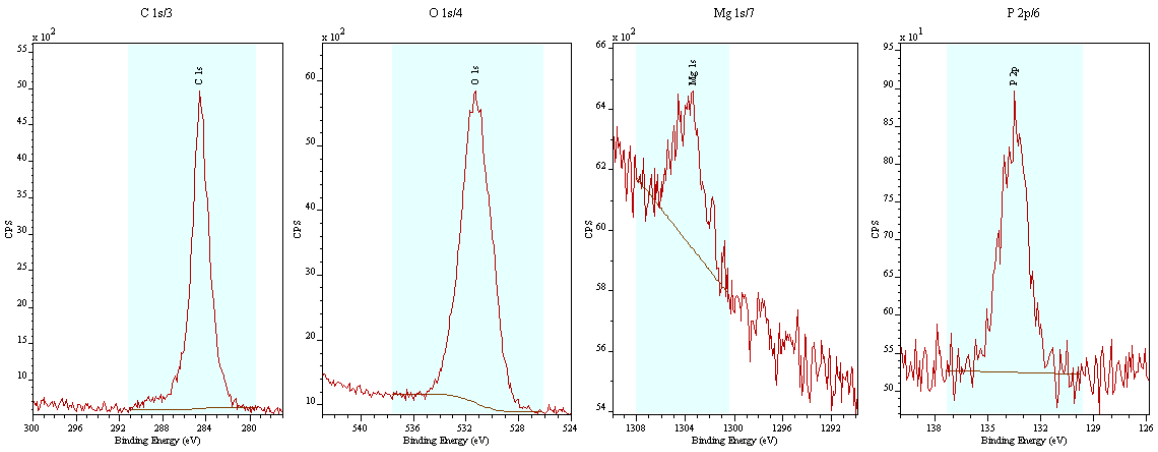

(a)

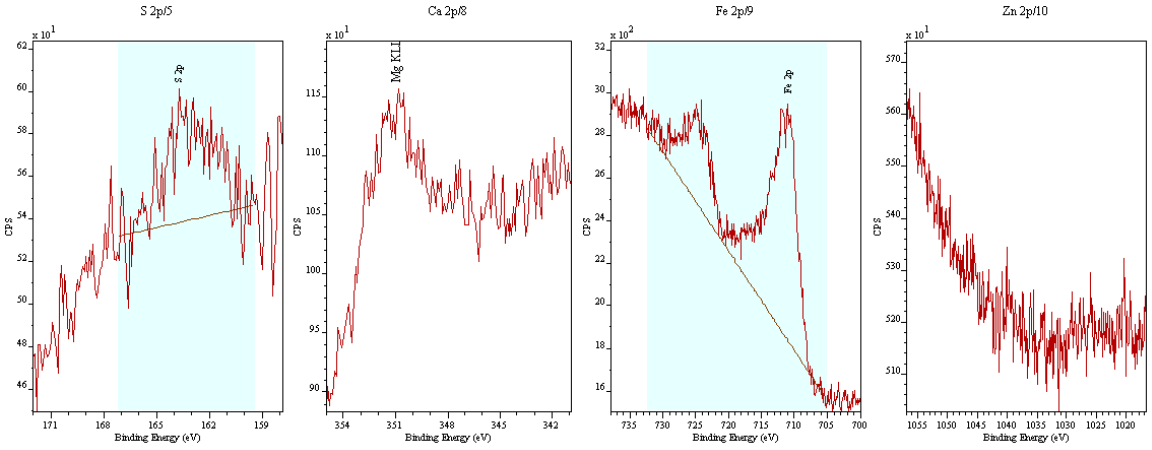

(b)

Figure D.2: XPS detailed spectra on RTB 81107 TN oven 24h (immersed) roller on centre region for tests performed with 75W90 oil.

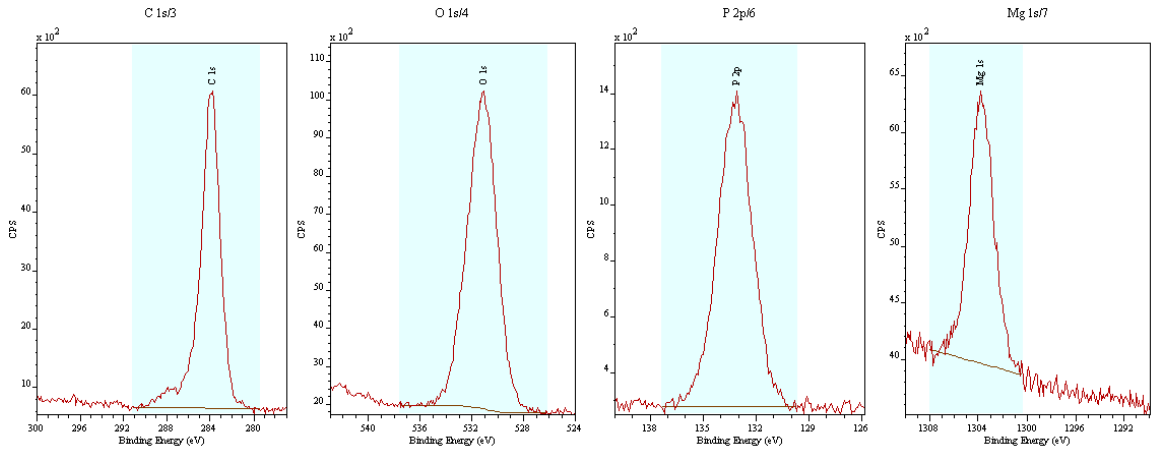

(a)

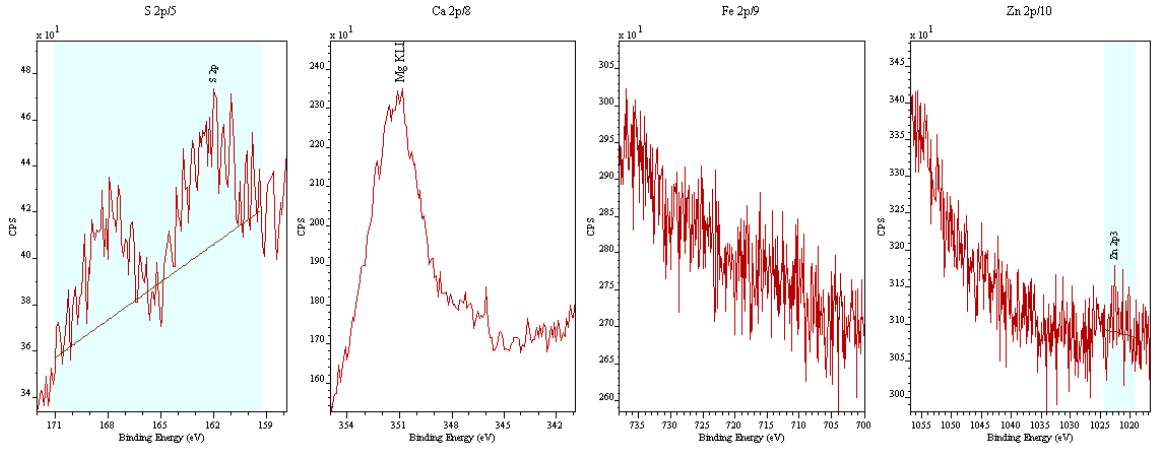

(b)

Figure D.3: XPS detailed spectra on RTB 81107 TN tested 24h roller on Z1 region for tests performed with 75W140 oil.

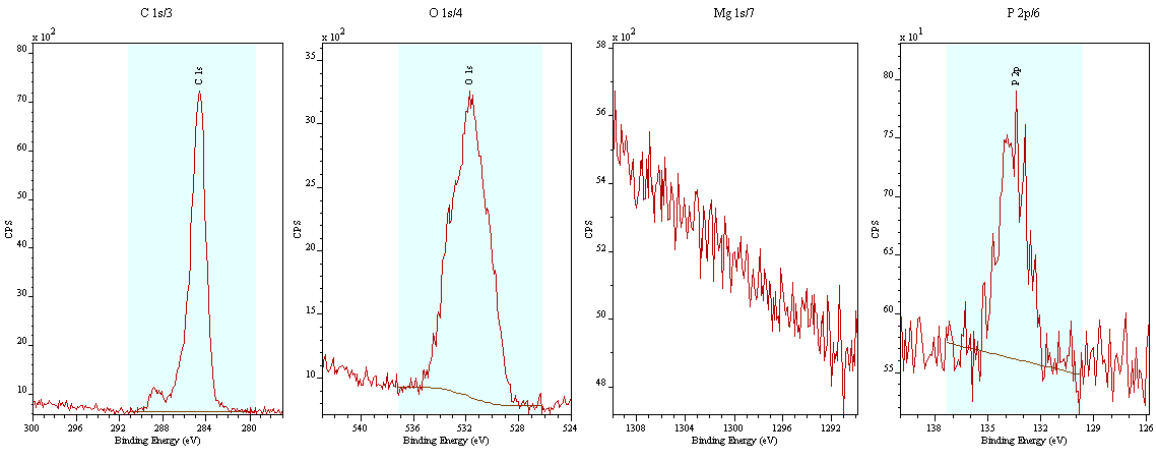

(a)

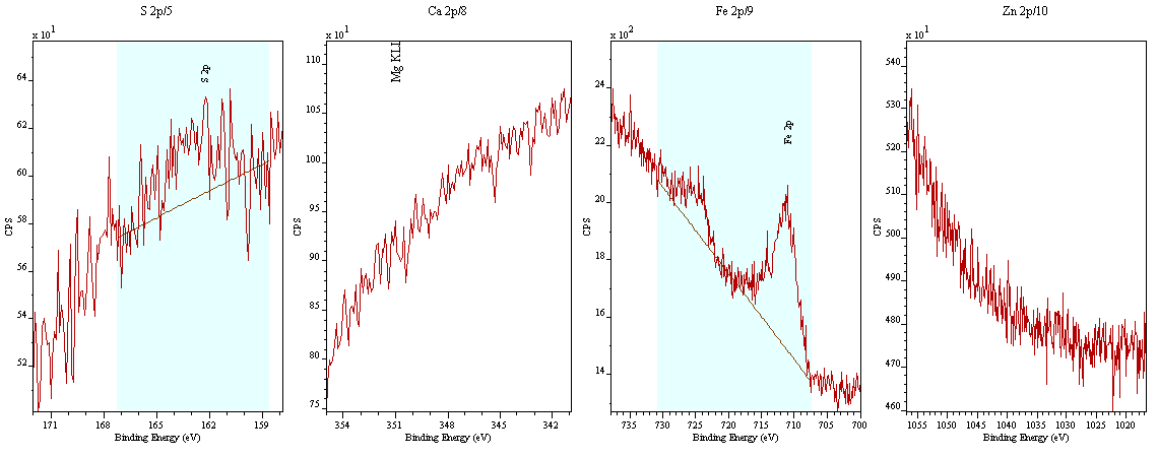

(b)

Figure D.4: XPS detailed spectra on RTB 81107 TN oven 24h (immersed) roller on centre region for tests performed with 75W140 oil.

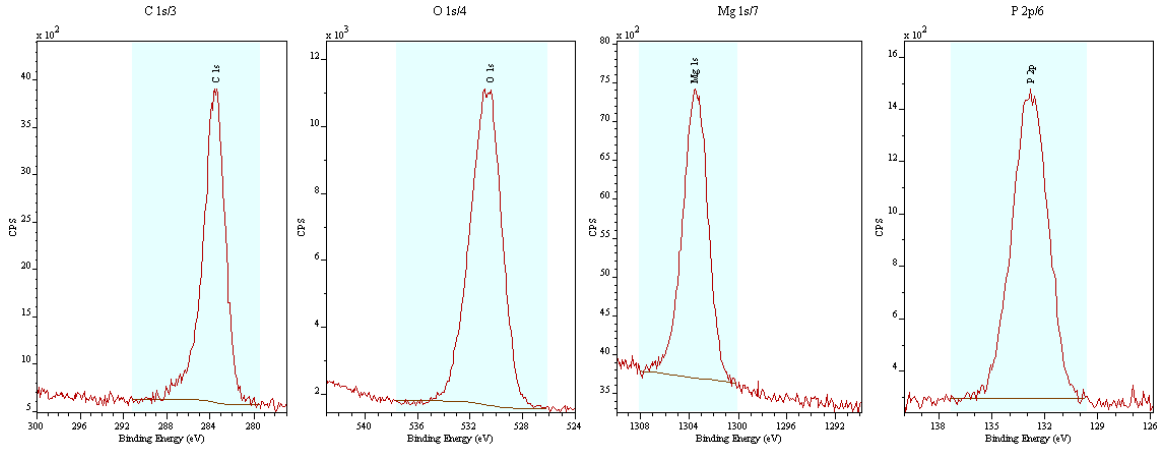

(a)

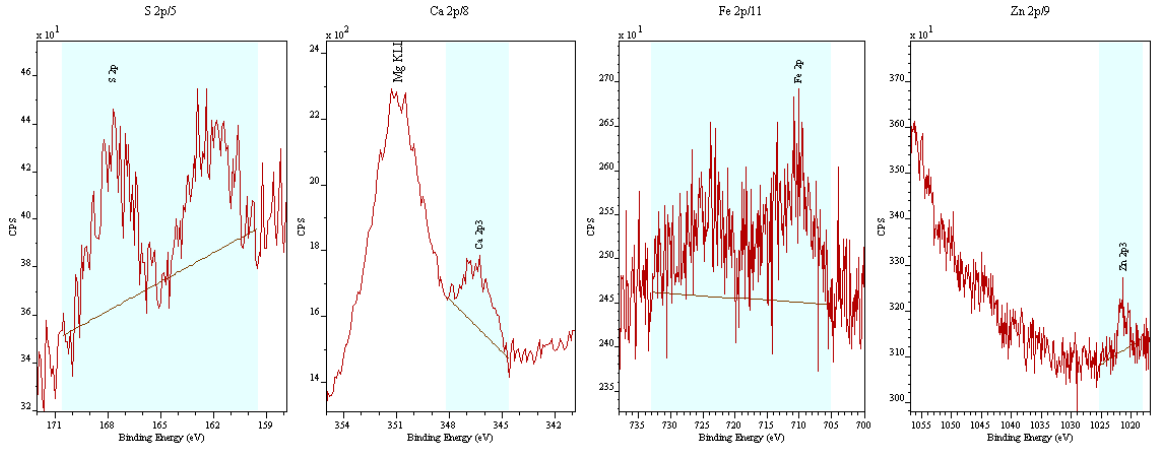

(b)

Figure D.5: XPS detailed spectra on RTB 81107 TN tested 24h roller on Z1 region for tests performed with 80W90 oil.

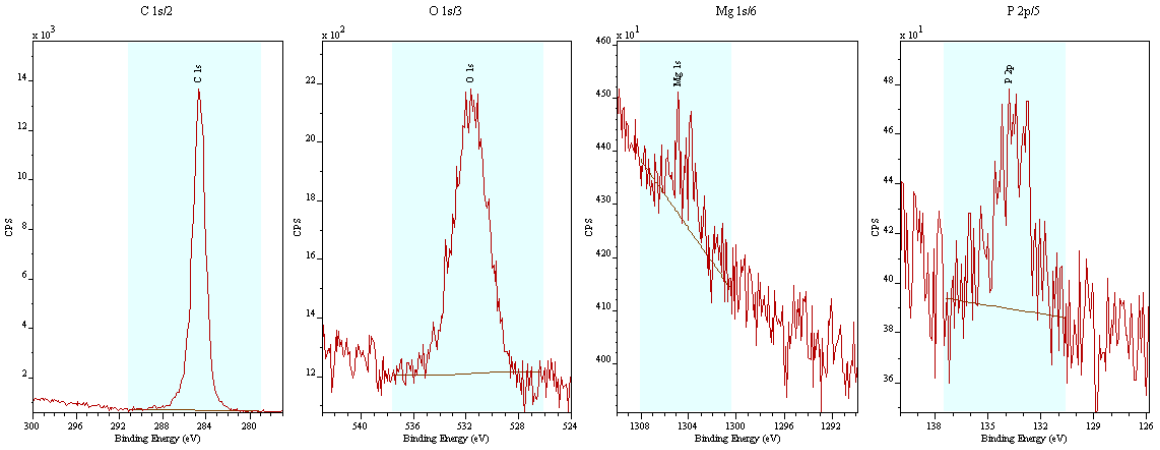

(a)

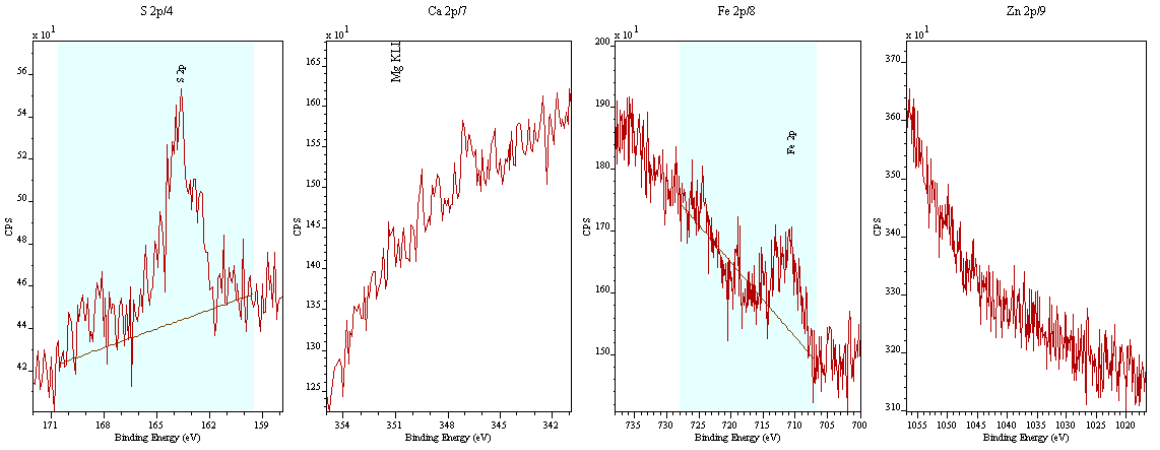

(b)

Figure D.6: XPS detailed spectra on RTB 81107 TN oven 24h (immersed) roller on centre region for tests performed with 80W90 oil.

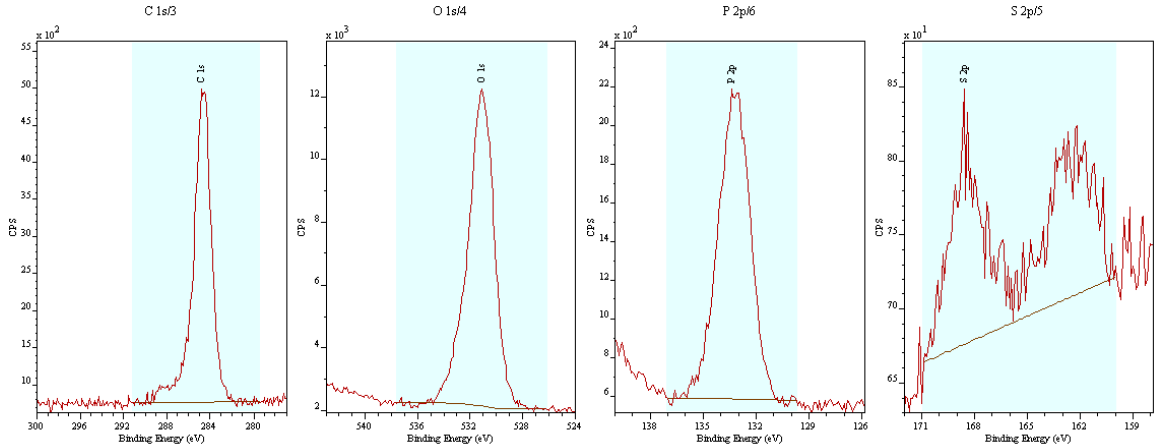

(a)

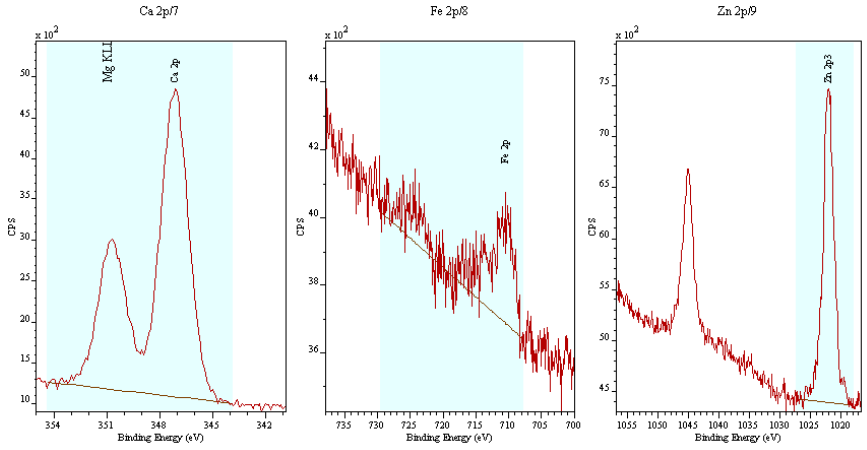

(b)

Figure D.7: XPS detailed spectra on RTB 81107 TN tested 24h roller on Z1 region for tests performed with 5W30 oil.

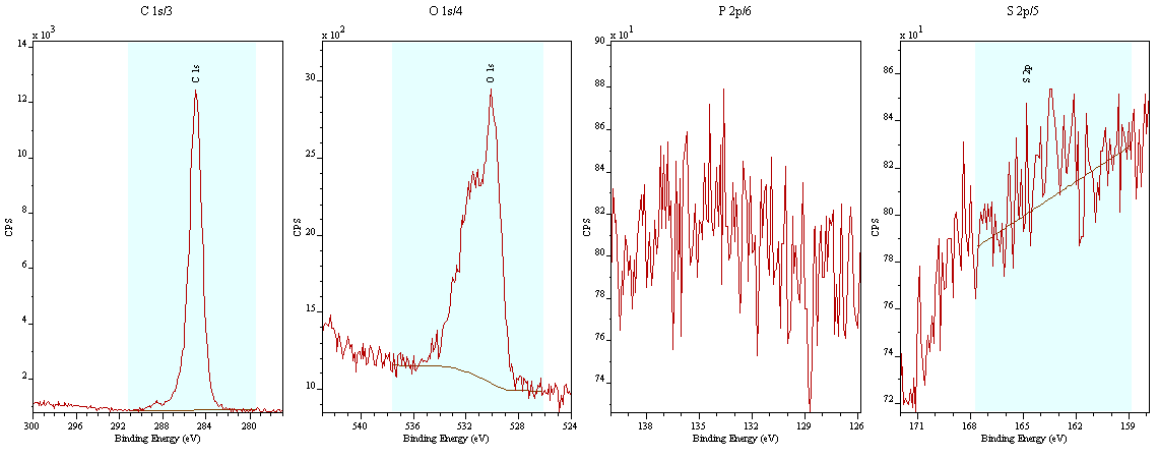

(a)

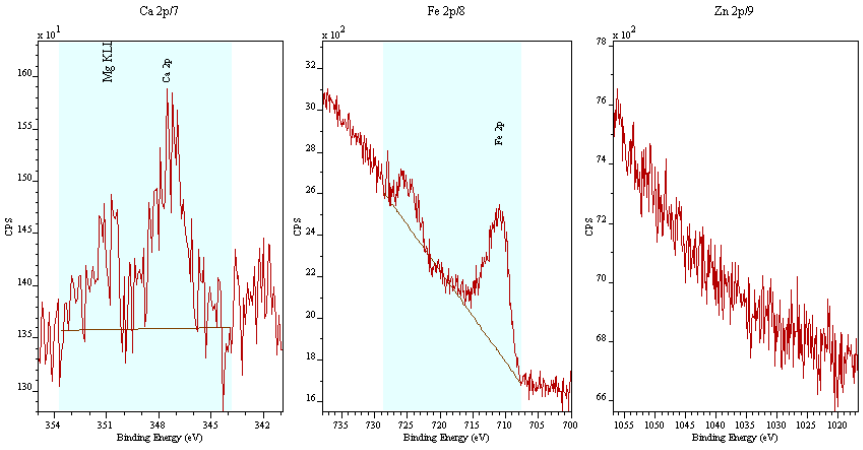

(b)

Figure D.8: XPS detailed spectra on RTB 81107 TN oven 24h (immersed) roller on centre region performed with 5W30 oil.

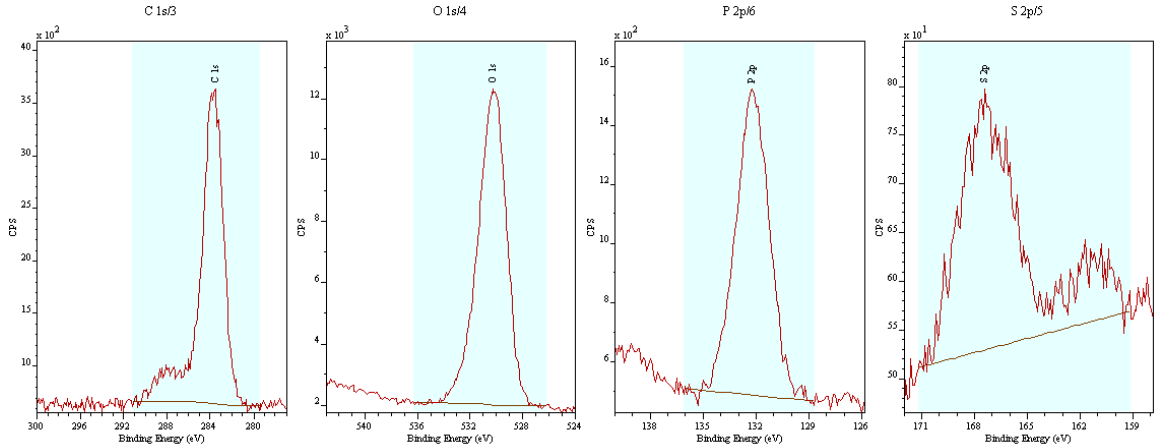

(a)

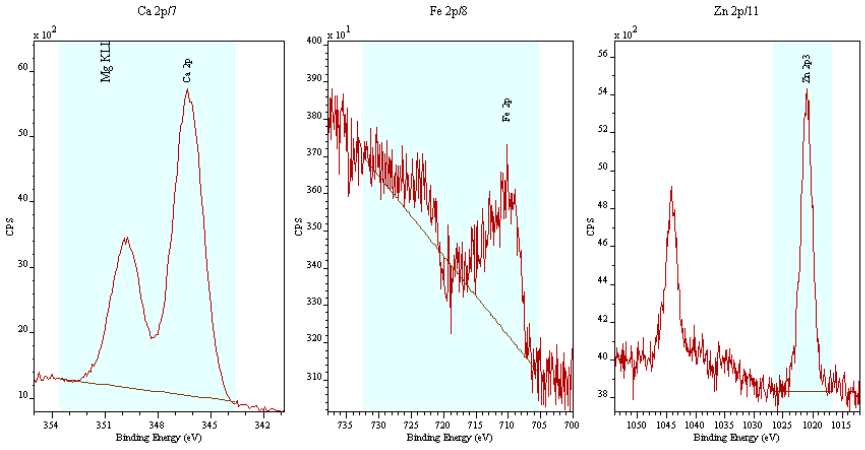

(b)

Figure D.9: XPS detailed spectra on RTB 81107 TN tested 24h roller on Z1 region for tests performed with 10W50 oil.

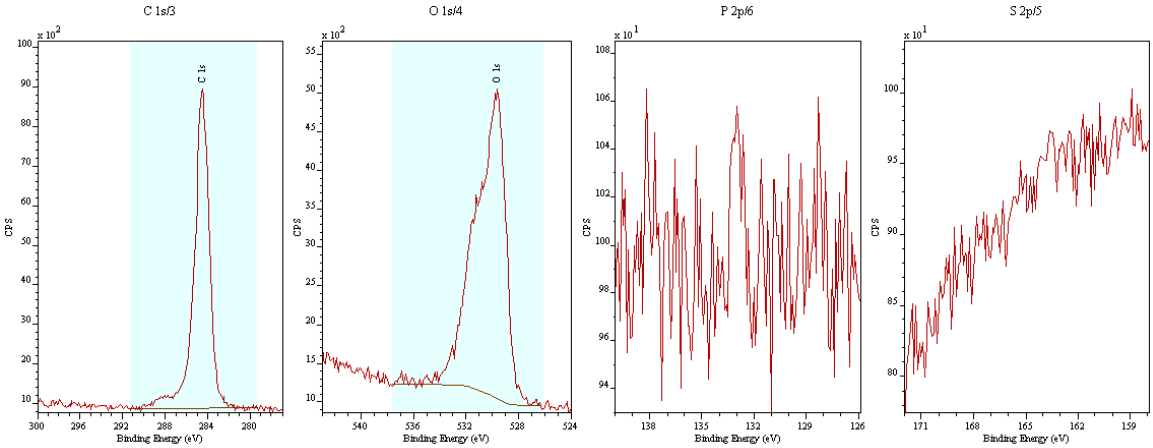

(a)

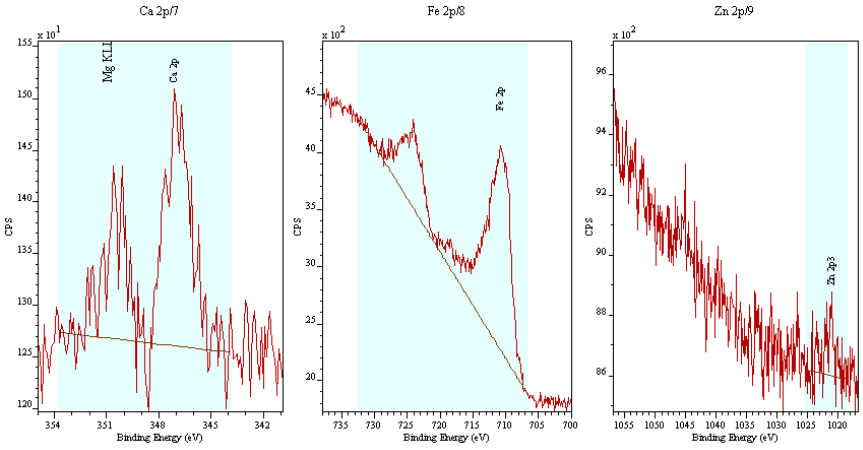

(b)

Figure D.10: XPS detailed spectra on RTB 81107 TN oven 24h (immersed) roller for centre region performed with 10W50 oil.

Appendix E

Analytical Ferrography Pictures

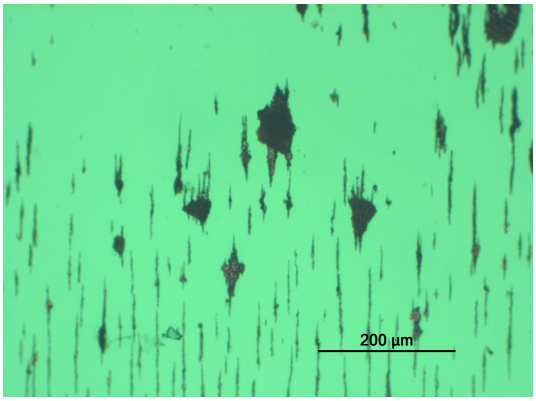

(a)

Magnification: 200x Dilution: 0.01
Local: Core Light: White/Green
Description: Small and large ferrous particles.

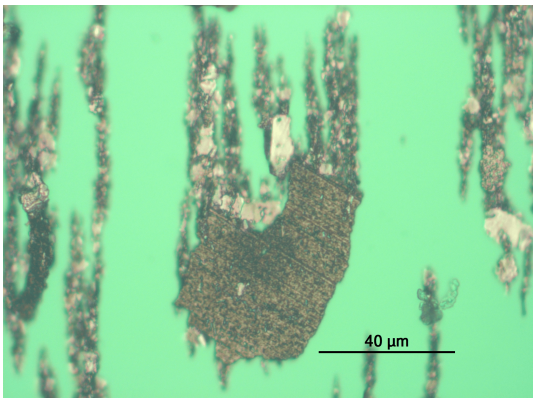

(b)

Magnification: 1000x Dilution: 0.01
Local: Core Light: White/Green
Description: Magnification of Figure E.1(a). Large ferrous particle resulting of severe sliding wear.

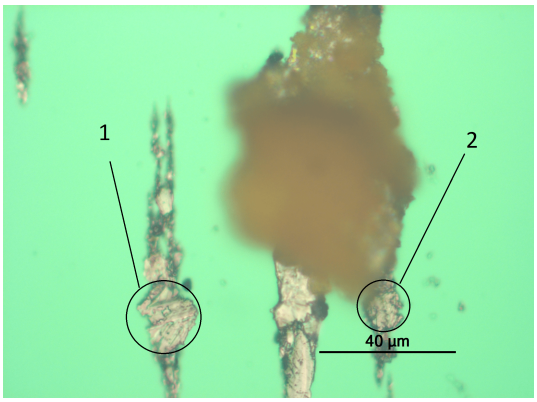

(c)

Magnification: 1000x Dilution: 0.01
Local: Core Light: White/Green
Description: Magnification of Figure E.1(a). Medium ferrous particles resulting of severe sliding (1) wear and fatigue wear (2).

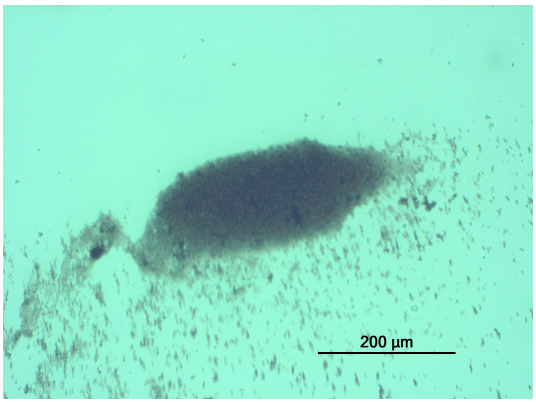

(d)

Magnification: 200x Dilution: 0.01
Local: End Light: White/Green
Description: Small wear particles cloud.

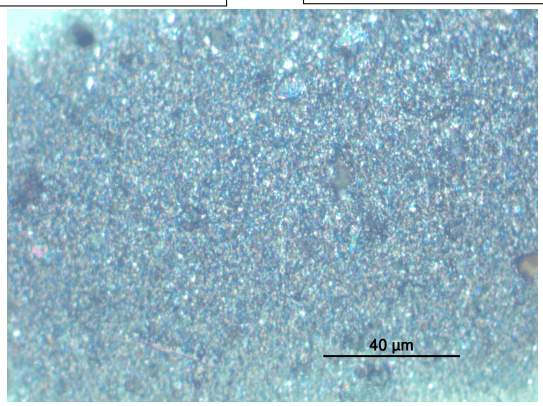

(e)

Magnification: 1000x Dilution: 0.01
Local: End Light: White/Green
Description: Magnification of Figure E.1(d) showing corrosive wear particles.

Figure E.1: Analytical ferrography: 75W90 oil.

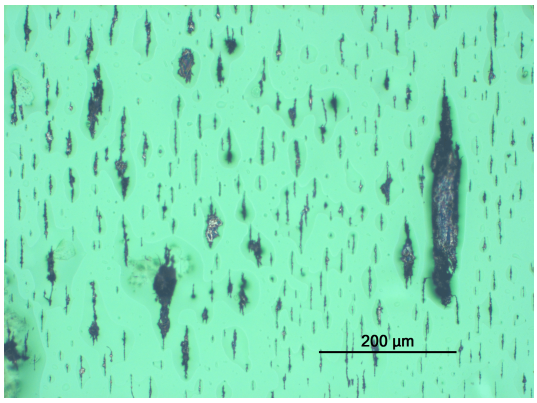

(a)

Magnification: 200x	Dilution: 0.01
Local: Core	Light: White/Green
Description: Medium and large ferrous particles.	

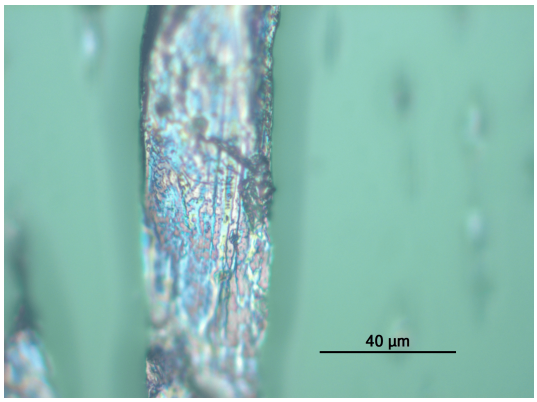

(b)

Magnification: 1000x	Dilution: 0.01
Local: Core	Light: White/Green
Description: Magnification of Figure E.2(a). Large ferrous particle resulting from severe wear.	

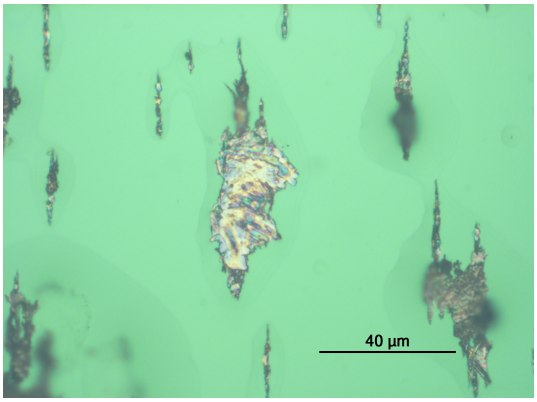

(c)

Magnification: 1000x	Dilution: 0.01
Local: Core	Light: White/Green
Description: Magnification of Figure E.2(a). Large ferrous particle resulting from fatigue wear.	

Figure E.2: Analytical ferrography: 75W140 oil.

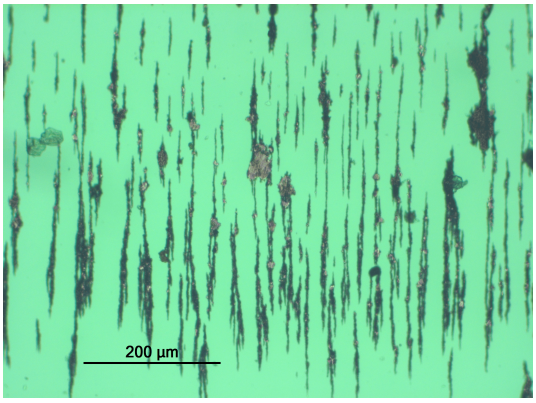

(a)

Magnification: 200x Dilution: 0.01
Local: Core Light: White/Green
Description: Medium and large ferrous particles.

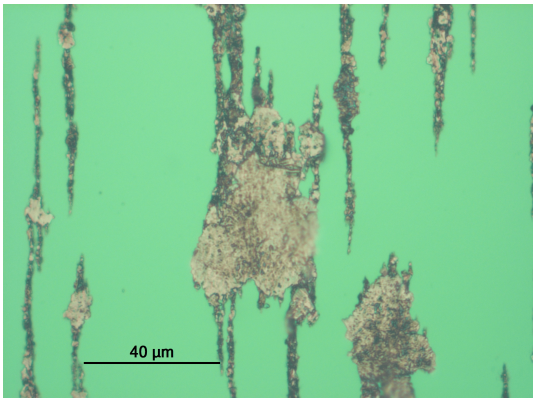

(b)

Magnification: 1000x Dilution: 0.01
Local: Core Light: White/Green
Description: Magnification of Figure E.3(a). Large ferrous particle resulting of fatigue wear.

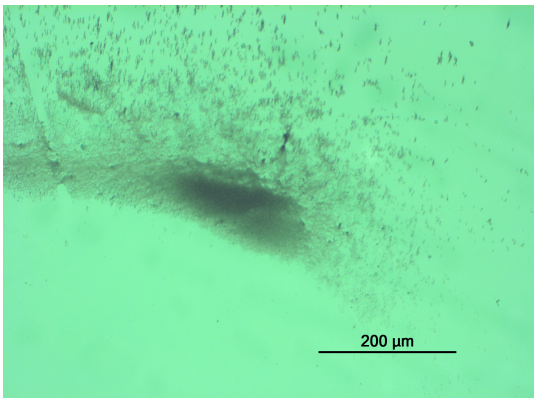

(c)

Magnification: 200x Dilution: 0.01
Local: End Light: White/Green
Description: Small wear particles cloud.

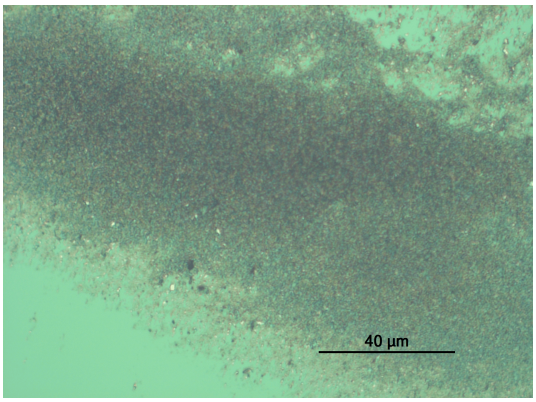

(d)

Magnification: 1000x Dilution: 0.01
Local: End Light: White/Green
Description: Magnification of Figure E.3(c) showing corrosive wear particles.

Figure E.3: Analytical ferrography: 80W90 oil.

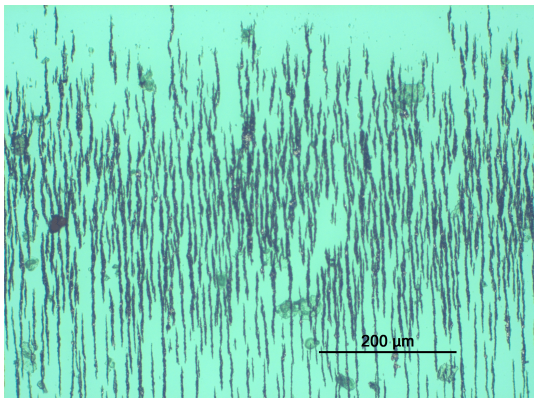

(a)

Magnification: 200x Dilution: 0.01
Local: Core Light: White/Green
Description: Few large particles and medium ferrous particles.

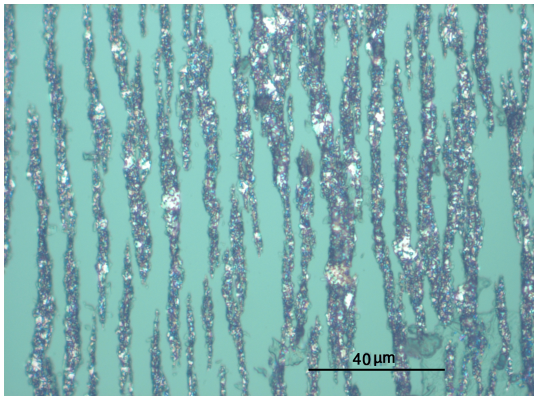

(b)

Magnification: 1000x Dilution: 0.01
Local: Core Light: White/Green
Description: Magnification of Figure E.4(a) Medium ferrous particles, closely disposed indicating a excessive rubbing wear. Some black particles resulting from thermal oxidation.

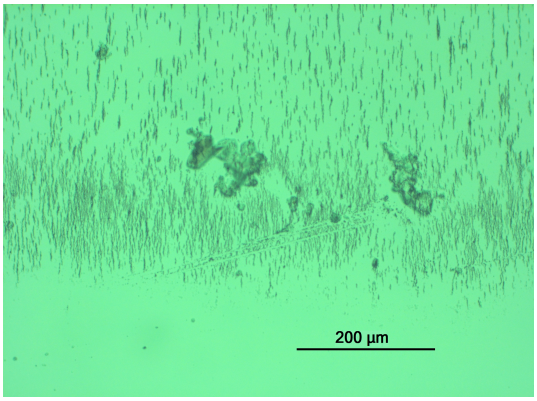

(c)

Magnification: 200x Dilution: 0.01
Local: End Light: White/Green
Description: Small wear particles and two larger particles (possibly friction polymers).

Figure E.4: Analytical ferrography: 5W30 oil.

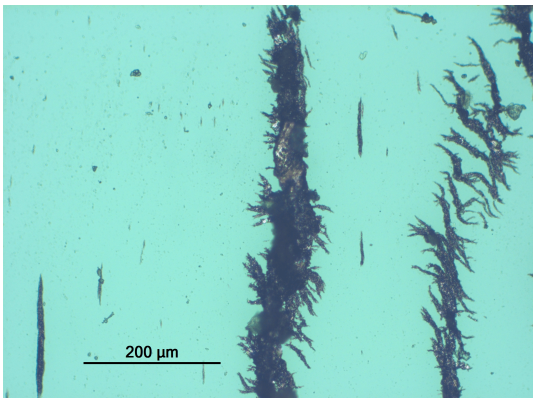

(a)

Magnification: 200x Dilution: 0.01
Local: Core Light: White/Green
Description: Large and medium ferrous wear particles.

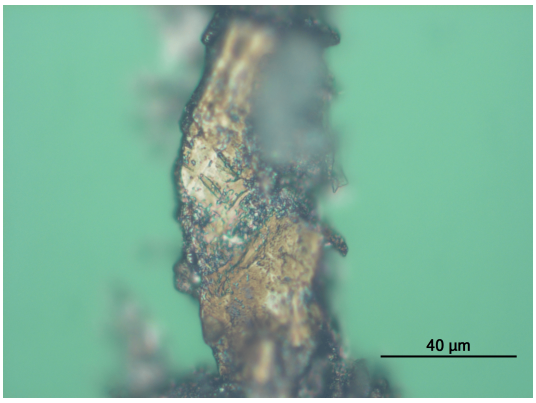

(b)

Magnification: 1000x Dilution: 0.01
Local: Core Light: White/Green
Description: Magnification of Figure E.5(a). Large ferrous particle particle resulting from severe wear.

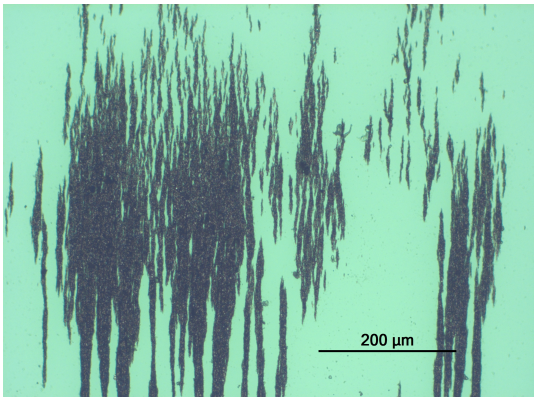

(c)

Magnification: 200x Dilution: 0.01
Local: Midle Light: White/Green
Description: Medium wear particles agglomerated.

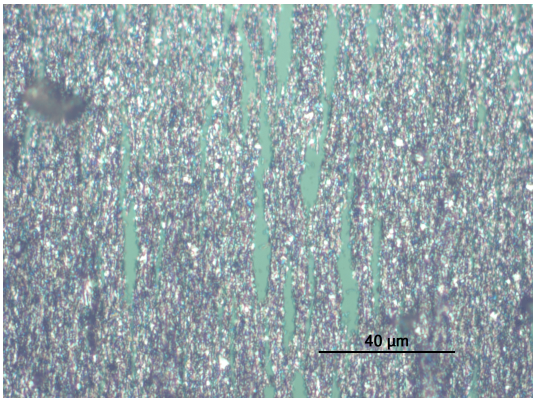

(d)

Magnification: 1000x Dilution: 0.01
Local: Midle Light: White/Green
Description: Medium black ferrous particles revealing thermal oxidation and a corrosive wear. Particles are closely disposed indicating a excessive wear.

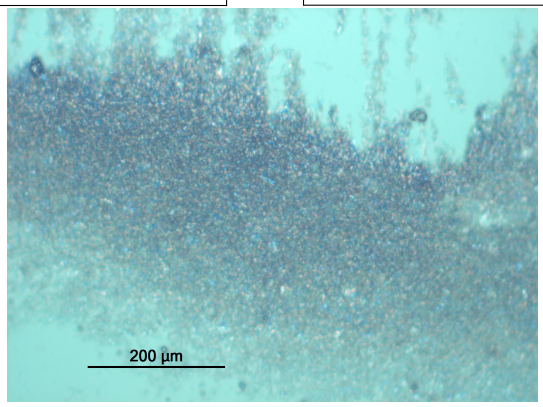

(e)

Magnification: 200x Dilution: 0.01
Local: End Light: White/Green
Description: Small wear particles indicating corrosive wear.

Figure E.5: Analytical ferrography: 10W50 oil.

Appendix F

Engine and Differential

F.1 Torque and Power Diagram

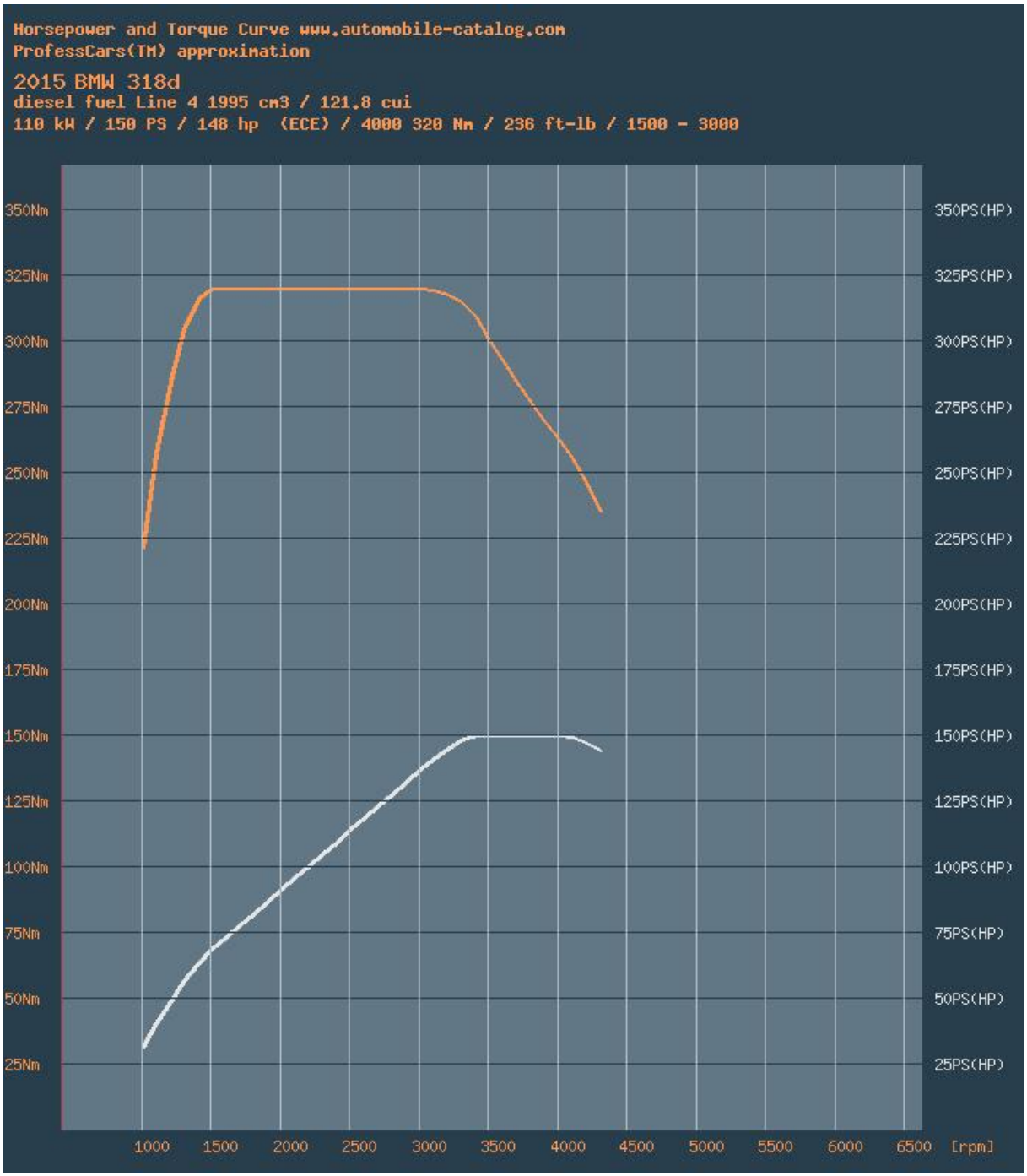

Figure F.1: BMW 318d engine torque (T_{eng}) and power (P_{eng}) diagram [57].

F.2 Meshing Loads

To calculate the meshing loads it is necessary to know the input pinion and the ring gear dimensions. Table F.1 presents the equations to calculate some reference parameters to obtain the meshing loads, and the corresponding values.

In this study, to obtain gear number of teeth and module, it was considered an approximation of the ring gear pitch diameter. Since there was no available dimensions information, it was used the Figure 5.1(b) and an image software *GIMP* to estimate ring gear dimension. Thus the gear differential ratio (i_{diff}) was predicted and the number of teeth estimated.

Table F.1: Helical bevel gears: calculation parameters. [66].

Item	Symbol	Expression	Differential	
			Pinion 1	Gear 2
Shaft angle	γ		1,571 rad	
Outside radial module	m		2,5	
Normal pressure angle	α_n		0,349 rad	
Spiral angle	β_m		0,611 rad	
No of teeth	Z_1 , Z_2		16	52
Gear Ratio	i_{diff}	$i_{diff} = \frac{Z_2}{Z_1}$	1/3,25	
Radial Pressure angle	α_t	$\alpha_t = \arctan(\frac{\tan\alpha_n}{\cos\beta m})$	0,418rad	
Pitch diameter	d'	$Z * m$	40	130
Pitch cone angle	δ_1	$\delta_1 = \arctan(\frac{\sin\gamma}{i_{diff} + \cos\gamma})$	0,3 rad	1,271 rad
	δ_2	$\delta_2 = \gamma - \delta_1$		
Cone distance	R_e	$R_e = \frac{d'_2}{2\sin\delta_2}$	68,04 mm	
Face width	b		23 mm	

Since the main purpose of these calculations was to determine the magnitude values for rolling bearing loads, it was not considered hypoid gears, but helical bevel gears instead to simplify the calculation procedure. No significant difference was expected on calculated rolling bearing loads.

In Figure F.2 the meshing loads are presented. F'_u represents the tangential load, F'_r the radial load and F'_a the axial load. The index 1 and 2 are related to the pinion or ring gear respectively, and represents the loads acting on each one. On Figure F.2(a) are represented the loads when the input shaft rotates in positive direction (vehicle is moving forward) and on Figure F.2(b) loads when the input shaft rotates in negative direction (vehicle is moving backwards). The equations used to calculate the meshing loads in both cases, are given in Table F.2.

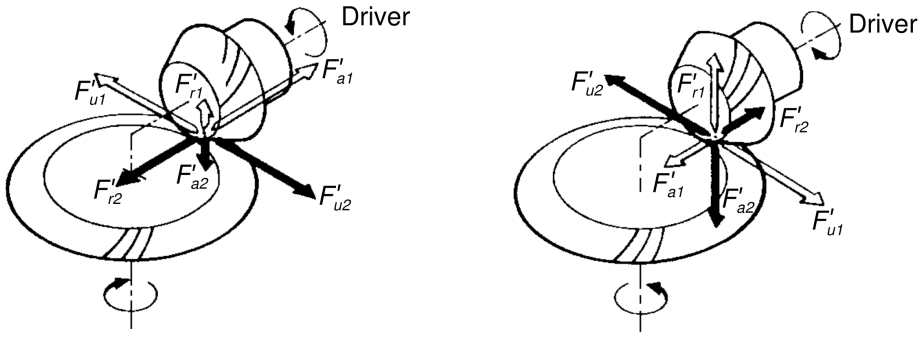

(a) Positive rotation direction. (b) Negative rotation direction.

Figure F.2: Helical bevel gear: load diagram [66].

Table F.2: Helical bevel gear: meshing loads [66].

	Fu_2	Fr_2	Fa_2
Foward	$\frac{T_{in} * 2000}{d'_1}$	$\frac{F'_{u2}}{\cos\beta_m}(\tan\alpha_n \cos\delta_2 + \sin\beta_m \sin\delta_2)$	$\frac{F'_{u2}}{\cos\beta_m}(\tan\alpha_n \sin\delta_2 - \sin\beta_m \cos\delta_2)$
Reverse	$\frac{T_{in} * 2000}{d'_1}$	$\frac{F'_{u2}}{\cos\beta_m}(\tan\alpha_n \cos\delta_2 - \sin\beta_m \sin\delta_2)$	$\frac{F'_{u2}}{\cos\beta_m}(\tan\alpha_n \sin\delta_2 + \sin\beta_m \cos\delta_2)$

F.3 Rolling Bearing Loads

Using *GIMP* software the position of rolling bearings and gears in each shaft were determined and presented in Table F.3.

Table F.3: Rolling bearings relative position within differential.

	Variable	Dimension [mm]		Variable	Dimension [mm]
Input shaft	l'_1	105	Differential cage	l'_2	234
	l'_A	30		l'_C	82
	l'_B	135		l'_D	152

To calculate the loads on supports, the *Henriot* [67] procedure was followed. The loads represented in diagrams of Figure F.3(a) and Figure F.3(b) correspond to forward and backward vehicle movement, respectively. In the input shaft are assembled the bearings A and B. The point O_1 and O_2 represents the centre of the drive pinion and ring gear, respectively. The rolling bearings assembled on ring gear shaft, are represented by C and D. The M marker represents the gear meshing point. For all rolling bearings positions, tapered rolling bearings were assumed.

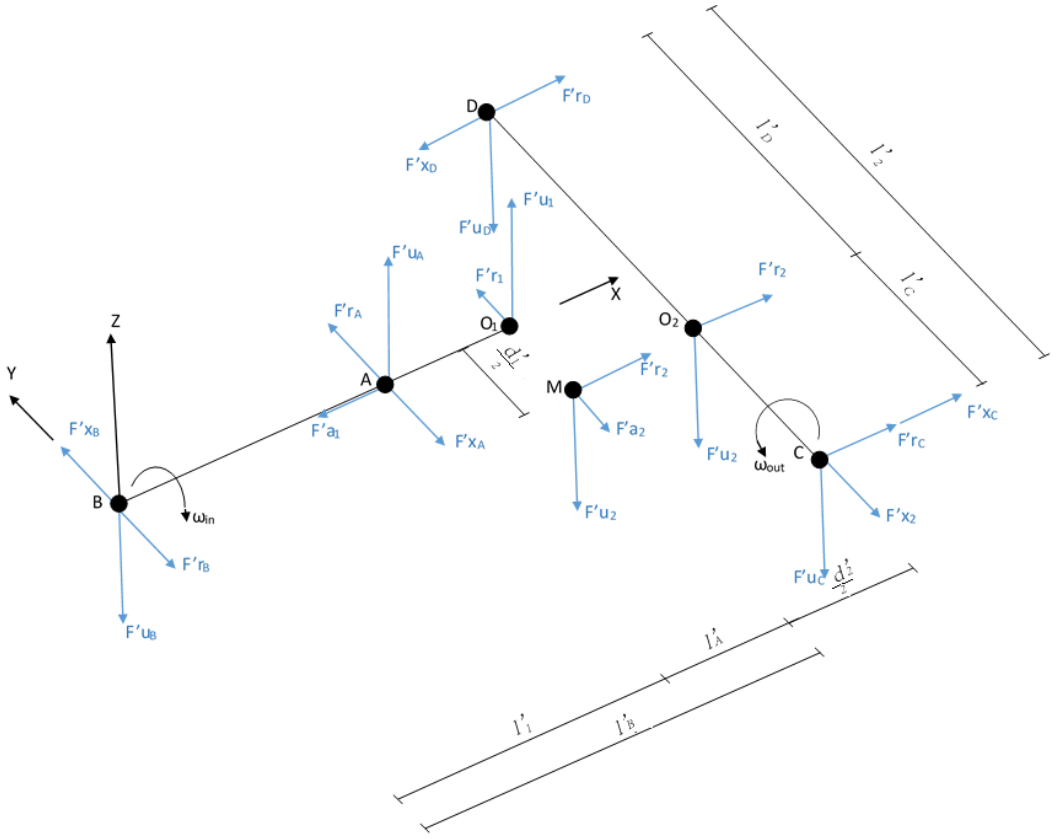

(a) Vehicle moving forward.

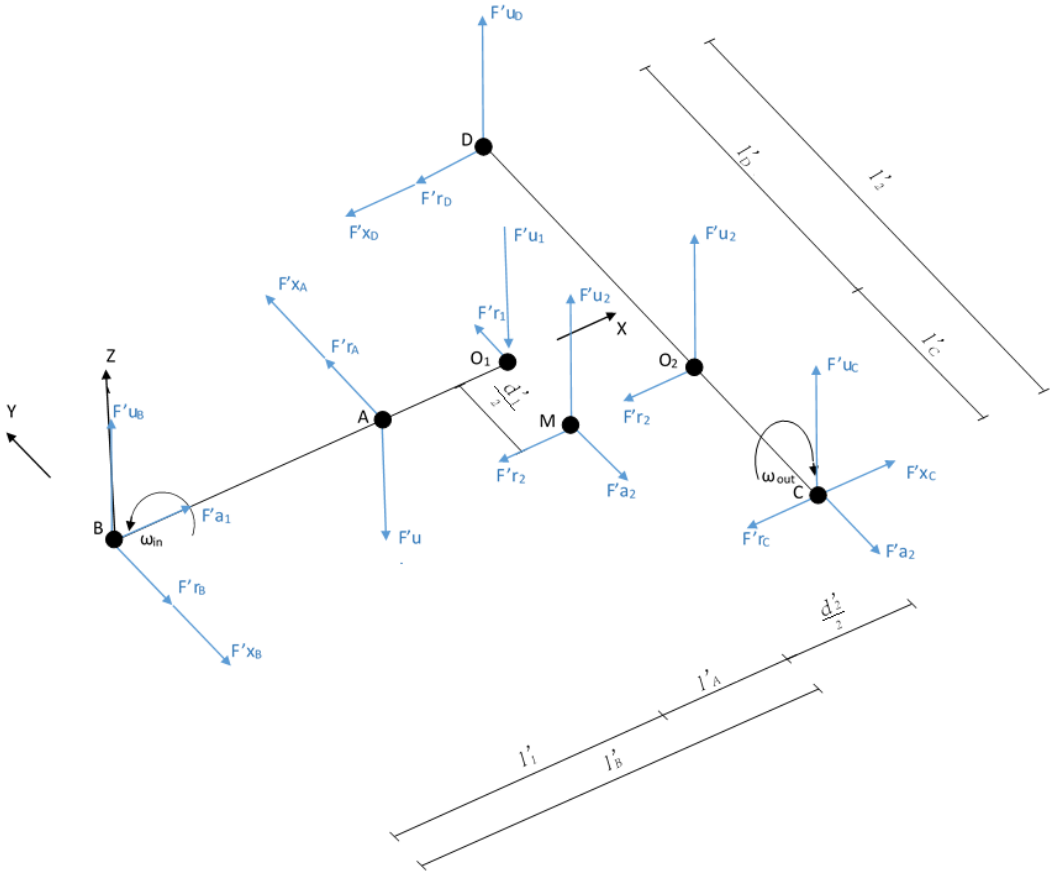

(b) Vehicle is moving backward.

Figure F.3: Rolling bearing's load diagrams.

The loads on each rolling bearing position, in x,y,z directions, for both positive and negative input shaft rotation, are presented in Table F.4.

Table F.4: Loads on rolling bearing positions on x,y,z directions.

Forces	Rotation Direction	A	B	C	D
R^x [N]	(+)	F'_{r2}	0	$-F'_{r2}\frac{l'_D}{l'_2} - F'_{a2}\frac{d'_2}{2l'_2}$	$-F'_{r2}\frac{l'_C}{l'_2} + F'_{a2}\frac{d'_2}{2l'_2}$
	(-)	0	$-F'_{r2}$	$F'_{r2}\frac{l'_D}{l'_2} - F'_{a2}\frac{d'_2}{2l'_2}$	$F'_{r2}\frac{l'_C}{l'_2} + F'_{a2}\frac{d_2}{2l'_2}$
R^y [N]	(+)	$F'_{r2}\frac{d'_1}{2l'_1} - F'_{a2}\frac{l'_B}{l'_1}$	$-F'_{r2}\frac{d'_1}{2l'_1} + F'_{a2}\frac{l'_A}{l'_1}$	F'_{a2}	0
	(-)	$-F'_{r2}\frac{d'_1}{2l'_1} - F'_{a2}\frac{l'_B}{l'_1}$	$F'_{r2}\frac{d'_1}{2l'_1} + F'_{a2}\frac{l'_A}{l'_1}$	F'_{a2}	0
R^z [N]	(+)	$-F'_{u2}\frac{l'_B}{l'_1}$	$F'_{u2}\frac{l'_A}{l'_1}$	$F'_{u2}\frac{l'_D}{l'_2}$	$F'_{u2}\frac{l'_C}{l'_2}$
	(-)	$F'_{u2}\frac{l'_B}{l'_1}$	$-F'_{u2}\frac{l'_A}{l'_1}$	$-F'_{u2}\frac{l'_D}{l'_2}$	$-F'_{u2}\frac{l'_C}{l'_2}$

When a radial load is applied to a single row tapered roller bearing, the load is transmitted from one raceway to the other, an internal axial load is induced, due to the angle between the bearing axis and the raceway (ψ) [9]. This was considered when axial rolling bearing loads were calculated in Table F.5.

According to *Eschmann et al.* [30], to ensure correct meshing and uniform load distribution over the tooth width between the input pinion and ring gear meshing, the bearing arrangement must have a very high degree of rigidity. Furthermore, to increase rolling bearing running accuracy and prevent its damage, a minimum axial load has to be ensured. Minimum axial load is given by, $F_{am} = \frac{0{,}02C}{2Y}$ [9], where C is the basic dynamic load rating and Y is the rolling bearing dynamic axial load factor.

The typical arrangements for tapered roller bearings are shown in Figure F.4. Two bearings can be mounted and preloaded following a back-to-back (Figure F.4(a)) or a face-to-face (Figure F.4(b)) arrangement.

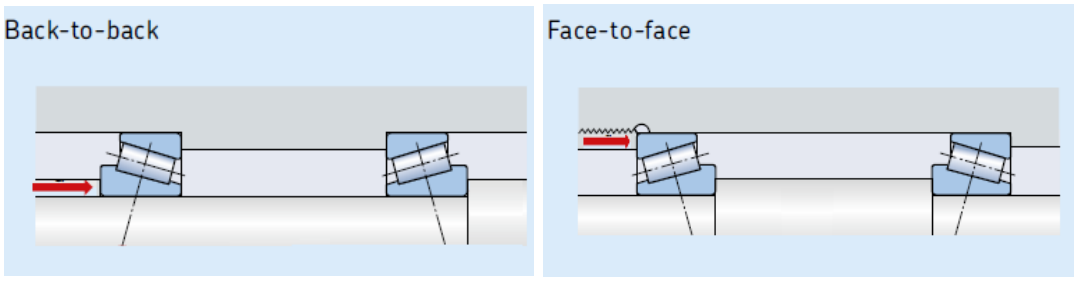

(a) Back-to-back [9]. (b) Face-to-face [9].

Figure F.4: Tapered roller bearing arrangements.

For both TRB arrangements described, preload is needed to ensure the correct gear engagement and prevent the sliding between the inner and outer raceway of rolling bearing. As transmission life progresses, tapered roller bearings may support higher loads, as result of preload loss due to the roller element width reduction caused by increase in sliding friction between roller end face and large flange face of the inner ring [68].

In ACBB, the contact problems related with roller face and the rib are solved, as the preload losses are avoided. These type of bearings reduces significantly the friction torque losses and oil temperature, thus the vehicle fuel efficiency improves. However, the ACBB present much lower load capacity than TRB [69].

In Figure F.5(a), F.5(b) and F.5(c) three possible situations in the rear differential are shown. K_a is the axial load (F'_{r2} and F'_{a2} in load diagrams of Figure F.3(a) and Figure F.3(b) for pinion shaft and ring gear shaft, respectively).

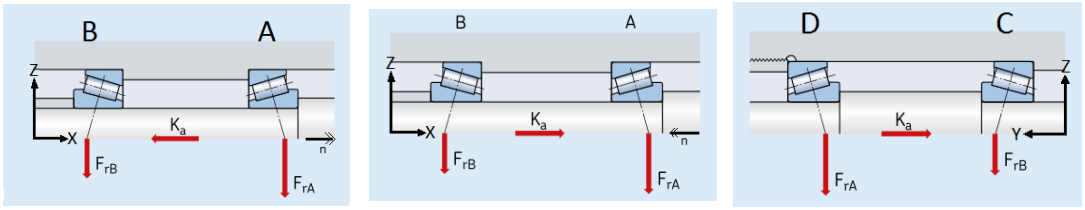

(a) Pinion shaft positive rotational direction.

(b) Pinion shaft negative rotational direction.

(c) Ring gear shaft both rotational directions.

Figure F.5: Axial loading of TRB arrangements depending on rotational speed direction of the shafts [9].

Considering positive rotational direction in the input shaft (x direction), the preload must ensure a minimum axial load in rolling bearing B in the positive axial direction (x direction).

On the other hand, when the input shaft rotates in negative x direction the preload must ensure a minimum load in rolling bearing A on negative axial direction (x direction).

For face-to-face arrangement mounted in the ring gear shaft, in both positive and negative rotational direction the preload must ensure a minimum load in rolling bearing D in y positive direction.

The radial and axial loads on rolling bearings are shown in Table F.5.

Table F.5: TRB radial and axial loads considering internal loads and preload.

Loads	Rotation Direction	A	B	C	D
F_r [N]	(+)	$\sqrt{R_A^{y^2} + R_A^{z^2}}$	$\sqrt{R_B^{y^2} + R_B^{z^2}}$	$\sqrt{R_C^{x^2} + R_C^{z^2}}$	$\sqrt{R_D^{x^2} + R_D^{z^2}}$
F_r [N]	(-)				
F_a [N]	(+)	$Preload + \frac{F_{rB}}{2Y_B} + K_a$	$Preload - \frac{F_{rB}}{2Y_B}$	$Preload + \frac{F_{rC}}{2Y_D} + K_a$	$Preload - \frac{F_{rC}}{2Y_D}$
F_a [N]	(-)	$Preload - \frac{F_{rB}}{2Y_A}$	$Preload + \frac{F_{rB}}{2Y_A} + K_a$		

The axial load equations on rolling bearings (F_a) presented in Table F.5, that ensure the

correct performance, are dependent on internal load conditions, settled by SKF [9], preload and external axial loads (K_a) and were obtained according to the equations presented in Table F.6.

Table F.6: Rolling bearing's axial loads [9].

Bearing	Input shaft positive rotational direction		Input shaft negative rotational direction	
	Condition	Axial load (F_a)	Condition	Axial load (F_a)
A	$\frac{F_{rA}}{Y_A} > \frac{F_{rB}}{Y_B}$	$Preload + \frac{F_{rB}}{2Y_B} + K_a$ (−)	$\frac{F_{rA}}{Y_A} > \frac{F_{rB}}{Y_B}$	$Preload - \frac{F_{rB}}{2Y_A}$ (−)
B	$K_a \geq \frac{1}{2}(\frac{F_{rB}}{Y_B} - \frac{F_{rA}}{Y_A})$	$Preload - \frac{F_{rB}}{2Y_B}$ (+)	$K_a \geq 0$	$Preload + \frac{F_{rB}}{2Y_A} + K_a$ (+)
C	$\frac{F_{rD}}{Y_D} < \frac{F_{rC}}{Y_C}$	$Preload + \frac{F_{rC}}{2Y_D} + K_a$ (+)	$\frac{F_{rD}}{Y_D} < \frac{F_{rC}}{Y_C}$	$Preload + \frac{F_{rC}}{2Y_D} + K_a$ (+)
D	$K_a \geq \frac{1}{2}(\frac{F_{rC}}{Y_C} - \frac{F_{rD}}{Y_D})$	$Preload - \frac{F_{rC}}{2Y_D}$ (−)	$K_a \geq \frac{1}{2}(\frac{F_{rC}}{Y_C} - \frac{F_{rD}}{Y_D})$	$Preload - \frac{F_{rC}}{2Y_D}$ (−)

Knowing the loads at the rolling bearings positions, several tapered roller bearings were selected. For each TRB, it was calculated the axial load (Table F.6), the preload required to assure a F_{am} and equivalent static and dynamic bearing load, P_0 and P. When the P_0 and P were lower than basic static and dynamic load C_0 and C, respectively, the TRB was selected. The equations to calculate P_0 and P are given in Table F.7.

Table F.7: Equivalent loads calculation [9].

Equivalent dynamic bearing load	Equivalent static bearing load
$\frac{F_a}{F_r} \leq e \Rightarrow P = F_r$ $\frac{F_a}{F_r} > e \Rightarrow P = \frac{2}{5}F_r + YF_a$	$P_0 = \frac{1}{2}F_r + Y_0F_a$

It should be noted that it is not known what rolling bearing are assembled in BMW 7599469-02 differential, and the selection was done according to the determined load described above. The TRB along with principal characteristics are shown in Table F.8.

Table F.8: Rolling bearings selected for assembly: main characteristics [9].

	Designation	Principal Dimensions			Basic load ratings		Dimensions		Calculation factors			No. Rollers
		d	D	T	C	C_0	d_1	C	e	Y	Y_0	z
		[mm]	[mm]	[mm]	[kN]	[kN]	[mm]	[mm]	–	–	–	–
A	32310 J2/Q	45	110	42.25	172	212	77.8	33	0.35	1.7	0.9	16
B	32308 J2/Q	40	90	35.25	117	140	62.9	27	0.35	1.7	0.9	16
C/D	32309 J2/Q	45	100	38.25	140	170	71.1	30	0.35	1.7	0.9	16

The calculated preload value for selected TRB presented in pinion gear and ring gear shaft was 8 kN and 18 kN, respectively. The resultant radial and axial loads acting in each rolling bearing, are presented in Table F.9.

Table F.9: Resultant loads in rolling bearings.

		Engine condition 1 250Nm @ 1500rpm				Engine condition 2 320Nm @ 3000rpm			
Shifts	[kN]	A	B	C	D	A	B	C	D
1	F_r	64.7	15.0	43.6	20.7	82.9	19.2	55.8	26.6
	F_a	52.5	3.6	41.7	5.2	65.0	2.3	48.4	1.6
2	F_r	34.1	7.9	23.0	10.9	43.7	10.1	29.4	14.0
	F_a	31.5	5.7	30.5	11.2	38.0	5.0	34.0	9.3
3	F_r	22.5	5.2	15.1	7.2	28.7	6.7	19.4	9.2
	F_a	23.4	6.5	26.2	13.6	27.8	6.0	28.5	12.3
4	F_r	16.2	3.8	10.9	5.2	20.7	4.8	14.0	6.6
	F_a	19.1	6.9	23.9	14.8	22.2	6.6	25.6	13.9
5	F_r	12.6	2.9	8.5	4.0	16.2	3.7	10.9	5.2
	F_a	16.7	7.1	22.6	15.5	19.1	6.9	23.9	14.8
6	F_r	10.4	2.4	7.0	3.3	13.4	3.1	9.0	4.3
	F_a	15.2	7.3	21.8	15.9	17.2	7.1	22.9	15.4
Reverse	F_r	-	-	-	-	92.2	23.5	39.3	29.5
	F_a	-	-	-	-	1.1	46.3	66.5	6.4

For both engine conditions, higher rolling bearing loads are achieved for higher gearbox ratios corresponding to "reverse", "1st" and "2nd" gearbox shifts. Thus, comparing both conditions, higher loads are achieved for engine condition 2, since higher engine torque is delivered to gearbox and consequently to differential rolling bearings.

F.3.1 Contact Load Calculations

The magnitude of F_a and F_r determines the range of the loading area when a portion or the entire raceway sustains the load, shown in Figure F.6 . When a part of the outer raceway sustains the load, the ratio between the projected length of the loading area and the raceway diameter (D) represented by ϵ, varies between 0 and 1. Thus, when the entire outer race is subjected to a load, ϵ is greatest than 1 ($\epsilon \geq 1$) and depends on the rolling element elastic

deformation under maximum and minimum load. [70].

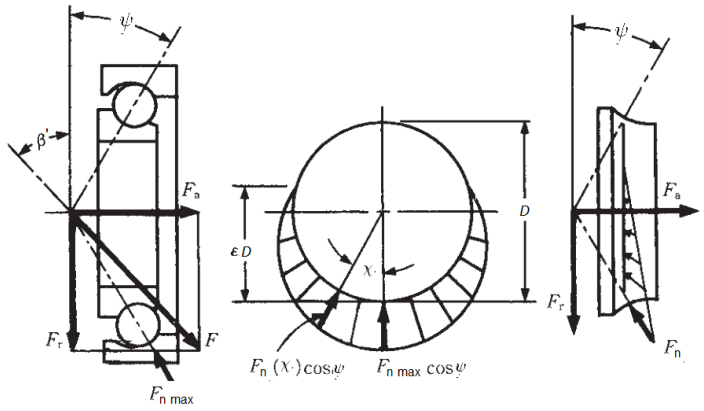

Figure F.6: Radial and axial forces acting on the rolling bearing [70].

Maximum normal load at a line contact is defined by equation (F.1).

$$F_{nmax} = \frac{F_r}{J_r \cdot z \cos\psi} \tag{F.1}$$

Where J_r is the line contact coefficient given by equation (F.2) and is presented in Table F.10.

$$J_r = \frac{F_r \cdot \tan\psi}{F_a} \tag{F.2}$$

It should be noted that only F_{nmax} was determined, and assumed as the normal contact load (F_n) for the entire rolling bearing raceway.

Table F.10: J_r parameter depending on radial and axial loads acting on rolling bearing [70].

ε	Line Contact $\frac{F_r \cdot \tan(\psi)}{F_a}$	J_r
0	1	0
0.1	0.9613	0.1268
0.2	0.9215	0.1737
0.3	0.8805	0.2055
0.4	0.8380	0.2286
0.5	0.7939	0.2453
0.6	0.7480	0.2568
0.7	0.6999	0.2636
0.8	0.6486	0.2658
0.9	0.5920	0.2628
1	0.5238	0.2523
1.25	0.3598	0.2078
1.67	0.2340	0.1589
2.5	0.1372	0.1075
5	0.0611	0.0544
∞	0	0

The pressure in the contact line is related with normal force F_n according to equation (3.8) and is used to calculate the film thickness. Knowing the contact roller raceway geomet-

rical characteristics, presented in Table F.11 it is possible determine the pressure in the centre of the line contact.

Table F.11: TRB selected: contact roller raceways characteristics.

Designation [-]	No. Rollers [-]	R_{x1} [m]	R_{x2} [m]	l [m]	σ [μm]
32310 J2	16	7.71×10^{-3}	32.50×10^{-3}	27.77×10^{-3}	0.25
32308 J2/Q	16	6.31×10^{-3}	25.87×10^{-3}	23.77×10^{-3}	
32309 J2/Q	16	7.11×10^{-3}	29.25×10^{-3}	24.68×10^{-3}	

In Table F.12 is presented the maximum pressure results by gearbox shift and engine condition for each rolling bearing.

Table F.12: Contact pressure (p) in selected rolling bearings.

		Engine condition 1 250Nm @ 1500rpm				Engine condition 2 320Nm @ 3000rpm			
Shifts		A	B	C	D	A	B	C	D
1	p [GPa]	2,2	1,9	2,1	1,5	2,4	1,7	2,3	1,8
2		1,6	0,9	1,7	1,0	1,8	0,9	1,8	1,0
3		1.4	0.8	1.5	1.1	1.5	0.9	1.6	1.1
4		1.2	0.8	1.4	1.1	1.3	0.8	1.5	1.1
5		1.1	0.8	1.3	1.1	1.2	0.8	1.4	1.1
6		1.1	0.8	1.3	1.1	1.2	0.8	1.4	1.1
Reverse		-	-	-	-	3.1	2.2	2.4	1.9

Appendix G

Friction Torque Results

Table G.1: Parameters obtained by performed tests for different load, temperature and rotational speed conditions, for TRB 30203 J2 and 10W50 oil (without running-in).

Load	θ (Condition)	n	θ (Recorded)	ν	M_t^{exp}	M_{rr}	M_{sl}^{exp}	μ_{sl}^{exp}	μ_{sl}^{opt}	error	μ_{bl}	μ_{EHL}	ϕ_{bl}	λ	k
[kN]	[°C]	[rpm]	[°C]	[cSt]	[Nmm]	[Nmm]	[Nmm]	[-]	[-]	[-]	[-]	[-]	[-]	[-]	[-]
4	70	75	70.1	39.65	916.08	19.99	896.09	0.249	0.249	1.84E-07	0.252	0.179	0.947	0.09	0.20
		150	70.2	39.53	911.50	30.17	881.33	0.244	0.243	1.78E-03			0.868	0.14	0.36
		300	70.8	38.81	843.55	45.02	798.53	0.221	0.230	8.41E-03			0.694	0.23	0.52
		600	69.9	39.90	810.74	68.63	742.11	0.206	0.206	9.03E-07			0.367	0.39	1.14
		900	87.5	24.33	824.92	65.07	759.85	0.211	0.209	1.55E-03			0.413	0.35	0.97
		1200	109.3	14.67	774.26	57.22	717.04	0.199	0.217	1.83E-02			0.521	0.28	0.73
	90	75	90.2	22.72	812.06	14.32	797.74	0.221	0.235	1.40E-02	0.239	0.084	0.976	0.05	0.11
		150	89.9	22.89	847.95	21.78	826.17	0.229	0.229	5.60E-07			0.936	0.09	0.21
		300	89.8	22.93	811.17	32.94	778.23	0.216	0.214	1.61E-03			0.840	0.15	0.31
		600	90.9	22.31	710.86	48.82	662.04	0.184	0.184	2.19E-07			0.642	0.24	0.64
		900	89.9	22.89	619.96	62.80	557.16	0.155	0.153	1.45E-03			0.444	0.33	0.92
		1200	90.2	22.70	484.55	73.76	410.80	0.114	0.131	1.70E-02			0.301	0.40	1.13
	110	75	109.8	14.53	660.20	10.96	649.25	0.180	0.186	5.75E-03	0.188	0.033	0.987	0.04	0.07
		150	109.7	14.54	698.79	16.60	682.19	0.189	0.183	6.68E-03			0.966	0.06	0.13
		300	109.7	14.56	653.08	25.13	627.95	0.174	0.174	1.05E-10			0.912	0.10	0.19
		600	109.9	14.49	594.84	37.82	557.02	0.154	0.154	1.76E-07			0.785	0.17	0.41
		900	109.9	14.48	537.90	48.00	489.89	0.136	0.134	1.91E-03			0.652	0.23	0.58
		1200	110.1	14.44	467.68	56.69	410.99	0.114	0.115	8.78E-04			0.529	0.28	0.72
7	70	75	69.8	40.06	1160.15	23.92	1136.23	0.180	0.182	1.91E-03	0.188	0.033	0.947	0.08	0.20
		150	69.6	40.27	1129.38	36.28	1093.10	0.173	0.173	7.81E-05			0.864	0.14	0.37
		300	70.0	39.77	1025.62	54.32	971.30	0.154	0.154	3.92E-09			0.685	0.23	0.53
		600	89.5	23.10	983.19	59.27	923.92	0.146	0.148	1.30E-03			0.628	0.24	0.66
		900	126.2	10.57	1138.36	47.41	1090.95	0.173	0.162	1.10E-02			0.760	0.16	0.42
		1200	-	-	-	-	-	-	-	-			-	-	-
	90	75	89.9	22.91	1182.01	17.12	1164.89	0.185	0.179	5.23E-03	0.182	0.072	0.975	0.05	0.11
		150	89.6	23.08	1130.18	26.03	1104.15	0.175	0.175	2.95E-08			0.935	0.09	0.21
		300	89.8	22.95	1076.30	39.20	1037.10	0.164	0.164	6.61E-05			0.840	0.14	0.31
		600	90.4	22.59	957.67	58.49	899.18	0.143	0.142	4.27E-04			0.637	0.23	0.65
		900	114.0	13.33	906.72	54.39	852.33	0.135	0.147	1.21E-02			0.683	0.20	0.53
		1200	-	-	-	-	-	-	-	-			-	-	-
	110	75	110.1	14.42	1110.32	12.97	1097.35	0.174	0.174	2.34E-02	0.176	0.001	0.987	0.04	0.07
		150	109.8	14.51	1087.02	19.72	1067.30	0.169	0.170	3.88E-02			0.966	0.06	0.13
		300	110.1	14.44	1103.71	29.75	1073.96	0.170	0.161	6.40E-02			0.913	0.10	0.19
		600	109.8	14.52	1062.70	45.04	1017.65	0.161	0.138	1.06E-01			0.784	0.16	0.41
		900	112.9	13.61	805.93	55.06	750.87	0.119	0.119	1.35E-01			0.676	0.20	0.54
		1200	-	-	-	-	-	-	-	-			-	-	-

Table G.2: Parameters obtained by performed tests for different load, temperature and rotational speed conditions, for TRB 30203 J2 and 10W50 oil (with running-in).

Load	θ (Condition)	n	θ (Recorded)	ν	M_t^{exp}	M_{rr}	M_{sl}^{exp}	μ_{sl}^{exp}	μ_{sl}^{opt}	error	μ_{bl}	μ_{EHL}	ϕ_{bl}	λ	k
[kN]	[°C]	[rpm]	[°C]	[cSt]	[Nmm]	[Nmm]	[Nmm]	[-]	[-]	[-]	[-]	[-]	[-]	[-]	[-]
4	70	75	70.1	39.74	733.32	20.01	713.31	0.198	0.196	1.71E-03	0.207	0.001	0.947	0.09	0.20
		150	70.2	39.66	678.12	30.23	647.89	0.180	0.180	6.96E-05			0.867	0.14	0.36
		300	70.2	39.58	482.60	45.54	437.06	0.121	0.143	2.13E-02			0.687	0.24	0.53
		600	70.1	39.74	283.55	68.48	215.07	0.060	0.077	1.75E-02			0.369	0.39	1.14
		900	70.0	39.90	212.11	86.60	125.51	0.035	0.036	1.39E-03			0.171	0.53	1.60
		1200	69.8	40.11	262.30	102.07	160.23	0.044	0.015	2.91E-02			0.070	0.65	2.01
	90	75	89.9	22.92	696.02	14.40	681.62	0.189	0.168	2.12E-02	0.172	0.001	0.975	0.05	0.11
		150	89.5	23.16	607.19	21.93	585.27	0.162	0.161	1.31E-03			0.935	0.09	0.21
		300	89.9	22.92	554.90	32.94	521.96	0.145	0.145	6.91E-05			0.840	0.15	0.31
		600	90.2	22.75	363.80	49.39	314.41	0.087	0.109	2.22E-02			0.634	0.25	0.65
		900	90.1	22.83	332.60	62.70	269.90	0.075	0.077	2.39E-03			0.446	0.33	0.91
		1200	90.1	22.83	249.93	74.00	175.93	0.049	0.052	3.27E-03			0.298	0.41	1.14
	110	75	110.2	14.42	584.85	10.91	573.94	0.159	0.164	4.50E-03	0.166	0.001	0.987	0.04	0.07
		150	110.2	14.43	661.39	16.53	644.86	0.179	0.160	1.86E-02			0.966	0.06	0.13
		300	110.1	14.45	617.57	25.02	592.55	0.164	0.151	1.29E-02			0.913	0.10	0.19
		600	109.8	14.55	507.46	37.92	469.54	0.130	0.130	8.94E-05			0.783	0.17	0.42
		900	110.2	14.44	392.75	47.93	344.82	0.096	0.109	1.30E-02			0.653	0.22	0.58
		1200	110.1	14.47	322.69	56.77	265.93	0.074	0.088	1.43E-02			0.528	0.28	0.72
7	70	75	69.9	40.03	1080.49	23.91	1056.58	0.167	0.178	1.02E-02	0.186	0.024	0.947	0.08	0.20
		150	70.0	39.86	1075.13	36.06	1039.07	0.165	0.165	6.89E-05			0.866	0.14	0.36
		300	69.9	39.95	1011.71	54.46	957.25	0.152	0.135	1.67E-02			0.684	0.23	0.53
		600	69.7	40.27	581.71	82.09	499.62	0.079	0.083	3.83E-03			0.363	0.38	1.15
		900	69.6	40.32	479.99	103.62	376.37	0.060	0.051	8.40E-03			0.167	0.50	1.61
		1200	69.8	40.07	346.54	121.34	225.20	0.036	0.036	7.15E-05			0.070	0.61	2.00
	90	75	90.2	22.79	1164.01	17.07	1146.94	0.182	0.177	4.92E-03	0.181	0.010	0.975	0.05	0.11
		150	89.7	23.04	1070.46	26.00	1044.46	0.166	0.170	4.51E-03			0.936	0.09	0.21
		300	90.0	22.87	1010.34	39.12	971.22	0.154	0.154	1.56E-04			0.840	0.14	0.30
		600	90.3	22.70	808.36	58.66	749.70	0.119	0.119	1.48E-04			0.635	0.23	0.65
		900	90.4	22.66	624.14	74.25	549.89	0.087	0.087	1.48E-04			0.449	0.31	0.91
		1200	90.2	22.77	529.75	87.89	441.86	0.070	0.061	8.59E-03			0.300	0.38	1.14
	110	75	110.0	14.50	985.63	13.02	972.61	0.154	0.154	8.50E-07	0.155	0.068	0.987	0.04	0.07
		150	110.1	14.45	977.00	19.67	957.32	0.152	0.152	5.82E-04			0.966	0.06	0.13
		300	110.2	14.42	1000.60	29.73	970.88	0.154	0.148	6.23E-03			0.913	0.10	0.19
		600	110.2	14.42	967.47	44.87	922.61	0.146	0.137	9.70E-03			0.786	0.16	0.41
		900	110.1	14.46	902.87	57.06	845.81	0.134	0.125	9.22E-03			0.653	0.21	0.58
		1200	110.1	14.45	663.80	67.47	596.33	0.095	0.114	1.94E-02			0.529	0.26	0.72

Table G.3: Parameters obtained by performed tests for different load, temperature and rotational speed conditions, for TRB 320/28X/Q and 75W90 oil (with running-in).

Load	θ (Condition)	n	θ (Recorded)	ν	M_t^{exp}	M_{rr}	M_{sl}^{exp}	$\mu_{sl}exp$	$\mu_{sl}opt$	error	μ_{bl}	μ_{EHL}	ϕ_{bl}	λ	k
[kN]	[°C]	[rpm]	[°C]	[cSt]	[Nmm]	[Nmm]	[Nmm]	[-]	[-]	[-]	[-]	[-]	[-]	[-]	[-]
4	70	75	69.9	39.53	892.89	56.87	836.02	0.259	0.244	1.49E-02	0.263	0.001	0.927	0.12	0.22
		150	69.9	39.61	782.27	86.02	696.24	0.216	0.216	3.76E-09			0.819	0.19	0.40
		300	69.9	39.57	411.85	129.41	282.44	0.087	0.156	6.83E-02			0.591	0.32	0.72
		600	69.8	39.70	330.15	193.63	136.52	0.042	0.066	2.37E-02			0.248	0.53	1.59
		900	69.9	39.53	302.90	242.64	60.26	0.019	0.024	5.01E-03			0.087	0.70	1.80
		1200	69.9	39.53	379.24	283.83	95.42	0.030	0.008	2.18E-02			0.026	0.85	2.20
	90	75	89.8	22.86	906.30	41.00	865.31	0.268	0.250	1.76E-02	0.259	0.001	0.966	0.07	0.13
		150	90.0	22.77	825.90	61.86	764.04	0.237	0.237	1.26E-07			0.912	0.12	0.23
		300	89.9	22.83	633.59	93.50	540.09	0.167	0.203	3.62E-02			0.784	0.20	0.42
		600	89.9	22.81	384.67	140.38	244.29	0.076	0.137	6.13E-02			0.526	0.33	0.91
		900	90.0	22.77	360.07	177.18	182.88	0.057	0.084	2.78E-02			0.323	0.44	1.03
		1200	90.0	22.75	341.24	208.40	132.84	0.041	0.049	7.57E-03			0.185	0.54	1.26
	110	75	110.1	14.43	832.85	31.13	801.73	0.248	0.248	2.45E-10	0.253	0.001	0.982	0.05	0.08
		150	109.6	14.58	905.49	47.41	858.08	0.266	0.241	2.50E-02			0.952	0.08	0.15
		300	109.8	14.50	851.24	71.42	779.82	0.242	0.222	1.91E-02			0.879	0.14	0.26
		600	109.9	14.49	477.28	107.55	369.73	0.115	0.180	6.57E-02			0.711	0.23	0.58
		900	109.6	14.58	322.05	136.78	185.27	0.057	0.138	8.11E-02			0.546	0.30	0.66
		1200	109.8	14.52	314.68	161.07	153.61	0.048	0.103	5.57E-02			0.406	0.37	0.81
7	70	75	69.5	40.06	1208.08	68.18	1139.90	0.202	0.098	1.04E-01	0.105	0.010	0.926	0.11	0.22
		150	69.9	39.61	599.20	102.32	496.88	0.088	0.088	2.87E-09			0.819	0.18	0.40
		300	69.3	40.31	373.00	155.59	217.41	0.038	0.066	2.70E-02			0.583	0.31	0.73
		600	70.2	39.25	353.83	228.84	124.98	0.022	0.034	1.21E-02			0.253	0.50	1.57
		900	69.7	39.86	410.75	289.93	120.82	0.021	0.018	3.18E-03			0.084	0.67	1.81
		1200	69.8	39.70	445.25	338.35	106.91	0.019	0.013	6.32E-03			0.025	0.81	2.21
	90	75	90.2	22.62	1460.16	48.45	1411.71	0.250	0.192	5.74E-02	0.199	0.001	0.966	0.07	0.13
		150	89.8	22.84	1100.29	73.72	1026.57	0.182	0.182	4.45E-07			0.912	0.12	0.23
		300	90.3	22.58	611.30	110.51	500.79	0.089	0.157	6.83E-02			0.787	0.19	0.41
		600	88.3	23.74	362.09	170.94	191.15	0.034	0.101	6.76E-02			0.507	0.33	0.95
		900	90.0	22.75	390.52	210.65	179.87	0.032	0.065	3.32E-02			0.323	0.42	1.03
		1200	90.0	22.77	422.62	247.99	174.63	0.031	0.038	6.63E-03			0.184	0.51	1.26
	110	75	110.2	14.38	1527.04	36.95	1490.09	0.264	0.129	1.35E-01	0.131	0.001	0.982	0.05	0.08
		150	110.0	14.46	1276.56	56.11	1220.45	0.216	0.125	9.13E-02			0.952	0.08	0.14
		300	110.1	14.43	735.80	84.71	651.10	0.115	0.115	7.54E-09			0.880	0.13	0.26
		600	110.4	14.33	373.77	127.09	246.67	0.044	0.094	5.02E-02			0.715	0.21	0.57
		900	110.3	14.35	358.32	161.19	197.13	0.035	0.073	3.79E-02			0.553	0.29	0.65
		1200	110.0	14.46	328.75	191.12	137.63	0.024	0.054	2.97E-02			0.408	0.35	0.80

Table G.4: Parameters obtained by performed tests for different load, temperature and rotational speed conditions, for TRB 320/28X/Q and 75W140 oil (with running-in).

Load	θ (Condition)	n	θ (Recorded)	ν	M_t^{exp}	M_{rr}	M_{sl}^{exp}	μ_{sl}^{exp}	μ_{sl}^{opt}	error	μ_{bl}	μ_{EHL}	ϕ_{bl}	λ	k
[kN]	[°C]	[rpm]	[°C]	[cSt]	[Nmm]	[Nmm]	[Nmm]	[-]	[-]	[-]	[-]	[-]	[-]	[-]	[-]
4	70	75	69.9	64.41	630.80	76.09	554.71	0.172	0.131	4.09E-02	0.149	0.020	0.861	0.18	0.36
		150	70.0	64.27	459.76	114.59	345.17	0.107	0.107	3.04E-08			0.675	0.29	0.64
		300	69.8	64.55	329.26	172.26	156.99	0.049	0.065	1.66E-02			0.352	0.49	1.17
		600	69.8	64.62	321.78	255.40	66.38	0.021	0.028	7.46E-03			0.063	0.80	2.58
		900	70.2	63.77	383.47	315.87	67.60	0.021	0.021	7.55E-07			0.008	1.04	2.90
		1200	72.0	60.06	516.05	355.19	160.86	0.050	0.020	2.98E-02			0.001	1.21	3.34
	90	75	89.9	35.35	740.43	53.19	687.24	0.213	0.194	1.88E-02	0.207	0.002	0.938	0.11	0.20
		150	90.1	35.12	645.22	80.09	565.14	0.175	0.175	3.55E-11			0.845	0.18	0.35
		300	89.8	35.47	287.50	121.34	166.15	0.051	0.132	8.10E-02			0.637	0.30	0.64
		600	89.9	35.35	274.54	181.11	93.43	0.029	0.065	3.59E-02			0.305	0.48	1.41
		900	89.8	35.44	316.67	228.16	88.51	0.027	0.027	2.21E-05			0.122	0.65	1.61
		1200	89.9	35.35	579.89	266.86	313.02	0.097	0.011	8.56E-02			0.044	0.79	1.96
	110	75	110.3	21.38	787.63	39.38	748.25	0.232	0.183	4.88E-02	0.189	0.001	0.969	0.07	0.12
		150	109.8	21.60	762.33	59.95	702.38	0.218	0.173	4.41E-02			0.918	0.12	0.22
		300	110.1	21.44	578.48	90.10	488.38	0.151	0.151	1.07E-06			0.800	0.19	0.39
		600	110.2	21.39	264.44	135.23	129.21	0.040	0.105	6.54E-02			0.556	0.32	0.86
		900	110.1	21.46	247.91	171.22	76.69	0.024	0.067	4.36E-02			0.353	0.43	0.98
		1200	110.1	21.46	250.86	201.58	49.28	0.015	0.041	2.54E-02			0.211	0.52	1.19
7	70	75	70.0	64.27	760.43	90.38	670.05	0.119	0.071	4.73E-02	0.080	0.015	0.862	0.17	0.36
		150	70.2	63.84	451.89	135.76	316.13	0.056	0.059	3.39E-03			0.677	0.28	0.64
		300	69.7	64.84	420.57	205.42	215.15	0.038	0.038	1.33E-08			0.350	0.46	1.18
		600	69.9	64.48	417.86	303.41	114.45	0.020	0.020	7.21E-04			0.064	0.75	2.58
		900	69.9	64.34	460.96	377.50	83.46	0.015	0.016	1.14E-03			0.008	1.00	2.92
		1200	73.4	57.41	508.60	412.59	96.01	0.017	0.016	1.46E-03			0.002	1.11	3.19
	90	75	89.9	35.31	1124.01	63.24	1060.77	0.188	0.112	7.58E-02	0.119	0.010	0.938	0.10	0.2
		150	90.0	35.22	670.22	95.41	574.81	0.102	0.102	3.57E-06			0.844	0.17	0.35
		300	90.1	35.19	343.85	143.64	200.21	0.035	0.079	4.40E-02			0.640	0.28	0.64
		600	90.0	35.25	293.91	215.09	78.82	0.014	0.043	2.92E-02			0.307	0.46	1.41
		900	89.4	35.86	400.49	273.19	127.29	0.023	0.023	1.29E-07			0.118	0.62	1.63
		1200	89.8	35.44	573.56	317.89	255.67	0.045	0.014	3.09E-02			0.043	0.75	1.97
	110	75	110.0	21.51	1303.73	47.01	1256.72	0.222	0.114	1.09E-01	0.117	0.001	0.968	0.07	0.12
		150	110.2	21.39	1073.26	70.90	1002.37	0.177	0.108	6.95E-02			0.919	0.11	0.21
		300	110.1	21.44	540.33	107.17	433.16	0.077	0.094	1.74E-02			0.800	0.18	0.39
		600	110.1	21.46	387.78	161.13	226.65	0.040	0.065	2.54E-02			0.554	0.30	0.86
		900	110.2	21.43	320.49	203.48	117.01	0.021	0.042	2.15E-02			0.354	0.40	0.97
		1200	110.2	21.41	384.39	239.46	144.93	0.026	0.026	5.38E-08			0.21	0.50	1.19

Table G.5: Parameters obtained by performed tests for different load, temperature and rotational speed conditions, for TRB 320/28X/Q and 80W90 oil (with running-in).

Load	θ (Condition)	n	θ (Recorded)	ν	M_t^{exp}	M_{rr}	M_{sl}^{exp}	μ_{sl}^{exp}	μ_{sl}^{opt}	error	μ_{bl}	μ_{EHL}	ϕ_{bl}	λ	k
[kN]	[°C]	[rpm]	[°C]	[cSt]	[Nmm]	[Nmm]	[Nmm]	[-]	[-]	[-]	[-]	[-]	[-]	[-]	[-]
4	70	75	70.3	36.21	868.49	53.96	814.53	0.252	0.222	3.05E-02	0.237	0.001	0.935	0.14	0.20
		150	70.1	36.46	722.95	81.88	641.06	0.199	0.199	2.47E-08			0.837	0.23	0.36
		300	70.3	36.21	536.46	122.81	413.64	0.128	0.149	2.12E-02			0.628	0.38	0.66
		600	69.9	36.63	356.61	184.87	171.75	0.053	0.069	1.56E-02			0.287	0.63	1.47
		900	69.9	36.67	307.75	232.58	75.17	0.023	0.027	3.79E-03			0.110	0.84	1.67
		1200	70.3	36.21	365.91	270.43	95.48	0.030	0.010	1.93E-02			0.039	1.01	2.01
	90	75	90.3	19.55	901.18	37.33	863.85	0.268	0.220	4.74E-02	0.226	0.001	0.972	0.08	0.11
		150	90.1	19.62	754.50	56.61	697.89	0.216	0.210	5.93E-03			0.928	0.14	0.20
		300	89.9	19.73	584.58	85.76	498.81	0.154	0.186	3.13E-02			0.820	0.23	0.36
		600	90.0	19.71	421.88	128.89	292.99	0.091	0.135	4.38E-02			0.592	0.37	0.79
		900	90.3	19.55	316.51	162.23	154.27	0.048	0.091	4.37E-02			0.401	0.50	0.89
		1200	89.9	19.75	377.58	192.24	185.34	0.057	0.057	1.74E-09			0.250	0.61	1.10
	110	75	109.9	11.98	900.93	27.84	873.08	0.270	0.154	1.16E-01	0.156	0.043	0.986	0.05	0.07
		150	110.3	11.88	737.19	41.95	695.25	0.215	0.152	6.34E-02			0.964	0.09	0.12
		300	110.2	11.89	533.23	63.45	469.78	0.145	0.145	8.46E-09			0.907	0.15	0.22
		600	110.4	11.85	424.85	95.47	329.38	0.102	0.130	2.84E-02			0.774	0.24	0.47
		900	109.9	11.98	304.67	121.91	182.76	0.057	0.114	5.77E-02			0.631	0.33	0.54
		1200	109.9	11.99	324.87	144.11	180.77	0.056	0.100	4.38E-02			0.502	0.40	0.67
7	70	75	69.7	36.88	1042.80	64.90	977.90	0.173	0.107	6.64E-02	0.114	0.006	0.934	0.13	0.20
		150	69.8	36.75	638.87	97.86	541.01	0.096	0.096	3.78E-04			0.835	0.22	0.37
		300	69.9	36.71	445.68	147.27	298.41	0.053	0.073	2.04E-02			0.623	0.36	0.67
		600	69.9	36.63	391.37	219.89	171.48	0.030	0.037	6.88E-03			0.287	0.60	1.47
		900	70.1	36.42	379.84	275.56	104.28	0.018	0.018	1.63E-07			0.113	0.79	1.66
		1200	69.8	36.80	409.72	324.54	85.19	0.015	0.010	4.83E-03			0.036	0.97	2.04
	90	75	90.1	19.66	1449.84	44.55	1405.29	0.249	0.101	1.48E-01	0.104	0.001	0.972	0.08	0.11
		150	89.8	19.78	954.71	67.66	887.05	0.157	0.096	6.08E-02			0.927	0.13	0.20
		300	89.9	19.77	583.32	102.12	481.20	0.085	0.085	3.88E-08			0.819	0.22	0.36
		600	89.8	19.78	399.22	153.64	245.58	0.043	0.062	1.82E-02			0.591	0.36	0.79
		900	89.9	19.77	319.80	194.21	125.60	0.022	0.042	1.94E-02			0.396	0.48	0.90
		1200	90.1	19.66	367.59	228.06	139.53	0.025	0.027	2.23E-03			0.252	0.58	1.09
	110	75	110.3	11.87	1603.07	32.94	1570.13	0.278	0.121	1.57E-01	0.123	0.001	0.986	0.05	0.07
		150	109.9	11.99	1155.24	50.16	1105.08	0.196	0.118	7.75E-02			0.963	0.09	0.12
		300	109.8	12.01	703.67	75.92	627.76	0.111	0.111	2.30E-08			0.906	0.14	0.22
		600	110.3	11.88	423.49	113.76	309.73	0.055	0.095	4.01E-02			0.773	0.23	0.48
		900	110.3	11.87	363.44	144.24	219.21	0.039	0.078	3.94E-02			0.635	0.31	0.54
		1200	110.1	11.93	347.25	170.88	176.37	0.031	0.062	3.11E-02			0.505	0.38	0.66

Table G.6: Parameters obtained by performed tests for different load, temperature and rotational speed conditions, for TRB 320/28X/Q and 5W30 oil (with running-in).

Load	θ (Condition)	n	θ (Recorded)	ν	M_t^{exp}	M_{rr}	M_{sl}^{exp}	μ_{sl}^{exp}	μ_{sl}^{opt}	error	μ_{bl}	μ_{EHL}	ϕ_{bl}	λ	k
[kN]	[°C]	[rpm]	[°C]	[cSt]	[Nmm]	[Nmm]	[Nmm]	[-]	[-]	[-]	[-]	[-]	[-]	[-]	[-]
4	70	75	69.7	25.33	941.51	43.59	897.92	0.278	0.278	3.75E-07	0.290	0.001	0.960	0.08	0.14
		150	69.8	25.31	932.19	65.89	866.30	0.268	0.260	7.96E-03			0.899	0.13	0.25
		300	70.0	25.12	593.74	98.96	494.77	0.153	0.219	6.61E-02			0.757	0.22	0.46
		600	69.7	25.36	357.85	149.35	208.51	0.065	0.138	7.34E-02			0.475	0.36	1.01
		900	69.9	25.24	242.56	188.00	54.56	0.017	0.079	6.23E-02			0.271	0.48	1.15
		1200	70.2	25.00	215.64	219.86	-4.22	-0.001	0.043	4.43E-02			0.145	0.58	1.39
	90	75	90.2	15.05	1019.65	31.92	987.73	0.306	0.231	7.46E-02	0.236	0.001	0.981	0.05	0.08
		150	89.8	15.20	821.83	48.60	773.22	0.239	0.224	1.56E-02			0.949	0.09	0.15
		300	89.4	15.34	736.56	73.85	662.71	0.205	0.205	8.00E-09			0.870	0.14	0.28
		600	90.0	15.14	457.41	110.37	347.03	0.107	0.165	5.71E-02			0.696	0.23	0.61
		900	89.9	15.17	303.35	139.96	163.39	0.051	0.125	7.42E-02			0.527	0.31	0.69
		1200	89.6	15.27	273.94	165.82	108.11	0.033	0.090	5.68E-02			0.380	0.39	0.85
	110	75	110.2	9.93	997.55	24.88	972.68	0.301	0.242	5.96E-02	0.244	0.001	0.989	0.04	0.06
		150	109.7	10.02	966.81	37.87	928.93	0.288	0.237	5.04E-02			0.971	0.06	0.10
		300	109.6	10.03	787.75	57.33	730.42	0.226	0.226	3.46E-08			0.926	0.10	0.18
		600	110.3	9.90	593.89	85.83	508.06	0.157	0.200	4.29E-02			0.819	0.16	0.40
		900	110.2	9.92	444.41	109.12	335.29	0.104	0.172	6.80E-02			0.702	0.22	0.45
		1200	110.0	9.95	352.87	129.28	223.60	0.069	0.144	7.48E-02			0.588	0.27	0.55
7	70	75	69.9	25.21	1337.21	51.70	1285.51	0.228	0.213	1.42E-02	0.222	0.001	0.961	0.08	0.14
		150	70.0	25.17	1207.25	78.11	1129.14	0.200	0.200	7.95E-08			0.900	0.13	0.25
		300	70.0	25.14	908.11	117.78	790.33	0.140	0.168	2.84E-02			0.757	0.21	0.46
		600	69.9	25.21	538.42	177.06	361.36	0.064	0.107	4.26E-02			0.478	0.34	1.01
		900	69.8	25.26	325.83	223.73	102.10	0.018	0.061	4.27E-02			0.271	0.46	1.15
		1200	70.2	24.98	380.33	261.37	118.96	0.021	0.033	1.22E-02			0.146	0.55	1.39
	90	75	89.8	15.21	1530.77	38.21	1492.56	0.264	0.227	3.73E-02	0.231	0.001	0.980	0.05	0.08
		150	89.9	15.17	1515.42	57.73	1457.69	0.258	0.220	3.83E-02			0.949	0.08	0.15
		300	90.3	15.04	1228.69	86.81	1141.88	0.202	0.202	2.74E-08			0.873	0.13	0.27
		600	90.0	15.14	449.84	131.28	318.56	0.056	0.161	1.05E-01			0.696	0.22	0.61
		900	89.7	15.23	386.36	166.84	219.52	0.039	0.122	8.32E-02			0.525	0.30	0.69
		1200	89.7	15.23	349.25	196.89	152.37	0.027	0.089	6.20E-02			0.382	0.37	0.85
	110	75	110.0	9.96	1640.43	29.65	1610.78	0.285	0.265	2.02E-02	0.268	0.001	0.989	0.03	0.06
		150	109.8	10.00	1567.93	45.01	1522.92	0.270	0.260	9.41E-03			0.971	0.06	0.10
		300	109.9	9.98	1469.90	67.98	1401.92	0.248	0.248	8.87E-08			0.926	0.09	0.18
		600	110.3	9.90	744.19	102.13	642.07	0.114	0.219	1.06E-01			0.819	0.16	0.40
		900	110.0	9.95	447.50	130.03	317.47	0.056	0.188	1.32E-01			0.701	0.21	0.45
		1200	110.1	9.95	395.69	153.71	241.98	0.043	0.158	1.15E-01			0.588	0.26	0.55

Table G.7: Parameters obtained by performed tests for different load, temperature and rotational speed conditions, for TRB 320/28X/Q and 10W50 oil (with running-in).

Load	θ (Condition)	n	θ (Recorded)	ν	M_t^{exp}	M_{rr}	M_{sl}^{exp}	μ_{sl}^{exp}	μ_{sl}^{opt}	error	μ_{bl}	μ_{EHL}	ϕ_{bl}	λ	k
[kN]	[°C]	[rpm]	[°C]	[cSt]	[Nmm]	[Nmm]	[Nmm]	[-]	[-]	[-]	[-]	[-]	[-]	[-]	[-]
4	70	75	70.5	39.21	950.35	56.59	893.76	0.277	0.189	8.78E-02	0.201	0.036	0.928	0.12	0.22
		150	69.4	40.47	636.50	87.13	549.37	0.170	0.170	3.50E-07			0.814	0.20	0.40
		300	70.1	39.65	514.23	129.56	384.67	0.119	0.133	1.40E-02			0.590	0.32	0.72
		600	69.9	39.85	462.77	194.08	268.69	0.083	0.076	6.92E-03			0.246	0.52	1.59
		900	70.0	39.81	448.12	243.60	204.51	0.063	0.050	1.37E-02			0.084	0.70	1.81
		1200	69.7	40.14	336.00	286.21	49.80	0.015	0.040	2.42E-02			0.024	0.86	2.23
	90	75	90.3	22.68	1067.86	40.80	1027.06	0.318	0.289	2.91E-02	0.299	0.001	0.966	0.07	0.13
		150	89.9	22.89	942.89	62.06	880.83	0.273	0.273	6.54E-07			0.911	0.12	0.23
		300	90.4	22.61	705.50	92.97	612.53	0.190	0.235	4.58E-02			0.786	0.20	0.41
		600	90.0	22.81	448.52	140.41	308.11	0.095	0.158	6.24E-02			0.526	0.33	0.91
		900	90.1	22.78	383.34	177.21	206.13	0.064	0.097	3.34E-02			0.323	0.44	1.04
		1200	89.9	22.87	373.58	209.03	164.55	0.051	0.055	4.42E-03			0.182	0.54	1.27
	110	75	110.1	14.44	1099.71	31.14	1068.57	0.331	0.321	9.77E-03	0.327	0.001	0.982	0.05	0.08
		150	110.2	14.40	1080.42	47.05	1033.37	0.320	0.312	8.33E-03			0.953	0.08	0.14
		300	110.0	14.46	1000.49	71.29	929.20	0.288	0.288	3.31E-09			0.879	0.14	0.26
		600	109.7	14.56	567.61	107.84	459.76	0.142	0.233	9.01E-02			0.710	0.23	0.58
		900	110.1	14.44	462.63	135.99	326.64	0.101	0.180	7.93E-02			0.550	0.30	0.66
		1200	110.0	14.45	359.59	160.59	198.99	0.062	0.134	7.27E-02			0.409	0.37	0.80
7	70	75	69.8	40.06	1796.72	68.18	1728.54	0.306	0.288	1.75E-02	0.311	0.001	0.926	0.11	0.22
		150	69.8	40.06	1540.33	103.00	1437.33	0.254	0.254	2.93E-08			0.816	0.18	0.40
		300	70.2	39.49	631.01	153.73	477.28	0.084	0.185	1.00E-01			0.592	0.30	0.72
		600	70.2	39.57	391.60	229.90	161.70	0.029	0.078	4.98E-02			0.249	0.50	1.58
		900	70.2	39.53	394.78	288.59	106.19	0.019	0.028	9.07E-03			0.087	0.66	1.80
		1200	70.2	39.53	364.95	337.57	27.38	0.005	0.009	4.13E-03			0.026	0.80	2.20
	90	75	89.8	22.93	1879.04	48.84	1830.20	0.324	0.251	7.27E-02	0.260	0.001	0.965	0.07	0.13
		150	90.1	22.76	1414.92	73.56	1341.37	0.237	0.237	2.10E-06			0.912	0.11	0.23
		300	90.1	22.79	1176.61	111.13	1065.48	0.189	0.204	1.56E-02			0.784	0.19	0.41
		600	89.9	22.87	383.55	167.25	216.30	0.038	0.137	9.87E-02			0.525	0.31	0.91
		900	89.8	22.97	367.41	211.80	155.61	0.028	0.084	5.60E-02			0.318	0.42	1.04
		1200	90.2	22.70	428.67	247.57	181.10	0.032	0.049	1.71E-02			0.186	0.51	1.26
	110	75	109.8	14.52	1454.27	37.16	1417.11	0.251	0.070	1.81E-01	0.071	0.037	0.982	0.05	0.08
		150	110.1	14.43	445.66	56.03	389.63	0.069	0.069	7.59E-11			0.953	0.08	0.14
		300	110.1	14.42	418.24	84.66	333.58	0.059	0.067	7.47E-03			0.880	0.13	0.26
		600	109.9	14.49	545.33	127.90	417.42	0.074	0.061	1.30E-02			0.712	0.21	0.58
		900	109.7	14.54	451.07	162.41	288.66	0.051	0.055	4.23E-03			0.547	0.29	0.66
		1200	109.9	14.48	398.56	191.25	207.31	0.037	0.051	1.39E-02			0.408	0.35	0.80

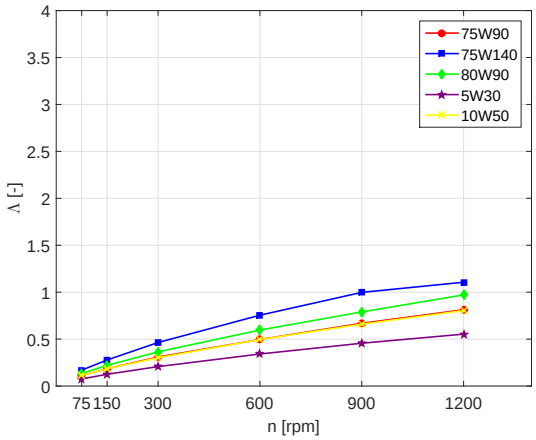

(a) 7 kN; 70 °C

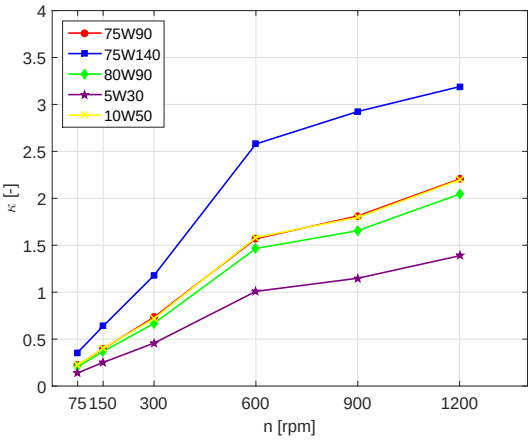

(b) 7 kN; 70 °C

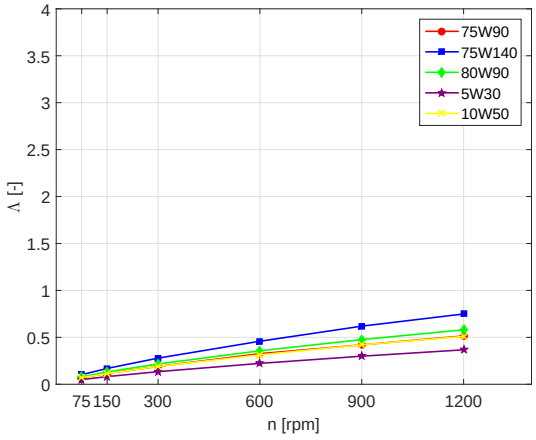

(c) 7 kN; 90 °C

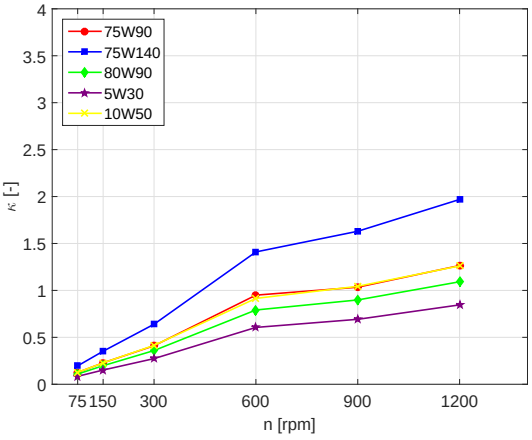

(d) 7 kN; 90 °C

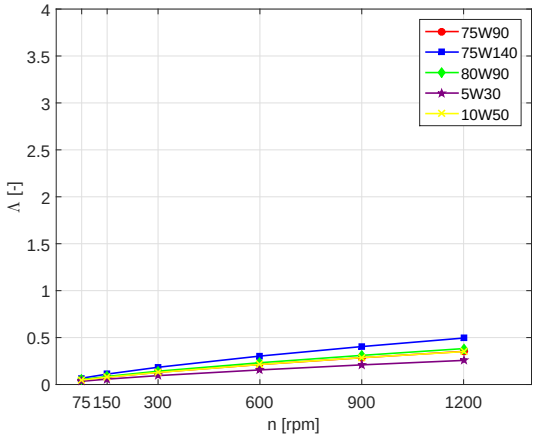

(e) 7 kN; 110 °C

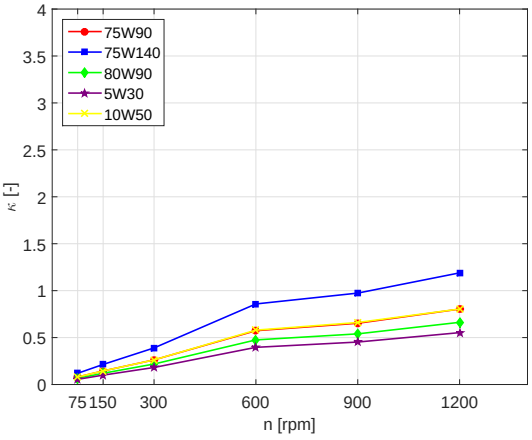

(f) 7 kN; 110 °C

Figure G.1: TRB 320/28X/Q calculated specific film thickness (Λ) and viscosity ratio (κ) for all tested oils at 7 kN

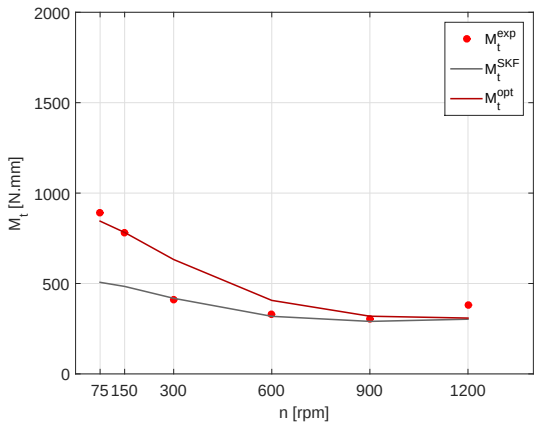

(a) 4 kN; 70 °C

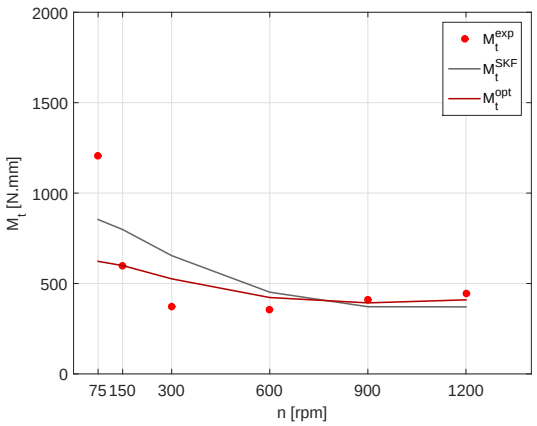

(b) 7 kN; 70 °C

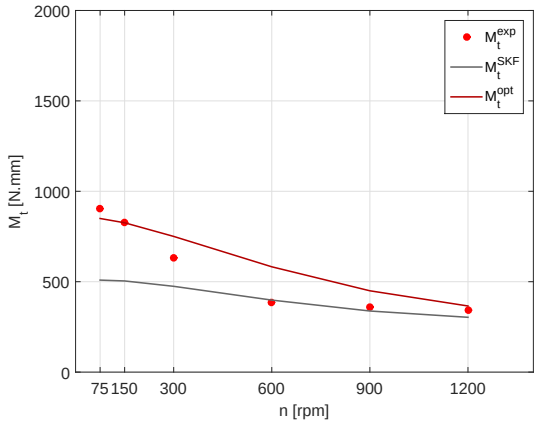

(c) 4 kN; 90 °C

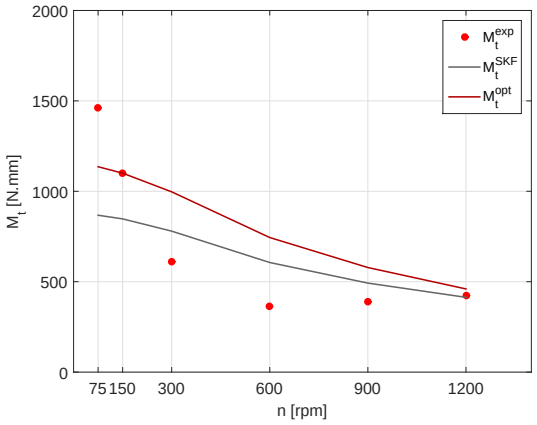

(d) 7 kN; 90 °C

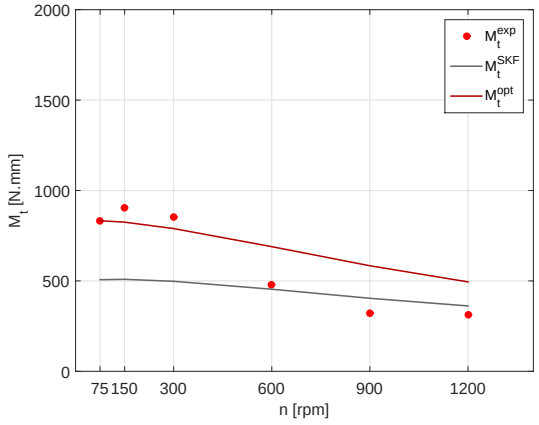

(e) 4 kN; 110 °C

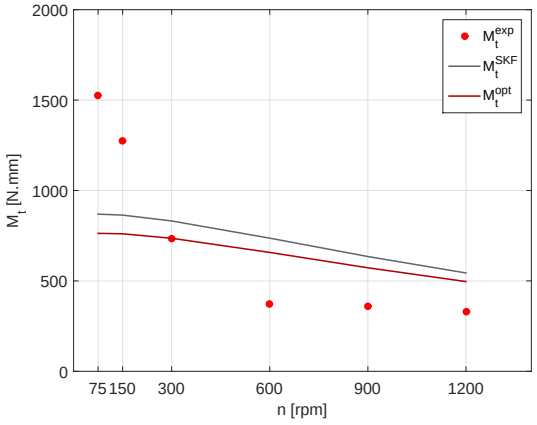

(f) 7 kN; 110 °C

Figure G.2: Experimental, SKF and Optimized Total Friction Torque (M_t) for TRB 320/28X/Q and 75W90 oil.

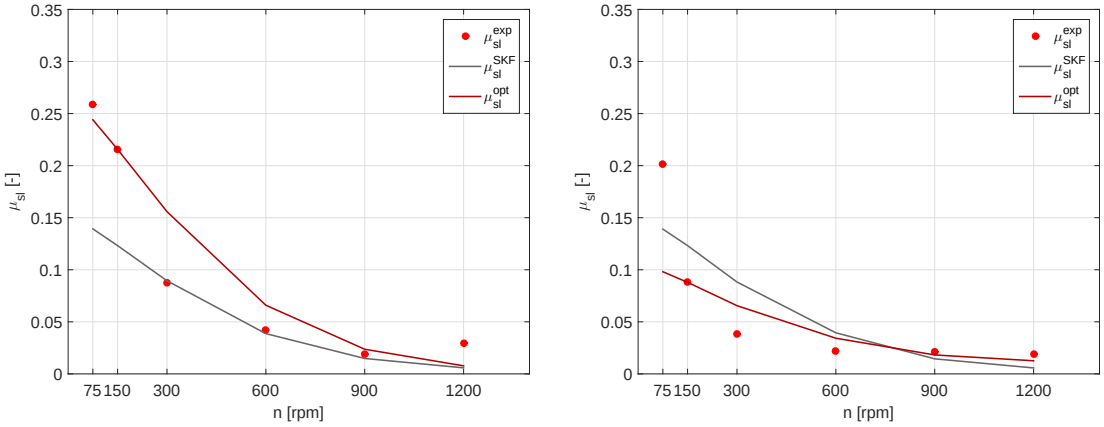

(a) 4 kN; 70 °C

(b) 7 kN; 70 °C

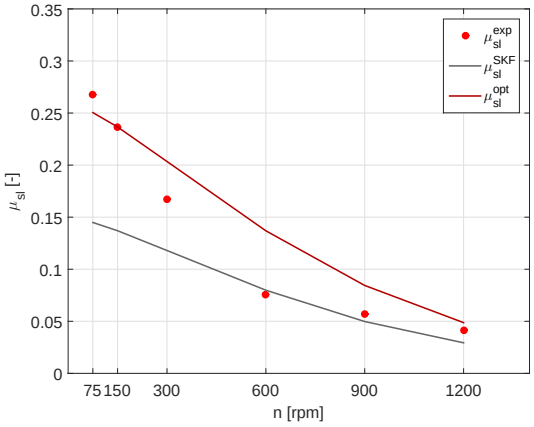

(c) 4 kN; 90 °C

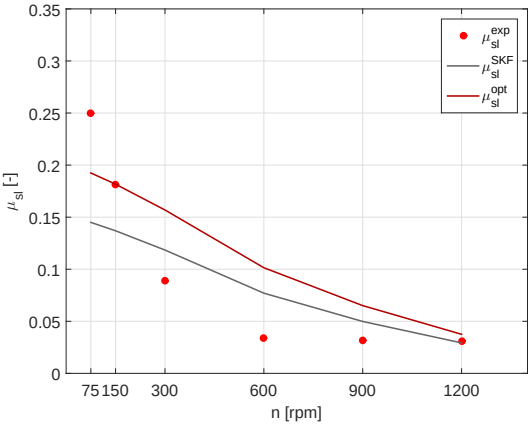

(d) 7 kN; 90 °C

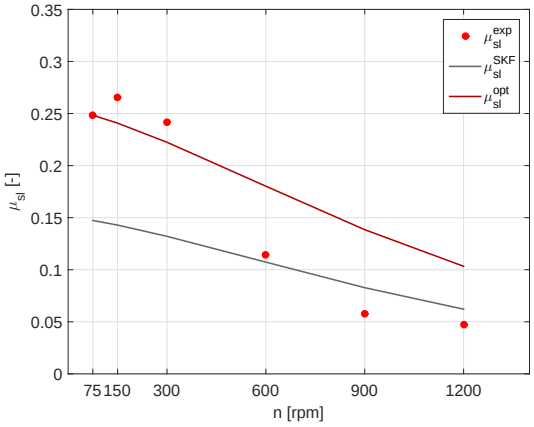

(e) 4 kN; 110 °C

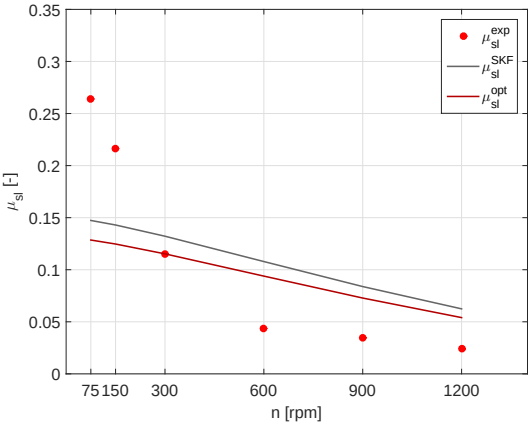

(f) 7 kN; 110 °C

Figure G.3: Experimental, SKF and Optimized Sliding Coefficient of Friction (μ_{sl}) for TRB 320/28X/Q and 75W90 oil.

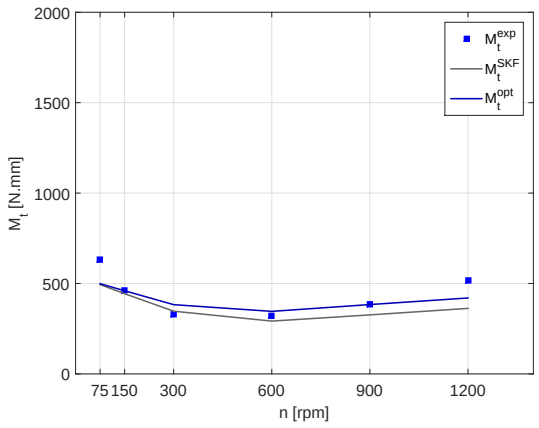

(a) 4 kN; 70 °C

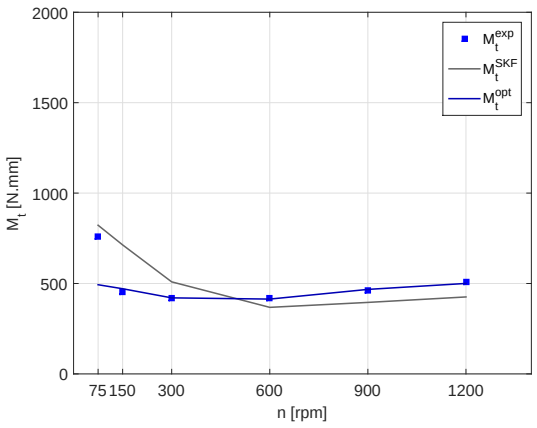

(b) 7 kN; 70 °C

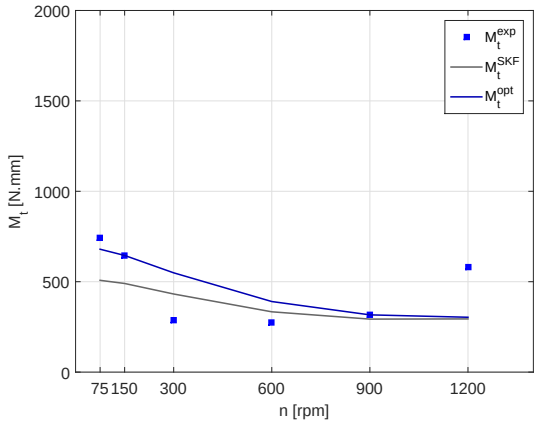

(c) 4 kN; 90 °C

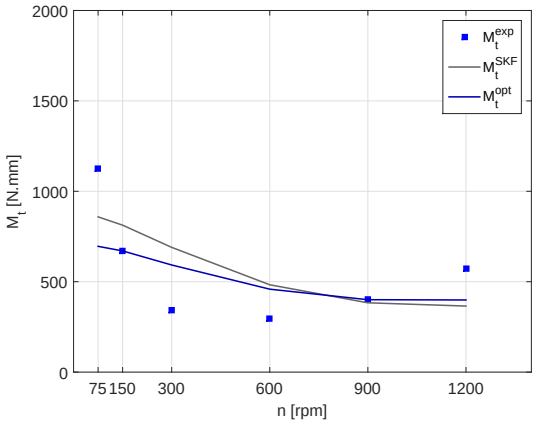

(d) 7 kN; 90 °C

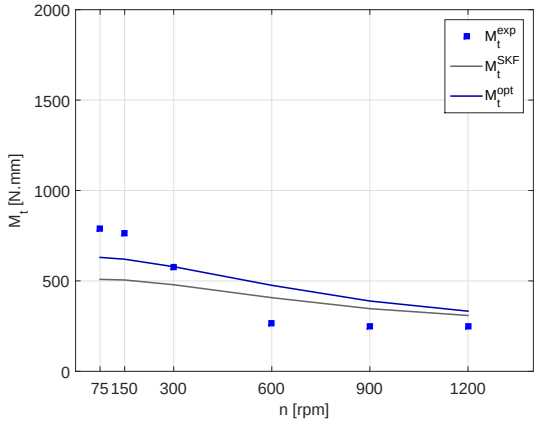

(e) 4 kN; 110 °C

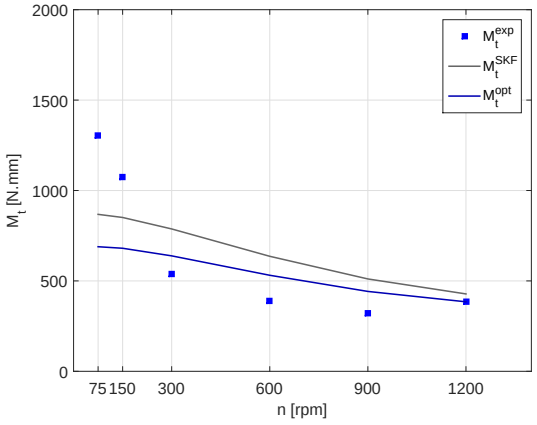

(f) 7 kN; 110 °C

Figure G.4: Experimental, SKF and Optimized Total Friction Torque (M_t) for TRB 320/28X/Q and 75W140 oil.

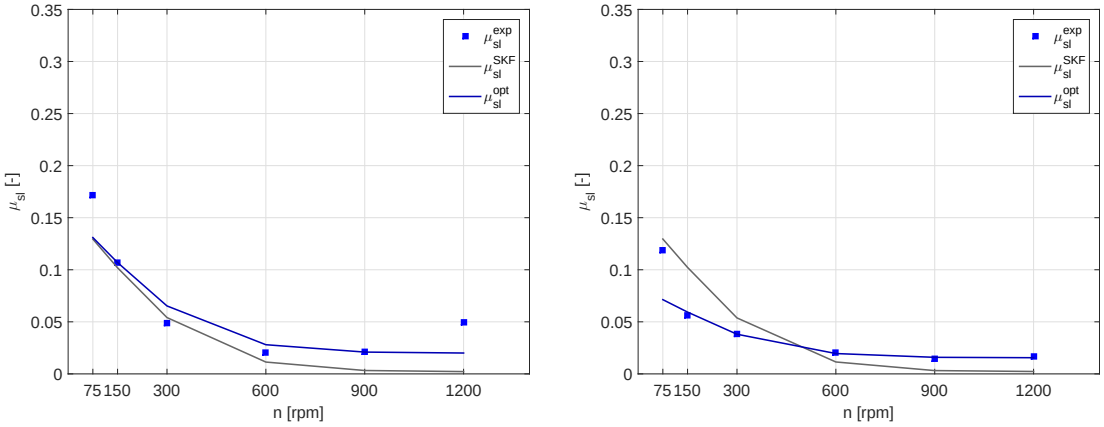

(a) 4 kN; 70 °C

(b) 7 kN; 70 °C

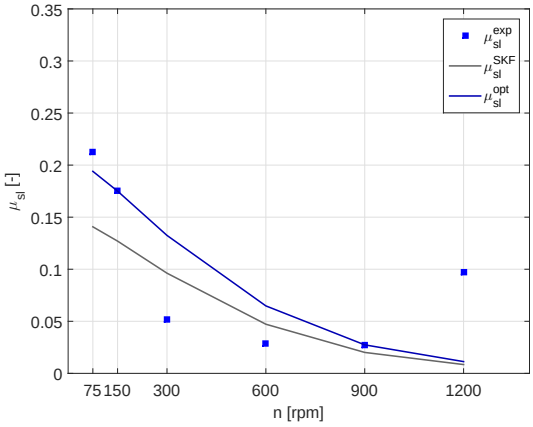

(c) 4 kN; 90 °C

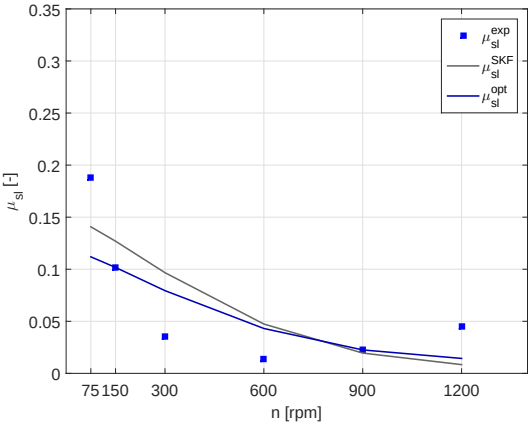

(d) 7 kN; 90 °C

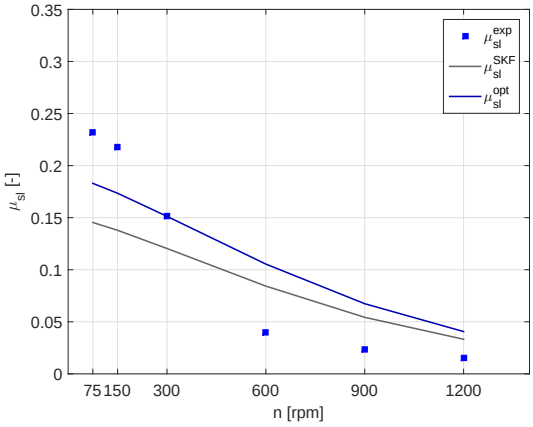

(e) 4 kN; 110 °C

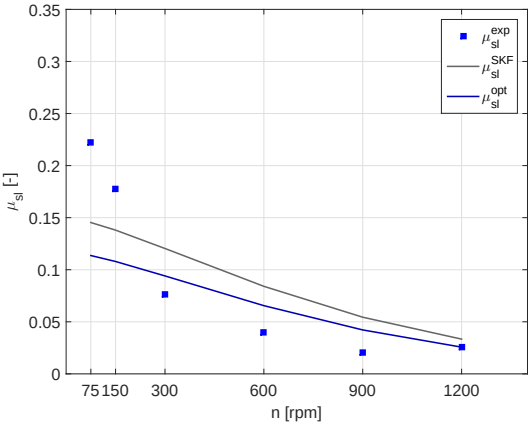

(f) 7 kN; 110 °C

Figure G.5: Experimental, SKF and Optimized Sliding Coefficient of Friction (μ_{sl}) for TRB 320/28X/Q and 75W140 oil.

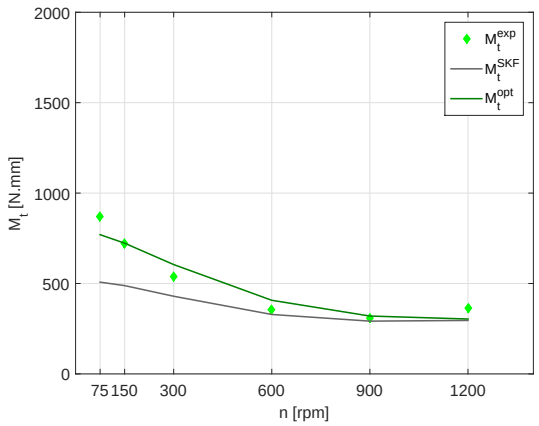

(a) 4 kN; 70 °C

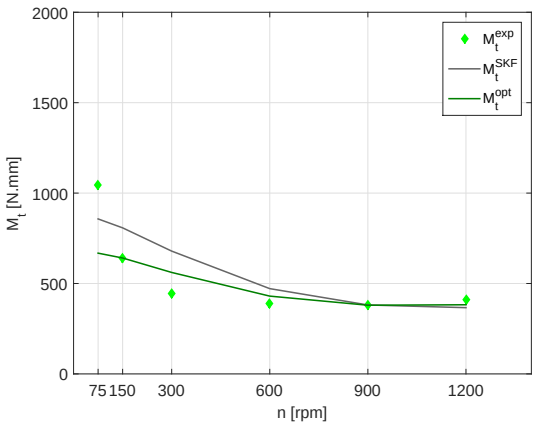

(b) 7 kN; 70 °C

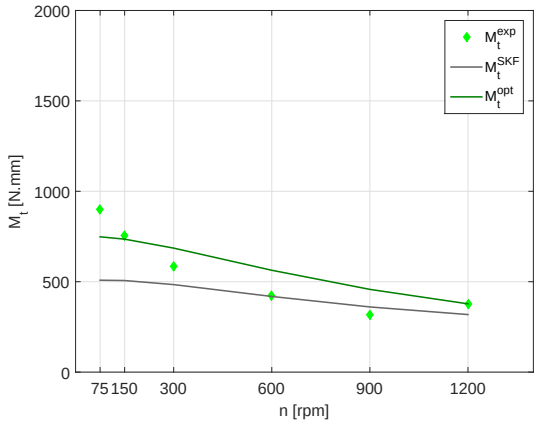

(c) 4 kN; 90 °C

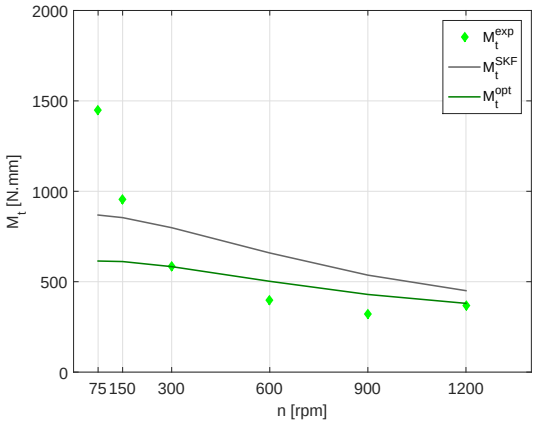

(d) 7 kN; 90 °C

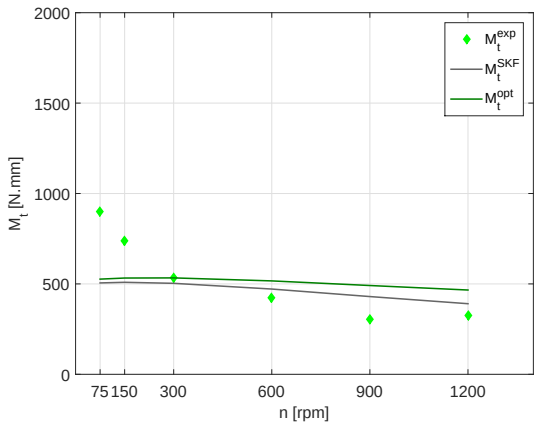

(e) 4 kN; 110 °C

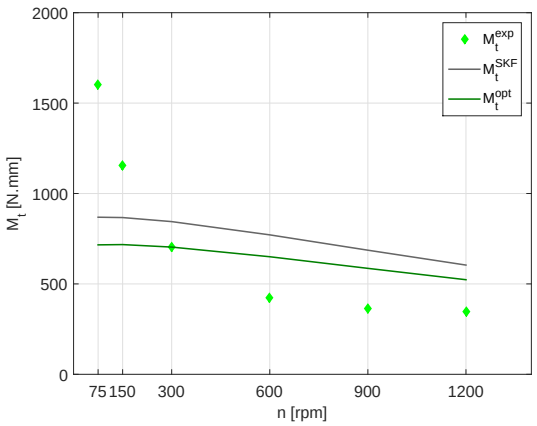

(f) 7 kN; 110 °C

Figure G.6: Experimental, SKF and Optimized Total Friction Torque (M_t) for TRB 320/28X/Q and 80W90 oil.

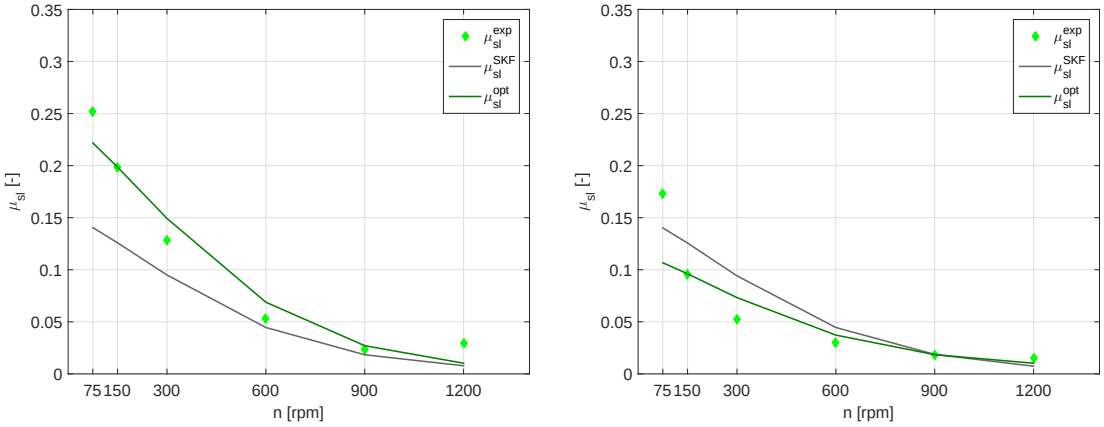

(a) 4 kN; 70 °C

(b) 7 kN; 70 °C

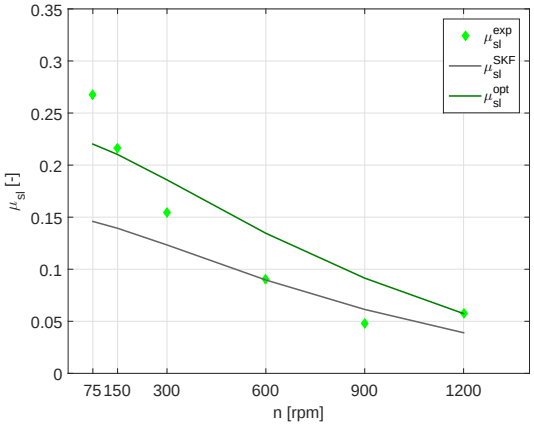

(c) 4 kN; 90 °C

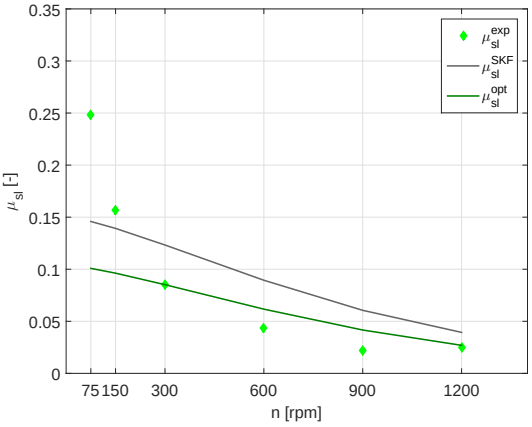

(d) 7 kN; 90 °C

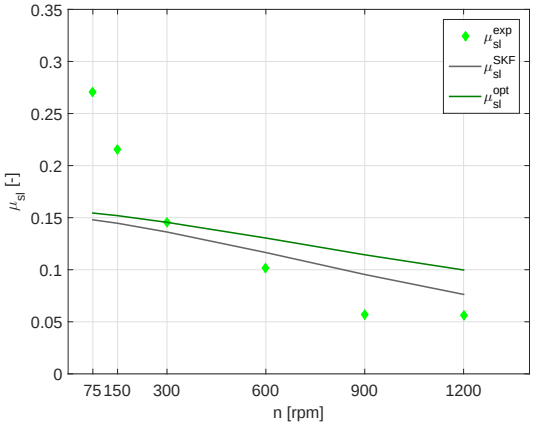

(e) 4 kN; 110 °C

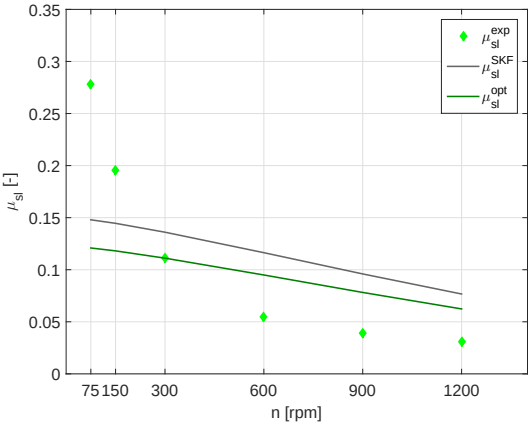

(f) 7 kN; 110 °C

Figure G.7: Experimental, SKF and Optimized Sliding Coefficient of Friction (μ_{sl}) for TRB 320/28X/Q and 80W90 oil.

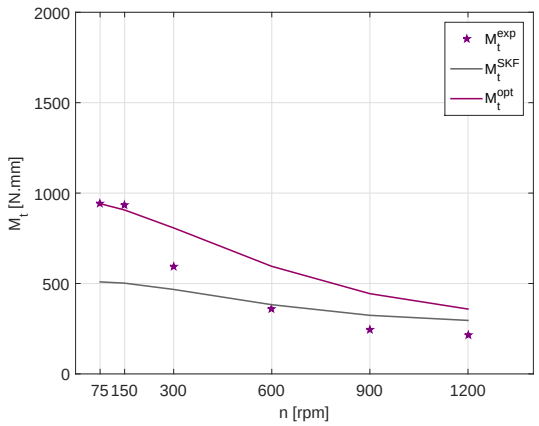

(a) 4 kN; 70 °C

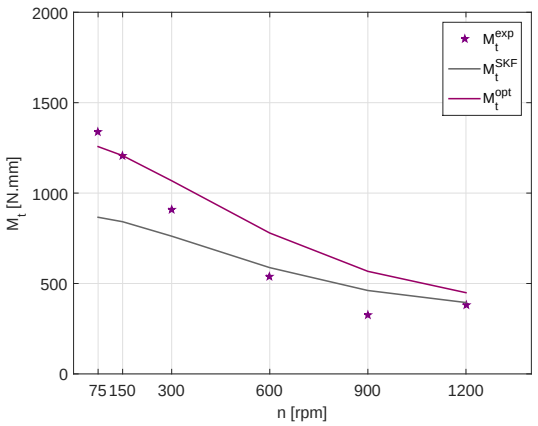

(b) 7 kN; 70 °C

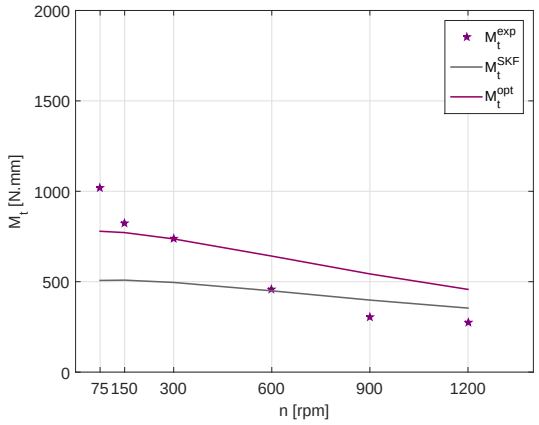

(c) 4 kN; 90 °C

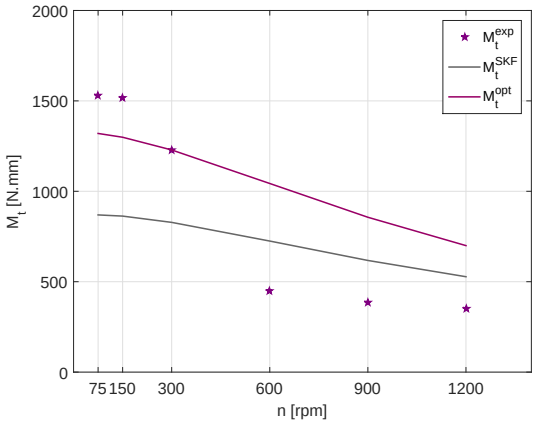

(d) 7 kN; 90 °C

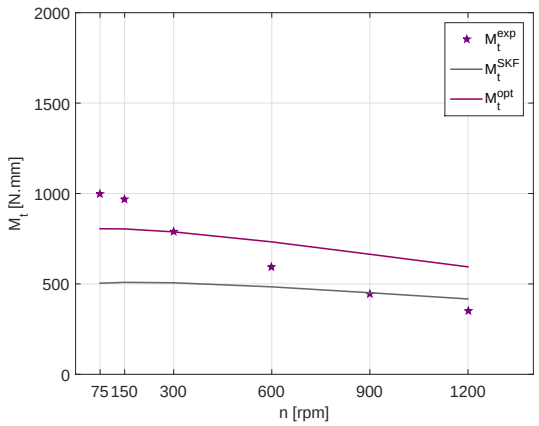

(e) 4 kN; 110 °C

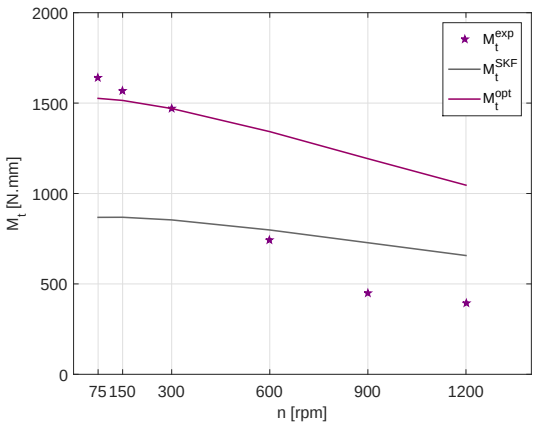

(f) 7 kN; 110 °C

Figure G.8: Experimental, SKF and Optimized Total Friction Torque (M_t) for TRB 320/28X/Q and 5W30 oil.

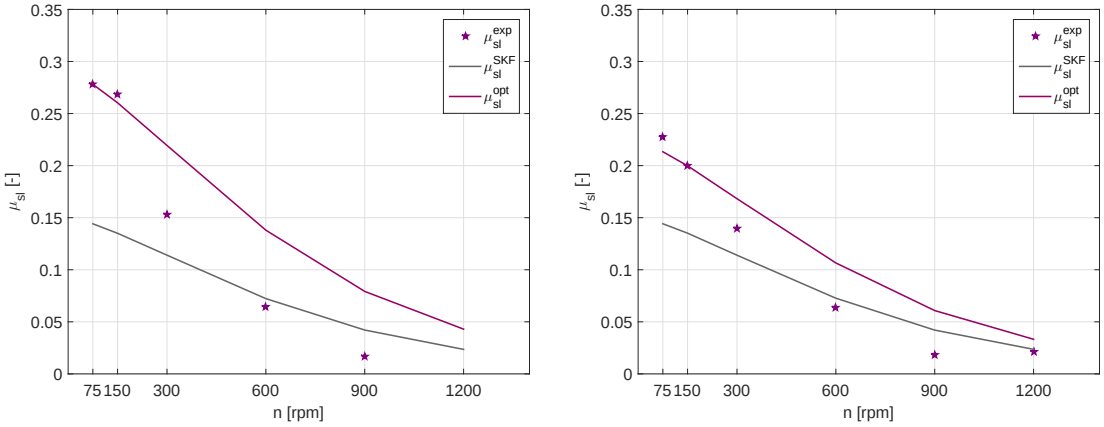

(a) 4 kN; 70 °C

(b) 7 kN; 70 °C

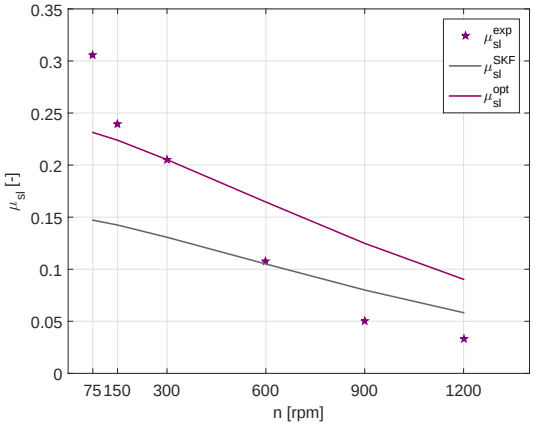

(c) 4 kN; 90 °C

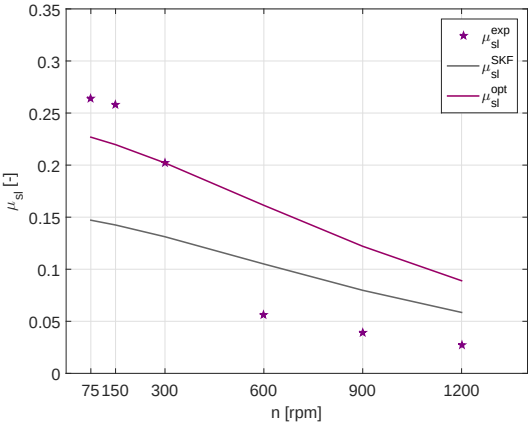

(d) 7 kN; 90 °C

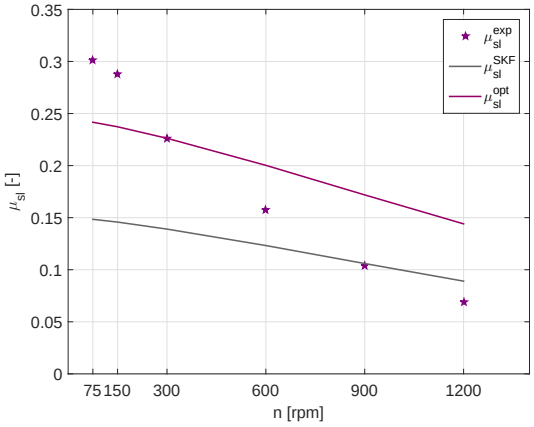

(e) 4 kN; 110 °C

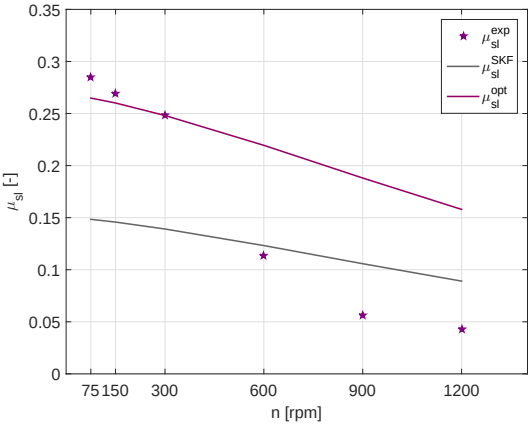

(f) 7 kN; 110 °C

Figure G.9: Experimental, SKF and Optimized Sliding Coefficient of Friction (μ_{sl}) for TRB 320/28X/Q and 5W30 oil.

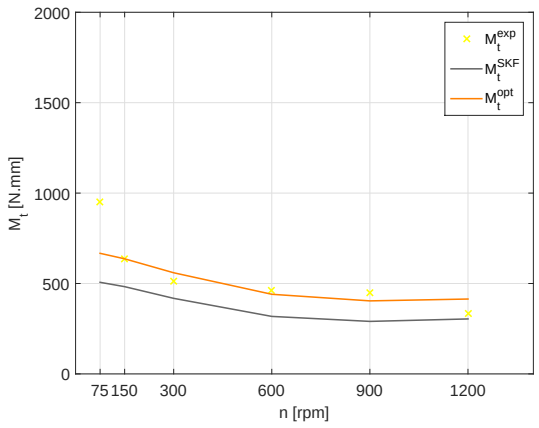

(a) 4 kN; 70 °C

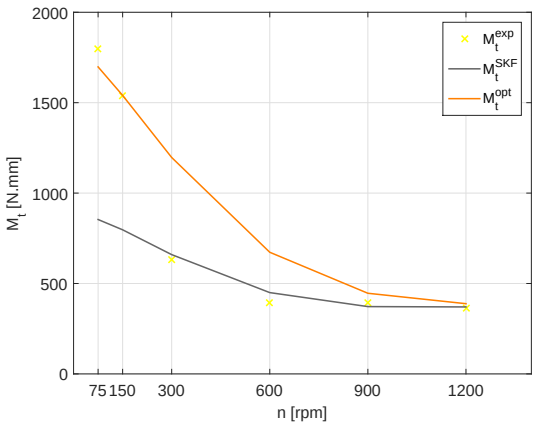

(b) 7 kN; 70 °C

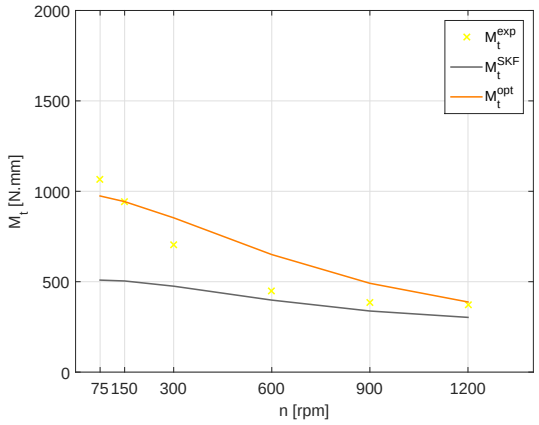

(c) 4 kN; 90 °C

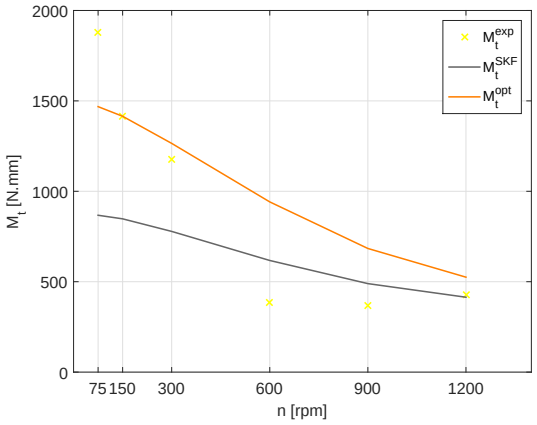

(d) 7 kN; 90 °C

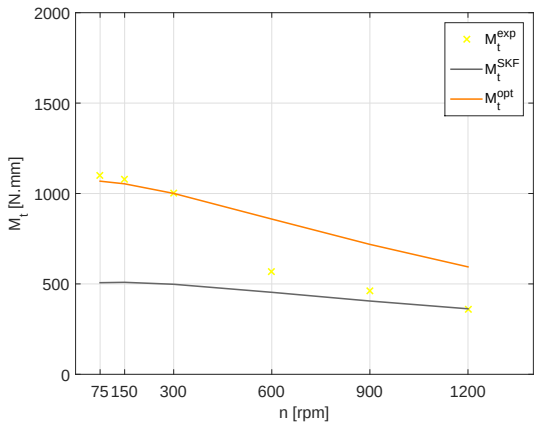

(e) 4 kN; 110 °C

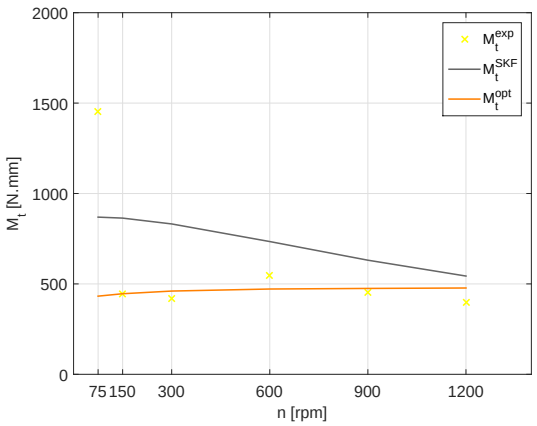

(f) 7 kN; 110 °C

Figure G.10: Experimental, SKF and Optimized Total Friction Torque (M_t) for TRB 320/28X/Q and 10W50 oil.

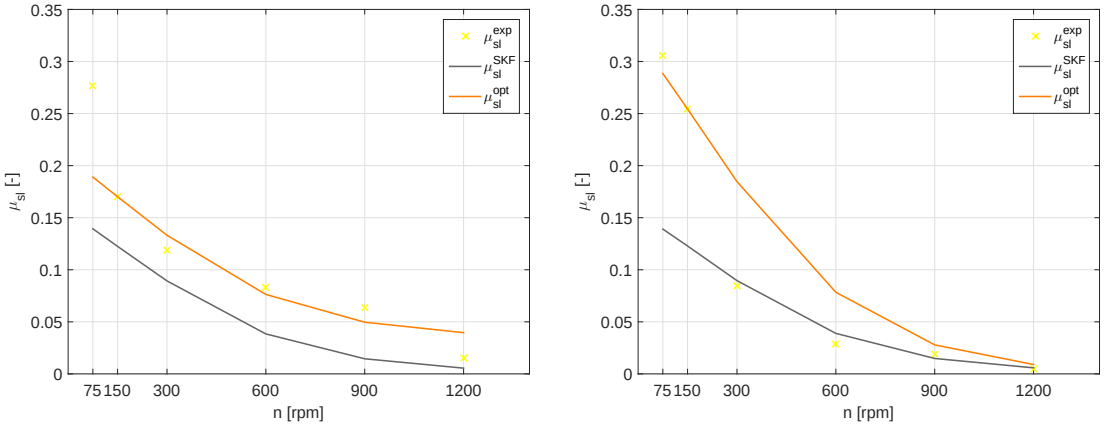

(a) 4 kN; 70 °C

(b) 7 kN; 70 °C

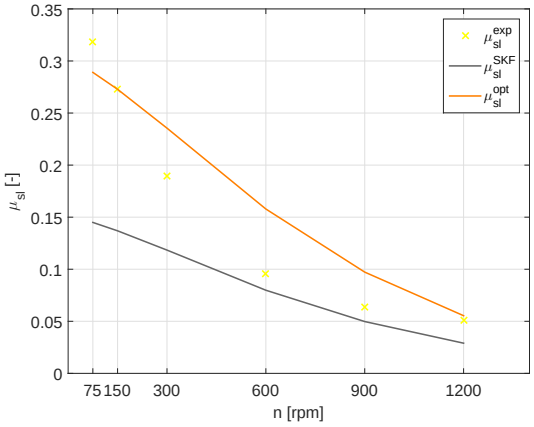

(c) 4 kN; 90 °C

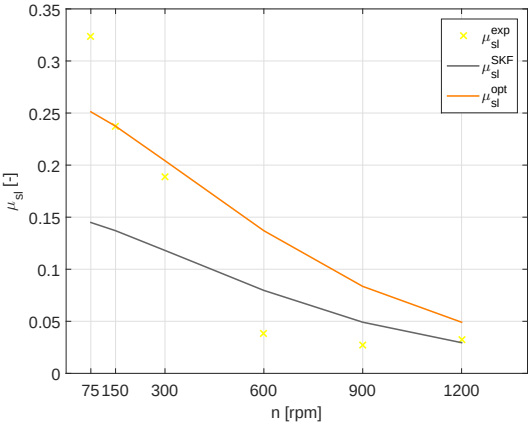

(d) 7 kN; 90 °C

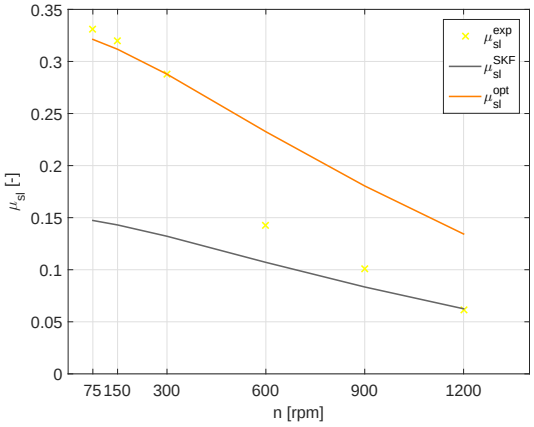

(e) 4 kN; 110 °C

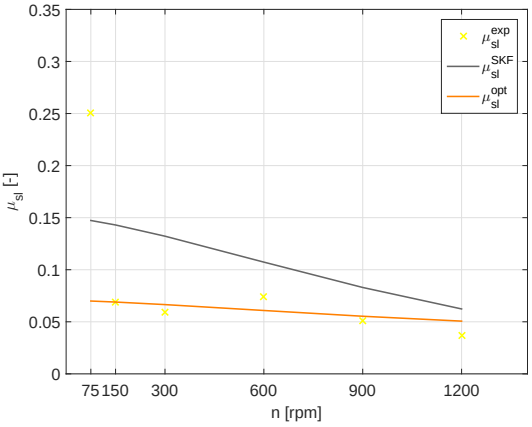

(f) 7 kN; 110 °C

Figure G.11: Experimental, SKF and Optimized Sliding Coefficient of Friction (μ_{sl}) for TRB 320/28X/Q and 10W50 oil.

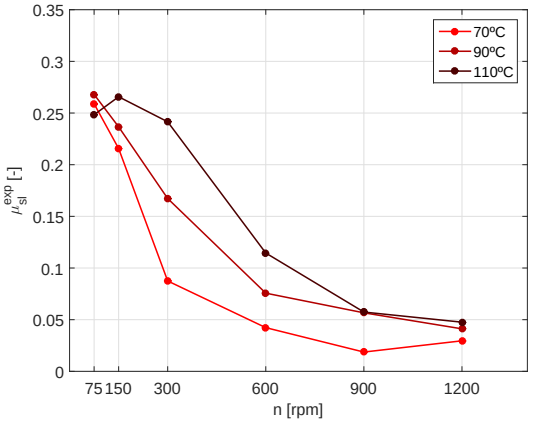

(a) 4 kN; 75W90

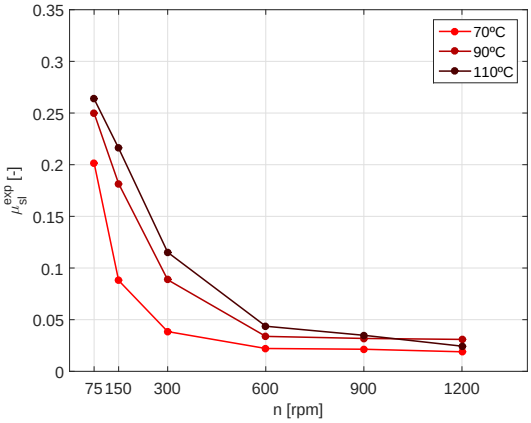

(b) 7 kN; 75W90

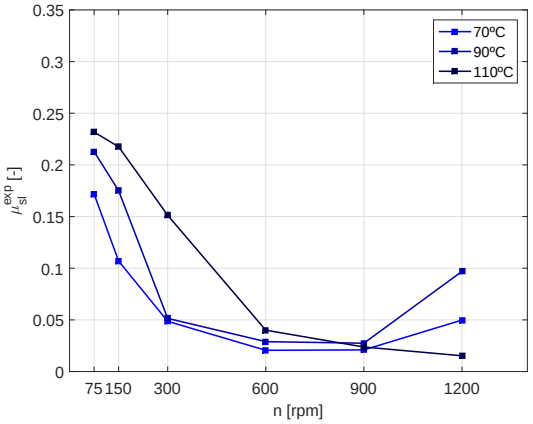

(c) 4 kN; 75W140

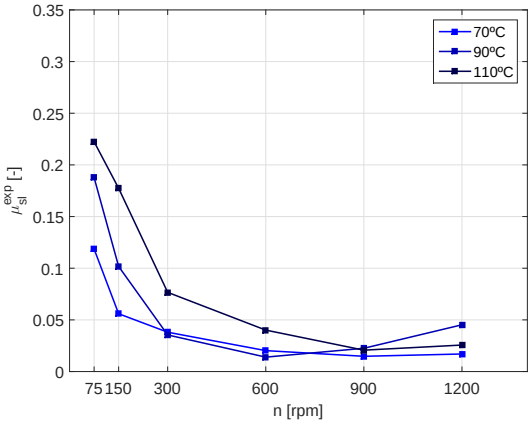

(d) 7 kN; 75W140

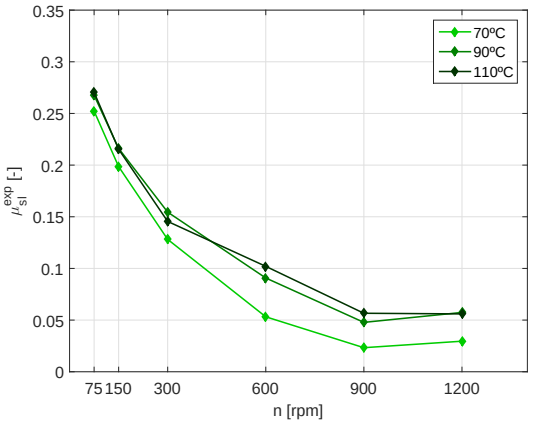

(e) 4 kN; 80W90

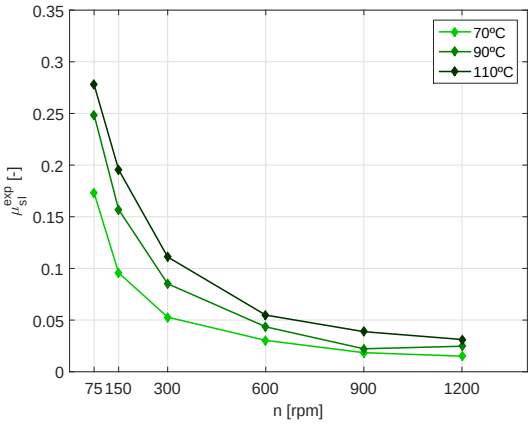

(f) 7 kN; 80W90

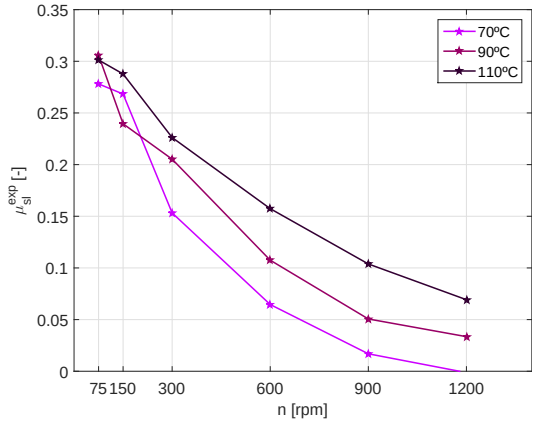

(g) 4 kN; 5W30

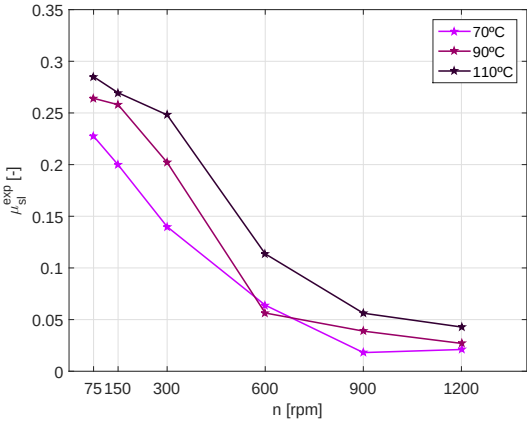

(h) 7 kN; 5W30

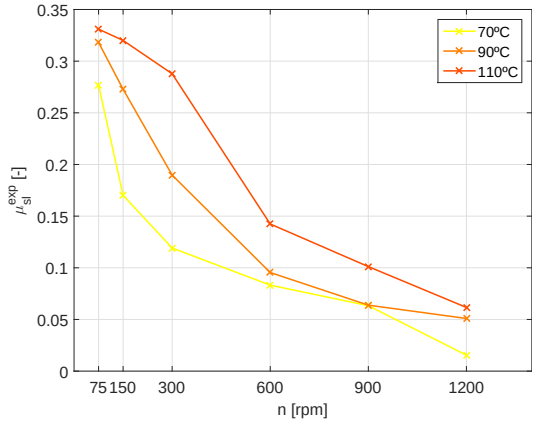

(i) 4 kN; 10W50

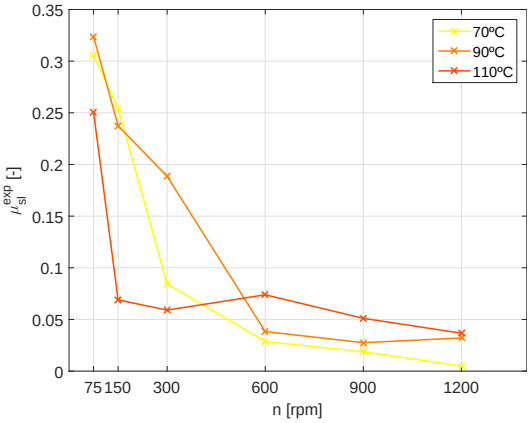

(j) 7 kN; 10W50

Figure G.12: Experimental Sliding Coefficient of Friction (μ_{sl}) for all oils at all tested conditions.